TECHNICKÁ UNIVERZITA V LIBERCI
Fakulta strojní

Geopolymer Composite for Fire-resistance

Disertační práce

Liberec 2020

Prohlášení

Prohlašuji, že svou disertační práci jsem vypracoval samostatně jako původní dílo s použitím uvedené literatury a na základě konzultací s vedoucím mé disertační práce a konzultantem.

Jsem si vědom toho, že na mou disertační práci se plně vztahuje zákon č. 121/2000 Sb., o právu autorském, zejména § 60 – školní dílo.

Beru na vědomí, že Technická univerzita v Liberci nezasahuje do mých autorských práv užitím mé disertační práce pro vnitřní potřebu Technické univerzity v Liberci.

Užiji-li disertační práci nebo poskytnu-li licenci k jejímu využití, jsem si vědom povinnosti informovat o této skutečnosti Technickou univerzitu v Liberci; v tomto případě má Technická univerzita v Liberci právo ode mne požadovat úhradu nákladů, které vynaložila na vytvoření díla, až do jejich skutečné výše.

Současně čestně prohlašuji, že text elektronické podoby práce vložený do IS/STAG se shoduje s textem tištěné podoby práce.

Beru na vědomí, že má disertační práce bude zveřejněna Technickou univerzitou v Liberci v souladu s § 47b zákona č. 111/1998 Sb., o vysokých školách a o změně a doplnění dalších zákonů (zákon o vysokých školách), ve znění pozdějších předpisů.

Jsem si vědom následků, které podle zákona o vysokých školách mohou vyplývat z porušení tohoto prohlášení.

10. srpna 2020   Ing. Su Le Van

TECHNICAL UNIVERSITY OF LIBEREC
FACULTY OF MECHANICAL ENGINEERING
DEPARTMENT OF MATERIAL SCIENCE
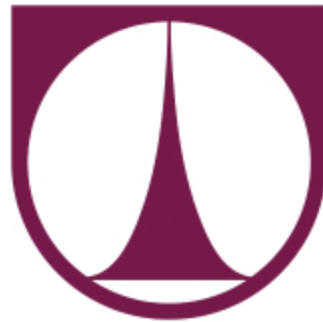
DISSERTATION THESIS

2020   **Ing. Le Van Su**

TECHNICKÁ UNIVERYITA V LIBEREC

FAKULTA STROJNÍ

KATEDRA MATERIÁLU
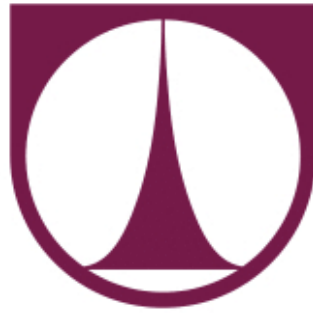
DISERTAČNÍ PRÁCE

Studijní obor: 2303v strojirenská technologie

Studijní program: p2301 strojní inženýrství

Zaměření: 3911v011 materiálové inženýrství

GEOPOLYMER COMPOSITE FOR FIRE-RESISTANCE
GEOPOLYMERNÍ KOMPOZIT PRO POŽÁRNÍ OCHRANU

Autor práce: Ing. Le Van Su

Školitel: prof. Ing. Petr Louda, CSc.

Rozsah práce   **Počet stran 218**

Počet obrázky 146

Počet tabulek 31

Počet příloh 1

Acknowledgments

Ing. Le Van Su

Liberec, 2020

Annotation

The thesis presents the research of fire-resistant materials and their application in building constructions for the purpose of preventing and protecting the safety of people when the fire occurs. The thesis author has applied the technology of surface treatment by coating fire-resistant composite materials on the surface of base materials in building structures. The coating fire-resistant composite materials on the structural surfaces can be fire-retardant and preventing the spread of fire to increase the time for evacuating the people in the case of fire. The fire-resistant composite materials developed in the thesis were based on geopolymer matrix commercialized in the Czech Republic.

The thesis author and colleagues conducted huge research work at the Technical University of Liberec (TUL) and the company of Pavus a.s. as well. The author has developed new geopolymer foams (GFs) as fire-resistant composite materials used for coating the base materials. The developed GFs have lightweight, low thermal conductivity, high-temperature resistance above 1000 °C, and flexible applicability. The GFs have coated on the substrate surfaces by laminating and spraying methods. The author has investigated and assessed the fire-resistance of GFs coated on the surfaces of the steel, concrete, wood, aluminum, and polystyrene structures at the TUL. In addition, the fire-resistance of GFs on the surfaces of concrete slabs, OSB panels, and steel plates has been examined and evaluated at the company Pavus a.s.

Research results at the TUL have shown that GFs are suitable coating materials for most substrates such as steel, concrete, wood, aluminum, and polystyrene materials. The fire-resistant time of the substrate materials coated with a GF protective layer is greatly improved. The fire-resistant periods of steel plates, concrete slabs, OSB panels, aluminum plates, and polystyrene boards covered with a GF protective layer with different thicknesses are 134, 100, 99, 125 and 15 min, respectively. In addition, research results at the company Pavus a.s indicated that the GFs coated on the concrete slabs, OSB panels, and steel plates had the respective fire-resistant times of 180, 130, and 50 min.

Moreover, in the thesis geopolymer reinforced with environmentally friendly materials (wool, basalt, rice husk) has shown a significant improvement in its mechanical properties and the fire-resistant time. The density, thermal conductivity coefficient, porosity, compressive and flexural strength of the GFs were measured as $546 - 1028$ kg.m^{-3}, $0.13 - 0.359$ W/m.K, $41.8 - 62.5$ %, $1.94 - 9$ MPa, $0.96 - 2.93$ MPa, respectively.

In short, the research results in this thesis have shown that the GF is an excellent coating material for the fire-resistant purpose at high-temperature.

Keywords: *geopolymer foam, concrete slab, waste fiber, fire-resistant test, OSB panel, aluminum powder, mechanical properties.*

Anotace

Disertační práce představuje výzkum materiálů odolných proti ohni a jejich použití ve stavebních konstrukcích za účelem prevence a ochrany bezpečnosti osob při vzniku požáru. Autor práce aplikoval technologii povrchové úpravy nanášením ohnivzdorných kompozitních materiálů na povrch základních materiálů ve stavebních konstrukcích. Povrstvené ohnivzdorné kompozity na konstrukčních površích jsou nehořlavé a mohou bránit šíření ohně, aby se prodloužil čas pro evakuaci lidí v případě požáru. Ohnivzdorné kompozitní materiály vyvinuté v práci byly založeny na geopolymerní matrici komerčně dostupné v České republice.

Autor práce s kolegy provedli výzkumné práce na Technické univerzitě v Liberci (TUL) a ve společnosti Pavus a.s. také. Autor vyvinul nové geopolymerní pěny (GF) jako ohnivzdorné kompozitní materiály pro povlakování základních materiálů. Vyvinuté GF mají nízkou hmotnost, velmi nízkou tepelnou vodivost, odolnost vůči vysokým teplotám nad 1000 °C a flexibilní použitelnost. GF se povlakovaly na povrch substrátu laminováním a nástřikem. Autor zkoumal a hodnotil požární odolnost GF povlakování na površích ocelových, betonových, dřevěných, hliníkových a polystyrenových materiálů na TUL. Kromě toho byla ve společnosti Pavus a.s. zkoumána a zhodnocena požární odolnost GF na površích betonových desek, OSB panelů a ocelových plechů.

Výsledky experimentů na TUL ukázaly, že GF jsou vhodné povlakové materiály pro většinu substrátů, jako jsou ocel, beton, dřevo, hliník a polystyren. Ohnivzdorná doba materiálů povlakovaných ochrannou vrstvou GF je výrazně zvýšená. Doba ohnivzdornosti ocelových a betonových desek, OSB panelů, hliníkových a polystyrénových desek pokrytých vrstvou GF o různých tloušťkách je u oceli 134 min, u betonu 100 min, u OSB panel 99 min, u hlinik 125 min a u polystyreny15 min.

Výsledky měření ve společnosti Pavus a.s ukázaly, že GF povlakování na betonových deskách, OSB panelech a ocelových deskách měly doby ohnivzdornosti 180 min (beton), 130 min (OSB panel) a 50 min (ocel).

Geopolymer vyztužený materiály šetrnými k životnímu prostředí (vlna, čedič, rýžová slupka) navíc v práci prokázal významné zlepšení svých mechanických vlastností a doby ohněvzdornosti. GF byla měřena měrná hustota ($546 - 1028$ kg.m^{-3}), koeficient tepelné vodivosti ($0,13 - 0,359$ W/m.K), pórovitost ($41,8 - 62,5\%$), pevnost v tlaku ($1,94 - 9$ MPa) a pevnost v ohybu ($0,96 - 2,93$ MPa).

Autorovy výzkumné výsledky ukázaly,že GF je vynikající povlakovací materiál pro ohnivzdorné účely při vysokých teplotách.

Klíčová slova: *geopolymerní pěna, betonová deska, odpadní vlákno, zkouška požární odolnosti, OSB panel, hliníkový prášek, mechanické vlastnosti.*

Preface

The Ph.D. thesis presents the author's research results in the field of the GF for fire-resistant applications. The main interest of the thesis focuses on research, evaluation and application of the GF for fire-resistance purposes.

The thesis consists of two parts. The first part is to present a brief overview of geopolymer materials, research methods, and equipment for the fire-resistant test. This part contains the experimental results conducted at the Technical University of Liberec (TUL) and the company Pavus a.s. (Praha). The research results specifically demonstrated the optimization and application of the GF for fire resistance. The second part includes crucial research results and is presented as a collection of the following papers (article A-F). The articles were published in prestigious journals indexed by Web of Science. The articles were created by the collaborative efforts of the team from idea to publication.

Article A. *Thermal conductivity of reinforced geopolymer foam*

Van Su Le, Pavlina Hajkova, Vladimir Kovacic, Totka Bakalova, Volesky Lukas, Chi Hiep Le, Kevin Ceccon Seifert, Amanda Pereira Peres, Petr Louda. Published in the Ceramics-Silikaty, volume 63 (4), pages 365-373. May 2019.

Article B. *Mechanical properties of geopolymer foam at high-temperature*

Van Su Le, Michal M. Szczypinski, Pavlina Hajkova, Vladimir Kovacic, Totka Bakalova, LukasVolesky, Le Chi Hiep, and Petr Louda. Published in the Science and Engineering of Composite Materials, volume 27 (4), pages 129-138. May 2020.

Article C. *Impact of flax and basalt fiber reinforcement on selected properties of geopolymer composites*

Miroslav Frydrych, Stepan Hysek, Ludmila Fridrichova, Su Le Van, Miroslav Herclik, Miroslava Pechociakova, Hiep Le Chi and Petr Louda. Published in the Sustainability, volume 1, pages 12. December 2019. Impact Factor: 2.592

Article D. *Permeable water-resistant heat insulation panel based on recycled materials and its physical and mechanical properties*

Stepan Hysek, Miroslav Frydrych, Miroslav Herclik, Ludmila Fridrichova, Petr Louda, Roman Knizek, Su Le Van, and Hiep Le Chi. Published in the Molecules, volume 12, pages 12. September 2019. Impact Factor: 3.06

Article E. *Fire-resistant sandwich-structured composite material based on alternative materials and its physical and mechanical properties*

Stepan Hysek, Miroslav Frydrych, Miroslav Herclik, Petr Louda, Ludmila Fridrichova, Su Le Van and Hiep Le Chi. Published in Materials, volume 24, pages 12. May 2019. Impact Factor: 2.972

Article F. *Water absorption properties of geopolymer foam after being impregnated with hydrophobic agents*

Hiep Le Chi, Pavlina Hajkova, Su Le Van, Petr Louda, Lukas Volesky. Published in Materials, volume 24, pages 12. December 2019. Impact Factor: 2.972

Contents

TABLE OF FIGURES

LIST OF TABLES

Part I. OVERVIEW

Chapter 1. INTRODUCTION

1. Fire-resistant materials

Fire-resistant materials can withstand high temperatures and are designed to slow the spread of fire. Fire-resistant material acts as an insulator, which is the reduction of heat transfer through the thickness of the material. It is used as a thermal insulation material in the buildings and construction sector. Fire-resistant materials which are commonly used in the buildings are presented as follows.

1.1 *Gypsum*

Gypsum is essentially a non-flammable material. Gypsum prevents the possibility of fire spreading, resisting the increase in the temperature of non-exposed surfaces. Ceiling systems and gypsum walls have fire-resistant time levels: 30 min, 60 min, or 120 min [1]. Gypsum ceilings used for office interior is presented in Figure 1.

Figure 1. Gypsum ceilings used for office interior [2].

1.2 *Concrete*

Concrete is a composite material and is one of the most frequently used construction materials worldwide [3, 4]. Concrete has excellent fire-resistance because it does not burn, has low thermal conductivity, and prevents fire from spreading (Figure 2). At temperatures below 400 °C, the concrete properties are the same as those at room temperature [5-8]. At a heating temperature of 600 °C, the compressive strength of concrete is only 85% of the value before heating [9].

Figure 2. Fire-resistance of concrete material [10].

1.3 *Wood treated with fire-resistance materials*

Wood is a trendy material in construction, both aesthetically pleasing and eco-friendly material. Nevertheless, the disadvantage of this material is that it has excellent flammable properties and burns quickly (Figure 3). To meet the needs of using wood in construction but still ensure safety, construction contractors have chosen wood treated with fire-resistant materials. The wood might be treated with Fire-resistant liquid, fire-retardant paint or other methods to reduce the flammability of wood [11]. Fire-treated wood has been a protective layer that can withstand high temperatures and fire spread [12].

Figure 3. The fire broke the roof of Notre-Dame de Paris cathedral in Paris [13].

1.4 *Steel*

Steel is widely used in the construction industry [14]. It has higher compressive and tensile strength than the concrete. The mechanical properties of steel depend on its grade. There are about 500 types of steel in the Czech Republic [15]. Steel can be applied to any shape and assembled quickly at the construction site. Steel is inherently non-flammable material. However, the stress of steel at the critical temperature reduces about 60% compared to that at room temperature [6, 16]. Standard methods of fire protection for the steel include plastering, calcium silicate coatings, and mineral wool coatings [8]. Geopolymer foam (GF) coated on the steel tubes at the company Plaga a.s is depicted in Figure 4.

Figure 4. Le Van Su sprayed the GF on the steel tubes at the company Plaga a.s.

1.5 *Fire-resistant paint*

Fire-resistant paint is the most used solution today for fire resistance. It has several types such as fire-resistant paint for wood and fire-resistant paint for steel (Figure 5). Depending on the fire-retardant paint rating, it has protection time from 30 to 120 min [17], even 150 min in different cases [18]. It has advantages in aesthetics and flexibility. The disadvantages of fire-resistant paint are high cost and short life. In addition, the paint production process causes many toxic emissions for the environment.

Figure 5. Fire-resistant paint for steel [19].

1.6 *Glass wool*

Glass wool is made from synthetic glass fiber manufactured from stone, slag, and clay (Figure 6). It has many features such as sound insulation, high electrical insulation, non-flammable, soft and good elasticity. Glass wool is widely used for buildings and construction, soundproofing, thermal and electrical insulation, and fire-resistant. Disadvantages of glass wool are allergies and skin irritation [20].

Figure 6. Glass wool building materials [21].

1.7 *Calcium silicate*

Calcium silicate used to protect electrical circuits and fire-resistant plasterings (Figure 7). Calcium silicate has excellent fire-resistance [22], even durable in wet weather. Besides, this material has good tensile strength, bending strength, excellent heat and sound insulation, and easy installation.
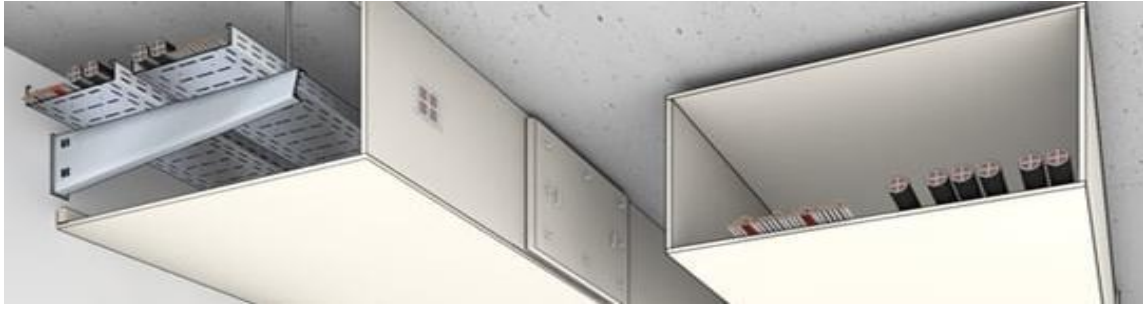
Figure 7. Calcium silicate board for electrical wiring [23].

2. Geopolymer materials

2.1 *Materials related to geopolymer composite used in ancient times [24]*

This section shows famous historical constructions and building materials related to geopolymer composite.

Mesopotamia

Eight million bricks built the Ziggurat of Ur (Figure 8). The bricks are dried and heated but also enameled. Prof. Davidovits and his colleague claimed the bricks of the Sumer [24]. The bricks have all the characteristics of today's ceramic bricks.

Figure 8. The Ziggurat of Ur [25].

Egypt

Today, 138 construction structures similar to the Cheops pyramid have been found in Egypt [26]. The book "The Pyramids: An Enigma Solved" written by Prof. Davidovits explained the construction techniques of the Cheops pyramid. Construction techniques of new blocks were produced directly on other blocks. The solidification of blocks is similar to that of today's geopolymer composite.

Figure 9. The Pyramid of Cheops [27].

Central and South America

The Inca civilization was the oldest in South America and flourished in the Andres. Inca people have excellent stone processing skills. In the Inca civilization, Inca citizens knew about stone casting techniques (Figure 10). The starting material (silicate or aluminosilicate) has been dissolved in an organic extract, and the liquid slurry is then poured into the mold.

Figure 10. Sacsayhuaman, Peru: Ancient people made rocks [28].

Ancient Rome

The Colosseum in Rome was made of high-quality pozzolanic concrete (Figure 11). The concrete was produced from calcium kaolin clay and volcanic rocks.

Figure 11. Colosseum in Rome, Italy [29].

2.2 *Geopolymers*

Prof. Joseph Davidovits is a French chemist who invented and developed a geopolymer material in the period 1970-1973 after the catastrophic fire in France. He established a

private company in 1972, which today is named CORD-GEOPOLYMERE. It focuses on the study of non-flammable materials.

The first application of geopolymer composite in the construction is the production of refractory plywood panels developed by J.J. Legrand (Figure 12). Refractory panels were manufactured in a one-step process (US Patents 3,950,47; 4,028,454) [30]. They comprised of a wooden core in the middle coating with two faces of nanocomposite SILIFACE Q. They were applied in industry and were commercialized in the French market from 1972 to 1976. However, refractory plywood panels were abandoned in 1976 by politics.

Figure 12. The fire-resistant wood-chipboards manufactured from geopolymer (na-poly(sialate)) [31].

Electrical fuses made by geopolymer composite SILIFACE COR70 (Figure 13). It has excellent mechanical properties, special thermal stability, and low thermal expansion. Unfortunately, it has high water absorption (0.3%), therefore the project developed SILIFACE COR70 was canceled.

Figure 13. Electrical fuses made by LEGRAND a.s [31].

The low-temperature geopolymer composite setting (L.T.G.S.) dries at temperatures of 50 - 250 °C, in an alkaline environment through an oligosialate precursor of (-Si-O-Al-O-) (Na) in concentrations from 2 to 6% by weight of the ceramic paste (Figure 14). Kaolinite in clay is transformed by L.T.G.S. technology into a three-dimensional composite of poly(sialate) Na-PS of the modality type. This manufacturing technology changes and modernizes the traditional industry. It has been patented (European Patent 0,101,714) about producing high-quality ceramics.

Figure 14. The geopolymer composite brick L.T.G.S. [31].

The new terminology, geopolymeric binder, is the key to the successful development of new materials. Geopolymer binders are polymers that set rapidly at ambient temperature within a few minutes. They are inorganic, hard, stable at high temperatures up to 1250 °C, and not flammable. This has brought a tremendous impetus to creativity and innovation. Some art objects made of geopolymer binders are depicted in Figure 15.
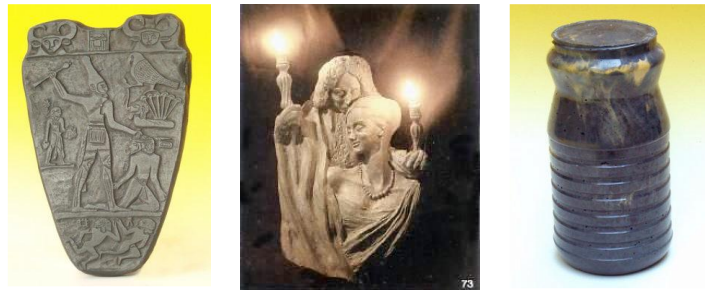
Figure 15. Art objects made of geopolymer material [31].

Liquid binders, which are the inorganic equivalent of organic resins, have been developed by a group of scientists, including Michel Davidovits and Nikolas Davidovits. The trade names of the binders include GEOPOLYMIT, TROLIT and WILLIT. The applications of these binders in aeronautical engineering, nuclear sector, artistic reproductions, thermal insulation of buildings, foundries, castings, metal production, furnace insulation (Figure 16) and archaeological research have found since 1979.

Figure 16. Example of foamed geopolymer materials [31].

A high-strength cement geopolymer, named QUAZITE, was invented in 1983. It is also the name of the company founded in 1983. The QUAZITE company developed, manufactured and marketed this new material for applications in the construction, architecture and engineering. QUAZITE material is made of mineral aggregates combined with polymer and monomer. It is defined as (K-Ca) (Si-O-Al-O-Si-O-) poly(sialate-siloxo)

cement. Understandably, QUAZITE material is concrete with organic adhesive. In August 1983, Lon Star Industries Inc. decided to set up a subsidiary under the name PYRAMENT (Figure 17).

Figure 17. PYRAMENT in the USA is used for road coverings and repairs [31].

The addition of ground blast furnace slag to the poly(sialate) type of geopolymer accelerates the setting time and significantly improves compressive and flexural strength [32]. Geopolymeric cements developed for the long-term containment of hazardous and toxic wastes (US Patents 4,859,367; 5,349,118) are acid-resistant cementitious materials with zeolitic properties [33]. Geopolymer cement includes the following compounds:

- Specific alumino-silicates of the kaolinitic clay species, calcined at 750 °C;

- Alkali-disilicates $(Na_2, K_2) (H_2SiO_4)_2$;

- Calcium disilicates $Ca(H_2SiO_4)_2$ produced by the alkali-reaction with blast furnace slag.

This acid-resistant cement hardens very quickly at room temperature and has a compressive strength up to 20 MPa after 4 hours of drying (Figure 18) when compressive strength was determined by the standard tests of hydraulic cement mortars. The 28-day compressive strength of the geopolymetric cement is 70-100 MPa.

PYRAMENT geopolymer cement is an ideal material for repairing runways originally made of concrete, sidewalks and highways. In the case of a runway for aircraft, 4-6 hours hardening is enough for Airbuses or Boeings to land here. When a plane catches fire, the survival chances of passengers are minimal. That is because the parts in the plane, such as the seat cushions, carpeting, walls, and luggage bins burn quickly and give off flammable gases leading to the explosion. Therefore, we need to give passengers more time to escape when the plane fires, the U.S. Federal Aviation Administration initiated a research program to develop low-cost, environmentally friendly, and fire-resistant materials in 1994. The geopolymer composite (Figure 19) was selected as the best candidate for this program.
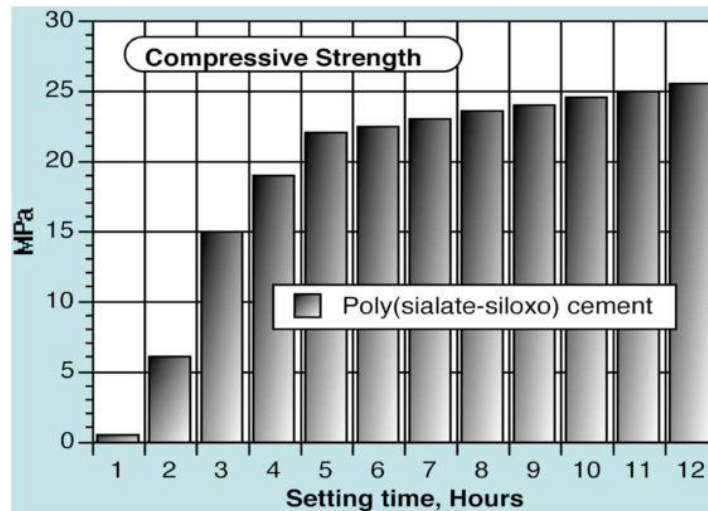
Figure 18. High-early strength of (K, Ca)-poly(sialate-siloxo) cement [34].

Figure 19. A carbon-epoxy aerospace composite (left) is burning while a carbon-geopolymer composite (right) still resists a 1200 °C fire [31].

2.3 *Summary of geopolymer materials*

Geopolymer is a compound of aluminum and silicon (-Si-O-Al-O bonds) which is the connecting block of chemical chains, similar to zeolite. However, geopolymer is an amorphous aluminosilicate whereas zeolite is crystalline microporous aluminosilicate material. The microstructure of geopolymers shows a 3-D molecular structure unit and small aluminosilicate clusters with pores dispersed within a highly porous network. The cluster sizes are from 5 to 10 nm [35]. Therefore, the geopolymer structure is perceived as a dense amorphous phase consisting of a semi-crystalline 3-D alumino-silicate microstructure [36].

Geopolymerization

There are many names that have been used to describe the term geopolymer, such as geocement [37], low-temperature synthesized aluminosilicate glasses [38], inorganic polymer concrete [39] aluminosilicate activated alkali systems [40], Alkali-bonded ceramics [41, 42], or alkaline-activated cement [43, 44]. They have the same nature as the synthesis of aluminosilicate from the reaction with alkaline solutions [45]. It can be described as a complex system of soluble reactions and precipitation in an alkaline medium [46]. Prof. Davidovits indicated that geopolymer synthesis consists of three steps:

- Dissolution of aluminosilicate in a strong alkaline solution,

- Reorientation of free ion clusters,

- Both polycondensation and all reactions can be carried out in many ways.

The most proposed mechanism of the geopolymerization process is divided into four main steps [47, 48]. The first step is the dissolution of aluminosilicate raw materials in an alkaline solution. At this stage, Si and Al are transferred from the solid phase to the liquid phase. Next, the formation of Si and/or Si–Al oligomers in the aqueous solution occurs in the second phase. In the third step, polycondensation of the oligomeric species or units in the aqueous phase is conducted to form an inorganic polymeric material [47]. Finally, the bonding of undissolved solid particles in the final geopolymeric structure occurs in the fourth step [47, 49].
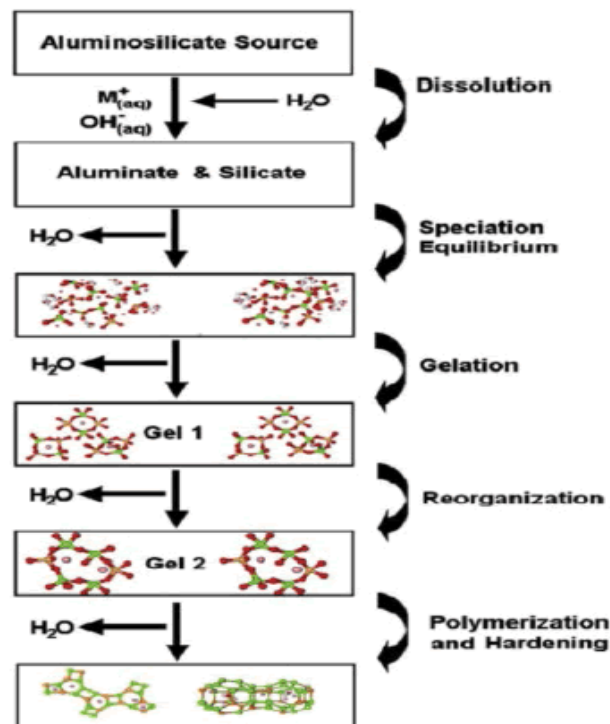
Figure 20. Conceptual model for geopolymerization [46].

Figure 20 describes a reaction mechanism occurring in the transformation of a solid aluminosilicate source into a synthetic alkali aluminosilicate for geopolymerization. Geopolymer contains mainly aluminum and silicon in amorphous form. From the studies, raw materials are divided into two main categories: (1) calcium-rich materials such as blast furnace slag, and (2) raw materials having low calcium and rich SiO_2 and rich Al_2O_3 such as metakaolin [50]. Because their reaction mechanisms are complex and different [51], any material containing mainly silicon (Si) and aluminum (Al) in an amorphous form and easily soluble in an alkaline environment can be used to produce geopolymer [52]. The reaction happens in the alkaline environment, therefore this material is also called alkali activation aluminosilicate [53], or alkaline activated cement [52]. Today, the most-used geopolymers are sodium polysialate ((Na) -PS), potassium polysialate ((K) -PS), sodium-potassium poly(siloxo-sialate) ((Na, K) -PSS) and potassium poly(siloxo sialate) ((K) -PSS) [47].

Source materials are usually as metakaolin or calcined kaolin [34, 54-67], fly ash [43, 64, 65, 67-78], natural Al-Si mineral [52, 79], combined flying and metakaolin [53, 68]. Besides, other sources of aluminum and silicon-rich materials can be used for industrial processes such as fly ash, because it is a waste product of coal-fired plants, slag and construction residues [53, 67, 80-85].

Geopolymer structure

The structure of geopolymers is based on a three-dimensional aluminosilicate phase. It has an empirical formula:

Mn (- (SiO_2)$_z$ - AlO_2)n . wH_2O
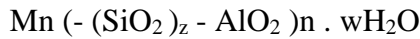
Where:

"M" is generally a monovalent cation, potassium or sodium,

"z" is a natural number denoting the number of SiO_2 units (1, 2, 3, etc.),

"n" represents the degree of polymerization [45, 86].

Based on the Si/Al ratio, four types of polysialates can be distinguished:

- Poly(sialate): Mn – (– Si–O–Al–O–)n M-PS Si: Al = 1:1

- Poly(siloxo-sialate): Mn – (–Si–O–Al–O–Si–O–) n M-PSS Si: Al = 2:1

- Poly(disiloxo-sialate): Mn – (–Si–O–Al–O–Si–O–Si–O–)n M-PSDS Si: Al = 3:1

- Poly(multisiloxo-sialate): (–Si–O–Al–O–) Si: Al >> 3:1

The geopolymer structure results from the interconnection of a poly(silicate) molecular structure by a chain or network - 2D (for the production of low-quality concrete reinforced mainly with particles) or 3D (solid and heat-resistant matrices reinforced not only with particles but also with fibers) [87]. Figure 21 shows some examples of poly(sialate) molecular structures. It includes at least four base units, where z is 1, 2, 3 and higher [88].

Figure 21. The structure of the geopolymer consists of a polymeric Si - O - Al chain [45].

2.4 *Preparation of geopolymer composites*

The raw clay material must have particles smaller than 20 microns with the volume fraction of at least 40%, and have thermal activation at a temperature lower than 800 °C,

Preparation of alkaline solution in molar ratios:

$$SiO_2 / Al_2O_3 / Na_2O (K_2O)$$
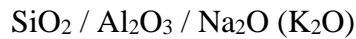
$$2\text{-}4 / 1 / 0.24 - 0.3$$

The water content is calculated in molar ratios as follows:

$$H_2O / Na_2O (K_2O)$$
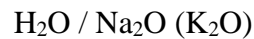
$$14 - 20 / 1$$

The mixing clay material with a massive amount of filler was conducted on a mixer with a powerful engine. At first, the activated clay was proportionally mixed with a calculated alkali solution. Next, the fillers were added to the mixture, and it was filled in the mold. The air bubbles of the mixture in the mold were eliminated by mechanical vibration. Finally, the obtained samples were wrapped by a thin plastic sheet (Figure 22).
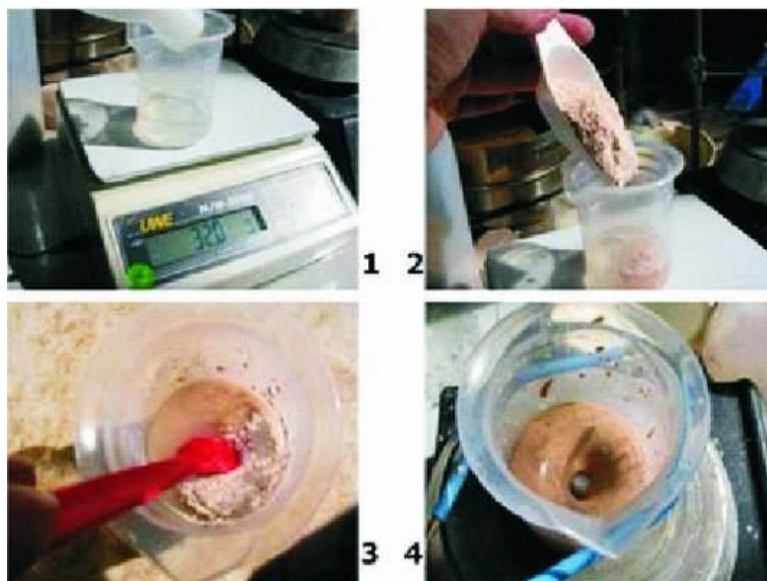
Figure 22. The process of mixing clay materials [24].

2.5 *Geopolymer foam*

Geopolymer foam (GF) is a lightweight material with a density of 200 to 1000 kg.m^{-3} [31, 33, 45, 89], stability at high temperatures [90, 91], fire-retardance in the case of geopolymer having potassium activator [92-94], quickly installed at low-temperatures [75, 95-97], thermal insulation [98-102]. GFs are considered as building materials [61, 73, 103-107], membranes and membrane support [42, 108-110], adsorbents and fillers [60, 66, 111, 112] or catalyst [91, 113]. The processing method of GFs is the thermal expansion of K-nano-poly(siloxo) at temperatures above 250 °C.

In addition, GFs can be produced by the geochemical method using foaming agents such as hydrogen peroxide (H_2O_2) [73, 114-116], aluminum powder [59, 67, 78, 85, 97, 100, 114, 117-126], sodium perborate [73], and silica fume [127, 128]. GFs can be used to develop a low density material with thermal insulation properties using thermal expansion agents or chemical methods [129].

Oxygen gas can be used as a foaming agent because of the decomposition of peroxides in an alkaline environment. The reaction process is the following:

$$2H_2O_2 \rightarrow 2H_2O + O_2$$
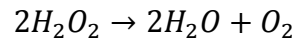
Besides, hydrogen gas also can be considered as the foaming agent. The hydrogen gas is created by the reaction of metal powder with water and hydroxide in an alkaline environment [93]. The reaction process is the following:

$$M + 3H_2O + OH^- \rightarrow M(OH)_4^- + \frac{3}{2}H_2$$
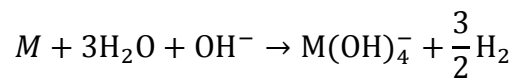
Where: M is metal.

GFs fabrication

GFs production requires the optimization of two parameters:

- Kinetics of peroxides decomposition with the creation of oxygen

- Increase in viscosity of the geopolymer precondensate.

It has no standard formula.

The specific examples of GFs fabrication are the following:

Foaming with sodium perborate

The first step was mixing 305g of MK750 (Na, K) – PSS geopolymeric reactant mixture containing H_2O_2 7.5 moles, Na_2O 0.246 moles, K_2O 0.164 moles, SiO_2 1.65 moles, Al_2O_3 0.43 moles with 90 g of muscovite mica. Then, the mixture was added 12 g of sodium perborate in 24 g of water and was stored at ambient temperature for 1 hour. Finally, the mixture is poured into a mold and cured at 60 °C.

Foaming with H_2O_2

Geopolymer foam is usually produced using H_2O_2 concentrations of 10, 30, and 110 in volume. To begin with, we mixed 860 g of an MK-750 (K)-PSS geopolymeric reactant mixture containing 17.33 moles H_2O, 1.63 moles K_2O, 4.46 moles SiO_2, and 1.081 moles Al_2O_3 with 220 g of muscovite mica and 90g of powdered filler (calcium fluoride). Subsequently, the mixture was added 50 g of H_2O_2 (110 Vol.), 120 g of Portland cement and 100 g of water, and then kept at ambient temperature for 1 hour. The mixture starts to expand after 1 hour and is solidified after 3 hours at ambient temperature. Portland cement may be replaced with blast furnace slag.

Foaming with aluminum

The industrial Trolit foams are manufactured with different geopolymeric raw materials such as silica fume and alumina fume [130]. The Trolit foam consists of 22 wt. % reactive solid (silica + alumina fumes), 34 wt. % filler (mica types), 36 wt. % hardener (K- silicate solution with MR = 1.62), and 8 wt. % H_2O_2 (30 vol.). Firstly, the reactive solid, filler and hardener were mixed homogeneously. After that, the blowing agent with determined quantities was added before pouring the mixture into a mold. The expansion of the mixture starts immediately and is completed after 10 min. Solidification begins with an exothermic reaction after 20 min and ends after 60 min.

2.6 *Properties and applications of geopolymer composite*

Geopolymer composite has outstanding properties such as fast curing, suitable for most commercial reinforced aggregates, relatively low water permeability, high-temperature resistance, low specific gravity, high strength and acid-resistance. It is slowly replacing traditional materials. It has been promising for use in many industrial applications.

Geopolymer composite's first application is to replace metal molds with geopolymer-molded casting in the plastic manufacturing process. It can suffer temperatures between 250-300 °C [131]. Later, the technical demands required materials to work at temperatures higher than 800 °C, initiated by Lyon in 1994-1995 at the American Federal Aviation Administration [131]. Geopolymer composite is an ideal material for high-temperature applications because it is a mineral polymer which is never burnt in nature. It can resist the temperature up to 1400 °C and has a low coefficient of thermal expansion like ceramic (4.10^{-6}/°C) [132]. Geopolymer composite shows a specific heat capacity being 1.5 times higher than bricks. It has the same value as insulating materials ranging from 1000 to 1600 W/m.K [45]. When the geopolymer is reinforced with carbon fiber, it retains 63% durability at 800 °C compared with that at room temperature [133, 134]. Although the brittleness of geopolymer composites reduces, their durability increases after reinforcing them with natural or synthetic fibers [78, 126, 135-149]. Geopolymer composite is a green material [116, 123, 124, 150-153].

The ordinary Portland cement industry was creating about 8% of carbon dioxide (CO_2) of worldwide man-made emissions [154]. Producing a ton of cement usually generates nearly a ton of CO_2 [151]. Completely replacing cement by geopolymer at present is impossible because of economic reasons and their popularity. To reduce the environmental pollution, industrial by-products such as fly ash and blast furnace slag are added to the cement. By this method, it reduces 20 to 30% of the carbon dioxide emissions into the environment [151]. The primary material that is used to produce a geopolymer is kaolin. Producing a ton of kaolin would emit 0.18 tons of CO_2 into the environment, but it is 6 times less than that of the Portland cement. Besides, the geopolymer is stable and is not destroyed in the acid environment compared with the Portland cement.

Geopolymer composite can mix with toxic materials, resulting in a decrease in hazardous waste [155]. The storage of hazardous waste in geopolymeric products can solve

the waste problem at landfills and prevent them from invading the environment [156, 157]. Geopolymer composite is used as a binder to restore ancient statues or structures [158].

In summary, geopolymers and potential applications are described in Figure 23 [42, 70, 131, 132].
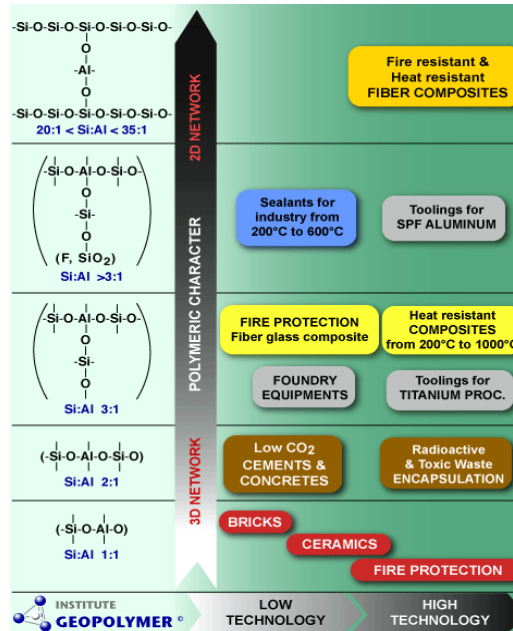
Figure 23. Geopolymers and potential applications [159].

3. Fire-resistance

Unlike other building materials, geopolymer composite materials have proven to increase the strength when exposed to fire. In addition, it can increase the fire-resistant time. The time and temperature of the fire depend on the fire type and place where the fire occurs [160].

Fire development can be divided into three stages (growth, flashover, decay stage) [161, 162]. Stages of fire development are described in Figure 24. The first stage of "Growth" is often overlooked because it is not affected by building structure during the fire [160].
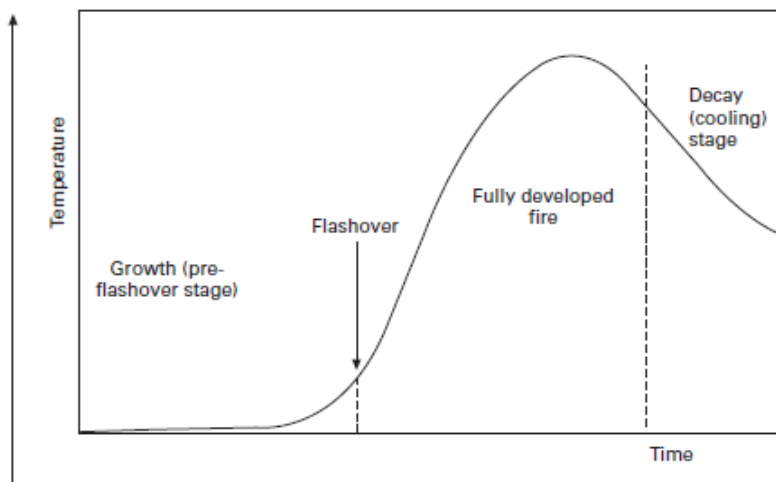
Figure 24. The development of fire [160].

Structural components in the construction are often required to resist the fire. Some standards for fire tests of building construction and materials are ISO 834, ASTM E119, Eurocode EN1991-1-2 (Figure 25) [163]. The fire curve is the relationship between temperature and time (Figure 25).
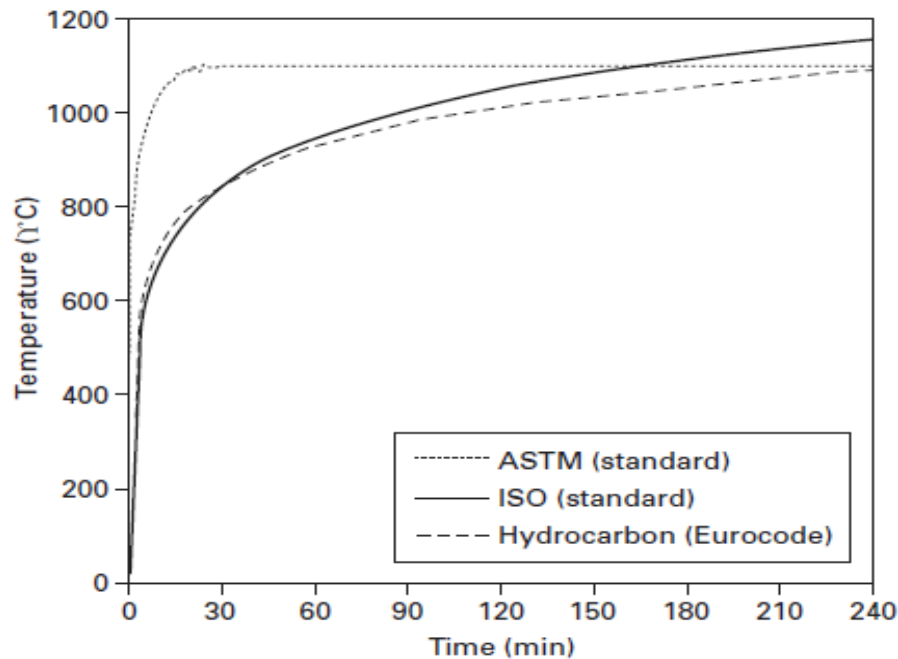
Figure 25. Temperature versus time relationship of a standard fire [160].

4. The objective of study

4.1 *Aims of the research*

The experimental investigation of passive fire resistance in construction materials at the TUL with the aim is to find a type of suitable GF applied in building construction. GF is the fire-resistant material, thus it is used as a coating material. The GF is coated on base materials such as wood, steel, concrete and polystyrene.

The main aims of this thesis are:

A. Finding the suitable GFs for fire-resistance purpose and improving their mechanical properties
  - The effect of basalt waste fiber on the mechanical properties of GFs curing at room temperature;
  - Effects of curing conditions on the mechanical properties of GFs;
  - Mechanical properties of GFs at high temperatures.
B. Performance of GFs for fire-resistance
  - GFs for passive fire-resistance of the structural steel plate;
  - GFs for passive fire-resistance of the wooden structural panels.
  - GFs for passive fire-resistance of the concrete slab

4.2 *Outline of the thesis*

The thesis is organized into two parts as follows:

Part 1 presents a general overview and contains chapters from 1 through 7. Chapter 1 portrays an overview of fire-resistant materials and a summary of geopolymer composites including history, definition, properties, applications. In addition, this chapter describes the objectives of the research and the outline of the thesis. Chapter 2 depicts the methods and equipment used in experimental investigations. This chapter also specifies the raw materials and the processing of geopolymer composites. Chapter 3 presents the empirical results conducted at the TUL. Chapter 4 reports on the results performed at the company Pavus a.s. Chapter 5 introduces a practical application. Chapter 6 presents conclusions and further perspectives. Chapter 7 presents an overview of the author's articles.

Part 2 shows the reprints of appended articles.

Chapter 2. EXPERIMENTAL METHODS

1. Preparation of GF

The GF was prepared by three following steps: (1) A geopolymer mortar is prepared by mixing throughout metakaolin with an alkaline solution of potassium in a predetermined ratio (liquid to solid) by mechanical stirring; (2) In the second step, silica sand and basalt waste fibers are added to the geopolymer mortar mixture. The mixture is homogenized by the mechanical stirring; (3) Lastly, aluminum powders are added to the mixture to create a protective porous geopolymer that can spray on the selected surface. Homogenization and foaming of the mixture are carried out by the mechanical stirring.

Note: the last step is omitted if the geopolymer mixture is prepared for a non-porous protective layer on the selected surface.

The curing times of 1, 3, 7, 14, 28 days for geopolymer samples are determined by each test method [55, 89, 164, 165]. The geopolymer specimens were cured in the different temperatures including room temperature, 50, 60, 70, 85, 90, 100 °C in the oven [89, 166]. The purpose of curing at high temperatures is to save time while the specimen retains the same properties as curing at room temperature. The processing of the geopolymer mortar is shown in Figure 26. Firstly, the raw materials (cement and its activator, silica sand, and basalt waste fibers, aluminum powders) are weighed. Next step, the cement (Figure 26.1) and activator (Figure 26.2) are mixed within 5 minutes at the speed of level 3 of the robot machine (or 500 rpm). After that, the silica sand and basalt waste fibers (Figure 26.3) were added, and then the mixture was stirred mechanically for another 5 minutes to obtain a uniform geopolymer mortar. Subsequently, aluminum powders (Figure 26.4) were added to the mortar mixture and then mixed for 5 minutes at high speed. Finally, a homogeneous mixture (Figure 26.6) is poured into the molds (Figure 26.7) [167-172].
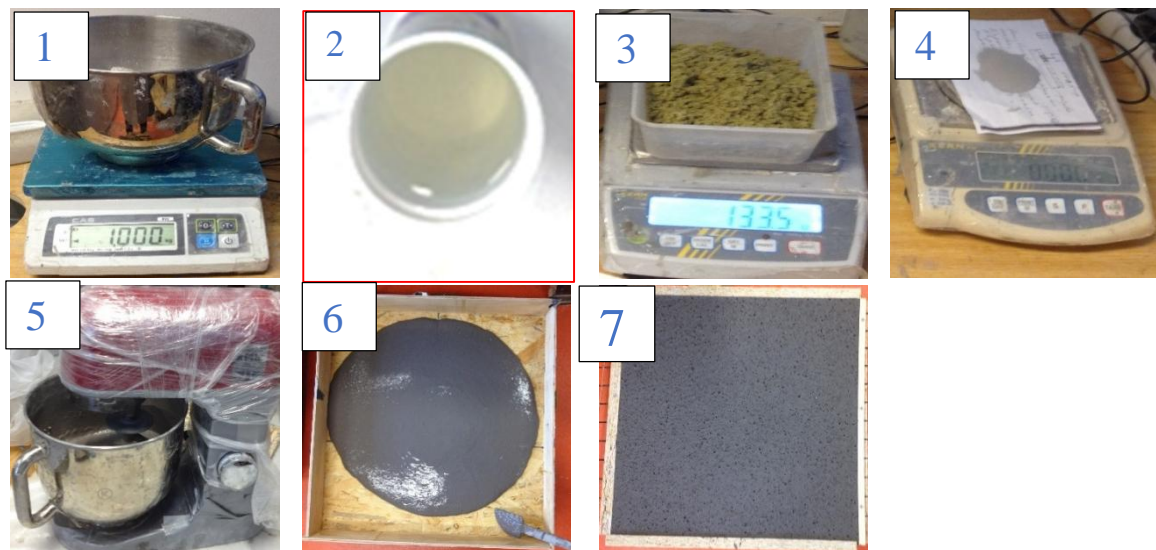
Figure 26. Processing of geopolymer mortar by Le Van Su

2. Coating the GF by spraying

The thesis author has coated the GF on base materials such as wood, steel, textile, concrete and polystyrene by direct spraying.

2.1 *Preparation of geopolymer mixtures*

The geopolymer mixing procedure is mentioned in subsection 2.1. Materials and equipment for preparing a geopolymer mixture are shown in Figure 27.

Figure 27. Materials and equipment for preparing a geopolymer mixture.

2.2 *Basic technical parameters of the spray gun*

Spray gun volume: 6 litres (Figure 28 left); airflow: 220 to 250 litres/min; required air pressure: 2 to 3 bar; unique holes for a chip size change (Figure 28 right). Recommendations for use: The maximum grain size of the components in geopolymer mortar is less or equal than 6 mm.

Figure 28. Reservoir spray gun with 6 litres volume (left) and sample nozzle size (right).

2.3 *Geopolymer protective layer*

The volume of the geopolymer mixture is determined by the surface area on which the surface protection layer will be applied (Figure 29). After securing the required amount, the geopolymer mixture settles into the reservoir of the spray gun and the size of the nozzle is selected (Figure 28 left).

Figure 29. Images illustrating the process of spraying geopolymer mixture and representation of unmodified surface (OSB panel) in the left and coated surface by GF (right).

3. Characterizations and testing

In this section, the apparent density, compressive and flexural strengths of a GF were measured. The analytical methods are discussed in detail in separate parts or the articles of the thesis author.

3.1 *Determination of the apparent density of geopolymer materials*

Apparent density of geopolymer materials was measured according to standard ČSN EN 1936 [173]. The following equation calculated apparent density:

$$Apparent\ density = \frac{Mass}{Volume} \tag{1}$$

where:

Apparent density of geopolymer material (kg/m^3),

Mass is the mass of the specimen (kg),

Volume is the volume of the specimen (m^3).

3.2 *Mechanical testing of GF*

A hydraulic press was used to measure the compressive and flexural strengths of a GF. The mechanical testing was conducted with a load cell of 10 kN at ambient temperature about 22 ± 3 °C using a universal testing machine INSTRON (Model 4202) (Figure 30). The mean strength of the GF was measured from three specimens.

Flexural strength was calculated from a three-point bending test on the samples of size 40 mm × 40 mm × 160 mm [174, 175]. The flexural tests are conducted with a crosshead speed of 2.0 mm/min and a span length of 120 mm. Three cubes of 40 mm were cut from the test bar, and they were used for compressive strength testing.
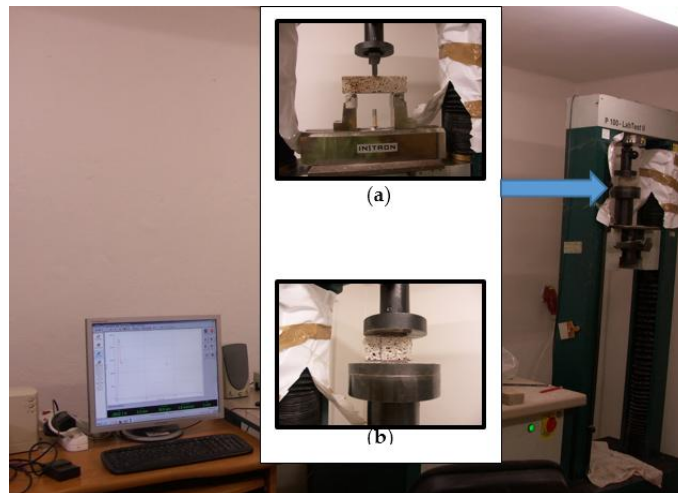
Figure 30. Universal testing machine INSTRON (Model 4202): a) set-up for flexural test b) set-up for compressive test.

3.3 *Thermal conductivity of geopolymer materials*

The measurement of the coefficient of thermal conductivity of geopolymer materials was performed on cubic samples with dimensions of 40 mm x 160 mm x 160 mm according to the ČSN EN 72 1105 standard using the ISOMET instrument. The coefficient of thermal conductivity λ [W/m. K] is a material parameter depending on physical and mechanical properties on the material. A material with a small λ is understood to be an excellent thermal insulator, whereas a material with a large λ is an excellent heat conductor.

3.4 *Scanning electron microscopy*

Electron microscopes have been widely used to analyze microstructures of geophysics due to their high resolution. In this thesis, a scanning electron microscope (SEM) Carl Zeiss Ultra Plus (Germany) was used to investigate microstructural morphology, pore analysis, and chemical composition of samples (Figure 31).

Figure 31. Carl Zeiss Ultra Plus SEM with Oxford micro-analytical system.

3.5 *Fire-resistant testing of geopolymer materials*

The testing of fire resistance for geopolymer materials was conducted at the TUL by the thesis author and team members from October 2015 to September 2019. Experimental results were measured by different size samples using two types of furnaces. The 2-D size for a test piece is 300 mm x 300 mm (Figure 32a) or 500 mm x 500 mm (Figure 32b) [101]. The test furnace was heated by a system of natural gas and regulated according to the relevant parts of the standard ISO 834 with furnace temperature showing in the following equation:

$$T/°C = 345 \log_{10}(8t/min + 1) + 20 \quad , \tag{3}$$

where T (°C) is the standard required furnace temperature at time t (min).

The thermocouples are mounted in the furnace and connected to the computer by the ADAM 4000 Series (Figure 32c, d).
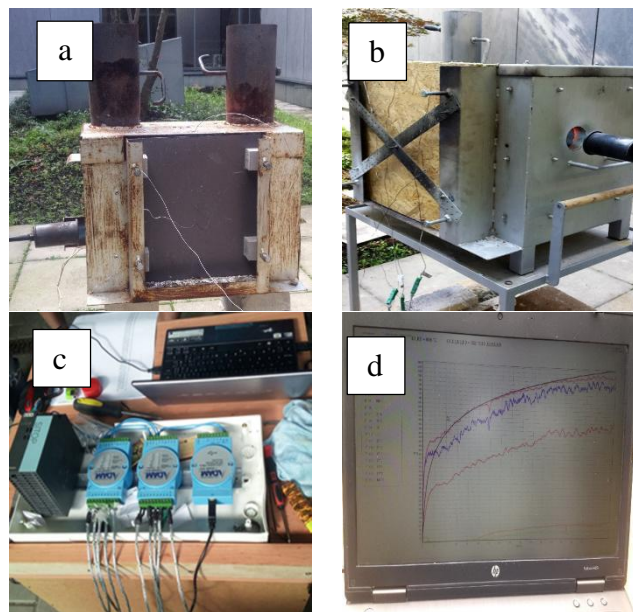
Figure 32. (a) Small furnace; (b) Big furnace; (c) ADAM 4000 series; (d) Results on laptop.

4. Other devices

The following devices were used during the experiments:

- Digital scale

Range 0 – 0.2 kg, accuracy 0.001 g Use for weighing small quantities that require high precision, such as bubble glass or fiber.

Range 0 – 5 kg, accuracy 1 g (0 – 2.5 kg) or 2 g (2.5 - 5 kg); It is used to measure raw materials such as sand, cement and gravel.

Range 0 – 25 kg, accuracy 1 g Use a scale of massive raw materials.

- Mixer Heidolph RZR 2020

Speed 35 up to 2200 per minute, powder 18 W and torque 1 Nm;

- Vibrating High-Frequency Table VSB 15

Area of bearing 250×250 mm^2, 11500 rpm, timer;

- The drying oven Binder can be used to dry specimens under test conditions with the temperature up to 300°C. The machine can schedule and automatically turn off according to the desired time.
- The furnace Binder can heat up to 1200°C;

Figure 33. Furnace BINDER (left) and GFs in the furnace at 1100 °C (right).

5. Raw materials

The raw materials used in the experiments were shown in the author's papers A to F. The following briefly describes them:

The industrially commercial material BAUCIS lk (České Lupkové Závody, a.s, Czech Republic) was a two-component aluminosilicate binder based on metakaolin and activator by potassium alkaline solution [176].

Table 1. The chemical composition of BAUCIS lk was determined by XRD.

Formula	SiO$_2$	Al$_2$O$_3$	CaO	MgO	TiO$_2$	Fe$_2$O$_3$	K$_2$O	SO$_3$	MnO	Na$_2$O	LOI
Concentration (%)	44.5	28.9	17.6	2.23	1.31	0.82	0.75	0.46	0.28	0.25	2.56

An aluminum powder (pkchemie Inc., Czech Republic) was used to create pores inside the GF. It has an aluminum content of 99 %, and the average grain size was 65 μm [177]. The chemical composition and particle size of the aluminum powder are shown in Table 2.

Table 2. The chemical composition and size of the aluminum powder.

Name	Diameter	Al	FeO	SiO	Cu
D50	65μm	98%	0.35%	0.4%	0.02%

The silica fume (produced by Kema Morava – sanační centrum a. s., Republic of Slovenia) contained 90 % SiO$_2$, and the average grain size was 1 mm [178].

Table 3. Chemical composition of silica fume as determined by XRD.

Formula	SiO$_2$	Cr$_2$O$_3$	K$_2$O	Al$_2$O$_3$	MgO	CaO	Fe$_2$O$_3$	SO$_3$	Na$_2$O	BaO	LOI
Concentration (%)	84,8	2.53	2.01	1.56	1.52	1.09	1.09	0.93	0.369	0.1	3.68

Sand (produced by Sklopísek Střeleč a.s., type ST 03-08) was used with a grain size from 0.3 to 0.8 mm [179].

Table 4. Chemical composition of sand as determined by XRD.

Formula	SiO$_2$	Al$_2$O$_3$	Other	LOI
Concentration (%)	99.4	0.35	0.25	0.07

Two types of basalt fiber, chopped basalt fiber and a waste ground basalt fiber made from recycled material, were produced by Basaltex a.s. (Figure 34 and Figure 35). The basalt fiber had a density of 2900 kg·m^{-3} and thermal conductivity of 0.027 ÷ 0.033 W/m.K [149].

Table 5. Chemical composition of chopped basalt fiber [180].

Formula	SiO$_2$	Al$_2$O$_3$	Fe$_2$O$_3$	CaO	MgO	Na$_2$O	K$_2$O	P$_2$O$_5$	MnO	Cr$_2$O$_3$	other
Concentration (%)	52.8	17.5	10.3	8.59	4.63	3.34	1.46	1.38	0.28	0.16	0.06

Table 6. Chemical composition of waste ground basalt fiber as determined by XRD.

Formula	SiO$_2$	CaO	Al$_2$O$_3$	MgO	Fe$_2$O$_3$	TiO$_2$	Na$_2$O	K$_2$O	MnO	SO$_3$	P$_2$O$_5$	LOI
Concentration (%)	33.6	26.1	14.4	8.26	6.61	1.98	1.38	1.21	0.0.76	0.29	0.14	2.05

Figure 34. The photographs showing original basalt waster fibers (left) and modified basal waste fibers after grinding (right).
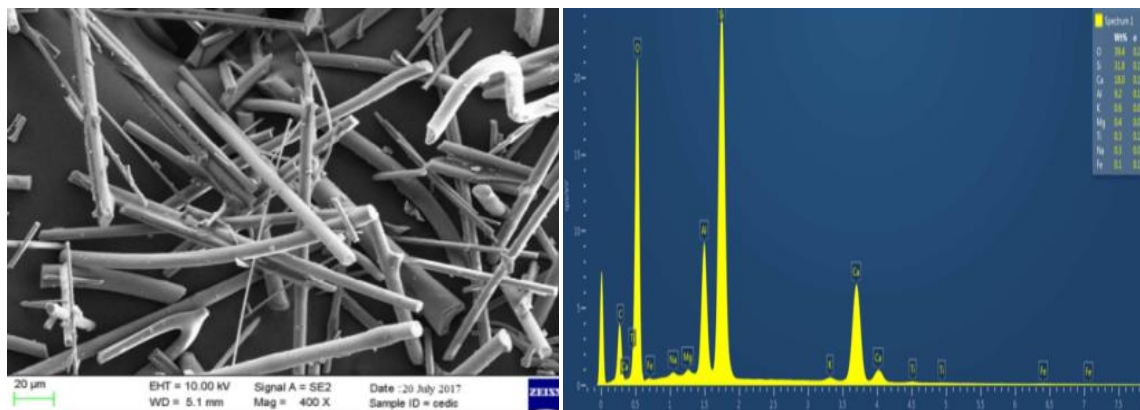
Figure 35. SEM micrograph and corresponding EDX energy spectrum of modified waste basalt fiber after grinding.

Chapter 3. FIRE-RESISTANT TEST AT TUL

The research results of fire-resistance presented in this chapter are directly related to the thesis topic. The fire-resistant test was conducted with the conditions at the TUL.

1. GFs for passive fire resistance of the wooden structural panels

This work aims at designing and evaluating the performance under thermal loading of the GF for passive fire protection of the OSB panels. Fire-resistant testing was conducted on the Oriented Strand Board (OSB) panels 500 mm ×500 mm × 22 mm with a fire exposure region of 300 mm × 300 mm by the flame of a gas burner into a furnace. The test was performed at the age of 21 days after the production of the specimens. The results showed that the fire-resistant period of treated OSB panels coated with a GF layer varied from 40 to 100 min compared to just 20 min of untreated OSB panels in the same testing condition.

1.1 *Materials and method*

Geopolymer is inorganic material as used a binder. Aluminum powder with a particle size of 65 µm and a purity of 99.5% was used for foaming. Siliceous sand with the particle size in the range of 0-0.6 mm and waste basalt fiber were used as reinforcements. A Geopolymer mortar was prepared in three steps. Firstly, geopolymer paste was created as a two-component system by mechanical mixing metakaolin with alkaline potassium solution in a liquid-to-solid weight ratio of 0.9 for around 5 min. Secondly, siliceous sand and waste basalt fiber were added into the pasta mixture. Then the mixture was mechanically stirred for 5 min. Finally, the aluminum powder was added into the geopolymer mortar mixture, and the mixture was mechanically stirred for a further 30 s. After mixing, the geopolymer mortar mixture was immediately poured on the surface of the OSB panel. It was laminated to create a GF layer with a given thickness (Figure 36). Five samples of the GF with different thickness layers before testing are shown in Table 7.

Figure 36. Materials and sample preparation steps to create a GF layer on the surface of the OSB panels.

The samples were exposed to fire at the age of 21 days after casting. A custom designed furnace was used for fire testing. OSB panels 500 mm × 500 mm × 22 mm with different thickness layers of GF on the OSB substrates were used for the fire testing. The fire exposure region of the specimens was 300 mm × 300 mm. Figure 37 shows the sample arrangement for the fire-resistant test.
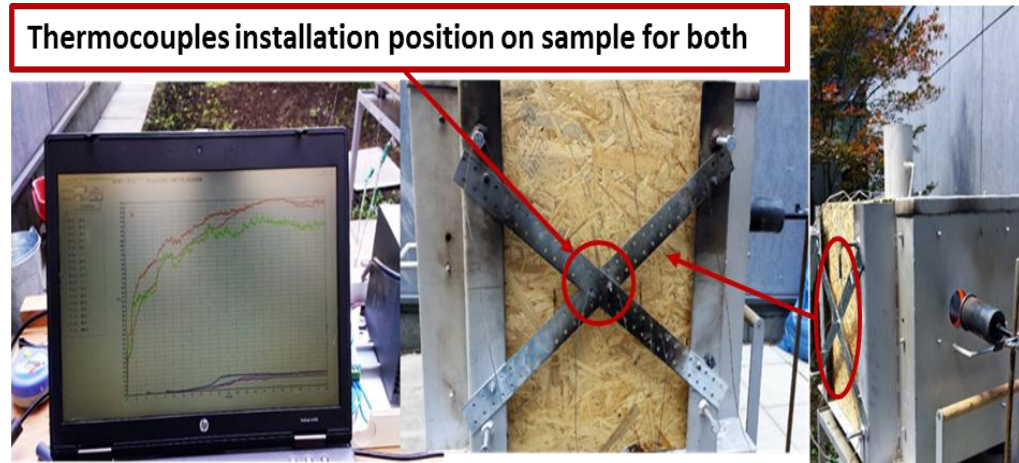
Figure 37. Photographs showing the sample arrangement for the fire-resistant test.

OSB panel without a GF layer (sample 1)   OSB panel with a GF layer (sample 3)
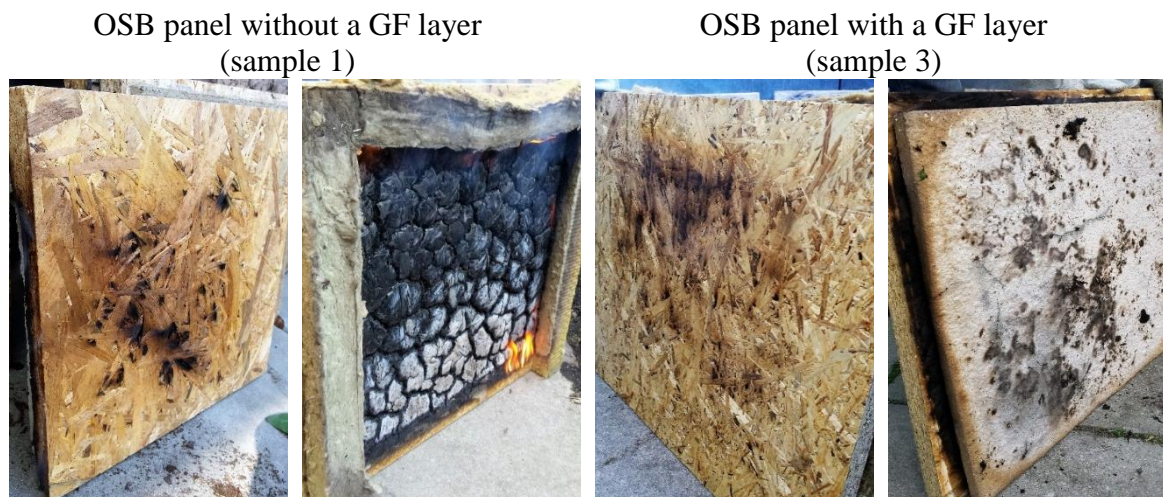
Figure 38. Images describing the OSB panels with and without a GF layer after testing.

Table 7. Mixture proportion of GF.

Samples [-]	Sand/binder [-]	Binder/liquid [-]	Basalt fiber/cement [%]	% wt. Al
No. 1	-	-	-	-
No. 2	1	0.9	30	0.25
No. 3	1	0.9	30	0.25
No. 4	-	0.9	60	2.5
No. 5	-	0.9	60	2.5

1.2 *Results and summary*

The fire-resistant curves of the samples are presented in Figure 39.
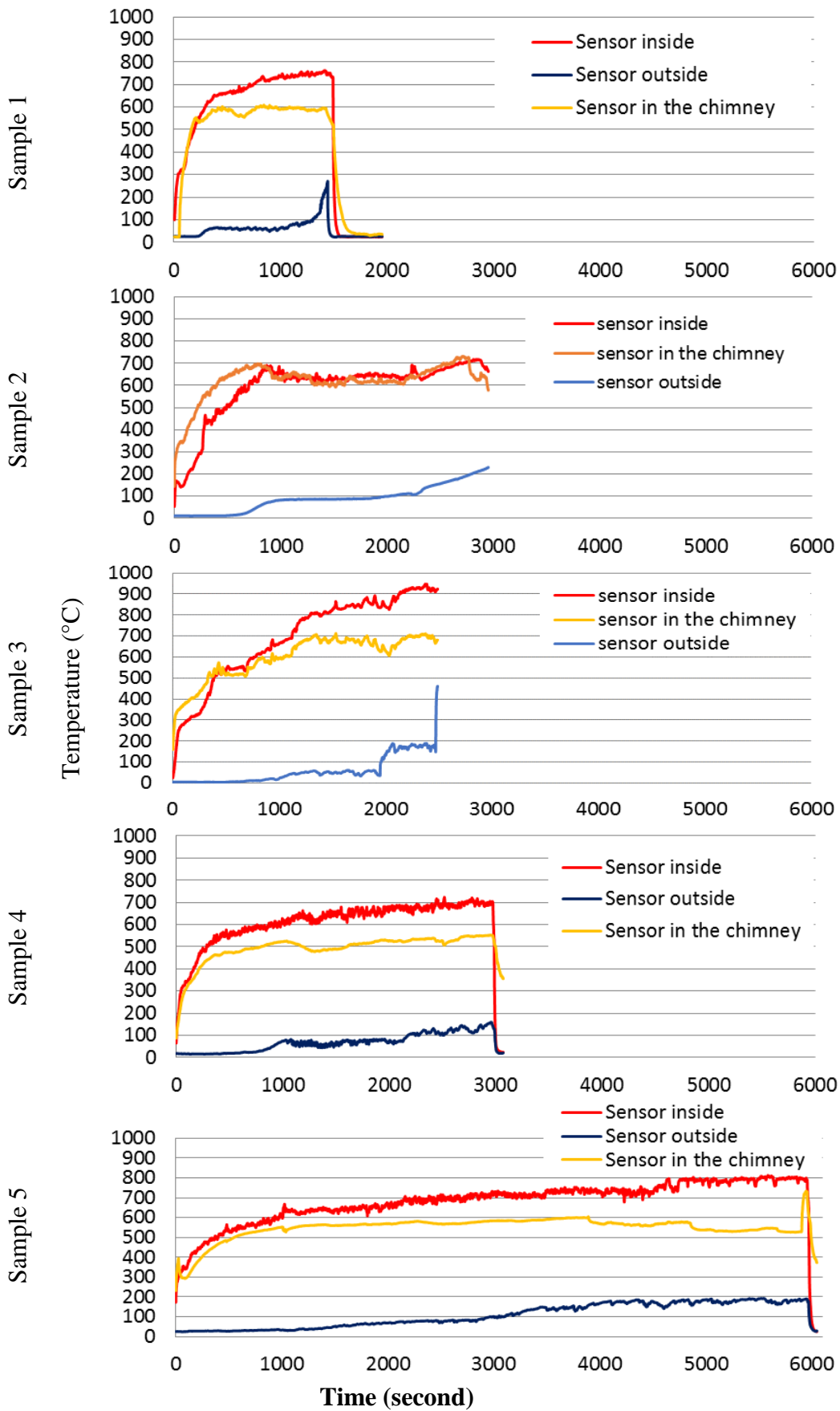
Figure 39. Evolution of the temperature versus time.

The results of the fire testing for the OSB panels with and without the GF layer in Figure 39 are described as follows:

- OSB panel without the GF layer had the fire-resistant time around 22 min;
- OSB panels with the GF layer could suffer the fire within 49 min for sample 2, 41 min for sample 3, 50 min for sample 4 and 99 min for sample 5;
- Sample 5 resisted the fire for the longest time. Its fire-resistant time was 4.5 times higher than that of the OSB panel without the GF layer. The maximal temperature in the furnace did not exceed 800 °C;
- Sample 2 and sample 4 had the same results. Their fire-resisted time was 2.3 times higher than the OSB panel without the GF layer. The temperature in the furnace did not exceed 700 °C during the test. However, the sample 4 was lighter than the sample 2.
- Sample 3 showed that its fire-resistant time was 1.9 times higher than that of sample 1, while the fire temperature in the furnace increased to 950 °C.

Experimental results confirmed that the geopolymer could be used for thermal insulation purposes, and it can be used as an excellent building material for fire-resistance.

2. GFs for passive fire resistance of the structural steel plates

This work aims at designing and evaluating the performance under thermal loading of GFs for passive fire protection of the steel plate. Two different thickness sizes of the GF layer were applied to the steel substrates. Fire testing was conducted on the steel plate 500 mm × 500 mm × 2 mm with a fire exposure region of 300 mm × 300 mm using natural gas.

2.1 *Materials and methods*

Materials and procedures were described in subsection 1.1. Table 8 presents the materials used to produce GFs.

Table 8. Materials used to produce GFs.

Samples [-]	Binder/liquid [-]	Basalt fiber/cement [wt. %]	Al [wt. %]
1	-	-	-
2	0.9	60	2.5
3	0.9	60	2.5
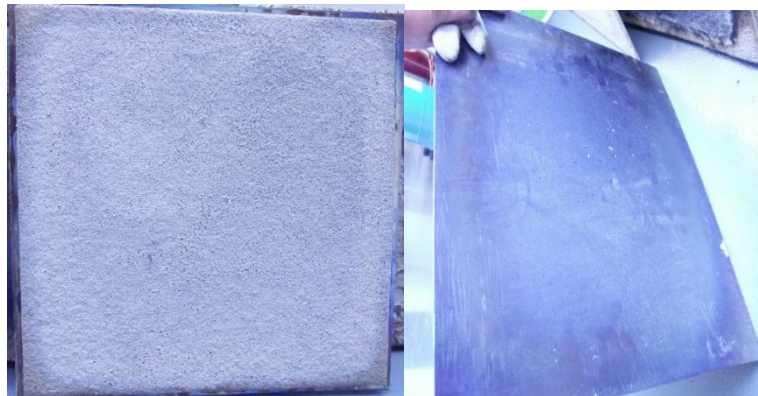
Figure 40. Images showing surfaces of the steel plate after the test (sample 2).

Figure 41. Pictures showing surfaces of the steel plate after the test (sample 3).

2.2 *Results and summary*
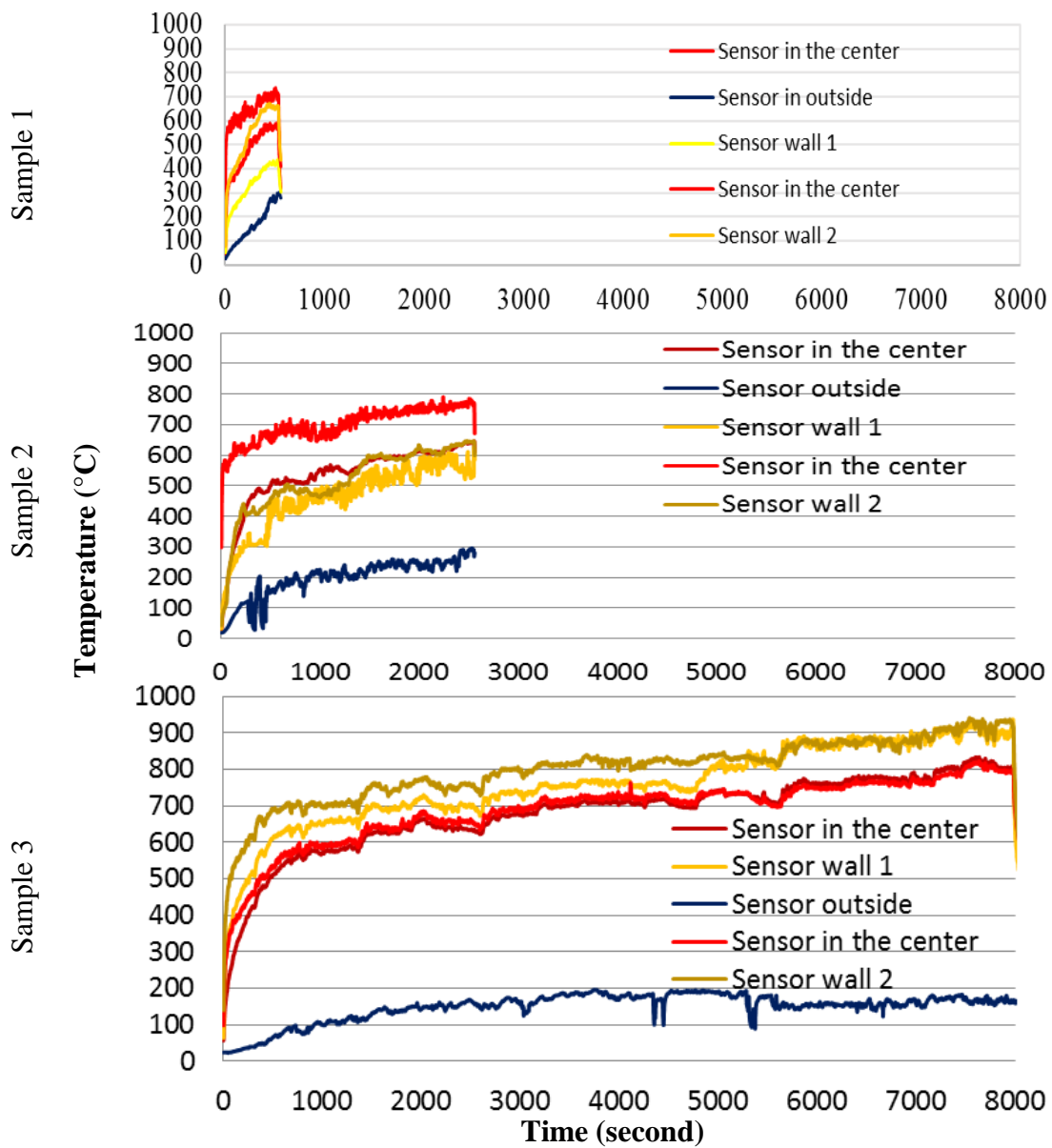
Figure 42. Evolution of the temperature versus time of the samples.

- The results showed that the fire-resistant time of the steel plate covered with the GF layer was 41 minutes for sample 2 and 134 minutes for sample 3. However, it was just 9 minutes for untreated steel panels in the same testing condition.
- Sample 3 resisted the fire at the longest time, and its fire-resisted time was 14.8 times higher than the steel plate without the GF layer. The maximal temperature in the furnace did not exceed 900°C (Figure 42).
- The fire-resistant time of sample 2 was 4.6 times higher than that of sample 1. The temperature in the furnace increased to 800 °C (Figure 42).

3. Evaluation of fire-resistance for concrete slabs

3.1 *Description of the problem*

The evaluation of the fire-resistance for the concrete slab was performed through test specimens covered with and without a GF layer. The GF layers with the thickness changing from 10 mm to 50 mm were applied to the concrete slab as a treated surface layer. The samples were fixed in a furnace and gradually heated to 1000 °C. Results obtained from the fire-resistant test for the concrete slab with and without the GF layer are given below.

3.2 *Experiment*

Table 9 presents the mixing ratio for concrete samples.

Table 9. Mixing ratio for concrete samples.

Sample	Sand /cement	Cement/activator	Basalt fiber/cement	Aluminum powder [%]
1	-	-	-	-
2	-	0.9	0.3	1.5
3	-	0.9	0.3	1.5
4	2	0.9	0.01	-
5	-	0.9	0.5	1.5

Description of samples:

Sample 1 – uncoated concrete slab with dimensions of 300 mm x 300 mm x 25 mm;

Sample 2 - 1.5% Al, 30% basalt-fiber waste, sand-free, the GF layer thickness of 11 mm;

Sample 3 - 1.5% Al, 30% basalt-fiber waste, sand-free, the GF layer thickness of 22 mm;

Sample 4 - 0% Al, 1% basalt fibers with a length of 3.2 mm, 200% sand, the GF layer thickness of 21 mm;

Sample 5 - 1.5% Al, 50% basalt-fiber waste, sand-free, the GF layer thickness of 50 mm.

The preparation of fillers for the mixture is shown in Figure 43. Test specimens with the GF layer are presented in Figure 44.

Figure 43. Preparation of fillers for the mixture.
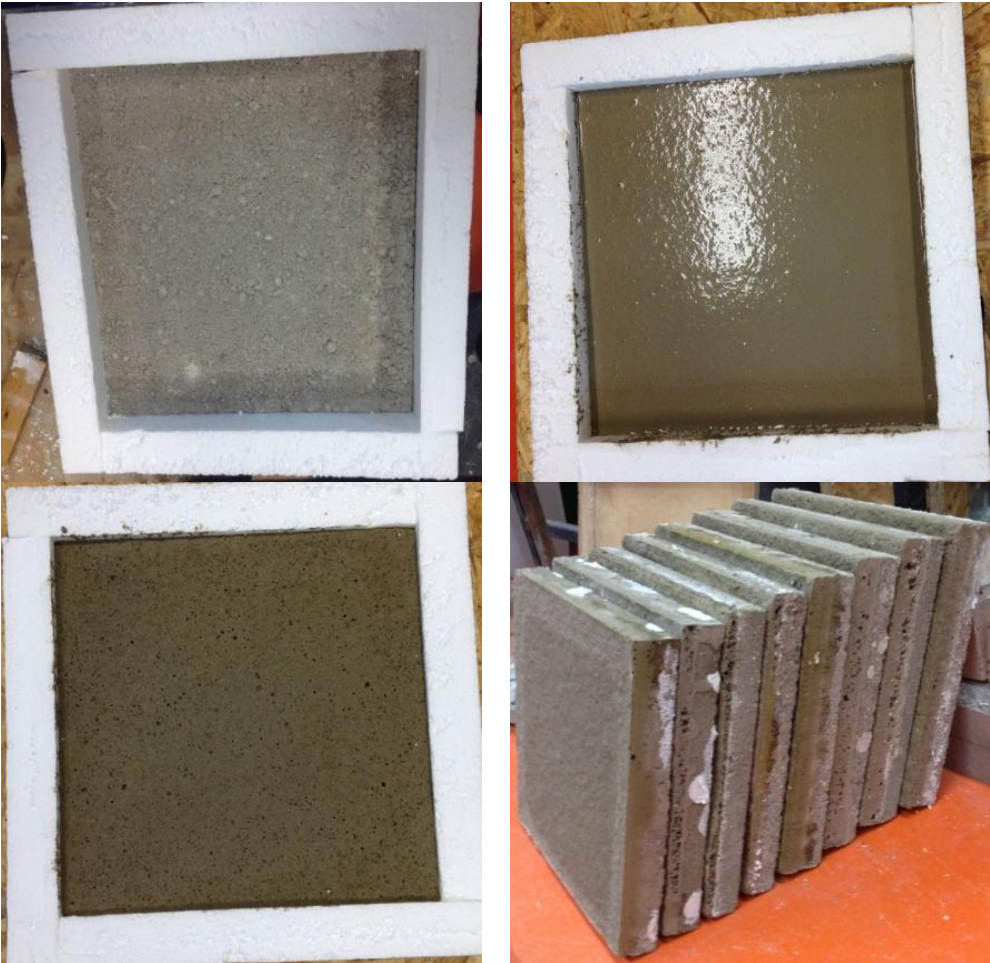
Figure 44. Test specimens with the GF layer.
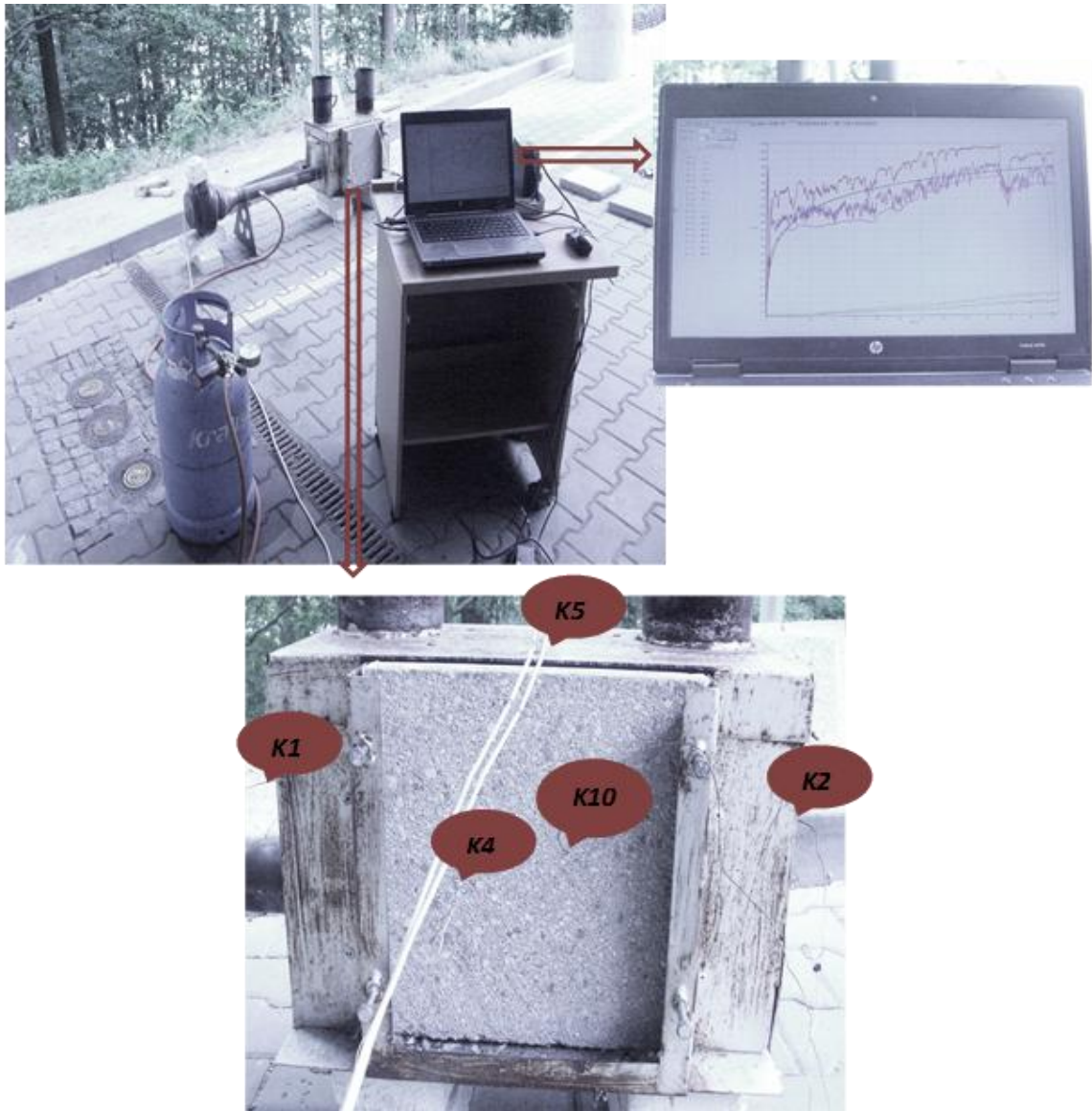
Figure 45. Layout of measuring equipment.

Note: Thermocouples *K1*, *K2*, and *K5* are located inside the furnace, whereas thermocouples K4 and K10 are located on the outside of the slab under investigation.

3.3 *Measured results*

The equipment shown in Figure 45 is prepared for the fire-resistant test of the samples. The temperatures outside and inside the concrete slab were measured using the thermocouples (Figure 45). Moreover, the temperature on the outside of the concrete slab after testing was measured using a thermal camera (model C. A1950). The fire-resistant test was interrupted when the outside temperature of the concrete slab reached 250 °C.
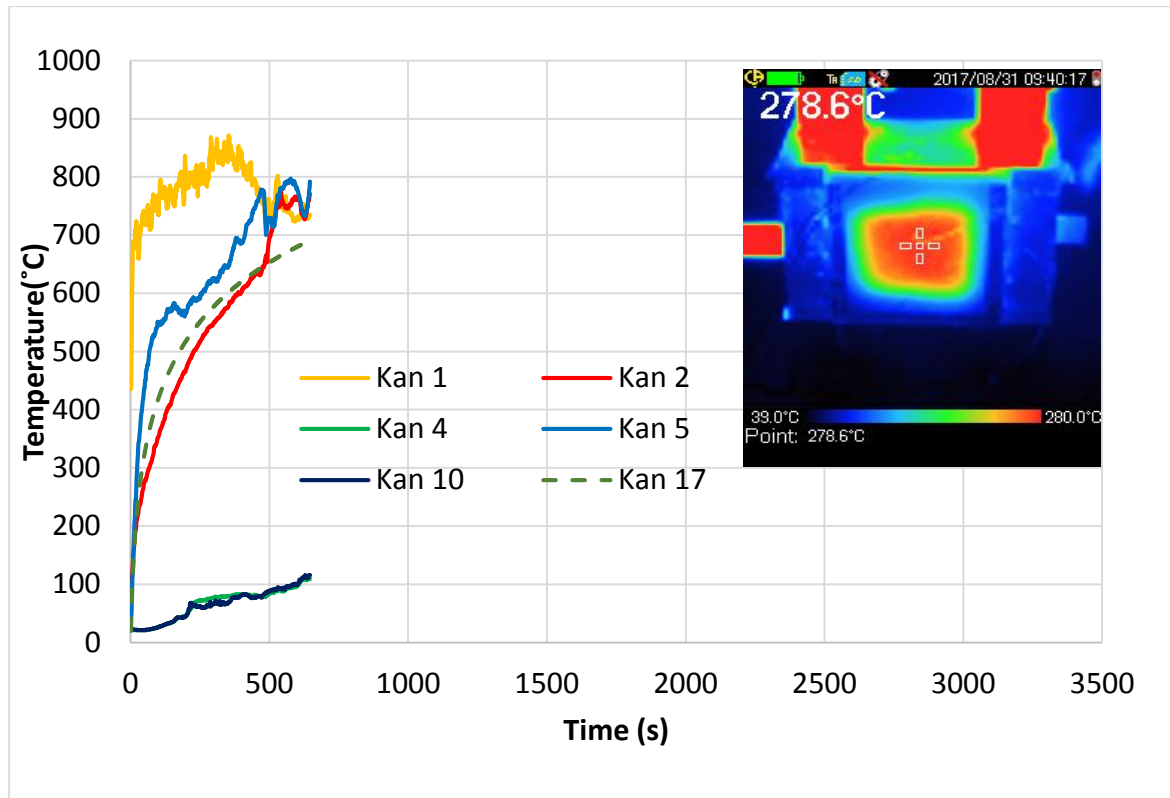
Figure 46. The temperature changes of thermocouples over time of uncoated concrete slab with dimensions of 300 mm x 300 mm x 25 mm. An inserted image showing the temperature of the thermal camera.

The surface was affected by the fire   Outer surface

Figure 47. The inner and outer surfaces of sample 1 after fire testing.
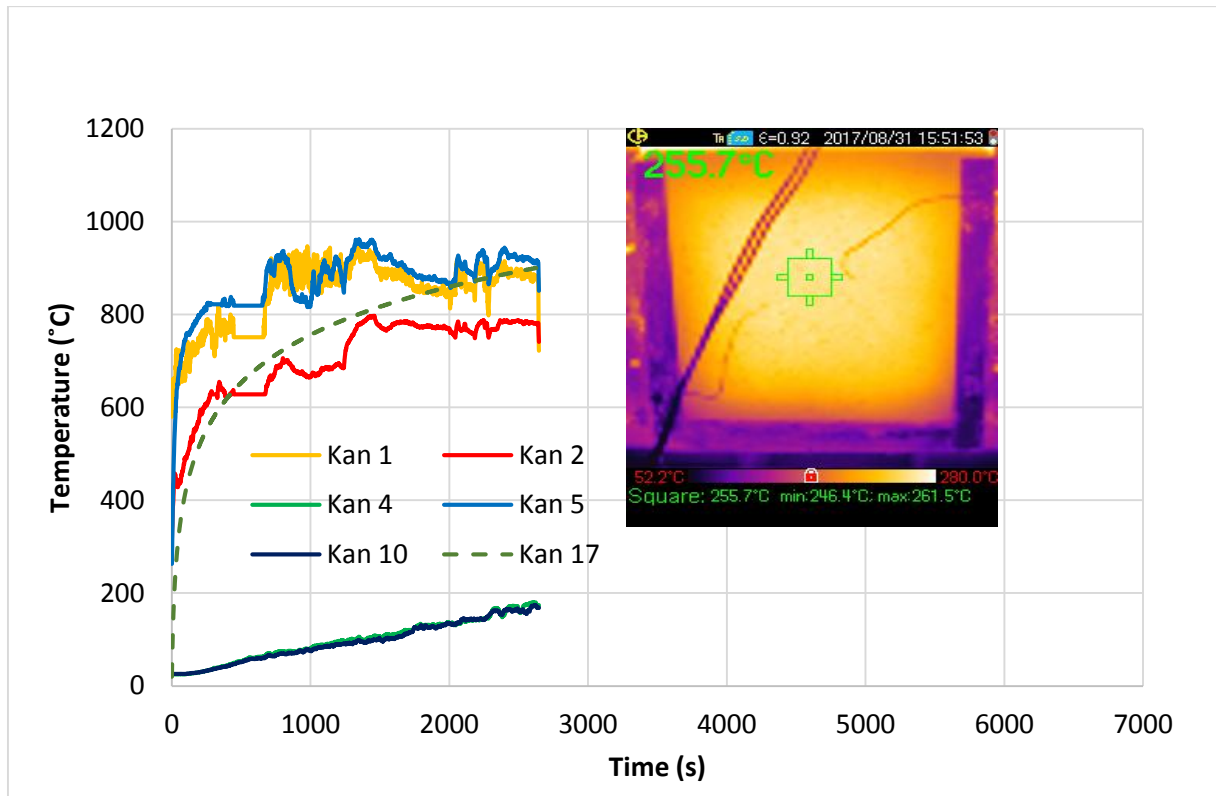
Figure 48. Sample 2, the temperature changes of thermocouples over time of concrete slabs covered by a protective GF with a thickness of 11 mm. An inserted image showing the temperature of the thermal camera.
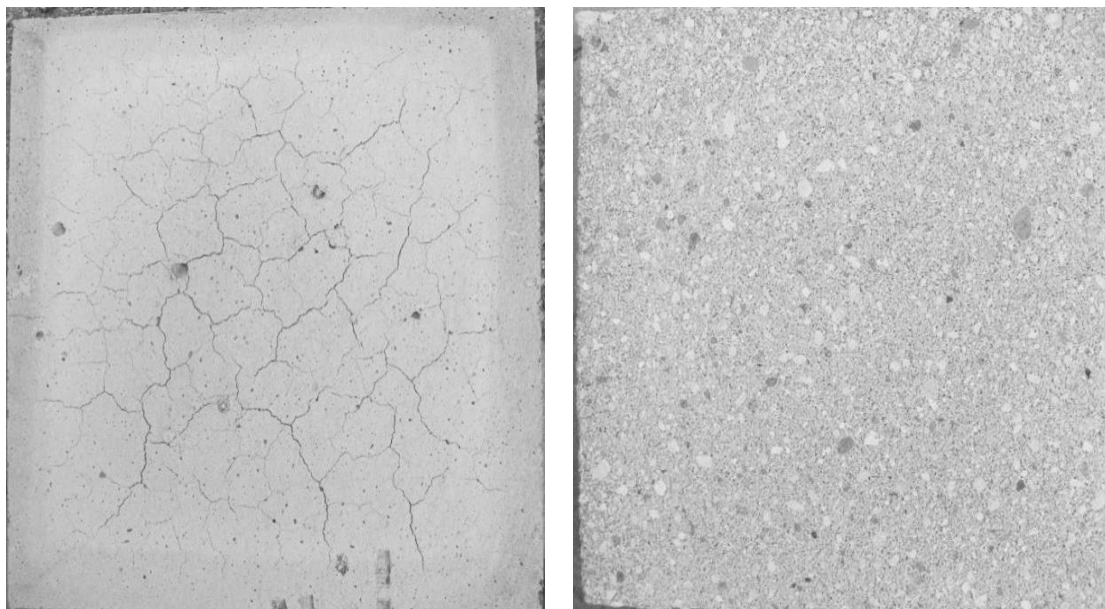
The surface was affected by the fire   Outer surface

Figure 49. The inner and outer surfaces of sample 2 after testing.
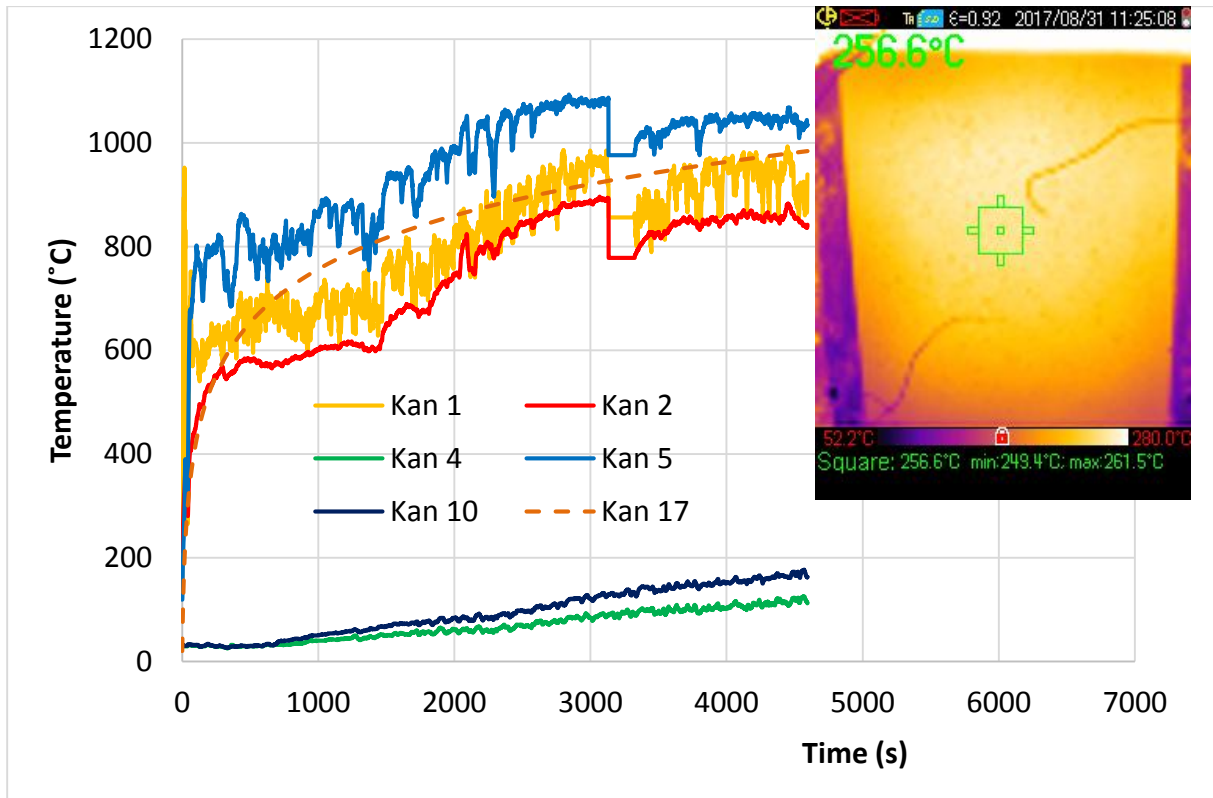
Figure 50. Sample 3, the temperature changes of thermocouples over time of concrete slabs covered by a protective GF with a thickness of 22 mm. An inserted image showing the temperature of the thermal camera.

The surface was affected by the fire   Outside surface

Figure 51. Sample 3, the inner and outer surfaces of the sample subjected to flame after finishing.
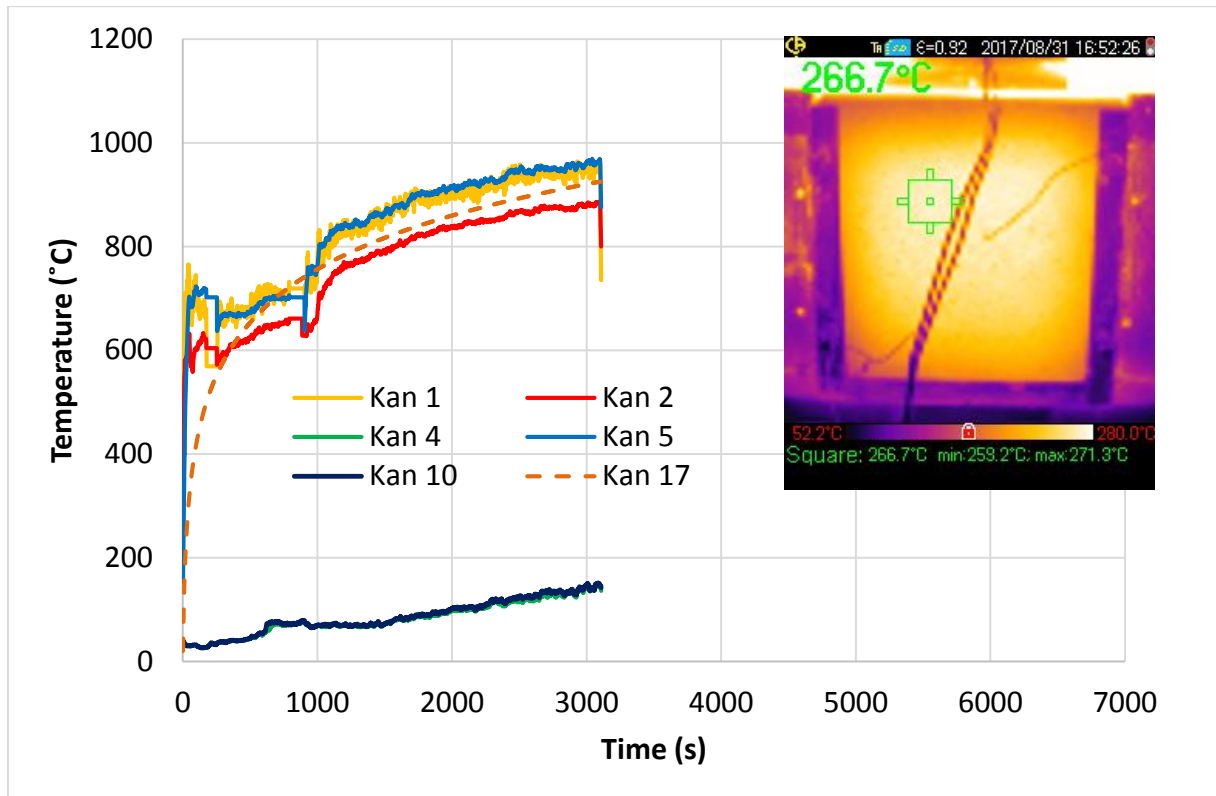
Figure 52. Sample 4, the temperature changes of thermocouples over time of concrete slabs covered by a protective GF with a thickness of 21 mm. An inserted image showing the temperature of the thermal camera.
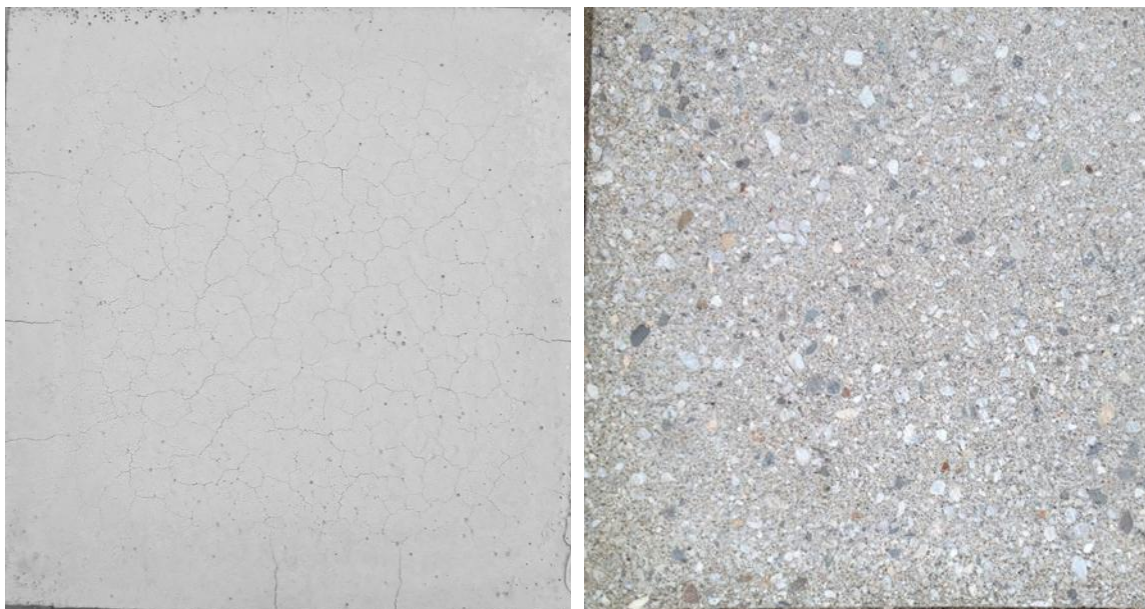
The surface was affected by the fire	Outer surface

Figure 53. Sample 4, the inner and outer surfaces of the sample subjected to flame after testing.
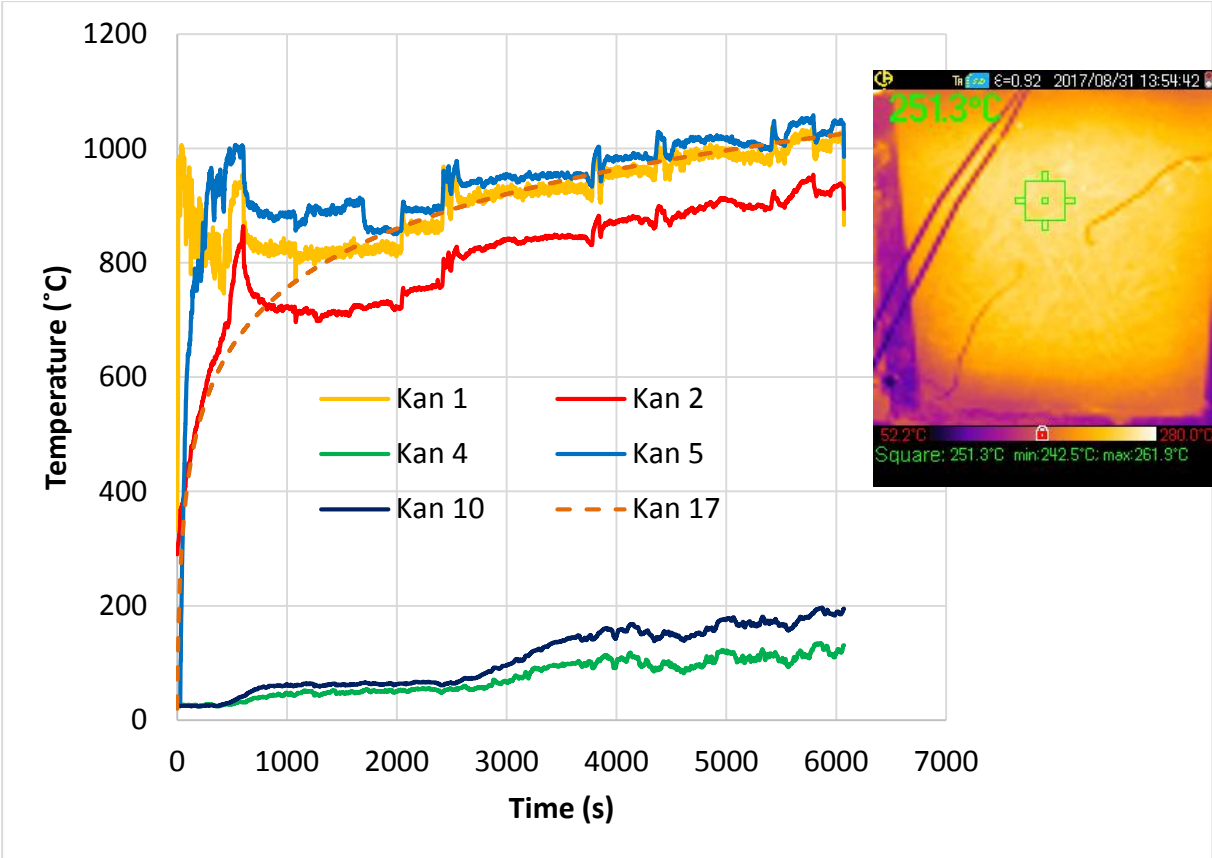
Figure 54. Sample 5, the temperature changes of thermocouples over time of concrete slabs covered by a protective GF with a thickness of 50 mm. An inserted image showing the temperature of the thermal camera.
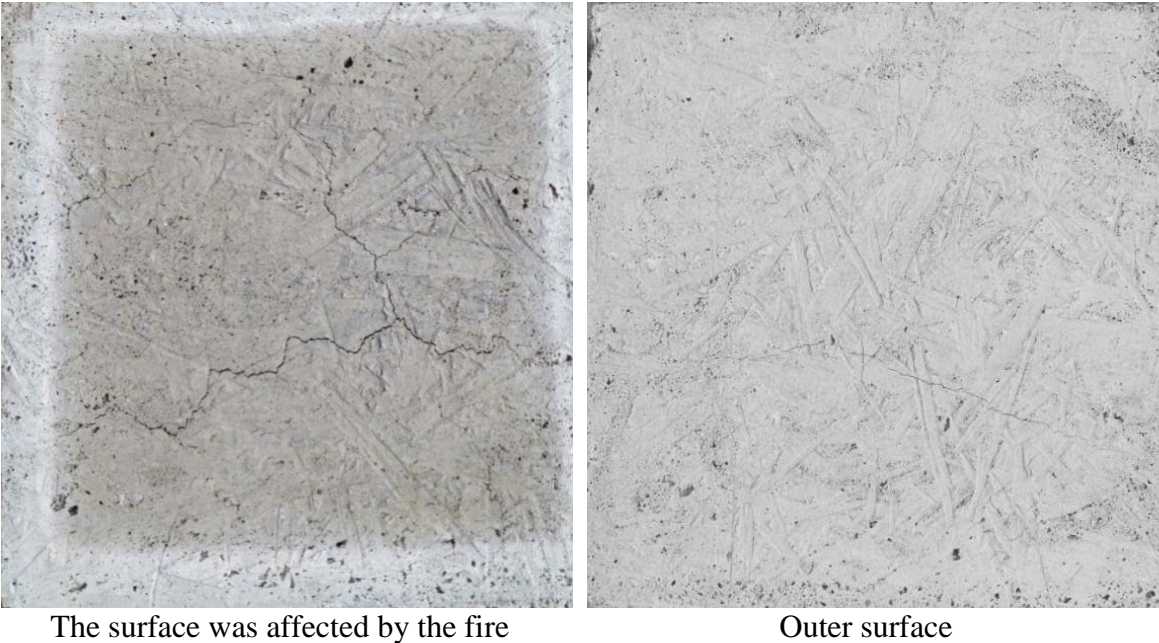
The surface was affected by the fire   Outer surface

Figure 55. Sample 5, the inner and outer surfaces of the sample subjected to flame after testing.

3.4 *Summary*

- The uncoated concrete slab had a fire-resistant time of 653 seconds (Figure 49).
- The application of a GF layer with a thickness of 11 mm led to an increase in the fire resistance several times. The fire-resistant time of the examined slab covered with an 11 mm GF layer was 2672 seconds (Figure 51).
- For the GF layer with a thickness of 22 mm, the fire-resistant time increased significantly and reached 4658 seconds (Figure 53).
- Using the GF layer with a thickness of 50 mm resulted in an increase in the fire-resistant time to 6000 seconds (Figure 57).

4. Evaluation of fire-resistance for polystyrene boards

4.1 *Description of the problem*

The improvement of the fire-resistance for the polystyrene board was performed through test specimens covered with and without a GF layer. The GF layer with a thickness of 10 mm with a different mixture, was applied to the polystyrene board as a treated surface layer. The samples were mounted in a furnace and gradually heated to 800 °C. The achieved fire-resistance results are given below.

4.2 *Experiment*

Firstly, geopolymer paste was mixed as a two-component system using metakaolin and alkaline potassium solution by mechanical stirring for around 5 min. Secondly, siliceous sand and waste basalt fiber were added into the pasta mixture. Then the mixture was stirred for 5 min. Finally, the aluminum powder was added into the geopolymer mortar mixture and then it was stirred continuously for further 30 seconds (Figure 56). After mixing, the slurry was evenly applied on polystyrene boards in 10 mm thickness of the GF coating (Figure 57).

Figure 56. Preparation of constituent materials for the GF production.

Figure 57. Test specimen with a GF layer.

Preparation of GF:

The mixing ratio of GF by weight for polystyrene boards is presented in Table 10.

Table 10. The mixing ratio of GF by weight for polystyrene boards.

Sample	Activator/ cement	Basalt fibers/ cement	Aluminum powder/ cement	Note:
1	0.8	0.03	0.015	Long basalt fiber
2	0.9	0.03	0.015	Long basalt fiber
3	0.9	0.3	0.015	Fine fiber

4.3 *Measured results*

The equipment shown in Figure 58 is prepared for the fire-resistant test of the samples. The temperatures outside and inside polystyrene boards were measured using the thermocouples (Figure 58 right). The test ends if the destruction of the polystyrene board can be visible to the naked eye.

Figure 58. Layout of measuring equipment.

The following graphs show the course of the experiment for the examined samples.
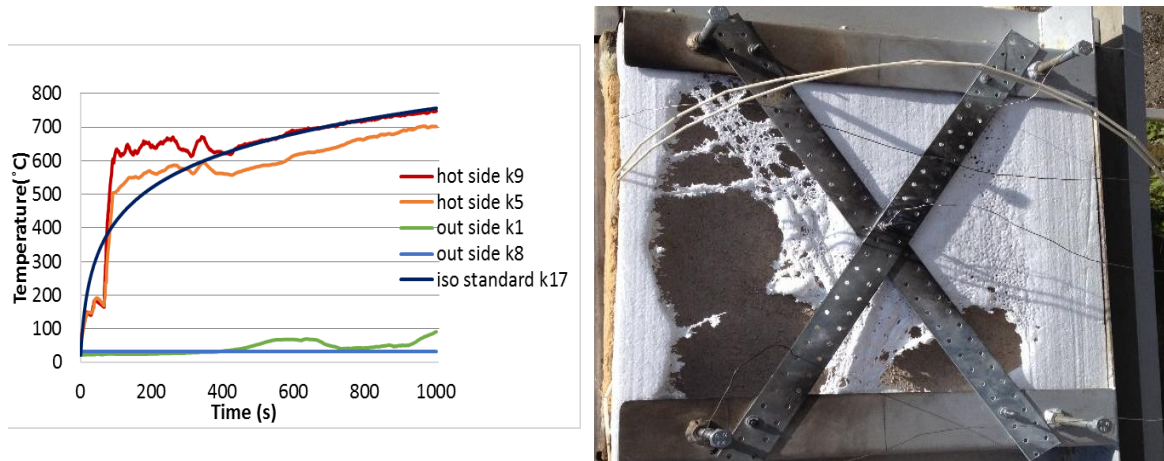
Figure 59. Fire-resistance curves (left) and the outer surface of sample 1 after testing (right).
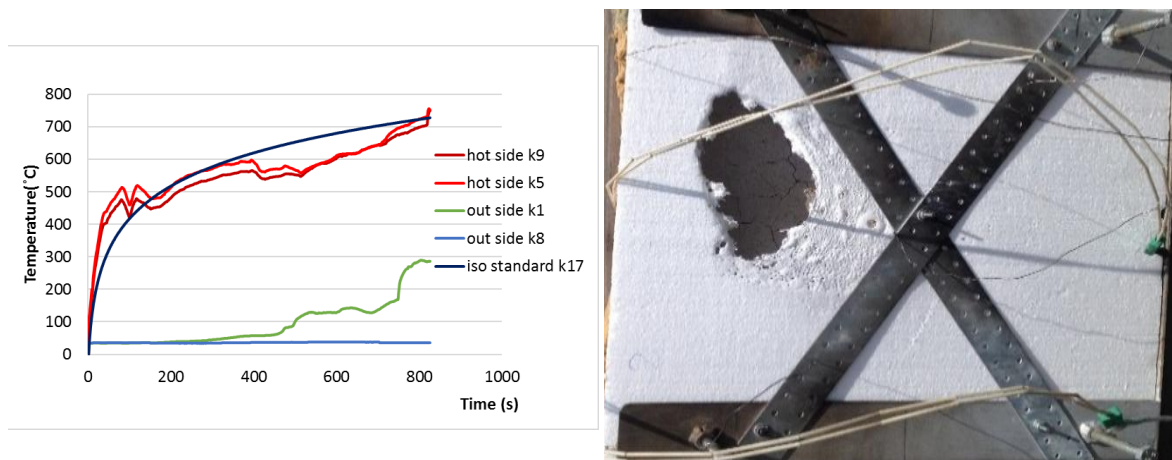
Figure 60. Fire-resistance curves (left) and the outer surface of sample 2 after testing (right).
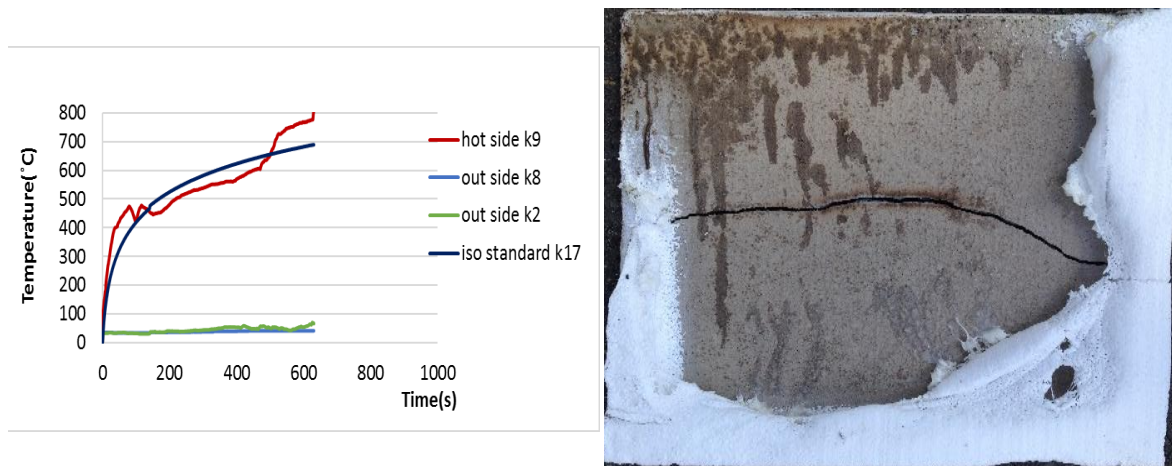
Figure 61. Fire-resistance curves (left) and the outer surface of sample 3 after testing (right).

4.4 *Summary*

The polystyrene boards showed the fire-resistant time ranging from 10 to 15 min (Figures 59-61). The GF layers under high temperatures improved significantly the fire-resistance period of polystyrene boards.

The results showed that the fire-resistance periods of treated polystyrene boards with a GF layer were 800 seconds for sample 2 and 600 seconds for sample 3, while the untreated polystyrene board in the same testing conditions destroyed instantaneously by the fire.

5. Evaluation of fire-resistance for aluminum plates

5.1 *Description of the problem*

The evaluation of the fire-resistance for the aluminum plate was performed using test specimens coated with and without the GF layer. The GF layers with a thickness of 11 mm and 20 mm were applied to the aluminum plate. The samples with and without the GF layer were fixed in the furnace and then were gradually heated to 800 °C. Results obtained from the fire-resistant test are given below.

5.2 *Experiment*

Materials and procedures were described in subsection 4.2. Table 11 presents the mixing ratio for aluminum samples.

Table 11. Mixing ratio for aluminum samples.

Sample	Cement/ activator	Basalt fiber/ cement	Aluminum powder [%]
1	-	-	-
2	0.9	0.4	1.5
3	0.9	0.4	1.5

Description of samples:

Sample 1 – uncoated aluminum plate with dimensions of 300 mm × 300 mm × 2.5 mm;

Sample 2 - 1.5% Al, 40% basalt-fiber waste, sand-free, the GF layer thickness of 11 mm;

Sample 3 - 1.5% Al, 40% basalt-fiber waste, sand-free, the GF layer thickness of 20 mm.

* Testing was interrupted when the outside temperature of the aluminum plate reached 210 °C [16].

The preparation of fillers for the GF mixture is shown in Figure 62.

The prepared aluminum plates were shown in Figure 63. In the next step, a geopolymer mixture was applied to the surface of the aluminum plate (Figure 64). The uncoated and coated with a GF layer samples are shown in Figure 65. Figure 66 shows the image layout on the test furnace.

Figure 62. Preparation of fillers for the mixture (left) and fillers for the mixture (right).

Figure 63. Both surfaces of an aluminum plate: original (left) and grinding (right).

Figure 64. Preparation of geopolymer mixture and its application on the surface of Al plates.

Figure 65. A photograph showing uncoated Al plate (left) and coated Al plates with 10 mm thickness of GF layer (middle) and 20 mm thickness of GF layer (right).

Figure 66. An image showing the sample layout on the test furnace.

*Note***:** Thermocouples Kan 1, Kan 2, and Kan 5 were located inside the furnace, whereas thermocouples Kan 4 and Kan 10 were located on the outside of the aluminum plate under investigation. A thermocouple labeled Kan 2 was attached to the burner and a thermocouple labeled Kan 5 was attached next to the burner.

5.3 *Measured results*

The equipment shown in Figure 66 is prepared for the fire-resistant test of the samples. The temperatures outside and inside the aluminum plate were measured using the thermocouples. Testing was interrupted when the outside temperature of the aluminum plate reached 200 °C.

Results of sample 1 are presented in Figure 67
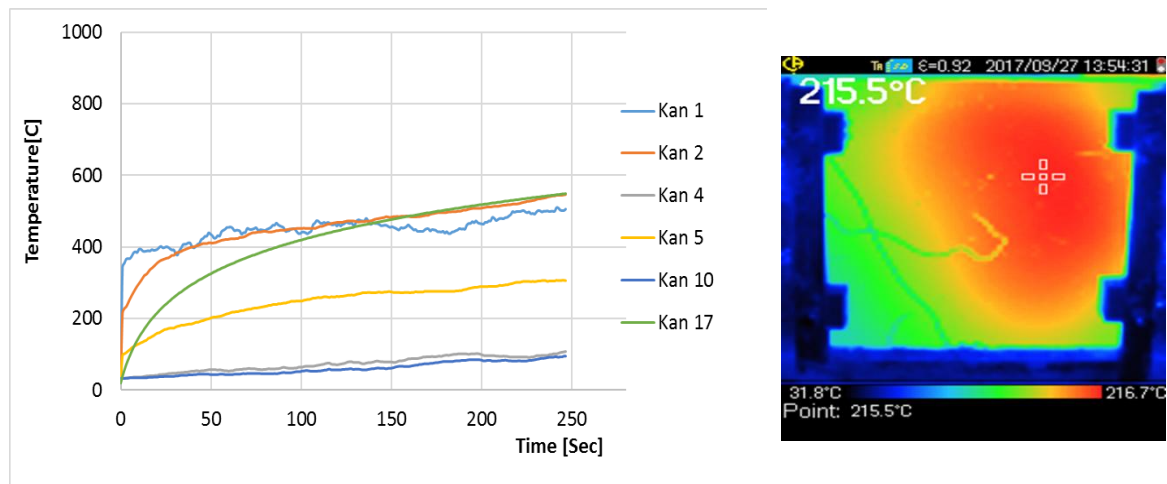
Figure 67. Fire-resistance curves of the uncoated aluminum plate (left) and an image showing the temperature of the outer surface of the aluminum plate (right).

The results of sample 2 are presented in Figures 68 and 69.
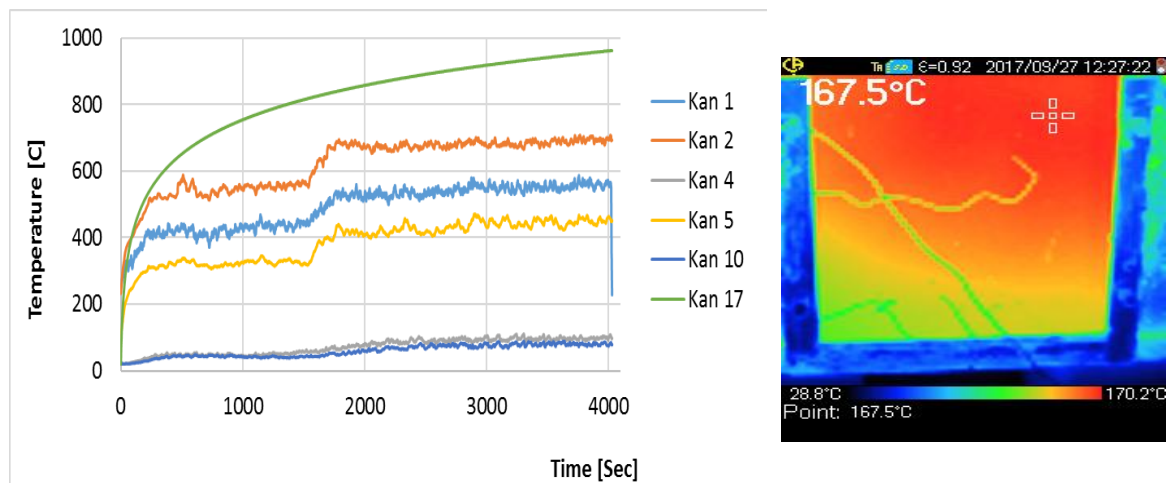
Figure 68. Fire-resistance curves of an aluminum plate with a GF layer of 11 mm thickness (left) and an image showing the temperature of the outer surface of the plate (right).
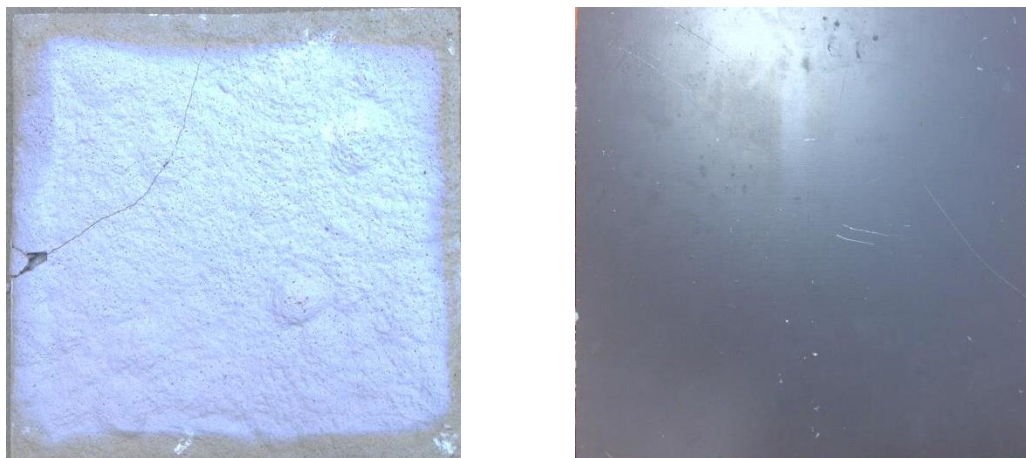
Figure 69. Pictures showing the surfaces of the sample after testing: the fire exposure surface (left), the back surface of the sample (right).

The results of sample 3 are presented in Figures 70 and 71.
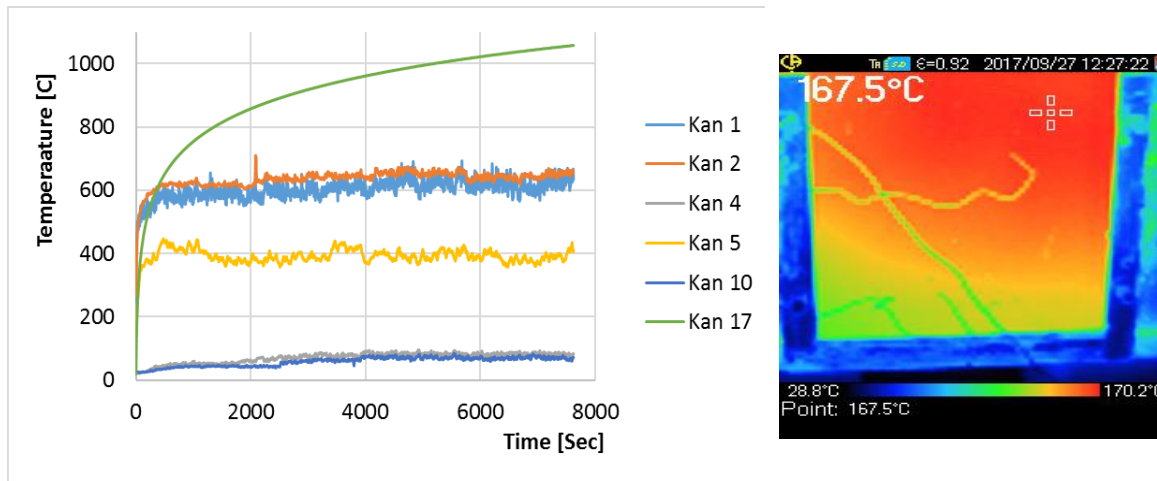
Figure 70. Fire-resistance curves of an aluminum plate with a GF layer of 20 mm (left) and an image showing the temperature of the outer surface of the plate (right).
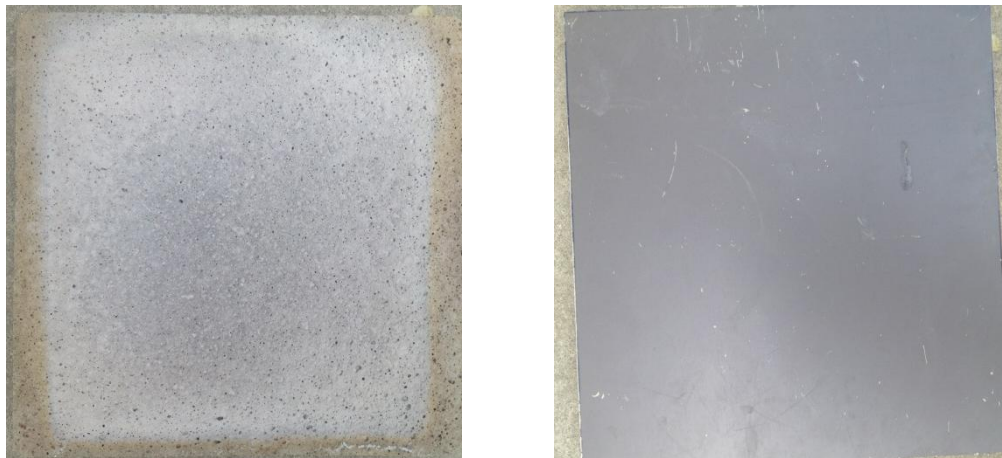
Figure 71. Photographs showing the surfaces of the sample after testing: the fire exposure surface (left), the back surface of the sample (right).

5.4 *Summary*

An uncoated aluminum plate had a fire-resistant time around 250 seconds, and the outside surface of the sample is above 200 °C (Figure 67).

The fire-resistance increases many times after the application of the GF layer with different thicknesses.

Sample 3 resisted the fire for the longest time. Its fire-resistant time was 30 times higher than that of the aluminum plate without the GF layer. The maximal temperature in the furnace did not exceed 600 °C (Figure 70).

Sample 2 showed that its fire-resistant time was 16 times higher than that of sample 1, while the fire temperature in the furnace increased to 600 °C (Figure 68).

6. Evaluation of fire-resistance for carbon steel column

6.1 *Description of the problem*

Fire-resistant coatings made of the GF are aimed at slowing the rise in the temperature of the carbon steel column and keeping its temperature below a critical value (about 600 °C). Therefore, GFs based on potassium activators were used to coat the steel column surface at room temperature in this subsection. A 6 mm thickness GF layer was sprayed on the steel column surface. The steel samples were mounted in a furnace and were gradually heated to a temperature of 1000 °C. The fire-resistant results of the GF are given below.

6.2 *Experiment*

Table 12. GF composition coating on the steel column samples.

Sand /cement	Cement/ activator	Basalt fiber/ cement	Aluminum powder [%]	Silica fume/cement [%]
1	0.9	0.2	1.5	5

Description of samples:

The GF layer with about 6 mm thickness and is sprayed on the surface of the column.

Note: All samples were tested after28 days of aging.

Figure 72. Preparing constituent materials (left) and mixing mortar for spraying (right).
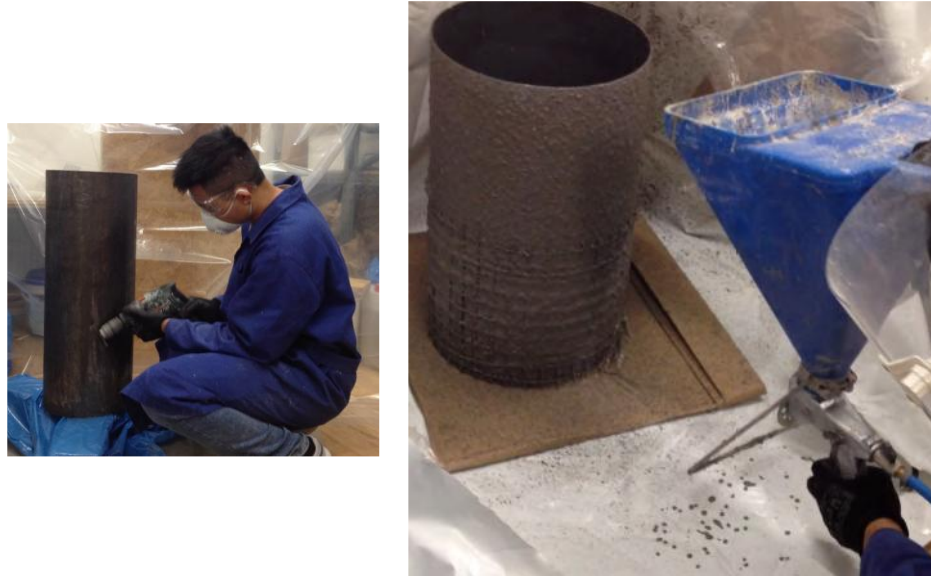
Figure 73. Sample preparation (left) and the GF spraying on the sample (right).

6.3 *Measured results*

The equipment shown in Figure 74 is prepared for the fire-resistant test of the samples. The temperatures outside and inside of the carbon steel column were measured using the thermocouples (Figure 75). Testing was stopped when the measured temperature on the cold-side of the column was 600 °C.

Figure 74. Device layout.

Note: A diagram of the location of the thermocouples can be seen in Figure 75 (left). Thermocouples from 1 to 4 were attached inner column of the cold side. Thermocouples 5, 9 and 10 were located inner furnace of the hot side.

Figure 75. The position of thermocouples (left) and an outer image after testing (right).
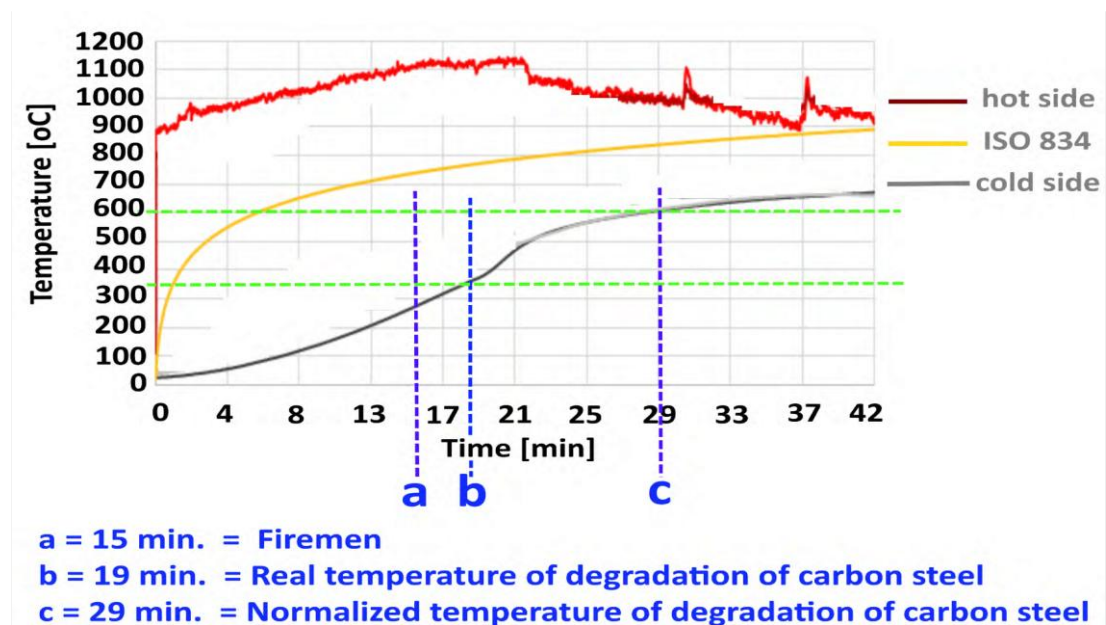
Figure 76. Fire-resistant curves of the carbon steel column.

6.4 *Summary*

The fire-resistance of the carbon steel column increases many times after the application of a GF layer with a thickness of 6 mm. The temperature of the carbon steel column reached 300 °C at the 19th minute, and it begins to affect the mechanical properties of the carbon steel column. The temperature of the column achieved 600 °C at the 29th minute (Figure 76). At this temperature, the mechanical strength of carbon steel decreases by 60% compared to its one at ambient temperature.

Chapter 4. FIRE-RESISTANT TEST AT PAVUS A.S.

This chapter presents the results of the fire-resistance of the GF coated on the surface of OSB panels, steel plate, and concrete blocks as a surface protection layer. The author and colleagues fabricated the test samples at the TUL. Fire-resistant tests are performed at the testing site of Pavus a.s. in Veselí nad Lužnicí.

1. Fire-resistant test for OSB panels and concrete slabs

The evaluation of the fire-resistance of GFs coated on the surface of OSB panels and concrete slabs are presented in this section. The GF layers with different thicknesses were applied to the surface of samples. The models are fitted with internal thermocouples and heated up by the test furnace, which is installed by the company Pavus a.s. Test results are summarized in the following subsections.

1.1 *Performance of the test*

General

The test was performed on 23 May 2018 using the standard ČSN EN 1363-1.

Conditioning of samples

From 20 April 2018 to 23 May 2018, the samples were stored in the environment with air temperature of 21 - 25 °C and relative humidity of 51 - 56%.

Preparing the furnace for test samples

The samples were attached to a vertical wall of 3 m (width) x 3 m (height) x 0.25 m (thickness) in the test furnace. The wall was constructed of cellular concrete blocks YTONG P-500.

Furnace regulation

A system of natural gas heated the test furnace by the standard ČSN EN 1363-1 Art. 5.

The plastic of thermoelectric cell (DST) measured the temperatures in the furnace according to the standard ČSN EN 1363-1 Art. 4.5.1.1:

$$T/°C = 345 \log_{10}(8t/min + 1) + 20 \qquad (3)$$

Where T (°C) is the standard required oven temperature at time t (min).

Tolerances of the average temperature in the furnace are given according to the standard ČSN EN 1363-1 Art. 5.1.2. The overpressure in the test furnaces was measured by a differential manometer and automatically regulated by the exhaust fan so that the values of the overpressure in the furnace correspond to the conditions of ČSN EN 1363-1 Art. 5.2.1 and 5.2.5.

Legend

TC	Thermoelectric cell
PST	The plastic of thermoelectric cell
DST	Board temperature sensor containing PTC ø 1mm
HS	Heated side of the sample
US	Unheated side of the sample

1.2 *Used materials*

Materials used to produce the GF by weight in Table 13. The author uses the ratio according to the article A.

Table 13. Materials used to produce the GF by weight.

Sand/ cement	Cement/ activator	Silica fume/ cement	Basalt fiber/ cement	Aluminum powder [%]
1	0.9	0.05	0.14	1.5

1.3 *The subject of the test*

For concrete slab samples

The concrete slab samples with dimensions of 300 mm x 300 mm x 140 mm were fabricated following the standard ČSN EN 13381-2, Article 6.3.1. Three thermocouples were installed in each slab sample at each depth from the concrete surface on the heated side of the sample (0, 15, 30, 45, 60, 75) mm.

For OSB panel samples

The OSB panels have five layers in which four layers have a thickness of 8 mm and one layer has a thickness of 22 mm. The sandwich OSB panel made from OSB/3 boards, as described in Figure 77. The list of samples is summarized in Table 14.
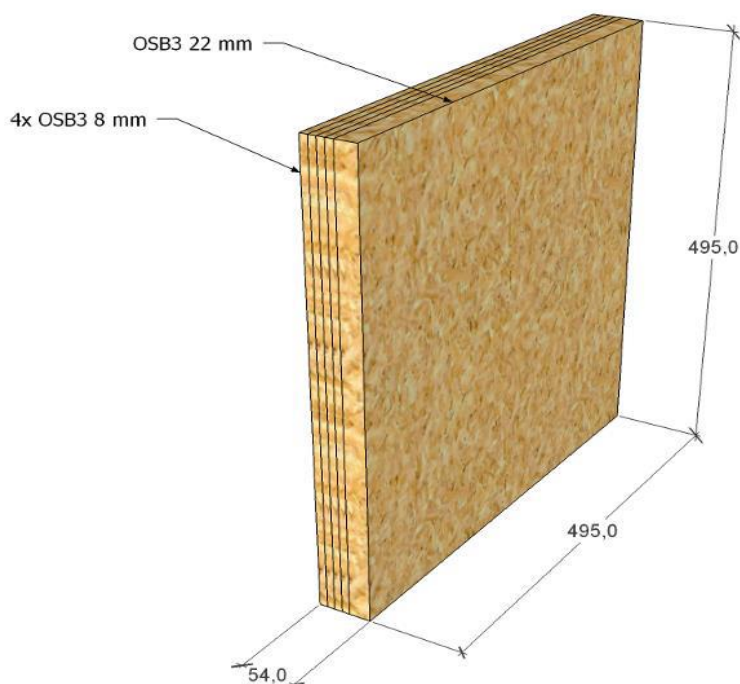
Figure 77. The sandwich OSB panel.

Table 14. Details of test specimens.

| Samples | The substrate sample | | Protection thickness (plan) | Protection thickness (reality) | Number Thermocouple |
| | Material | Thickness | | | |
		(mm)	(mm)		(number/sample)
1	Concrete 30/37 normal bulk density (2000 to 2600) kg/m³	140	0	0	12
2		140	0	0	12
3		140	10 + mesh	13.6	12
4		140	10	16	12
5		140	20 + mesh	23.5	12
6		140	20	23.2	12
7	Sandwich of OSB panel	4 x 8 + (20-22)	0	0	15
8			20	21.4	15
9			20	21	15
10			10 + mesh	10.2	15
11			10 + mesh	10	15
12			20 + mesh	20.4	15
13			20 + mesh	21	15
14			40 + mesh	37.7	15
15			40 + mesh	37.1	15
16	„Design element" TUL	OSB+izolation+OSB	20+5	20+1[a]	9
17			20+5	20+1[a]	9
		Total amount TC			225

Note: [a] The both surfaces of base material samples were coated by two layers (20 mm thickness of foamed geopolymer composite and 1 mm thickness of non-foamed geopolymer).
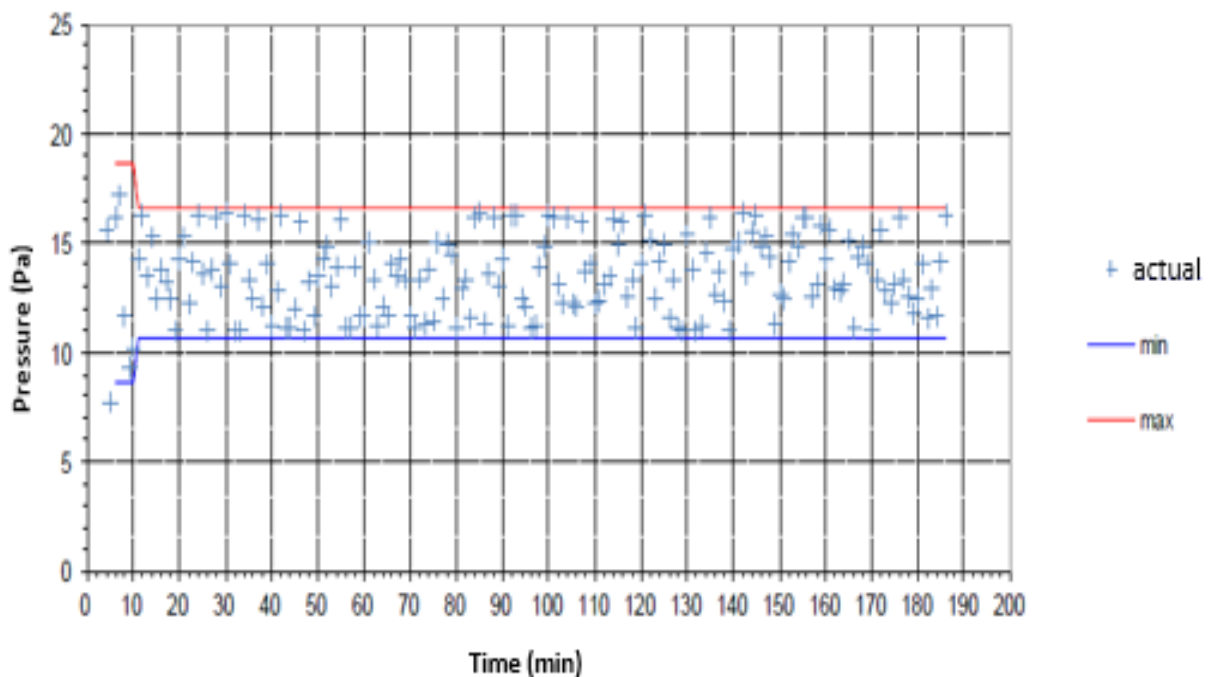
Figure 78. Pressure in a furnace, according to CSN EN 1363-1: 5.2.

Pressure and temperature in the furnace

The pressure in a furnace was measured according to the standard CSN EN 1363-1: 5.2 (Figure 78). The average temperature in a furnace was measured according to the standard CSN EN 1363-1: 5.1 (Figure 79).
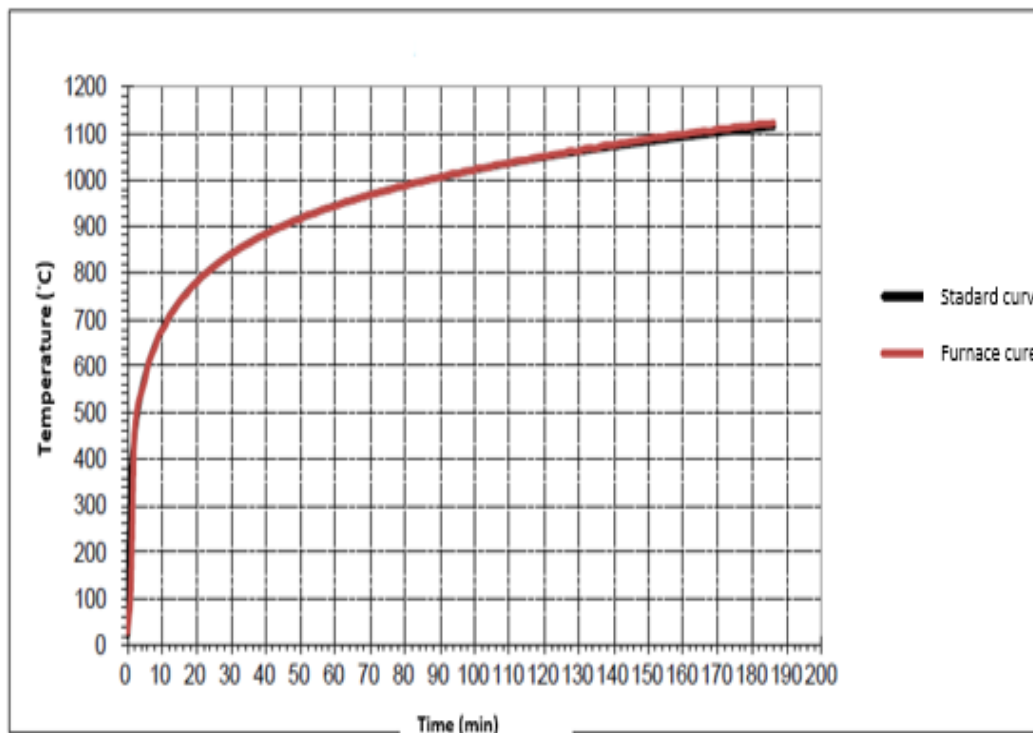
Figure 79. The average temperature in a furnace, according to CSN EN 1363-1: 5.1.

1.4 *Measured results of concrete samples*

Evaluation of measured results

The evaluation of the test results was performed according to the standard ČSN EN 13381-3. The equivalent thickness ε is determined by comparing the temperature fields in the unprotected concrete slab and the protected sample.

$\varepsilon = f (d_p, t)$

where t is the fire-resistant time of the protected concrete element in min.

The temperature field in an unprotected concrete slab with 400 mm thickness was taken from the standard ČSN EN 13381-3.

For the evaluation of concrete slabs with a thickness of 140 mm and the protective layer with the thickness d_p, it is necessary to use a thermal field in an unprotected concrete slab with a thickness of at least 140 mm + ε.

The procedure for determining the equivalent thickness ε is described in the standard ČSN EN 13381-3.

The characteristic temperatures of samples 1 – 6 are presented in Figure 80.
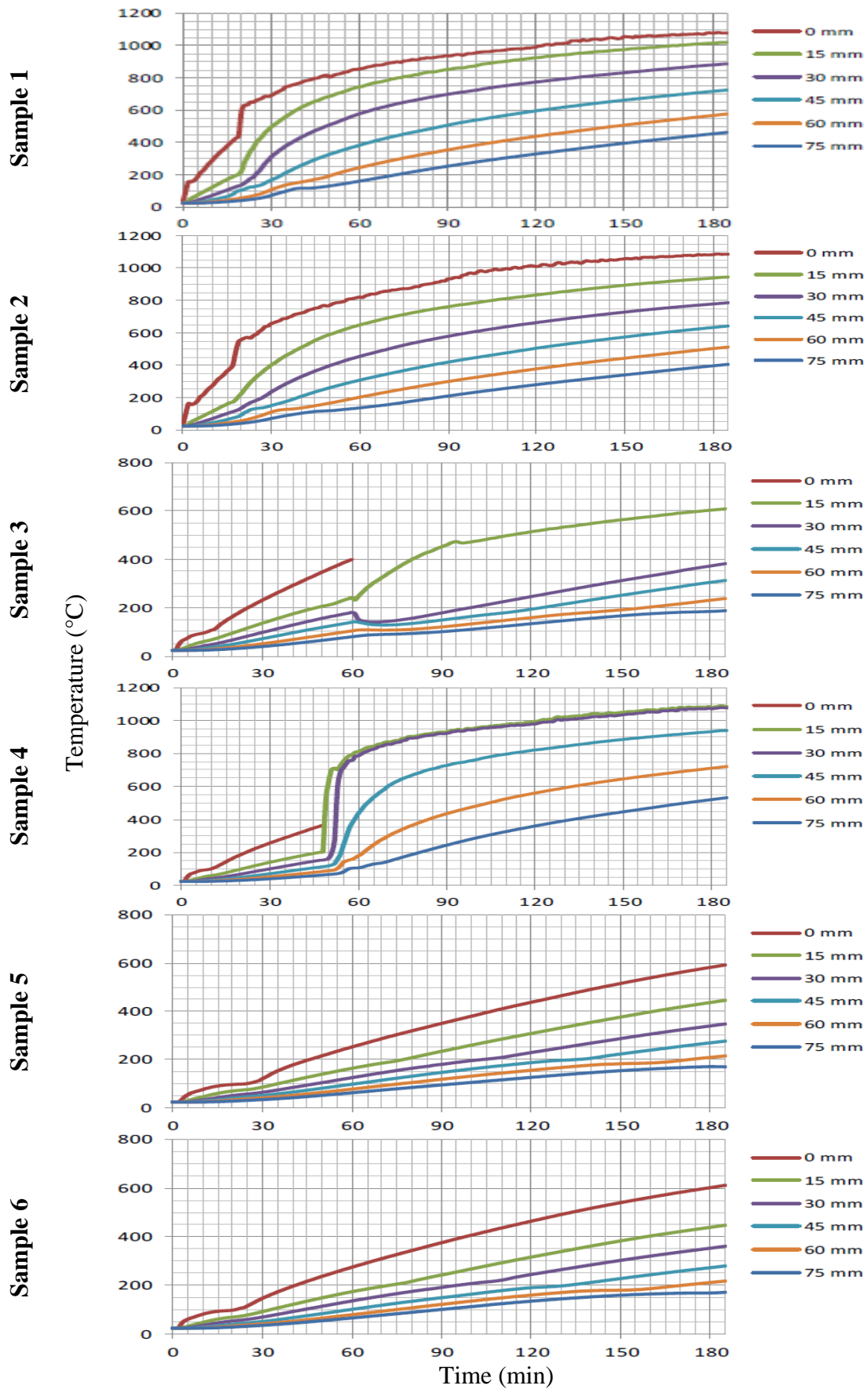
Figure 80. The characteristic temperatures of samples 1 - 6.

Results of regression analysis for the dependence of equivalent thicknesses ε on the protection thickness d_p and the required fire-resistant time t are presented as follows.
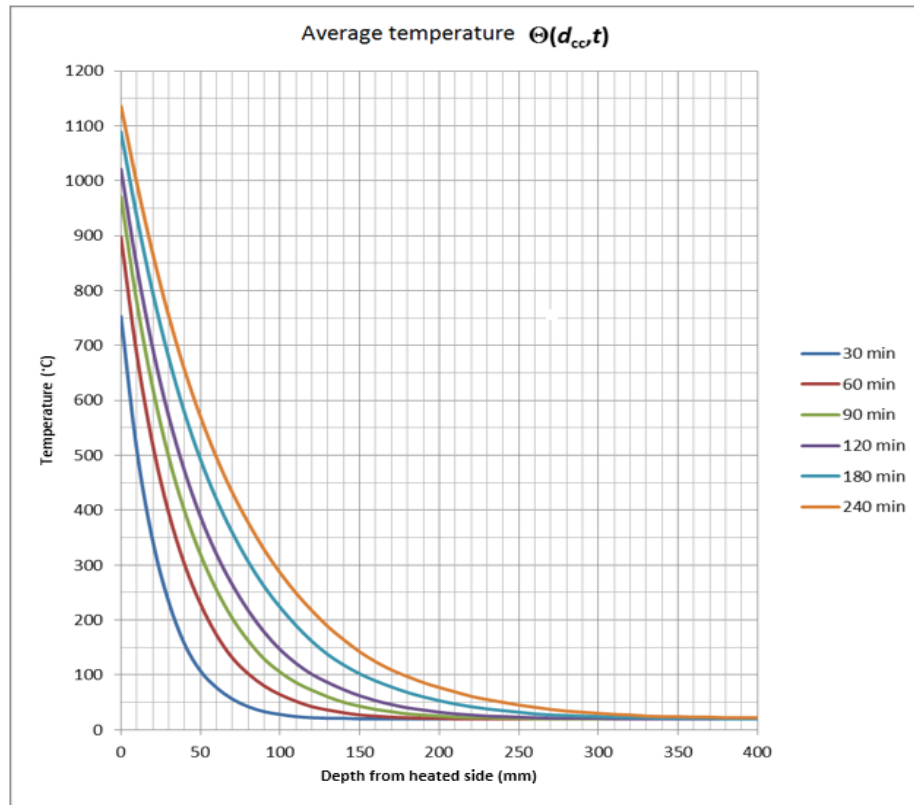
Figure 81. The temperature field in an unprotected concrete slab.

The average temperature increase of samples 1 and 2 are presented in Figures 82.
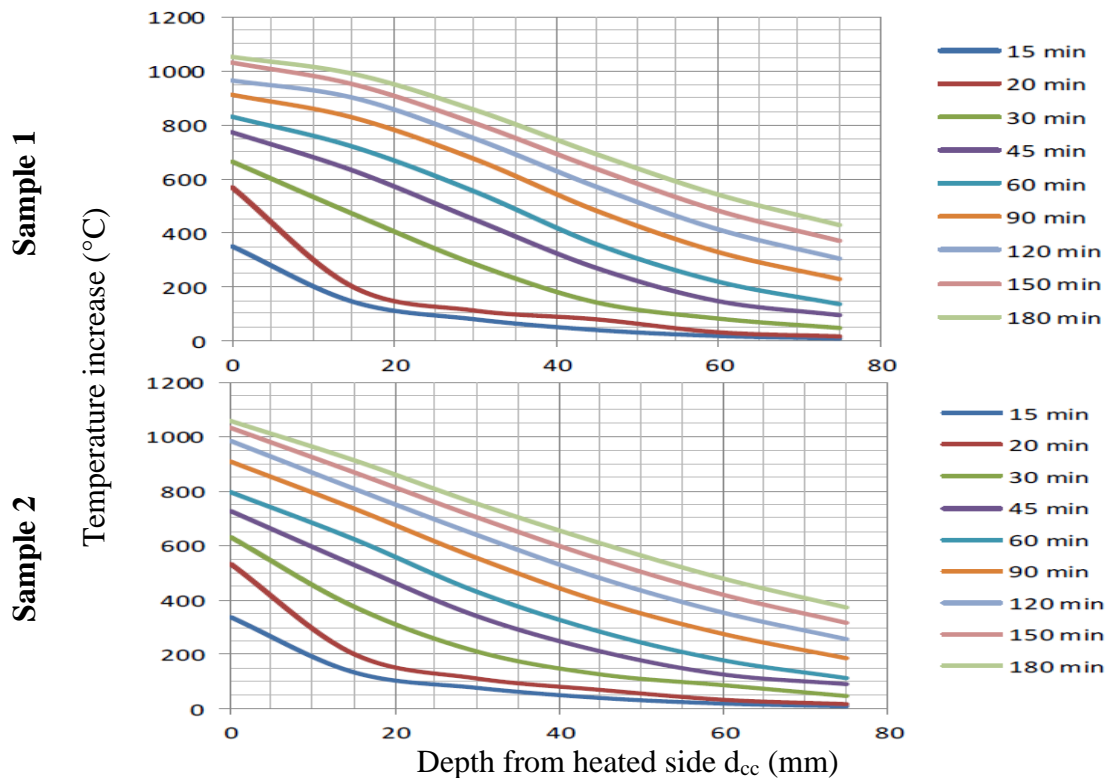
Figure 82. The average temperature increase of sample 1 (top) and sample 2 (bottom).

The results of the fire-resistant test for sample 3 with the protective GF layer having a thickness of 13.6 mm are presented in Figures 83-84 and Tables 15-16.
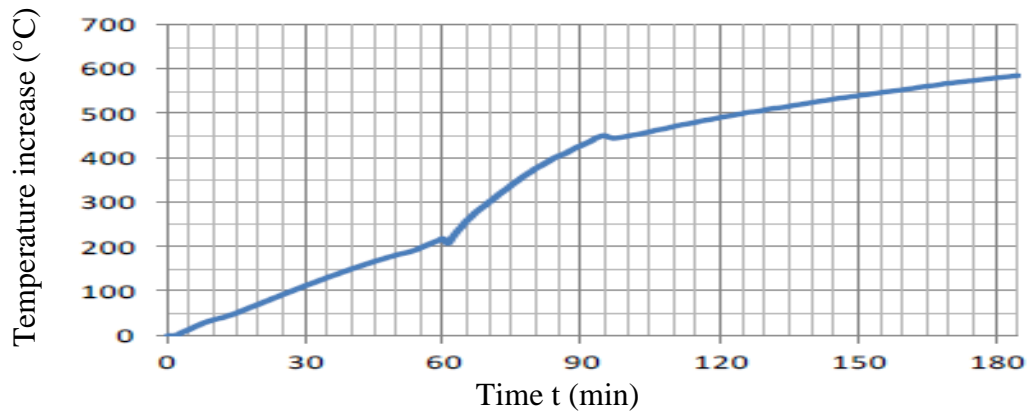
Figure 83. The increase in the characteristic temperature $\Delta\Theta(d_{cp}, t)$ at a depth d_{cp} =15 mm for the protected sample.
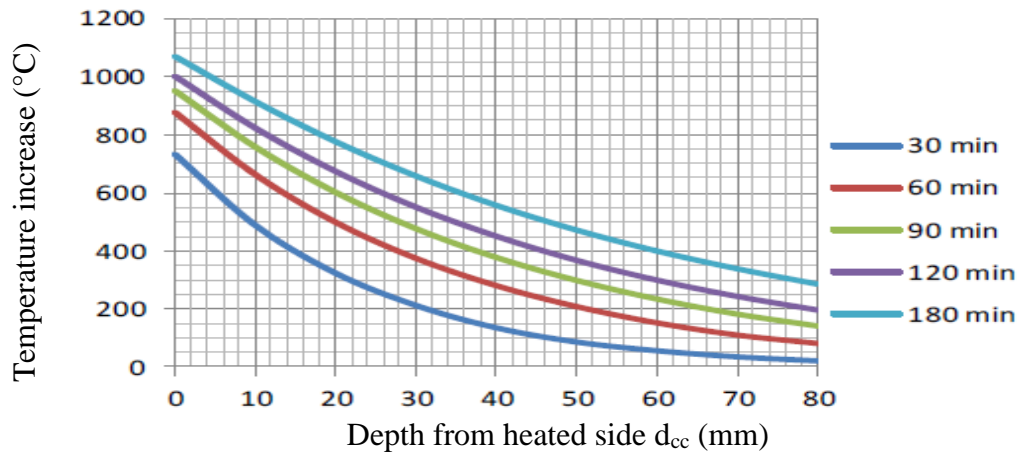
Figure 84. The temperature increase $\Delta\Theta(d_{cc}, t)$ in the unprotection slab as a function of the depth d_{cc} and time t.

Table 15. Calculation of equivalent thickness (sample 3).

t (min)	$\Delta\Theta(d_{cp}, t)$ (°C)	d_{cc} (mm)	ε (mm)
30	112.4	44.8	45
60	218.3	48.7	49
90	427.5	35.0	35
120	490.6	36.0	36
180	579.9	37.7	38

Table 16. The average temperature increase in the unprotected slab (sample 3).

Time t (min)	Depth d_{cc} from heated side (mm)								
	0	10	20	30	40	50	60	70	80
	Temperature increase $\Delta\Theta(d_{cc},t)$ (°C)								
30 min	733	489	324	213	136	87	57	36	22
60 min	877	663	499	375	281	209	153	111	82
90 min	951	758	602	477	378	299	235	183	142
120 min	1001	823	674	551	451	368	300	244	197
180 min	1069	914	776	658	557	472	400	339	286

Legend

t	(min)	Time
d_{cp}	15 mm	The depth from the concrete surface on the heated side of the protected sample
$\Delta\Theta(d_{cp}, t)$	(°C)	The increase of the characteristic temperature at the depth d_{cp} and at time t compared to the initial temperature of the protected sample
$\Delta\Theta(d_{cc},t)$	(°C)	The increase in temperature at the depth d_{cc} from the heated side and at time t compared to the initial temperature of the unprotected slab
d_{cc}	(mm)	$\Delta\Theta(d_{cc},t) = \Delta\Theta(d_{cp},t)$ The depth from the heated side of the unprotected slab calculated according to the standard ČSN EN 13381-3.
$\varepsilon = d_{cc} - d_{cp}$	(mm)	Equivalent concrete thickness
x		Concrete was chipped from the 61st minute. Thus evaluation for fire-resistance is performed when the time is less than or equal to 60 min.

The results of the fire-resistant test for sample 4 with the protective GF layer having a thickness of 16 mm are presented in Figures 85-86 and Tables 17-18.
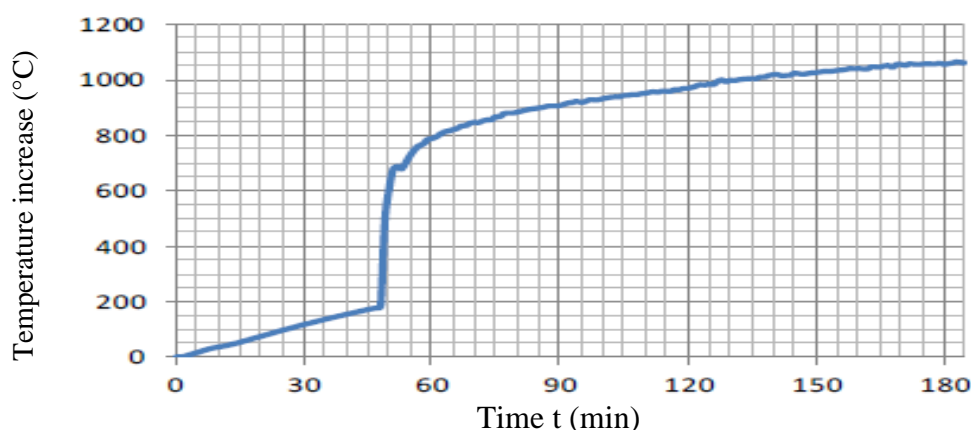
Figure 85. The increase in the characteristic temperature $\Delta\Theta(d_{cp}, t)$ at a depth $d_{cp} =15$ mm for the protected sample 4.
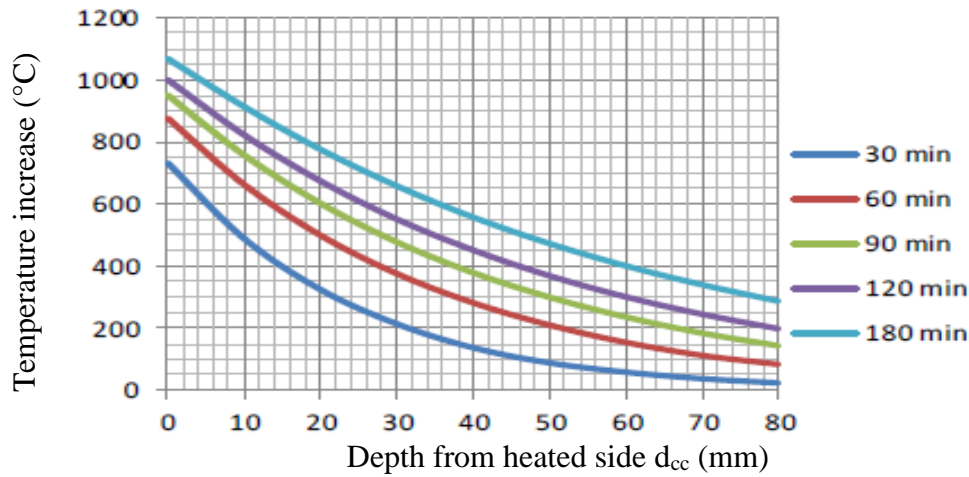
Figure 86. The temperature increase $\Delta\Theta(d_{cc}, t)$ in the unprotection slab as a function of the depth d_{cc} and time t.

Table 17. Calculation of equivalent thickness (sample 4).

t (min)	$\Delta\Theta(d_{cp}, t)$ (°C)	d_{cc} (mm)	ε (mm)
30	116	44.1	44
60	788	4.2	4
90	907	2.3	2
120	969	1.8	2
180	1056	0.9	1

Table 18. Increase of average temperature in unprotected slab (sample 4).

Time t (min)	Depth d_{cc} from heated side (mm)								
	0	10	20	30	40	50	60	70	80
	Temperature increase $\Delta\Theta(d_{cc}, t)$ (°C)								
30 min	733	489	324	213	136	87	57	36	22
60 min	877	663	499	375	281	209	153	111	82
90 min	951	758	602	477	378	299	235	183	142
120 min	1001	823	674	551	451	368	300	244	197
180 min	1069	914	776	658	557	472	400	339	286

Note:

ε from (60 min) to (180 min)   From the 49th minute, the concrete was chipped off, the equivalent thicknesses marked in red are not important; it is possible to evaluate it for fire resistance less than or equal to it.

The results of the fire-resistant test for sample 5 with the protective GF layer having a thickness of 23.5 mm are given in Figures 87-88 and Tables 19-20.
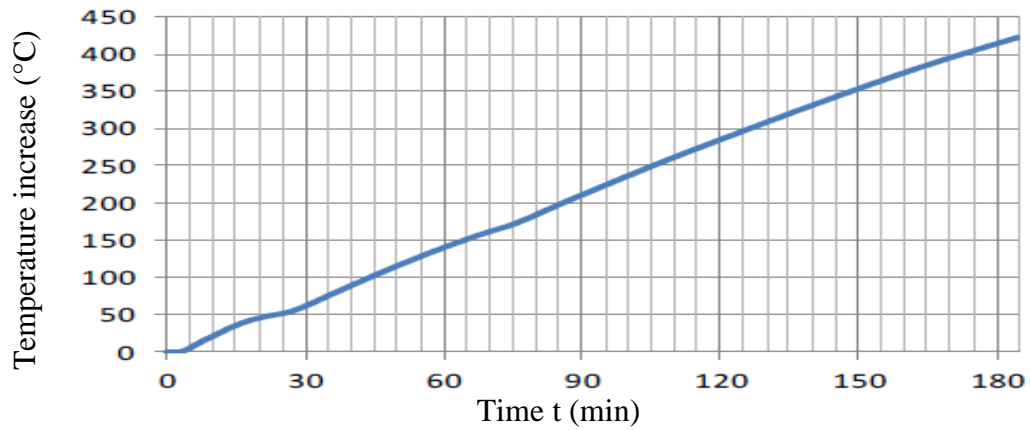
Figure 87: The increase in the characteristic temperature $\Delta\Theta(d_{cp}, t)$ at a depth $d_{cp}=15$ mm for the protected (sample 5)
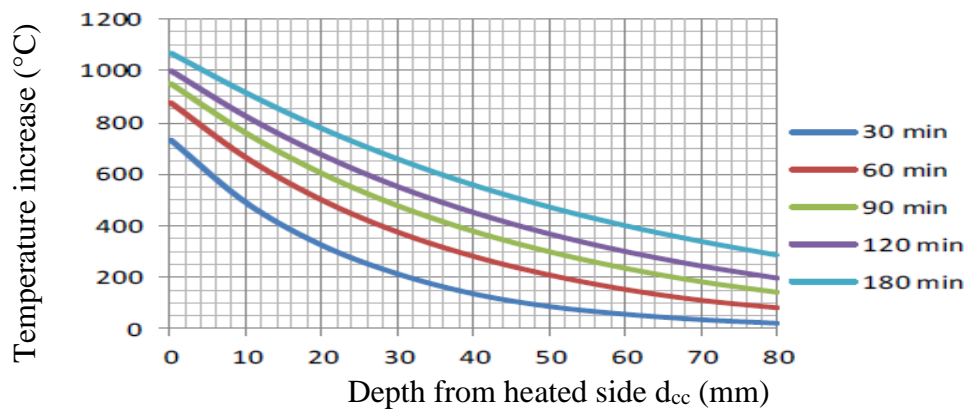
Figure 88. The temperature increase $\Delta\Theta(d_{cc}, t)$ in the unprotection slab as a function of the depth d_{cc} and time t.

Table 19. Calculation of equivalent thickness of sample 5.

t (min)	$\Delta\Theta(d_{cp}, t)$ (°C)	d_{cc} (mm)	ε (mm)
30	61.8	58.4	58
60	140.0	63.1	63
90	210.5	64.7	65
120	284.4	62.8	63
180	413.1	57.9	58

Table 20. Increase of average temperature in unprotected slab (sample 5).

Time t (min)	Depth d_{cc} from heated side (mm)								
	0	10	20	30	40	50	60	70	80
	Temperature increase $\Delta\Theta(d_{cc}, t)$ (°C)								
30 min	733	489	324	213	136	87	57	36	22
60 min	877	663	499	375	281	209	153	111	82
90 min	951	758	602	477	378	299	235	183	142
120 min	1001	823	674	551	451	368	300	244	197
180 min	1069	914	776	658	557	472	400	339	286

The results of the fire-resistant test for sample 6 with the protective GF layer having a thickness of 23.2 mm are given in Figures 89-90 and Tables 21-22.
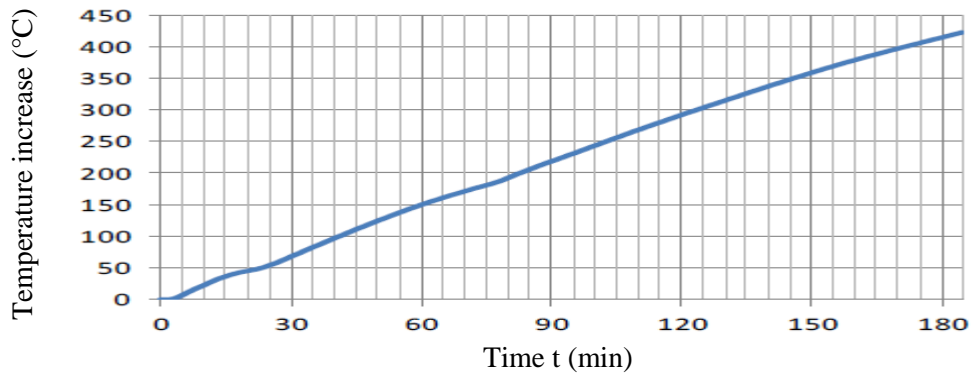
Figure 89. The increase in the characteristic temperature $\Delta\Theta(d_{cp}, t)$ at a depth d_{cp} =15 mm for the protected (sample 6).
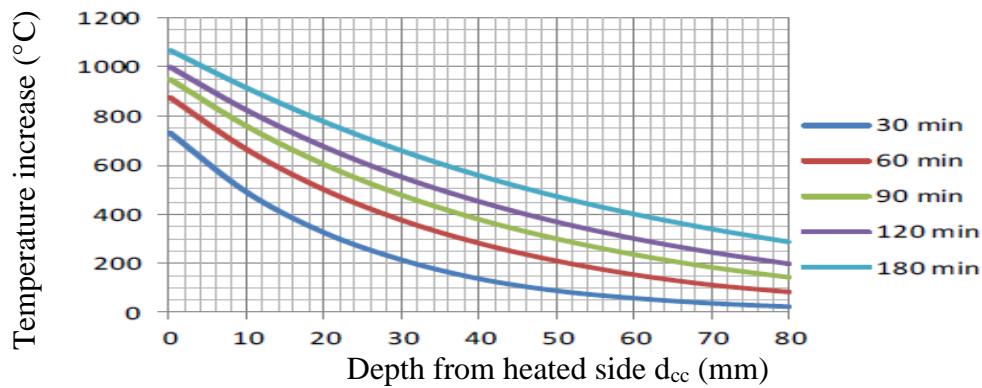
Figure 90. The temperature increase $\Delta\Theta(d_{cc}, t)$ in the unprotection slab as a function of the depth d_{cc} and time t (sample 6).

Table 21. Calculation of equivalent thickness of sample 6.

t (min)	$\Delta\Theta(d_{cp}, t)$ (°C)	d_{cc} (mm)	ε (mm)
30	67.8	56.4	56
60	149.8	60.8	61
90	218.4	63.2	63
120	291.8	61.5	61
180	414.4	57.6	58

Table 22. Increase of average temperature in unprotected slab (sample 6).

Time t (min)	Depth d_{cc} from heated side (mm)								
	0	10	20	30	40	50	60	70	80
	Temperature increase $\Delta\Theta(d_{cc}, t)$ (°C)								
30 min	733	489	324	213	136	87	57	36	22
60 min	877	663	499	375	281	209	153	111	82
90 min	951	758	602	477	378	299	235	183	142
120 min	1001	823	674	551	451	368	300	244	197
180 min	1069	914	776	658	557	472	400	339	286

Regression analysis

The results of the regression analysis for the dependence of the equivalent thicknesses ε on the protection thickness d_p and the required fire-resistant time t are summarized below (Table 23).

Table 23. The equivalent thickness for concrete slabs depending on the thickness of the protection and fire-resistant time.

Fire-resistant time t (min)	Thickness protection d_p (mm)	Equivalent thickness ε (mm)
30	13.6	44
	16.0	45
	23.5	58
	23.2	56
60	13.6	4
	16.0	49
	23.5	63
	23.2	61
90	13.6	2
	16.0	35
	23.5	65
	23.2	63
120	13.6	2
	16.0	36
	23.5	63
	23.2	61
180	13.6	1
	16.0	38
	23.5	58
	23.2	58
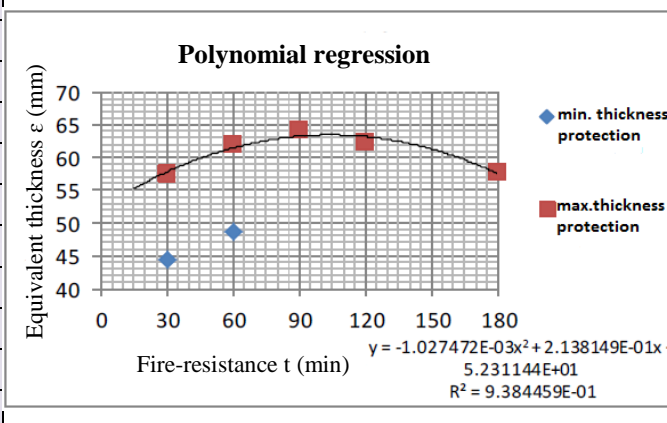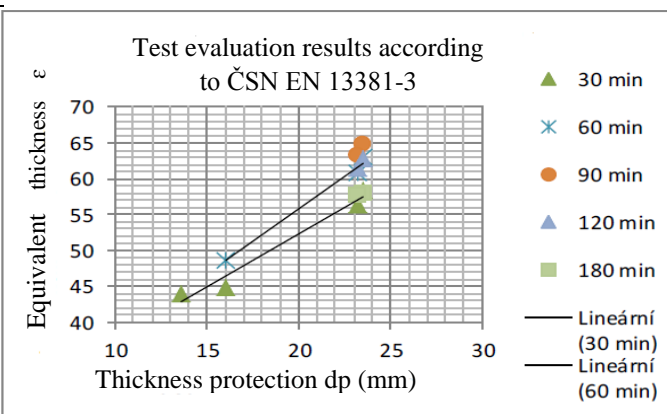
Note: From the 49th minute and the 61st minute, respectively, the concrete was chipped off in the samples. Therefore, the evaluation for fire-resistance is performed when the fire-resistance time is less or equal to this value.

The photographs illustrating the course of fire-resistant test are presented below.

Figure 91. The front view from outside before testing.

Figure 92. The samples inside furnace numbered from left to right in the 1st row
(11, 7, 17, 16) and the 2nd row (12, 9, 8, 10).

Figure 93. The samples inside furnace numbered from left to right in the 3rd row
(15, 14, 13, 6) and the 4th row (5, 4, 2, 3, 1).

Figure 94. The view from outside after 30 min testing.

Figure 95. The view from outside after 183 min testing.

Figure 96. Detail of unprotection slab samples 1 and 2.

Figure 97. Detail of samples 3 to 6 with different protection thicknesses.

1.5 *Measured results of OSB panel samples*

The characteristic temperatures of the OSB panel samples are depicted in Figures 98 and 99.
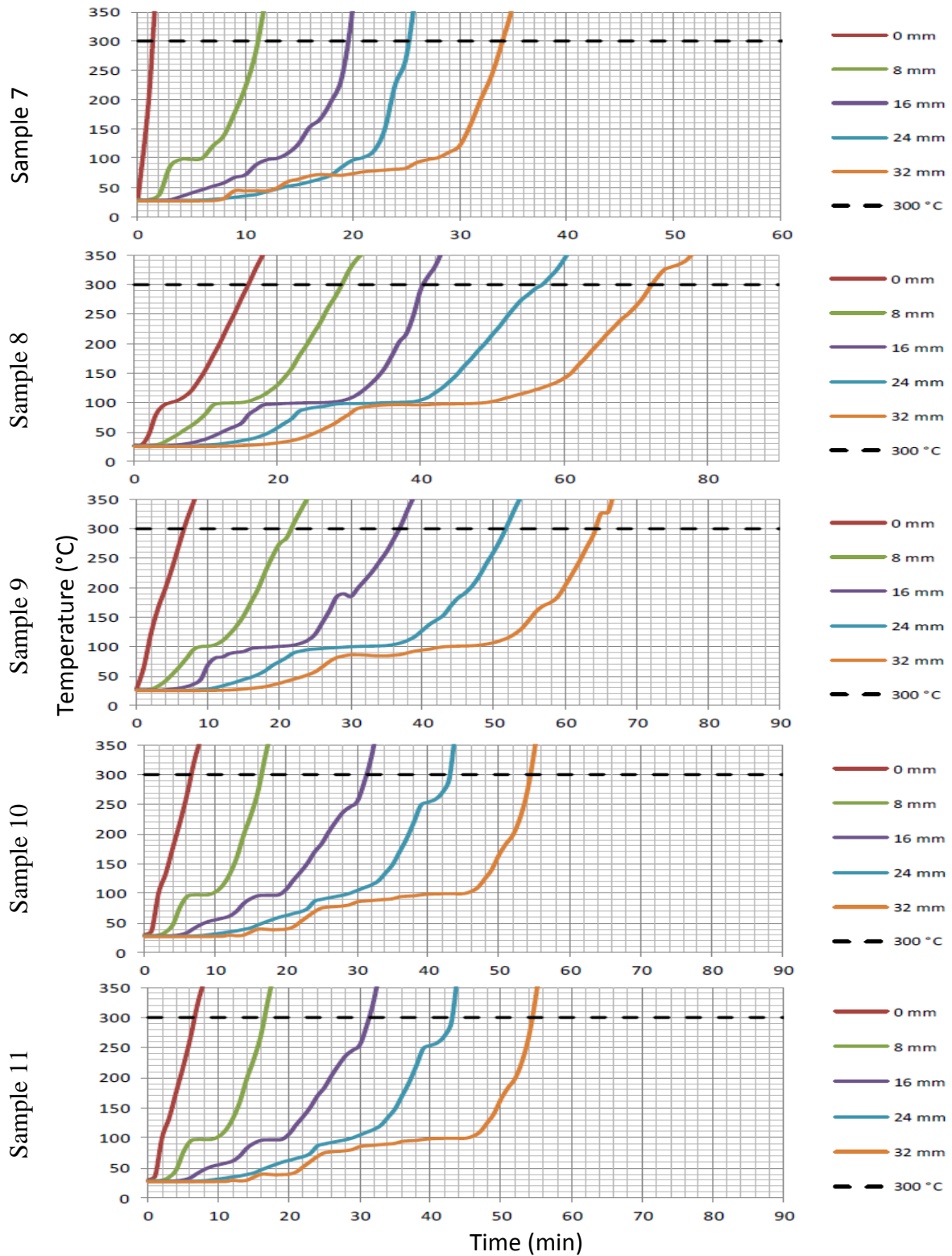
Figure 98. The characteristic temperature of samples 7-11.
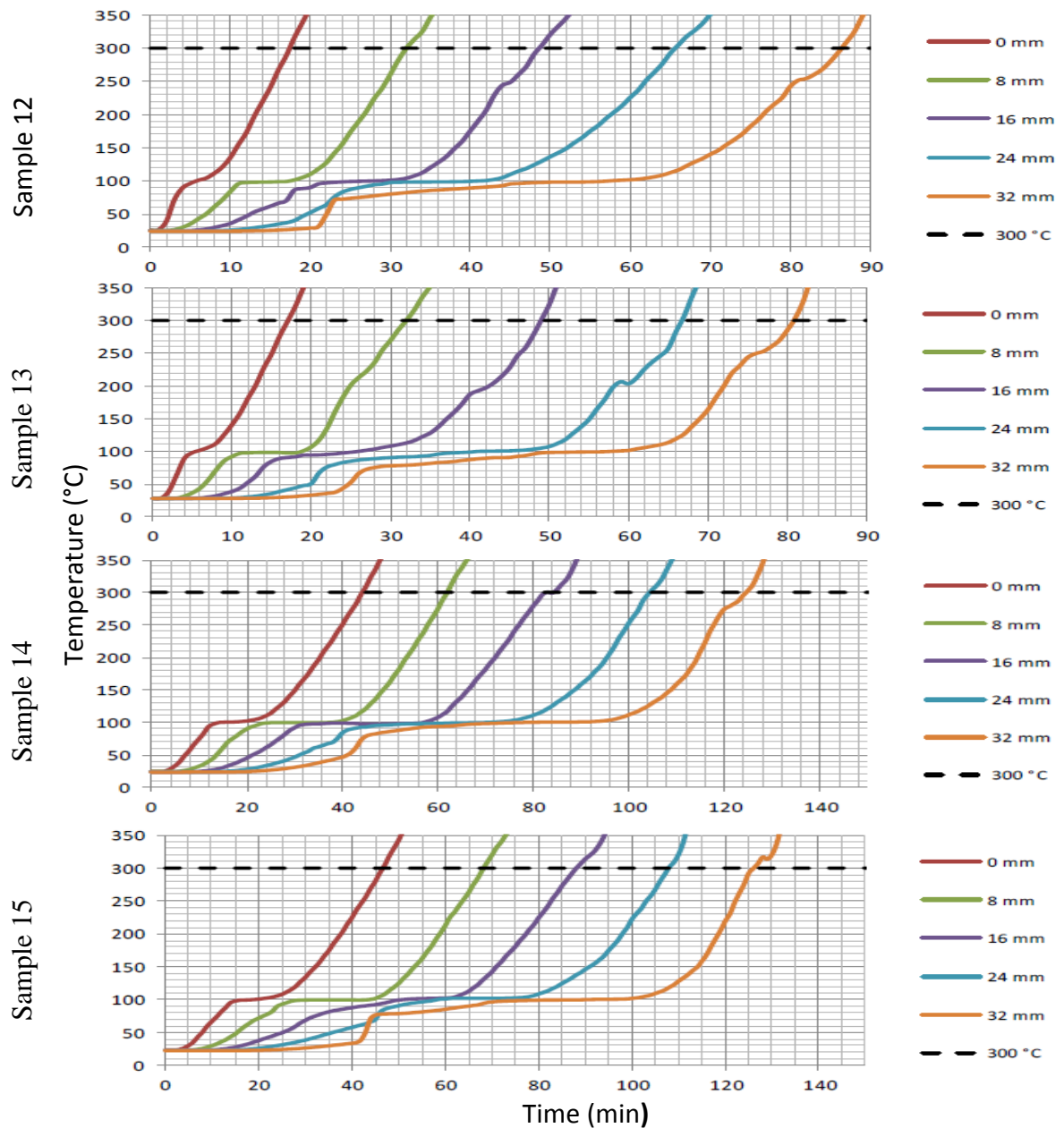
Figure 99. The characteristic temperature of samples 12-15.

Evaluation of the results of different samples from 7 to 15

Evaluation of measured results of the sample 7 (OSB board without protection) and samples from 8 to 15 (OSB boards with fire protection layer) was performed according to the standard prEN 13381-7: 2017-07 and Eurocode 5 (ČSN EN 1395-1-2). The carbonization limit in the sample is defined as an isotherm at 300 °C. The charring depth d_{char} (in mm) is defined as the distance of the carbonate boundary from the original surface of the sample (exposed surface of the unprotected sample or the interface of the fire protection layer and OSB panel is protected samples). The time of start of charring t_{ch} (in min) is determined as the time of reaching the temperature of 300 °C at the HS of the unprotected sample or the interface of the fire protection layer and the OSB board of the protected samples. The charring depth d_{char} for each sample above depends on test time t in min. In the linear phase

of this dependence, a regression line is interpolated by the least-squares method and its direction is used to estimate the charring rate as follows:

• For the unprotected sample 7 the charring rate was ß, in mm/min;

• For protected samples 8 to 15 the charring rate was ß2 = ß . K2, in mm / min, and was determined in the 2nd phase (from the beginning of charring t_{ch} to the end of the test), where K2 is the dimensionless protection coefficient.

Note: The test was terminated after 61 minutes due to the fire damage of samples 16 and 17. During the first 60 minutes of the test, the fire protection layer did not fall off. Therefore, it was not possible to determine other parameters such as the fire-resistant time and charring rate in the next phase 3.

Sample 7 without fire protection layer

Charring depth and charring rate (sample 7)

Phase	t (min)	d_{char} (mm)	$\Delta d_{char}/\Delta t$ (mm/min)	Slope (mm/min)	Intercept (mm)
"0"	0.0	0			
	1.4	0			
"1"	1.4	0			
	11.2	8	0.82		
	19.6	16	0.96	1.00	-2.3
	25.3	24	1.40		
	34.0	32	0.91		

y = 1.00x - 2.32
R² = 0.99
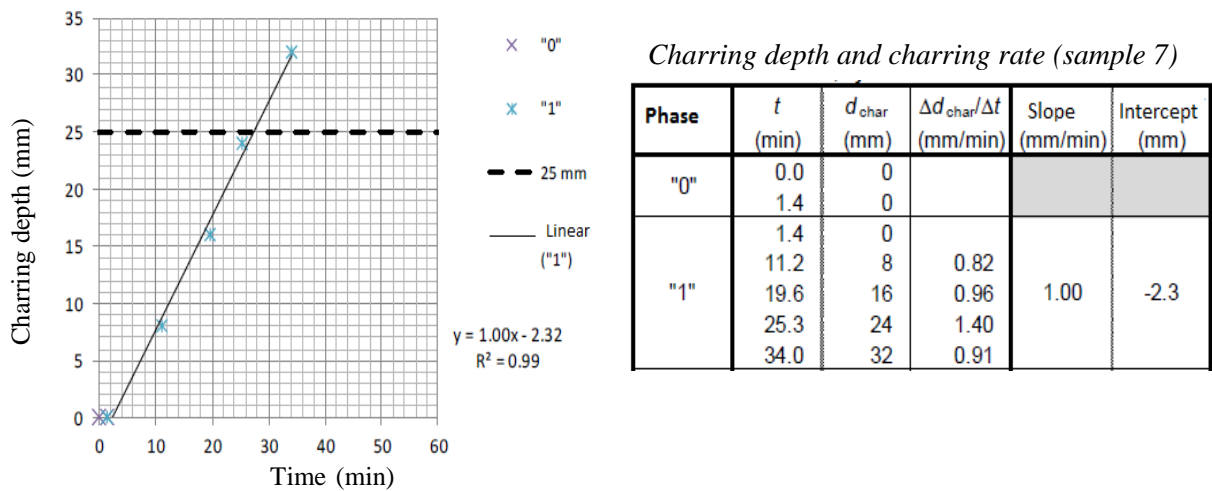
Figure 100. Charring depth and charring rate of sample 7.

Charring rate β was selected according to the standard prEN 13381-7: 2017-07.

ß= 1.00 mm / min

Sample 8 with the fire protection layer having a thickness of 21.4 mm.

Charring depth and charring rate (sample 8)

Phase	t (min)	d_{char} (mm)	$\Delta d_{char}/\Delta t$ (mm/min)	Slope (mm/min)	Intercept (mm)
1	0.0	0			
	15.9	0			
2	15.9	0			
	29.0	8	0.61		
	40.4	16	0.70	0.57	-8.3
	56.9	24	0.48		
	72.3	32	0.52		

y = 0.57x - 8.29
R² = 1.00
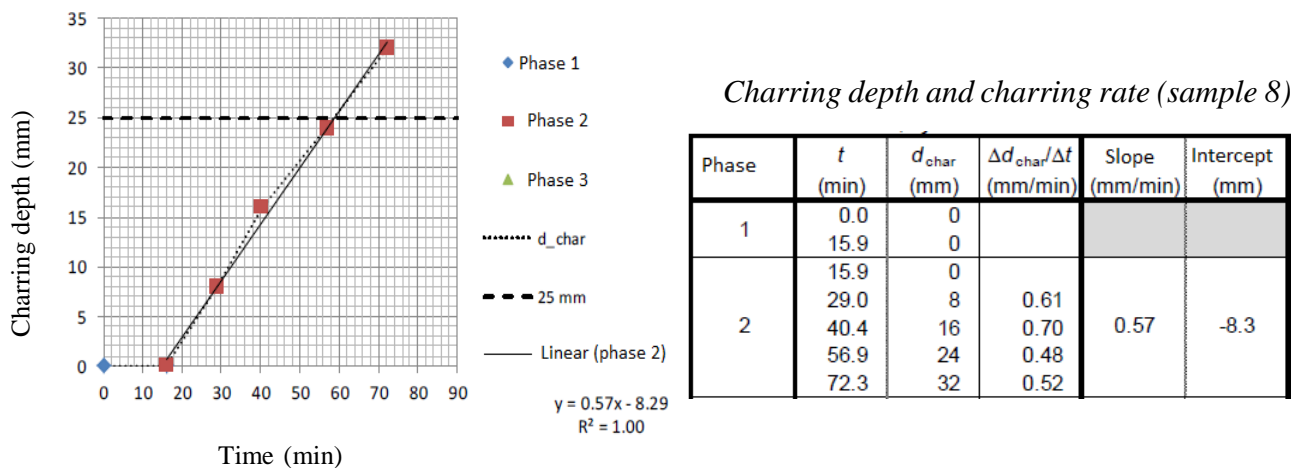
Figure 101. Charring depth and charring rate of sample 8.

t_{ch} =   15.9 min   the time of start of charring

$ß_2$ =   0.57 mm/min   charring rate under protection

t_f =   N/A min   the time of loss of stickability of the fire protection system

Sample 9 with the fire protection layer *having a thickness of 21 mm.*

Charring depth and charring rate (sample 9)

Phase	t (min)	d_{char} (mm)	$\Delta d_{char}/\Delta t$ (mm/min)	Slope (mm/min)	Intercept (mm)
1	0.0	0			
	18.7	0			
2	18.7	0			
	35.8	8	0.47		
	53.6	16	0.45	0.46	-8.7
	71.4	24	0.45		
	87.4	32	0.50		

y = 0.46x - 8.68
R² = 1.00
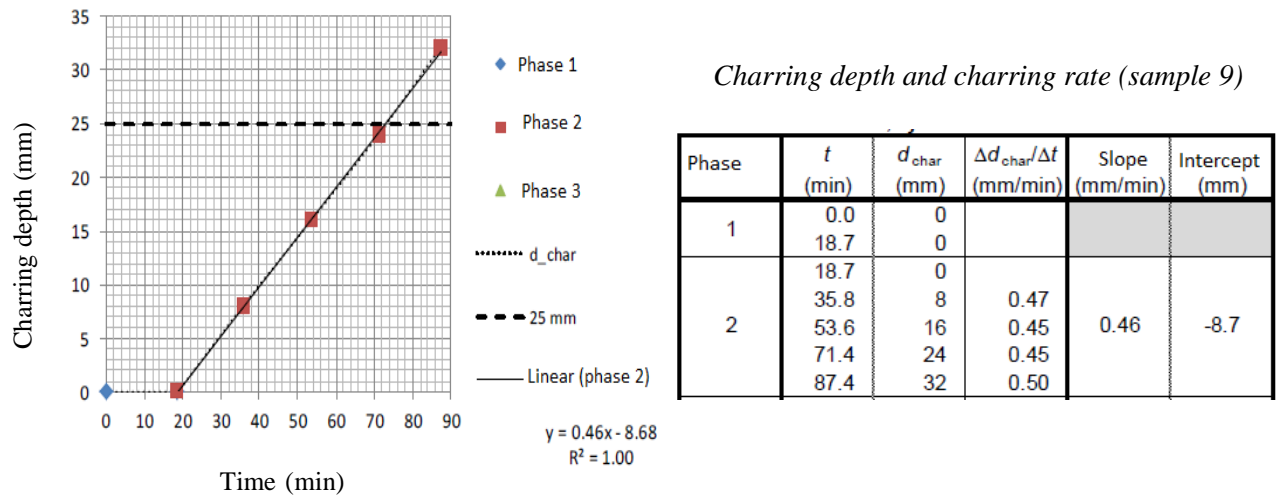
Figure 102. Charring depth and charring rate of sample 9.

t_{ch} =   18.7   min   the time of start of charring

$ß_2$ =   0.46   mm/min   charring rate under protection

t_f =   N/A   min   the time of loss of stickability of the fire protection system

Sample 10 with the fire protection layer having a thickness of 10.2 mm.

Charring depth and charring rate (sample 10)

Phase	t (min)	d_{char} (mm)	$\Delta d_{char}/\Delta t$ (mm/min)	Slope (mm/min)	Intercept (mm)
1	0.0	0			
	6.6	0			
2	6.6	0			
	21.6	8	0.53		
	36.8	16	0.53	0.55	-3.9
	51.7	24	0.54		
	64.3	32	0.64		

y = 0.55x - 3.91
R² = 1.00
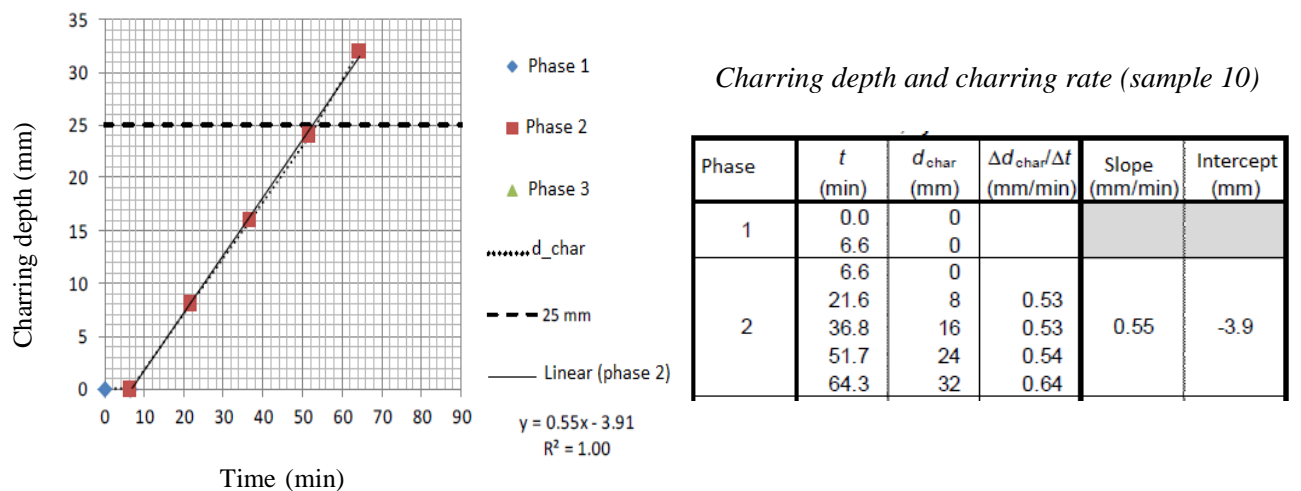
Figure 103. Charring depth and charring rate of sample 10.

t_{ch} =   6.6   min   the time of start of charring

$ß_2$ =   0.55   mm/min   charring rate under protection

t_f =   N/A   min   the time of loss of stickability of the fire protection system

Sample 11 with the fire protection layer having a thickness of 10 mm.

Charring depth and charring rate (sample 11)

Phase	t (min)	d_{char} (mm)	$\Delta d_{char}/\Delta t$ (mm/min)	Slope (mm/min)	Intercept (mm)
1	0.0	0			
	6.6	0			
2	6.6	0			
	16.5	8	0.81		
	31.3	16	0.54	0.65	-3.8
	43.1	24	0.68		
	54.4	32	0.71		

$y = 0.65x - 3.84$
$R^2 = 1.00$
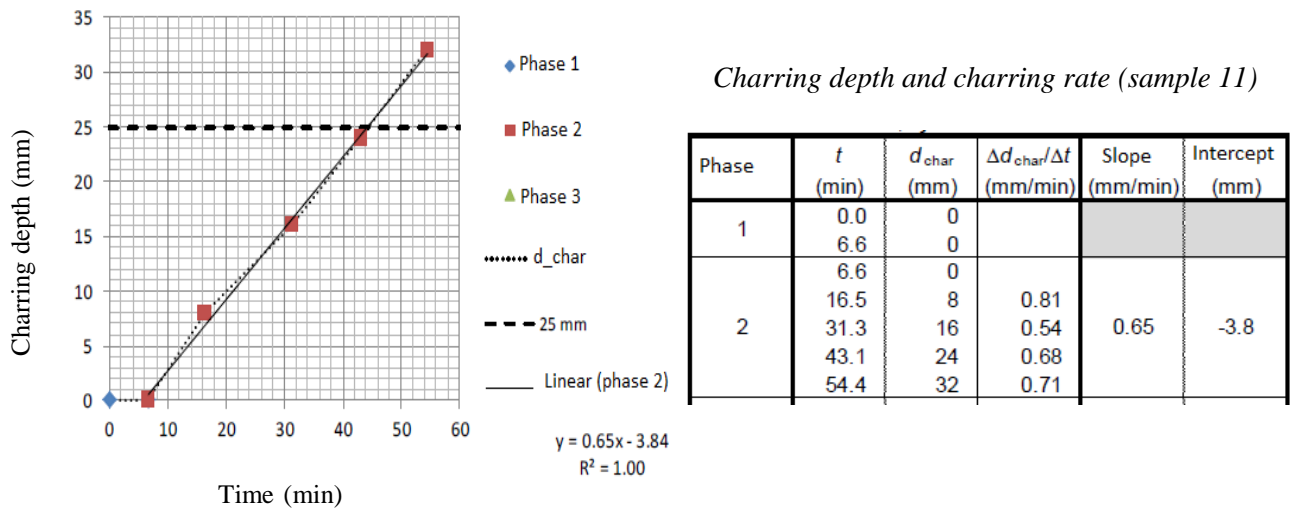
Figure 104. Charring depth and charring rate of sample 11.

$t_{ch} = 6.6$	min	the time of start of charring
$\beta_2 = 0.65$	mm/min	charring rate under protection
$t_f = $ N/A	min	the time of loss of stickability of the fire protection system

Sample 12 with the fire protection layer having a thickness of 20.4 mm.

Charring depth and charring rate (sample 12)

Phase	t (min)	d_{char} (mm)	$\Delta d_{char}/\Delta t$ (mm/min)	Slope (mm/min)	Intercept (mm)
1	0.0	0			
	17.1	0			
2	17.1	0			
	32.0	8	0.54		
	49.0	16	0.47	0.49	-8.2
	66.7	24	0.45		
	80.8	32	0.57		

$y = 0.49x - 8.18$
$R^2 = 1.00$
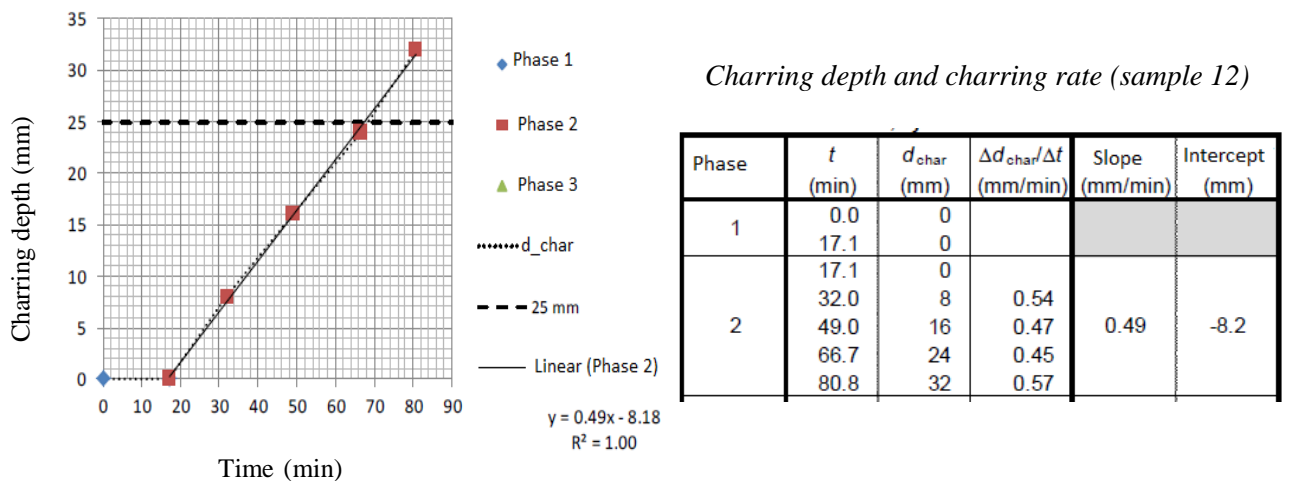
Figure 105. Charring depth and charring rate of sample 12.

$t_{ch} = 17.1$	min	the time of start of charring
$\beta_2 = 0.49$	mm/min	charring rate under protection
$t_f = $ N/A	min	the time of loss of stickability of the fire protection system

Sample 13 with the fire protection layer having a thickness of 21 mm.
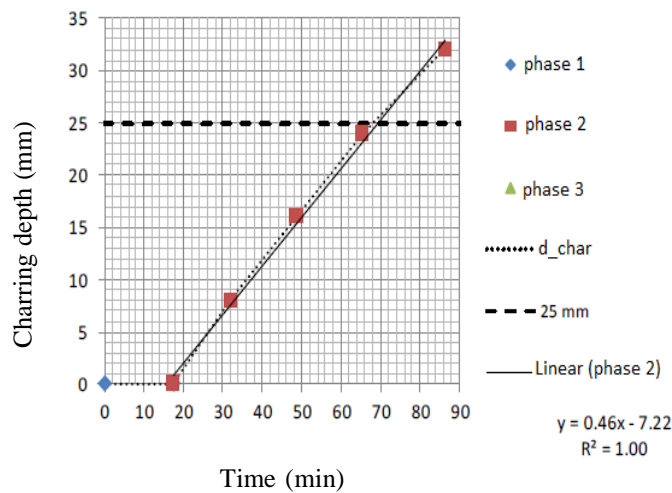
Charring depth and charring rate (sample 13)

Phase	t (min)	d_{char} (mm)	$\Delta d_{char}/\Delta t$ (mm/min)	Slope (mm/min)	Intercept (mm)
1	0.0	0			
	17.4	0			
2	17.4	0			
	32.0	8	0.55		
	48.6	16	0.48	0.46	-7.2
	65.6	24	0.47		
	86.4	32	0.38		

y = 0.46x - 7.22
R² = 1.00

Figure 106. Charring depth and charring rate of sample 13.

$t_{ch} = 17.4$ min   the time of start of charring
$ß_2 = 0.46$ mm/min   charring rate under protection
$t_f = $ N/A min   the time of loss of stickability of the fire protection system

Sample 14 with the fire protection layer having a thickness of 37.7 mm.
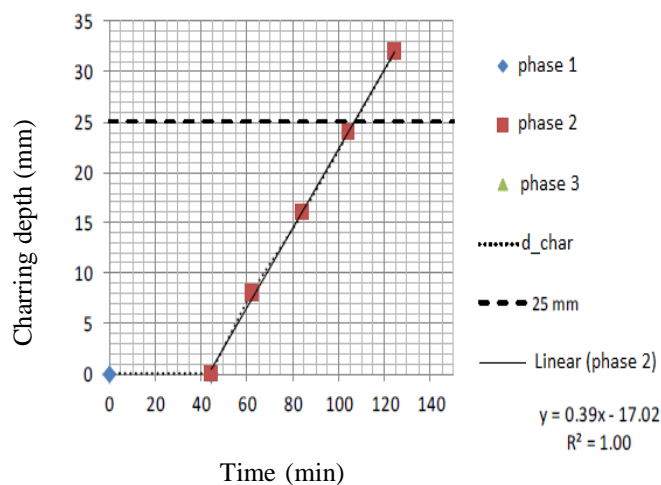
Charring depth and charring rate (sample 14)

phase	t (min)	d_{char} (mm)	$\Delta d_{char}/\Delta t$ (mm/min)	Slope (mm/min)	Intercept (mm)
1	0.0	0			
	44.3	0			
2	44.3	0			
	62.0	8	0.45		
	84.2	16	0.36	0.39	-17.0
	104.5	24	0.39		
	124.6	32	0.40		

y = 0.39x - 17.02
R² = 1.00

Figure 107. Charring depth and charring rate of sample 14.

$t_{ch} = 44.3$ min   the time of start of charring
$ß_2 = 0.39$ mm/min   charring rate under protection
$t_f = $ N/A min   the time of loss of stickability of the fire protection system

Sample 15 with the fire protection layer having a thickness of 37.1 mm.

Charring depth and charring rate (sample 15)

phase	t (min)	d_{char} (mm)	$\Delta d_{char}/\Delta t$ (mm/min)	Slope (mm/min)	Intercept (mm)
1	0.0	0			
	46.7	0			
2	46.7	0		0.40	-19.2
	68.2	8	0.37		
	88.1	16	0.40		
	107.9	24	0.40		
	126.1	32	0.44		
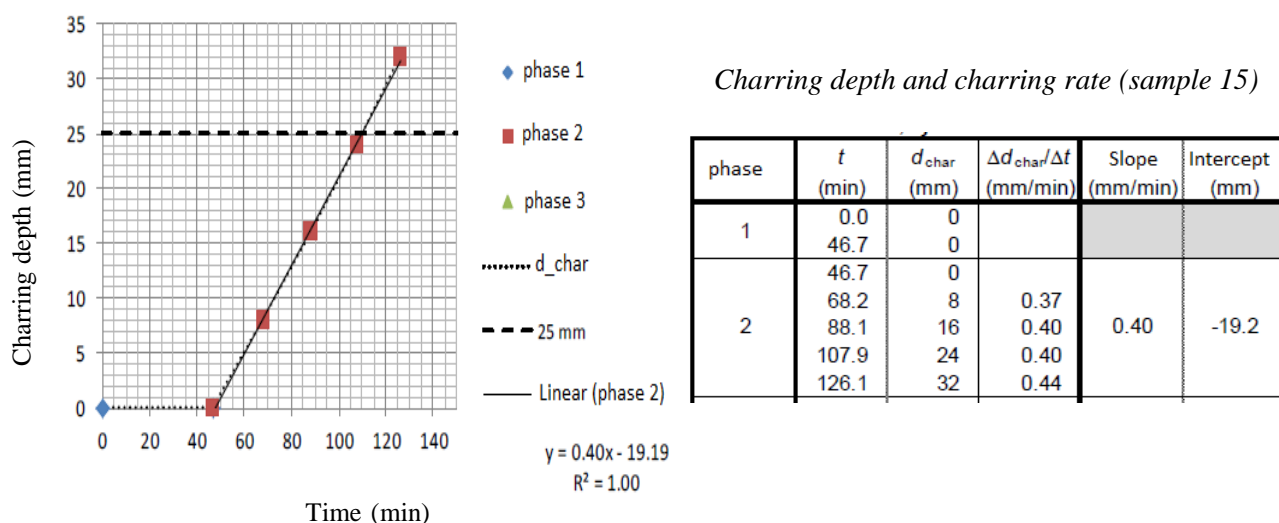
Figure 108. Charring depth and charring rate of sample 15.

$t_{ch} =$	46.7	min	the time of start of charring
$\beta_2 =$	0.4	mm/min	charring rate under protection
$t_f =$	N/A	min	the time of loss of stickability of the fire protection system

Regression analysis

The results of the regression analysis for the dependence of the different samples from the OSB panels according to the standard prEN 13381-7: 2017-07 and Eurocode 5 (ČSN EN 1395-1-2) are summarized below.

Sample	Test date	Thickness protection d_p (mm)	Charring rate (without/with protection layer) (mm/min)		Protection coefficient k_2 (-)	Charring time t_{ch} (mm)
11	18-01-05	0	ß	0.88	1.00	1.3
7	18-05-23	0		1.00	1.00	1.4
Average		0		0.94		
12	18-01-05	5.8	β_2	0.67	0.713	2.9
13	18-01-05	5.4		0.69	0.734	2.7
14	18-01-05	10.7		0.55	0.585	10.7
15	18-01-05	11.4		0.51	0.543	12.9
16	18-01-05	18.9		0.44	0.468	17.7
17	18-01-05	18.0		0.47	0.500	19.1
8	18-05-23	21.4		0.57	0.606	15.9
9	18-05-23	21.0		0.46	0.489	18.7
10	18-05-23	10.2		0.55	0.585	6.6
11	18-05-23	10.0		0.65	0.691	6.6
12	18-05-23	20.4		0.49	0.521	17.1
13	18-05-23	21.0		0.46	0.489	17.4
14	18-05-23	37.7		0.39	0.415	44.3
15	18-05-23	37.1		0.40	0.426	46.7

Regression (polynomial 2nd row)

Thickness protection d_p (mm)	Charring rate under protection β_2 (mm/min)	Coefficient protection k_2 (-)	Charring time t_{ch} (mm)
10.0	0.59	0.628	7.6
20.0	0.48	0.505	17.9
30.0	0.41	0.439	32.1
40.0	0.40	0.429	50.1
a_0	7.59E-01	8.08E-01	9.78E-01
a_1	-1.95E-02	-2.08E-02	4.68E-01
a_2	2.66E-04	2.83E-04	1.90E-02

d_p	(mm)	thickness of protection layer
β	(mm/min)	charring rate of the unprotection sample
		where $\beta = \beta_0$ (rate of one-dimensional carbonation)
β_2	(mm/min)	charring rate of the sample with the protection layer
k_2	(-)	coefficient of protection
t_{ch}	(min)	the time of start of charring

$$y = 2.66E\text{-}04x^2 - 1.95E\text{-}02x + 7.59E\text{-}01$$
$$R^2 = 7.91E\text{-}01$$
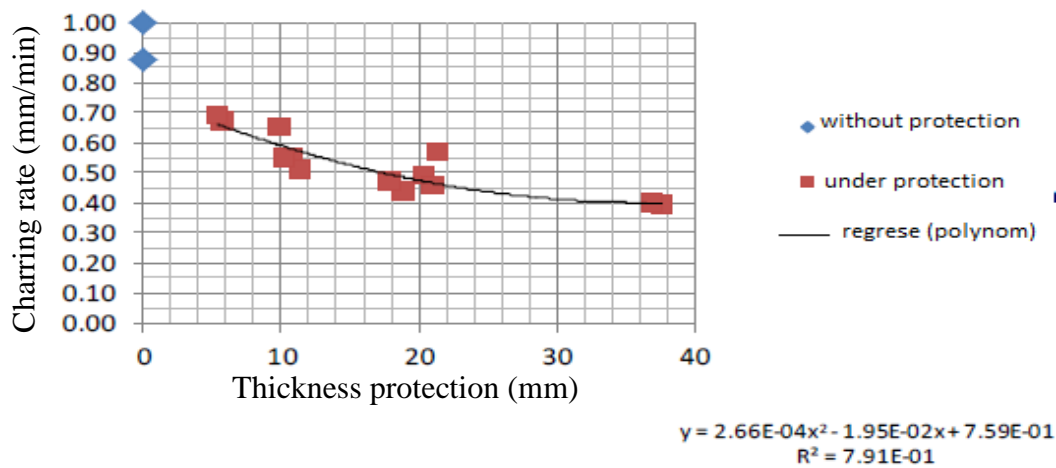
Figure 109. Charring rate depending on the thickness of the protection layer.

$$y = 1.90E\text{-}02x^2 + 4.68E\text{-}01x + 9.78E\text{-}01$$
$$R^2 = 9.70E\text{-}01$$
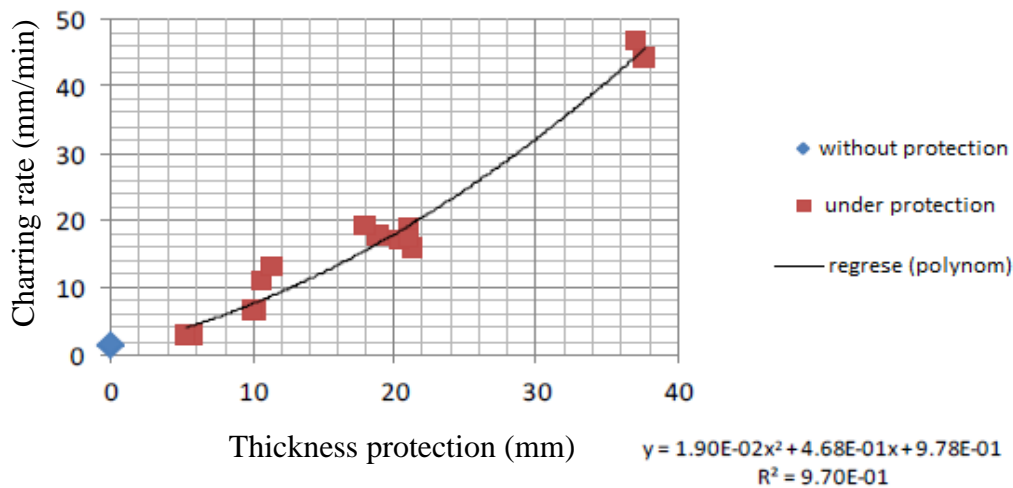
Figure 110. Coefficient of protection depending on the thickness of the protection layer.

$$y = 2.83E\text{-}04x^2 - 2.08E\text{-}02x + 8.08E\text{-}01$$
$$R^2 = 7.91E\text{-}01$$
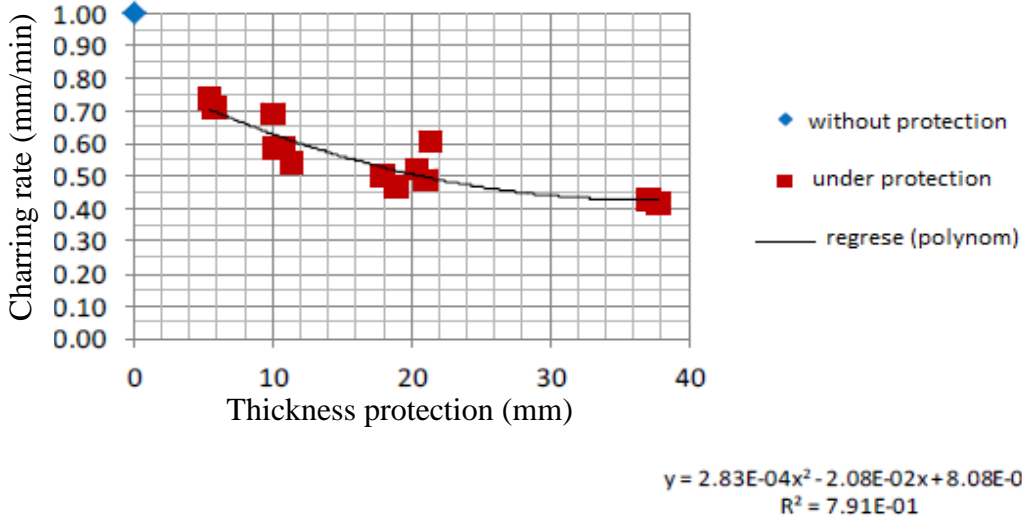
Figure 111. The time of start of charring depending on the thickness of the protection layer.

Samples before the test

Figure 112. Samples 11,7,17,16 (1st row) and 12,9,8,10 (2nd row) view from left to right.

Figure 113. Samples 15,14,13,6 (3rd row), 5,4,2,3,1 (4th row), view from left to right.

Sample after the test:

Figure 114. Samples 11,7,17,16 (1st row), 12, 9,8,10 (2 nd row), view from left to right.

Figure 115. Samples 15,14,6 (3rd row), 5, 4, 2 ,3,1 (4th row) view from left to right.

2. Fire protection system applied to steel plate

2.1 *General information*

The procedure for producing a test sample is described in subsection 1.2. Test samples were fabricated at the TUL and then were tested at Pavus a.s.

The GF protection layer for passive fire-resistance was coated on the surface of test samples. The process of fabricating the protected GF layer for the steel plate is portrayed in subsection 1.2.

2.2 *Performance of the test*

General

The test was performed on 5 January 2018 using the standard ČSN EN 1363-1 and EAD 350140-00-1106 art. E.9.

Conditioning of samples

From 20 December 2017 to 5 January 2018, the samples were stored in the environment with an air temperature of 21 - 25 °C and relative humidity of 51 - 56%.

Preparing the furnace for test samples

The samples were attached to a vertical wall of 3 m (width) x 3 m (height) x 0.25 m (thickness) in the test furnace. The wall was constructed of cellular concrete blocks YTONG P-500.

The samples were insulated on the unheated side with Rockwool Techrock 100 stone wool boards with a thickness of 50 mm and a bulk density of 100 kg / m^3 supplied from the manufacturer ROCKWOOL, a.s.

Furnace regulation

A system of natural gas heated the test furnace by the standard ČSN EN 1363-1 Art. 5.

The plastic of thermoelectric cell (DST) measured the temperatures in the furnace according to the standard ČSN EN 1363-1 Art. 4.5.1.1:

$$T/°C = 345 \log 10(8t/min + 1) + 20 \qquad (3)$$

Where T (°C) is the standard required oven temperature at time t (min).

Tolerances of the average temperature in the furnace are given according to the standard ČSN EN 1363-1 Art. 5.1.2.

Legend

TC	thermoelectric cell
PST	the plastic of thermoelectric cell
DST	board temperature sensor containing PTC ø 1 mm
HS	heated side of the sample
US	unheated side of the sample

2.3 *The subject of the test*

The selection of samples was performed according to the principles of the standard ČSN EN 13381-4 Article 6.6.3.1, as follows:

• four different sheet thicknesses t = (2, 3, 5, 10) mm representing steel profiles with three various cross-sectional factors ($A_p/V = s_p = 1/t_a$ for a perfectly thermally insulated unheated side of the sample);

• four different thicknesses of fire protection material d_p = (5, 10, 15, 20) mm.

Following ČSN EN 13381-4, the coefficients of the thickness/cross-section range used for the selection of samples according to equations (1) and (2) of this standard are given as follows.

The relation between the thickness of the fire protection material and the thickness range factor according to the standard is presented.

$$d_p = K_d (d_{max} - d_{min}) + d_{min} \qquad (1)$$

Where

d_p	is the thickness of the protective material corresponding to the thickness range factor K_d;
d_{max}	is the maximum thickness of the protective material corresponding to a thickness range factor of 1;

d_{min} is the minimum thickness of the protective material corresponding to a thickness range factor of 0.

The relationship between the cross-sectional coefficient and the cross-sectional extent coefficient is as follows.

$$s_p = K_s (s_{max} - s_{min}) + s_{min} \qquad (2)$$

Where

s_p is the cross-sectional factor corresponding to the cross-sectional extent factor Ks;

s_{max} is the maximum cross-sectional factor corresponding to the cross-sectional extent factor 1;

s_{min} is the minimum cross-sectional factor corresponding to the cross-sectional extent factor 0.

The selection of samples depending on the required values of the cross-sectional range/thickness coefficients is summarized in the following tables (the stated thicknesses of the fire protection material are nominal values):

Table 24. The cross-sectional range coefficient and thickness range factor.

Coefficient cross-sectional range k_s	Coefficient thickness range K_d			
	0.0 (d_{min})	0.2 to 0.5	0.5 to 0.8	1.0 (d_{max})
0.0 (S_{min})	Sample 1	Sample 2	Sample 3	
0.2 to 0.5	Sample 4		Sample 5	
0.5 to 0.8		Sample 6		Sample 7
1.0 (S_{max})		Sample 8		Sample 10

Table 25. Different cross-sectional coefficient of the protected profile.

Thickness plate (mm)	Coefficient s_p (m^{-1})	Coefficient K_s (-)	Thickness protection d_p (mm)	Coefficient K_d (-)
2	500	1.00	d_{max}/mm = 20	1.00
3	333	0.58	15	0.65
5	200	0.25	10	0.35
10	100	0.00	d_{min}/mm = 5	0.00

Ten samples were tested. Steel plates measuring with dimensions of 200 mm x 300 mm and four different thicknesses were used as the base plate to simulate four different section factor of the protected profile. The list of samples is given in the following table.

Table 26. Information on samples.

Sample	Substrate sample		Geopolymer composite thickness (mm)	Unheated side	Section factor A_p/V (m^{-1})
	Material	Thickness (mm)			
1		10	5.4 ±0.5		100
2		10	10.0 ±0.8		100
3		10	16.3 ±0.6		100
4		5	5.1 ±0.6		200
5	Steel plate	5	16.2 ±0.5	Mineral wool	200
6		3	11.4 ±0.5		333
7		3	20.6±0.7		333
8		2	11.7 ±0.5		500
9		2	16.6 ±0.9		500
10		2	20.7 ±0.8		500

Table 27. Apparent density of GF protection.

Sample Number	Avg. thickness (mm)	Weight (kg)	Apparent density (kg/m^3)
1	5.4	0.258	802
2	10.0	0.470	785
3	16.3	0.830	847
4	5.1	0.282	922
5	16.2	0.812	835
6	11.4	0.551	803
7	20.6	1.090	882
8	11.7	0.574	818
9	16.6	0.861	862
10	20.7	1.093	880
Selection average			844
Selection standard deviation			43
Extended uncertainty			87

Legend:

Thickness of fire protection material = total sample thickness - thickness plate

Weight plate = 0.2 m * 0.3 m * thickness plate * 7 850 kg / m^3

Weight of fire protection material = weight of the sample - weight of the plate steel

Apparent density of fire protection material = weight of fire protection material /

(0.2 m * 0.3 m * thickness of fire protection material)

Pressure and temperature in the furnace
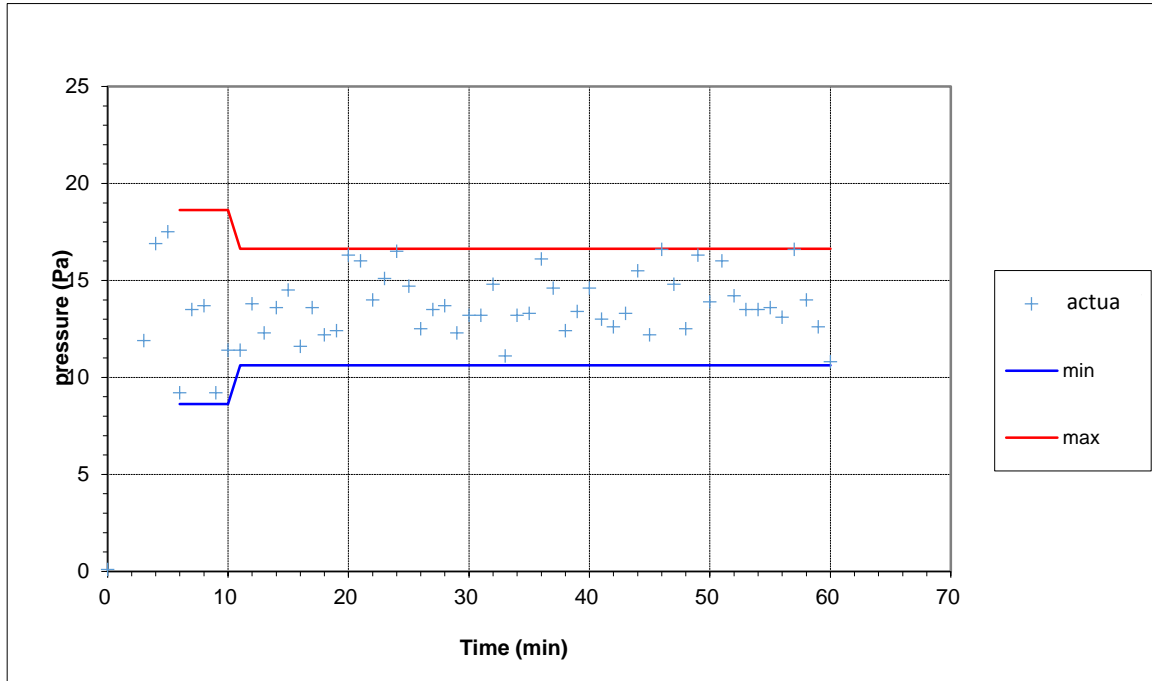
Figure 116. Pressure in a furnace, according to CSN EN 1363-1: 5.2.
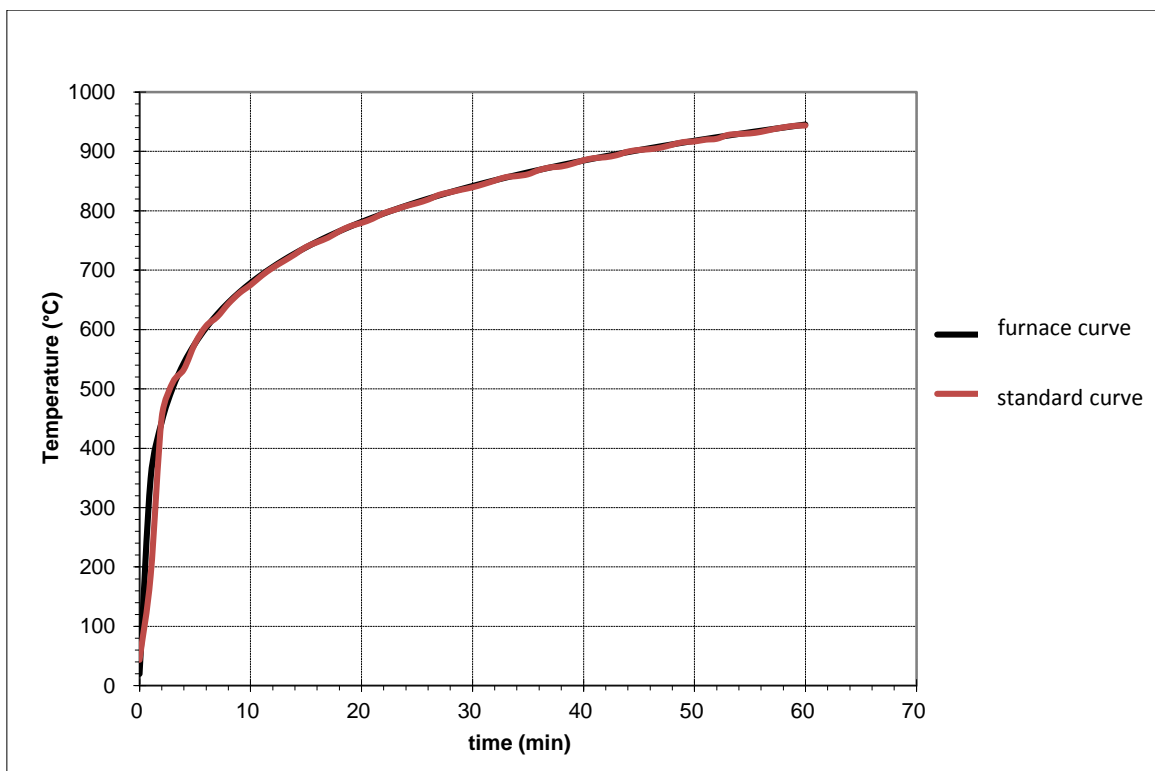
Figure 117. Average temperature in a furnace, according to CSN EN 1363-1: 5.1.

2.4 *Measured results*

The temperatures of measured samples using different thermocouples are presented in Tables 28 and 29. The average temperatures of samples are given in Table 30 and Figures 118-120.

Table 28. The sample temperature measured by different thermocouples (samples 1-5).

time	sample 1		sample 2		sample 3		sample 4		sample 5	
	temperature steel plate, **thermocouple number**									
	20	*21*	*22*	*23*	*24*	*25*	*26*	*27*	*28*	*29*
(min)	(°C)	(°C)	(°C)	(°C)	(°C)	(°C)	(°C)	(°C)	(°C)	(°C)
0	10	10	10	10	10	10	10	10	10	10
5	104	103	73	74	42	42	136	139	67	67
10	198	197	126	127	88	88	296	295	104	104
15	292	291	198	201	113	111	424	420	163	159
20	381	379	266	270	157	156	518	515	240	238
25	456	455	334	338	208	207	593	590	313	310
30	525	524	399	404	259	258	657	655	381	379
35	584	583	455	460	308	307	708	706	439	437
40	635	634	508	513	356	355	744	744	493	491
45	679	678	556	560	402	400	771	774	542	539
50	717	716	598	602	446	443	792	796	586	583
55	740	741	638	642	488	484	810	814	626	623
60	764	766	672	676	526	522	827	830	661	659

Table 29. The sample temperature measured by different thermocouples (samples 6-10).

time	sample 6		sample 7		sample 8		sample 9		sample 10	
	temperature steel plate, **thermocouple number**									
	30	*31*	*32*	*33*	*34*	*35*	*36*	*37*	*38*	*39*
(min)	(°C)	(°C)	(°C)	(°C)	(°C)	(°C)	(°C)	(°C)	(°C)	(°C)
0	10	10	10	10	10	10	10	10	10	10
5	98	97	64	64	102	105	90	89	62	62
10	200	195	98	98	241	250	106	109	98	98
15	330	322	120	123	390	397	205	206	111	109
20	438	430	203	202	498	503	323	321	186	181
25	521	513	285	284	578	583	425	422	275	272
30	586	578	360	358	641	646	501	500	358	355
35	642	634	427	426	693	698	567	566	432	429
40	688	680	485	484	734	738	619	618	493	491
45	725	718	537	536	765	767	665	664	547	544
50	749	743	582	581	788	794	702	702	592	589
55	773	767	623	623	806	813	731	734	633	631
60	792	787	661	659	820	828	750	758	669	667

Table 30. The average temperature of samples.

Sample	1	2	3	4	5	6	7	8	9	10
A_p/V*m	100	100	100	200	200	333	333	500	500	500
d_p/mm	5.4	10.0	16.3	5.1	16.2	11.4	20.6	11.7	16.6	20.7
time	Average temperature									
(min)	(°C)	(°C)	(°C)	(°C)	(°C)	(°C)	(°C)	(°C)	(°C)	(°C)
0	10	10	10	10	10	10	10	10	10	10
5	103	74	42	137	67	97	64	104	89	62
10	197	126	88	295	104	198	98	245	107	98
15	292	200	112	422	161	326	121	394	205	110
20	380	268	157	516	239	434	202	500	322	183
25	456	336	208	592	311	517	284	581	424	274
30	525	401	259	656	380	582	359	643	500	357
35	583	457	307	707	438	638	427	696	566	431
40	635	510	355	744	492	684	485	736	619	492
45	678	558	401	772	541	721	536	766	664	545
50	717	600	444	794	584	746	582	791	702	590
55	740	640	486	812	624	770	623	810	732	632
60	765	674	524	828	660	789	660	824	754	668
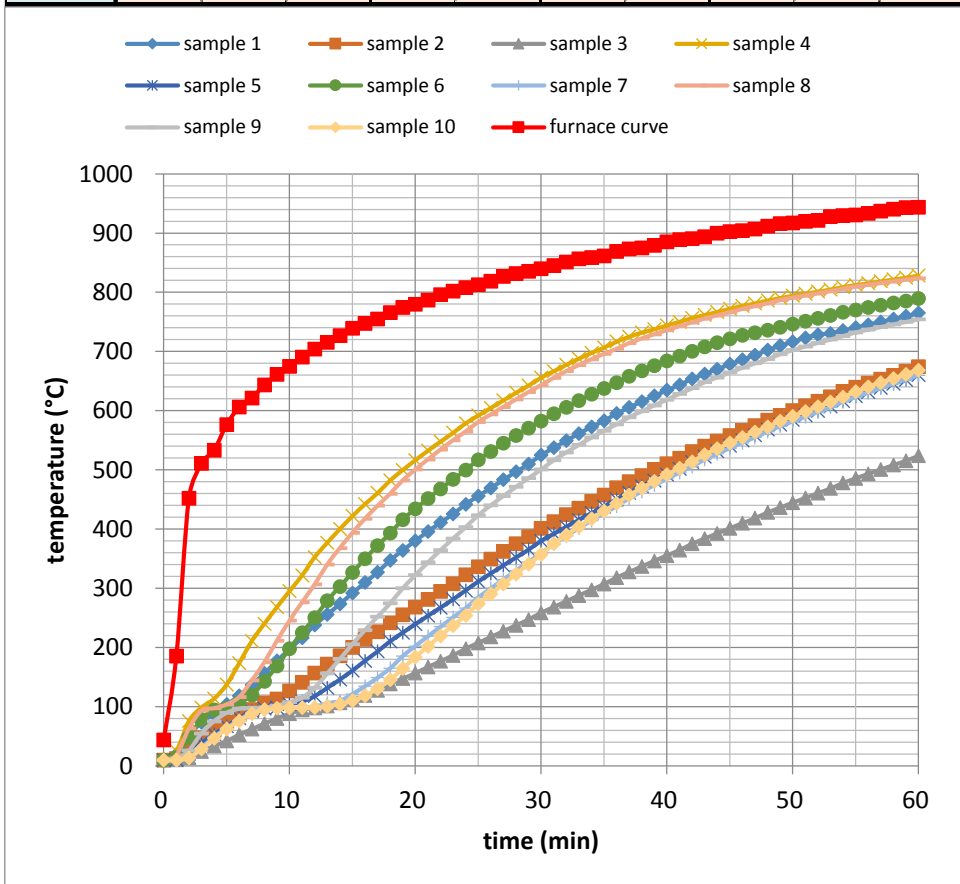
Figure 118. The average temperature of samples.

Legend:

d_p The thickness of fire protection layer, in mm

A_p/V The cross-section factor of the protected steel element, in m^{-1}, see ČSN EN 13381-4 Art. 3.1.9.1 and Figure 1
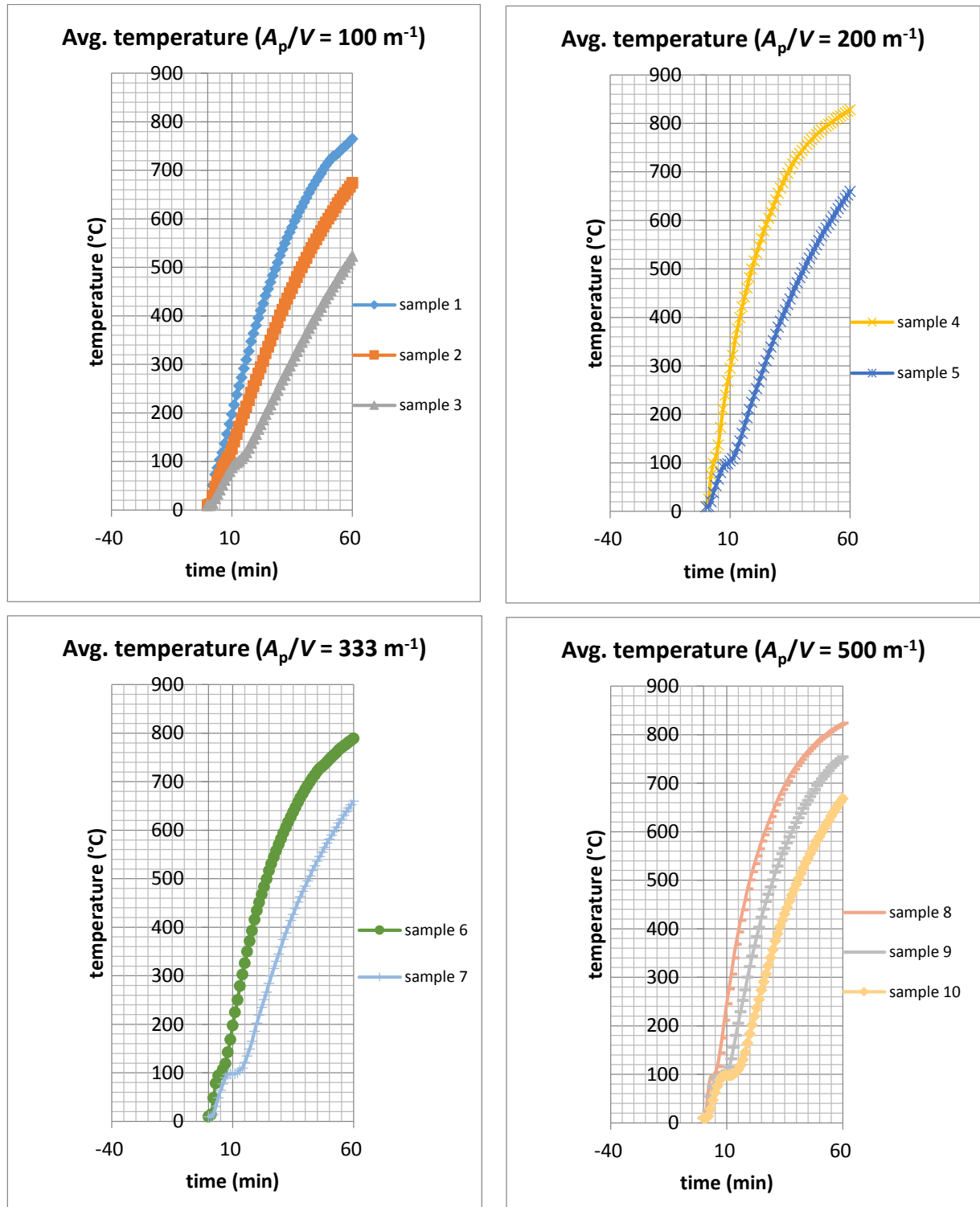
Figure 119. The average temperature for a given nominal thickness of the substrate (the cross-section factor A_p/V).
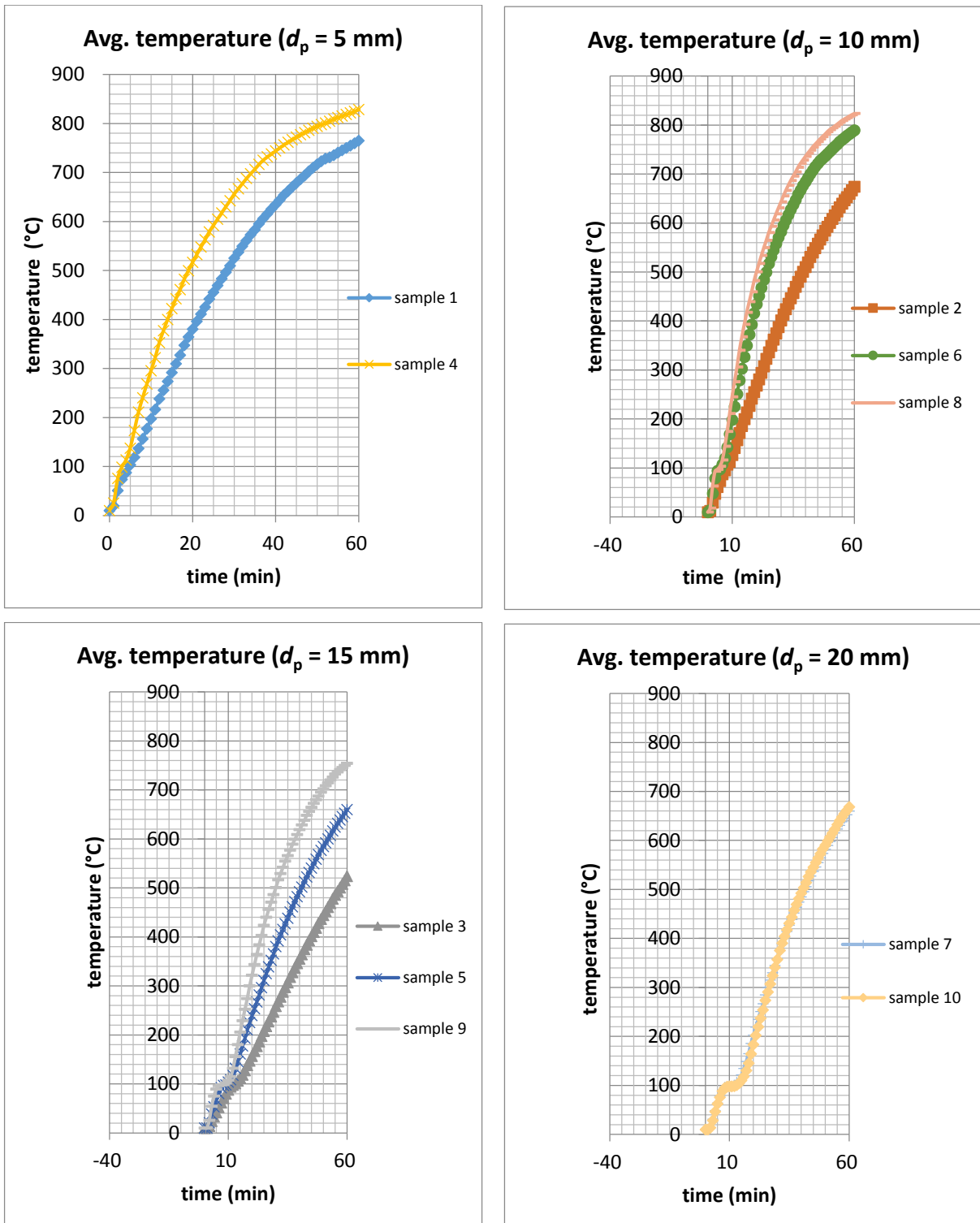
Figure 120. The average temperature of samples for a given nominal thickness of d_p.

The time to reach design temperature

The measured periods at design temperatures are presented in table 31.

Table 31. The time to reach temperature.

sample	1	2	3	4	5	6	7	8	9	10
A_p/V*m	100	100	100	200	200	333	333	500	500	500
d_p/mm	5.4	10.0	16.3	5.1	16.2	11.4	20.6	11.7	16.6	20.7
Tem. Design (°C)	The time to reach design temperature									
	(min)	(min)	(min)	(min)	(min)	(min)	(min)	(min)	(min)	(min)
350	18.2	26.1	39.4	11.9	27.9	16.0	29.4	13.4	21.3	29.6
400	21.3	29.9	44.8	14.0	31.7	18.3	32.9	15.3	23.8	32.7
450	24.6	34.3	50.7	16.4	36.0	20.9	36.9	17.5	26.6	36.5
500	28.3	39.0	56.9	19.0	40.8	24.0	41.5	20.0	30.0	40.7
550	32.1	44.1	N/A	22.2	46.0	27.4	46.5	23.0	33.6	45.5
600	36.5	50.0	N/A	25.6	52.0	31.5	52.3	26.5	38.1	51.2
650	41.6	56.5	N/A	29.6	58.7	36.3	58.7	30.6	43.2	57.4
700	47.7	N/A	N/A	34.3	N/A	42.0	N/A	35.5	49.7	N/A
750	57.0	N/A	N/A	41.0	N/A	50.8	N/A	42.2	59.0	N/A

Legend

d_p The thickness of fire protection material, in mm

A_p/V The cross-section factor of the protected steel element, in m^{-1}, see ČSN EN 13381-4 Art. 3.1.9.1 and Figure 1

Evaluation of measured results

The samples simulated to some extent protected short steel profiles with a cross-section factor $A_p/V = 1/t_a$ and a thickness of fire protection layer d_p. The test results can be evaluated according to ČSN EN 13381-4 part 13 and Annex E.5 ("Numerical regression analysis"NRA). The regression function is described by the relation (E.12) in Article E.5.3 of the standard ČSN EN 13381-4 as:

$$t = a_0 + a_1 d_p + a_2 \frac{d_p}{A_P/V} + A_3 \theta_a + a_4 d_p \theta_a + a_5 d_p \frac{\theta_a}{A_P/V} + a_6 \frac{\theta_a}{A_p/V} + a_6 \frac{1}{A_p/V} \tag{1}$$

Where:

t	the time of reaching the steel temperature Θ_a	(min)
d_p	the thickness protection material	(mm)
A_p/V	the cross-section factor protection steel profile	(m^{-1})
a_i	regression coefficient	i=0,1…7;
Θ_a	steel temperature	(°C)

Note: For this regression evaluation the cross-section factor of the unprotected profile A_m / V was replaced by the cross-section factor of the protected profile A_p/V.

The input data listed in Table 27 were used to calculate regression coefficients according to ČSN EN 13381-4 Art. E.5.4. "Characterization data" of the fire protection system:

Regression coefficient	unmodified	modified
a_0	-2.269730E+01	-2.180400E+01
a_1	6.588565E-01	6.329259E-01
a_2	5.992840E+01	5.756980E+01
a_3	4.185922E-02	4.021177E-02
a_4	2.067953E-03	1.986565E-03
a_5	2.546356E-02	2.446139E-02
a_6	3.814886E+00	3.664744E+00
a_7	-3.940369E+01	-3.785288E+01

Linear modification factor x = 0.960643

The maximum cross-section factor of a protected steel element is derived from the equation (1) as:

$$(A_P/V)_{max} = \frac{a_2 d_p + a_5 d_p \theta + a_6 \theta + a_7}{t_R - (a_0 + a_1 d_p + a_3 \theta + a_4 d_p \theta)} \qquad (2)$$

Where:

t	required time for fire-resistance	(min)
d_p	thickness protection layer	(mm)
$(A_p/V)_{max}$	the maximum cross-sectional coefficient of the protected steel element, the temperature of which at the time of the required fire-resistance t_R does not exceed the design temperature Θ	(m^{-1})
a_i	modified regression coefficient	i=0,1…7;
Θ	design temperature steel	(°C)

- Evaluation results calculated from relation (2) in the range time for fire-resistance (15, 20, 30, 45, 60, 90, 120) min;

- thicknesses of fire protection layer (5, 10, 15, 20, 25) mm, where the protection thickness of 25 mm has not been tested, and the corresponding extrapolated results are given in italics;

- design temperatures (350 - 750) °C;

- cross-section factor of the protected steel profile (50/100 to 500) m^{-1} for protection copying the cross-sectional surface, cross-sectional coefficients from the range (50 to 100) m^{-1} are the results of extrapolation.

The evaluation results are summarized in the following table.

Fire-resistance (min)	Thickness protection (mm)	maximum section factor (m⁻¹), for which temperature is below Design temperature (°C)								
		350	400	450	500	550	600	650	700	750
15	5	98	130	176	250	385	500	500	500	500
	10	202	326	500	500	500	500	500	500	500
	15	500	500	500	500	500	500	500	500	500
20	5	75	95	122	158	211	295	449	500	500
	10	132	184	272	459	500	500	500	500	500
	15	287	500	500	500	500	500	500	500	500
	20	500	500	500	500	500	500	500	500	500
30	5	51	62	75	91	111	136	169	214	280
	10	78	98	125	161	216	306	479	500	500
	15	126	170	244	389	500	500	500	500	500
	20	230	387	500	500	500	500	500	500	500
	25	500	500	500	500	500	500	500	500	500
45	5	N/A	N/A	N/A	56	65	75	87	102	119
	10	N/A	58	69	82	98	118	144	178	225
	15	68	83	102	127	162	212	292	439	500
	20	98	125	164	225	334	500	500	500	500
	25	148	207	316	500	500	500	500	500	500
	30	251	437	500	500	500	500	500	500	500
60	5	N/A	N/A	N/A	N/A	N/A	52	59	67	75
	10	N/A	N/A	N/A	55	63	73	85	98	114
	15	N/A	55	65	76	90	107	129	157	194
	20	62	75	90	109	135	170	222	305	460
	25	84	104	130	168	227	329	500	500	500
	30	116	151	205	301	500	500	500	500	500
90	≤ 15	N/A	N/A	N/A	N/A	N/A	54	61	68	77
	20	N/A	N/A	N/A	54	62	70	81	93	108
	25	N/A	52	60	69	81	94	111	133	161
	30	56	65	77	91	108	131	163	208	278
120	≤ 25	N/A	N/A	N/A	N/A	N/A	55	62	70	79
	30	N/A	N/A	N/A	53	60	69	78	90	104

Extrapolation for $A_p/V < 100$ m⁻¹ is informative

Photo documentation

Figure 121. The sample before the test.

Figure 122. The sample after 60 min testing. The view from outside.

Figure 123. The sample before the test.

Sample 3, protection
thickness of 16.3 mm

Sample 2, protection
thickness 10mm

Sample 1, protection
thickness 5.4 mm

Sample 6, protection
thickness 11.4 mm

Sample 5, protection
thickness 16.2 mm

Sample 4, protection
thickness 5.1 mm

Sample 9, protection
thickness 16.6 mm

Sample 3, protection
thickness 11.7 mm

Sample 3, protection
thickness 20.6 mm

Sample 3, protection
thickness 20.7 mm

Figure 124. The samples after the test.

Chapter 5. PRACTICAL APPLICATION

1. Introduction

Fire-resistance of the carbon steel pillars of the liquefied gas tank (Figure 125) of Plaga a.s. is necessary. Therefore, we performed a passive protection solution for the pillars by coating a GF layer on their surface in October 2018.

The purpose of the project is to protect the steel pillars from the fire damage. The GF layer with a thickness of 20 mm was coated on 48 pillars with a diameter of 273 mm and a length of 4200 mm (Figure 126).

Raw materials and the mixing process were presented in subsections 1.2, and the spraying technique was described in subsection 2.2 of the chapter 2. High-pressure sandblasting was used to treat the surface of the pillars before GF spraying (Figure 127).

2. Photo documentation

The gas tank in Plaga a.s., and spray-coating the GF on the surface of the pillars by the thesis author are depicted in Figures 125 and 126, respectively.

Figure 125. The gas tank in Plaga a.s.

Figure 126. Spray-coating the GF on the surface of the pillars by the thesis author.

Figure 127. The surface of the pillars before (left) and after (right) spray-coating the GF layer.

Chapter 6. CONCLUSIONS AND FURTHER RESEARCH

The thesis presents the research results of fire-resistance of GFs coated on the surface of the base building materials (steel, wood, concrete, polystyrene, and aluminum). The main aim of the thesis is to find out the most appropriate GF for fire-resistance. In addition, improving the mechanical properties of GFs were conducted and presented in the thesis. The experimental investigation of GFs for fire-resistance was funded by the project "Application of GFs as a fire barrier (AGK)" at TUL from 2015-2019. The main results of this thesis are as follows.

Results of the fire-resistant test conducted at the TUL:

The OSB panel 500 mm x 500 mm x 22 mm coated with 20 mm thickness of the GF layer resisted the fire with the longest time of 99 min. Its fire-resisted time was 4.5 times higher than that of the OSB panel without a GF layer. The maximal temperature in the furnace did not exceed 800 °C.

The longest fire-resistant time of the steel plate 500 mm x 500 mm x 2 mm coated by the protective GF lamina with a thickness of 10 mm was 134 min. It was 14.8 times higher than that of the steel plate without the GF layer. The maximum temperature in the furnace did not exceed 900 °C

The concrete slab 300 mm x 300 mm x 25 mm covered by the GF layer with a thickness of 50 mm resisted the fire with the longest time of 100 min, and its fire-resistant time was 9.18 times higher than that of the concrete slab without the GF layer. The highest temperature in the furnace did not exceed 1050 °C.

The polystyrene board 500 mm x 500 mm x 50 mm coated by the GF layer with a thickness of 10 mm resisted the fire at the longest time of 15 min. The maximum temperature in the furnace did not exceed 700 °C.

The longest fire-resisted time of the aluminum plate 300 mm x 300 mm x 2 mm covered by 20 mm thickness of the GF layer was 125 min. This fire-resistant time was 30 times greater than that of the aluminum plate without the GF layer. The maximal temperature in the furnace did not exceed 600 °C.

The fire-resistant time of the carbon steel pillars with 273 mm in diameter and 10 mm in thickness coated by the GF layer with a thickness of 6 mm was 29 min when the outer-surface temperature reached 600ºC, while the temperature in the did not exceed 1000 °C.

Results of fire-resisted measurements performed at Pavus a.s. (Praha):

The concrete slab 300 mm x 300 mm x 140 mm coated by the GF layer with a thickness of 23.2 mm resisted the fire at the longest time of 180 min, and its fire-resisted time was three times higher than that of the concrete slab without the GF layer. The maximal

temperature in the furnace did not exceed 1100 °C, while the outside temperature of the slab was 414 °C.

The longest fire-resistant time of the OSB panel 495 mm x 495 mm x 54 mm covered by the GF lamina with a thickness of 37.7 mm was 130 min. It was 3.8 times higher than that of the OSB panel without the GF layer. At the same time, the maximum temperature in the furnace did not exceed 1065 °C.

The steel plate 300 mm x 200 mm x 2 mm coated with 20.7 mm thickness of the GF layer resisted the fire with the longest time of 50 min. In addition, the temperature in the furnace did not exceed 910 °C.

Results from papers of the thesis author:

The measurement of thermal conductivity of GFs reinforced by basalt fibers was conducted and presented in the paper A. Results indicated that the basalt waste fiber has a significant effect on the mechanical properties of the GFs. It has been shown that a higher addition of basalt waste fibers reduces the thermal conductivity of the GFs due to small, homogenized and regular pore distribution. The use of basalt waste fiber as a by-product for reinforcing the GFs conducted at only the ambient temperature significantly improves the physical, thermal and mechanical properties of the GFs, enabling a reduction in the cost of the GFs and creating an environmentally friendly material. The lowest thermal conductivity of the GFs is 0.13 $W \cdot m^{-1} \cdot K^{-1}$. Moreover, the thermal conductivity is increased by increasing the fillers with a larger proportion of chopped basalt fibers. Besides, GFs reinforced with chopped basalt fibers have improved the durability of GFs. The measured compressive and flexural strengths of GFs are about 5 - 9 MPa and 2 - 3 MPa, respectively. In addition, the silica fume considered as a harmful waste by-product was added to GFs for improving their mechanical properties and pores.

In the paper B, GFs containing waste basalt fiber (10, 30, and 50 wt. %) were exposed to elevated temperatures of 200, 400, 600, 800 and 1000 °C to investigate the effects of fiber content and temperature on their mechanical properties. The compressive and flexural strengths of the GFs increased with increasing the fiber content. Although the compressive and flexural strengths of the composites at low fiber content (10 wt. %) decreased with the rise of the temperature till 800°C, they enhanced significantly at high fiber contents. The maximal strengths of the composites achieved with the weight content of 50% and at the temperature of 1000°C. Therefore, it could be confirmed that the GF composites were stable at high temperatures. Reinforcing the right content of basalt fibers in the geopolymer can be created a GF having the heat-resistant property. Moreover, the research showed the influence of the fiber content on the formation of pores, crack propagation and the formation of structural changes of the GF.

In the paper C, the GF was reinforced with flax fibers in nonwoven fabric, and the fibers spread over the entire board thickness. Flax reinforcement of GFs with a density of 448 kg/m^3 increased the impact bending of composites up to 0.62 J/cm^2, and the variability also increased. Although the impact bending of flax-reinforced GFs was statistically significantly higher than that of basalt-reinforced GFs, the bending strength of both composites reinforced

with fibers was comparable. Geopolymers reinforced with basalt exhibited a different pattern of joint failure than geopolymers reinforced with flax. While basalt fibers peeled off when the composite was breached, flax fibers remained anchored in the geopolymer and ruptured.

Paper D investigated the properties of a sandwich panel that was made from recycled materials and coated by a GF layer and a nanofibrous membrane. It was shown that the addition of wheat husk to the thermal insulation core increased the thermal conductivity coefficient up to 0.0452 W/ (m.K), but this negative increase can be compensated by the increase in specific heat capacity of the insulation core with husks up to the value of 0.126 MJ/ (m^3.K). The theoretical value of the thermal conductivity coefficient of the developed panels achieves excellent values on the level of 0.05 W/ (m.K). The sandwich panel coated by the GF layer and nanofibrous membrane can be used for thermal insulation, fire-resistance, and water resistance. The panel coated by the GF layer resisted the fire for the longest time of 13 min. In addition, the nanofibrous membrane covered on the panel enhanced the water-resistance with a column height of 0.8 m.

The paper E evaluates the physical and mechanical properties of the developed sandwich composite material based on particles of winter rapeseed stalks, GF and reinforcing lattices. The fundamental influence of particleboard density on the resulting mechanical properties of the entire sandwich panel was demonstrated. The density of the second layer of the sandwich panel and the GF did not have the same impact on its mechanical properties as the particleboard density. The reinforcing lattice made of basalt fiber positively influenced the mechanical properties of sandwich composites only if it was sufficiently anchored in the particleboard structure. The developed materials reached a higher bending strength than 0.3 MPa in only two cases, and the tensile strength perpendicular to the board plane was also low. However, these low values are due to the low density of the material and the low adhesive content. On the contrary, good thermal and fire protection properties were achieved, namely the thermal conductivity coefficient of the sandwich composite with the lowest density value was 0.111 W/ (m.K) and all developed sandwich composites resisted flame for more than 13 min.

In the paper F, the GFs were treated with two types of hydrophobic agents at the age of 7 days after casting. The physical-mechanical properties of GFs such as flexural strength, compressive strength, bulk density, water absorption capacity, and water absorption coefficient were measured and assessed. Samples with hydrophobic agents of Lukosil M130 (LS) have the bulk density higher than the hydrophobic samples of Lukofob ELX (LF) and untreated samples because holes on the surface of the sample are filled with hydrophobic agents. The physical and mechanical properties of the GFs treated by LS are better than those by LF. Moreover, using LS for surface treatment of the samples also improved the mechanical strength of GFs significantly if they are cured at high temperatures. The LF samples indicate that their total water absorption capacity is much higher than that of LS samples. The water absorptions of the LS and LF samples respectively was 8.58% and 35.49%, which was lower than the water absorption of untreated samples (47.41%). However, under capillary water uptake test, the water absorption coefficient of the LF samples was higher than that of the LS samples. The untreated sample had a high water

absorption coefficient of 90.39, whereas the LF sample and LS samples showed the values of 6.47 and 2.27, respectively. LS has proved that it is an excellent hydrophobic agent for surface treatment of the GF.

In conclusion, the author's research results have shown that a GF is an excellent coating material for the fire-resistant purpose at high-temperature.

Several topics for research, development, and application of geopolymer composite in the future are the following:

• Use geopolymer composite for creating molds that can withstand high temperatures,

• Apply geopolymer composite for decoration,

• Improving the durability of geopolymer composite by reinforcing natural fibers

• Optimize the adhesion of geopolymer composite on substrate materials.

• Use GFs for filtering toxins of water.

Chapter 7. SUMMARY OF APPENDED ARTICLES

Article A. *Thermal conductivity of reinforced geopolymer foam.*

Van Su Le, Pavlina Hajkova, Vladimir Kovacic, Totka Bakalova, Volesky Lukas, Chi Hiep Le, Kevin Ceccon Seifert, Amanda Pereira Peres, Petr Louda. Ceramics-Silikaty,63 (4),365-373, 2019.

Reinforced GFs were studied in this work as potential building materials. It has been widely assumed that for a given thermal conductivity λ [W·m⁻¹·K⁻¹], GFs can have a lighter density than other materials. The study sought to test this assumption by comparing the thermal conductivity between GFs. The thermal conductivity λ was measured using an ISOMET 2014 device. In all the experiments, the GFs were obtained by adding aluminum powder and several combinations: silica fume and fine sand reinforced by short basalt fibers. Curing was carried out at room temperature and then in a furnace at 70 °C. After the curing process, the properties of the samples were tested at 7 and 28 days. The results show that the thermal conductivity, porosity, compressive strength, flexural strength and density for all of the tests ranged in the following values: 0.13 - 0.359 W/m·K; 41.8 - 62.5 %; 1.94 - 9 MPa; 0.96 - 2.93 MPa; 546 - 1028 kg·m⁻³, respectively. It was proven that the filler in the GFs has a significant influence on the mechanical and physical properties of the tested samples.

The effect of the content of reinforcing fillers and fibers on the compressive and flexural strength and the thermal conductivity coefficient of GFs is shown in Figure 128. The formation of pores in a geopolymer composite is significantly affected by the percentage increase of aluminum powder and filler (Figure 129).
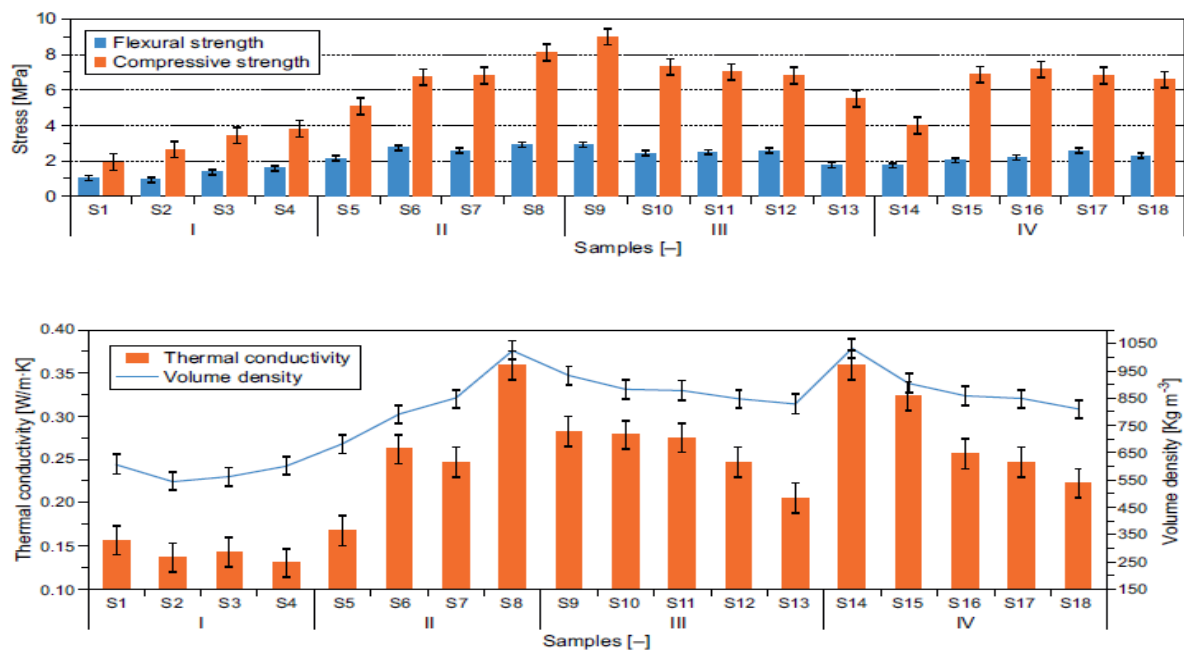
Figure 128. The compressive and flexural strength (up), and thermal conductivity and density of GFs (down).
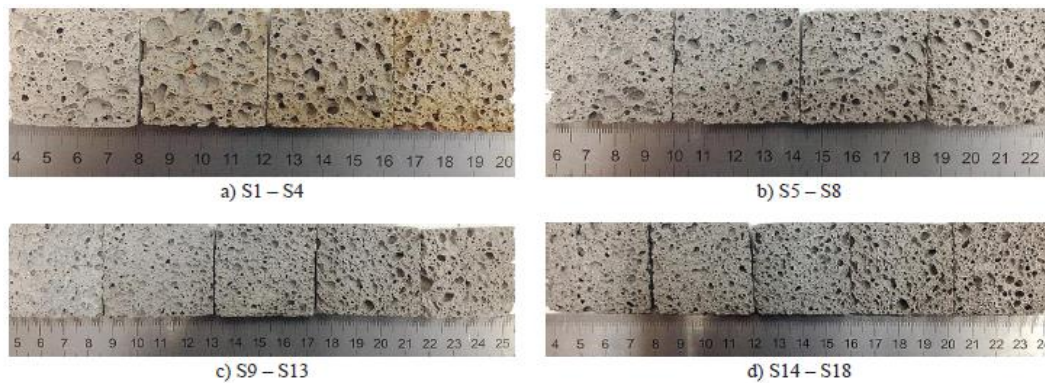
Figure 129. Photos are showing the different types of GFs with dimension 40 x 40 mm^2.

Article B. *Mechanical properties of geopolymer foam at high-temperature*

Van Su Le, Michal M. Szczypinski, Pavlina Hajkova, Vladimir Kovacic, Totka Bakalova, LukasVolesky, Le Chi Hiep, and Petr Louda. Science and Engineering of Composite Materials, 27 (4), 129-138, 2020.

In this work, GFs containing waste basalt fiber (10, 30, and 50 wt. %) were exposed to elevated temperatures of 200, 400, 600, 800 and 1000 °C. With an increase in high-temperature, the GF materials exhibits a decrease in compressive strength and bending strength. When heated above 600 °C, GF materials exhibit a significant reduction in mechanical properties. It shows clearly with the naked eye that surface cracks in case of samples containing 10% of basalt filler. However, when increasing fillers with basalt fibers up to 30% and 50%, the cracking of the sample surface is no longer visible to the naked eye. Especially when the temperature increases, the mechanical properties also increase without decreasing in the sample of 50% by weighing to the binder (see Figure 130).
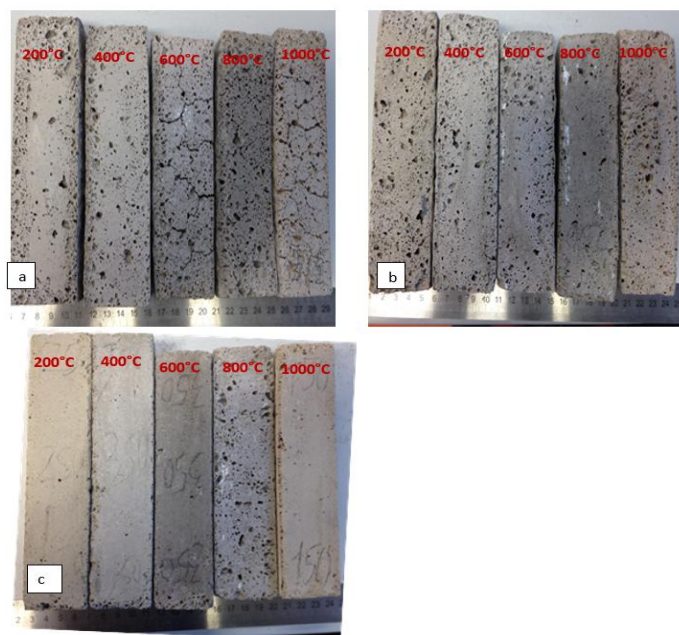
Figure 130. Color change and cracks occurrence of GFs with different content of basalt waste fiber a) 10%, b) 30% and c) 50% after heating at various temperatures.

The results show that reinforcing the GFs with basalt ground fibers improved the mechanical properties of GFs at high temperatures (Figure 131 and Figure 132).
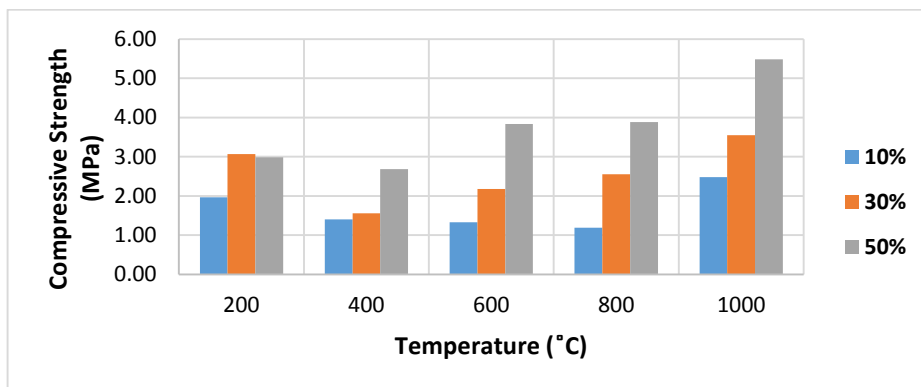
Figure 131. The compressive strength of GFs at different heating temperatures
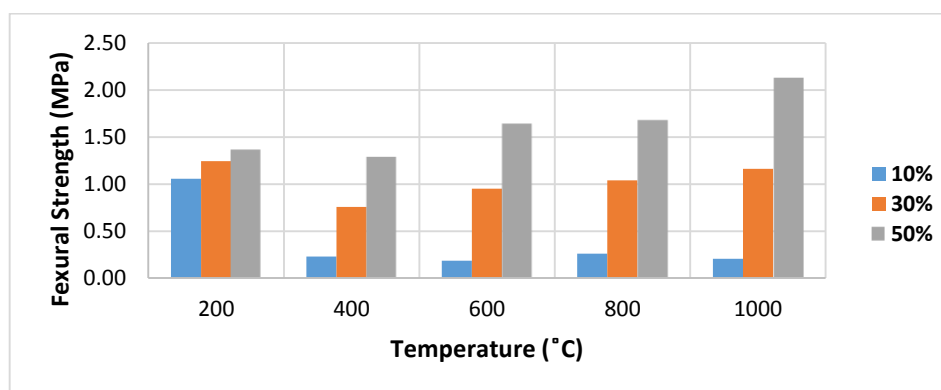
Figure 132. The flexural strength of GFs at different heating temperatures.

Article C. *Impact of flax and basalt fiber reinforcement on selected properties of geopolymer composites*

Miroslav Frydrych, Stepan Hysek, Ludmila Fridrichova, Su Le Van, Miroslav Herclik, Miroslava Pechociakova, Hiep Le Chi and Petr Louda. Sustainability, 1(12), 2019.

The submitted paper deals with the physical and mechanical properties of GF materials reinforced with natural fibers. For this study, we aimed to develop a GF reinforced with long flax fibers, which were implemented in the GF in the form of a nonwoven fabric that reinforced the structure of the GF over the entire thickness of the board. To compare the properties of the developed composite with natural fibers, a GF without fibers and a geopolymer reinforced with basalt fibers were also produced. The monitored mechanical properties were impact bending, bending strength and compressive strength. Differential scanning calorimetry (DSC), thermogravimetric analysis (TGA), Fourier transform infrared spectroscopy (FTIR) and microscopic analysis was also carried out.

The results clearly showed the positive effect of the addition of natural fibers on impact bending (Figure 133) and bending strength (Figure 134). However, the reinforcement of natural fibers in the form of a nonwoven fabric significantly increased the variability of the

properties of the developed composites (Figure 135). In addition, a different pattern of joint failure between the geopolymer reinforced with flax fibers and the geopolymer reinforced with basalt fibers as described in Figure 136.
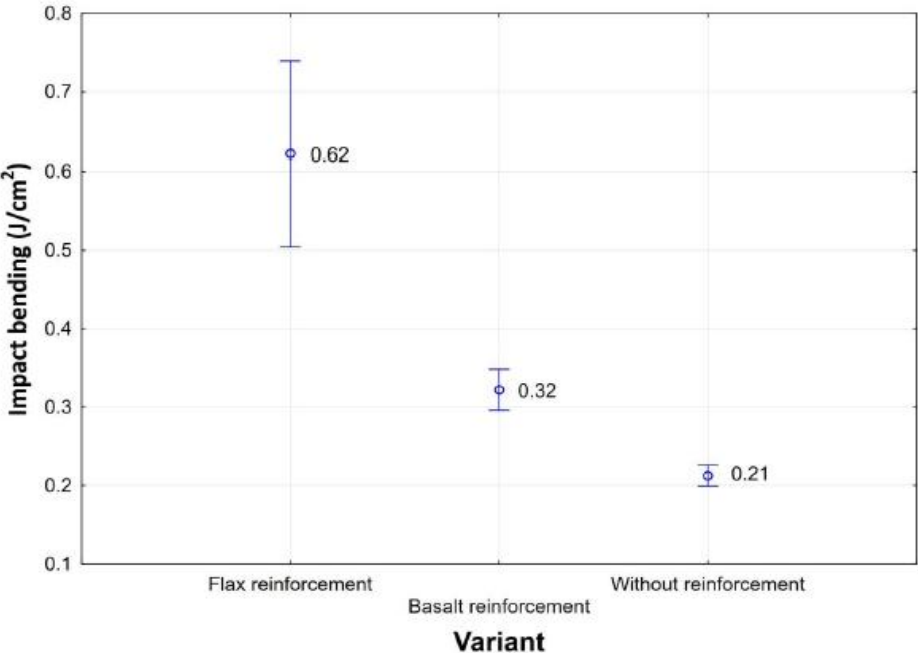
Figure 133. Impact bending of geopolymers reinforced with different fibers.
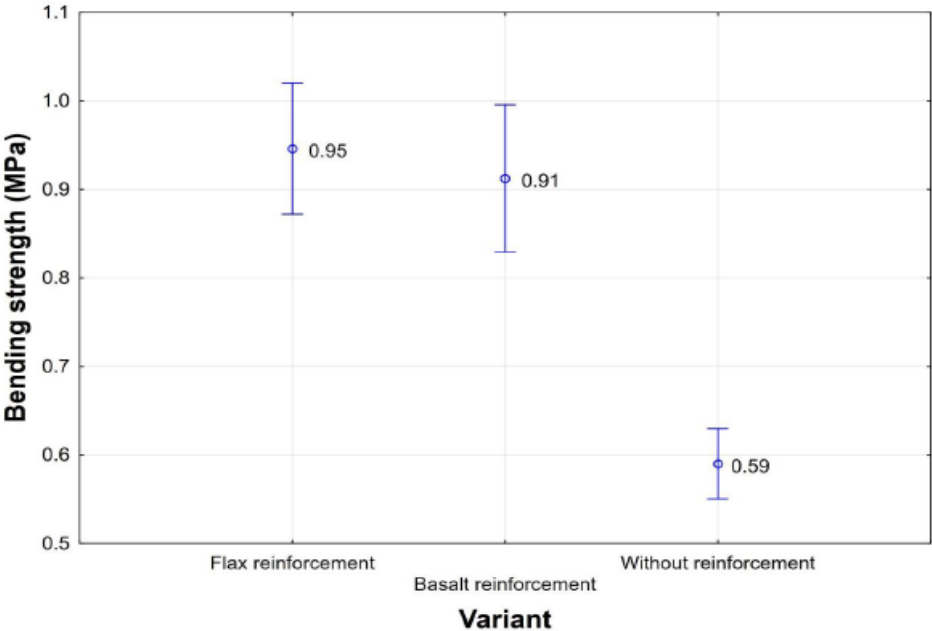
Figure 134. Bending strength of geopolymers reinforced with different fibers.
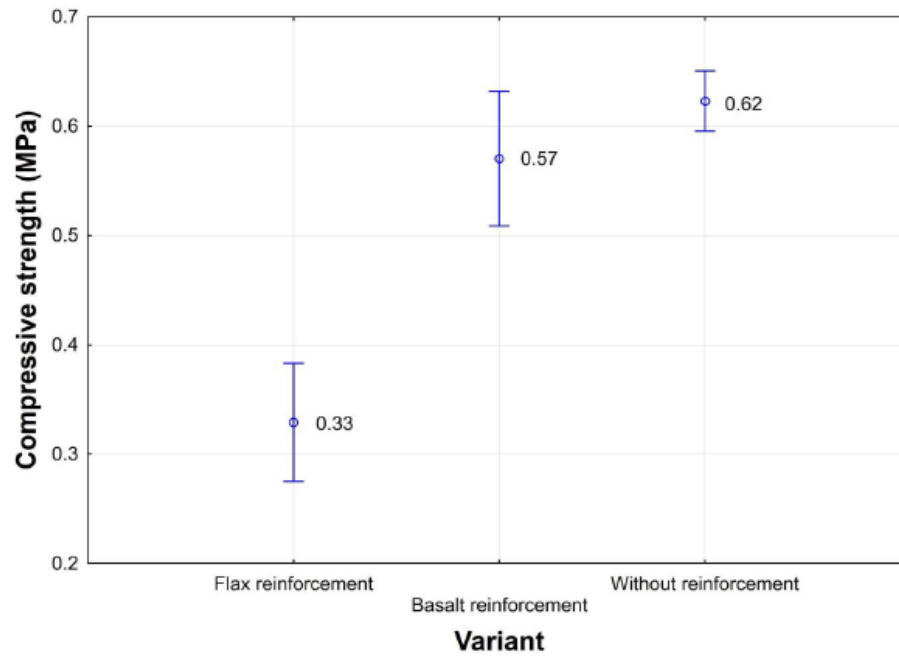
Figure 135. Compressive strength of geopolymers reinforced with different fibers.
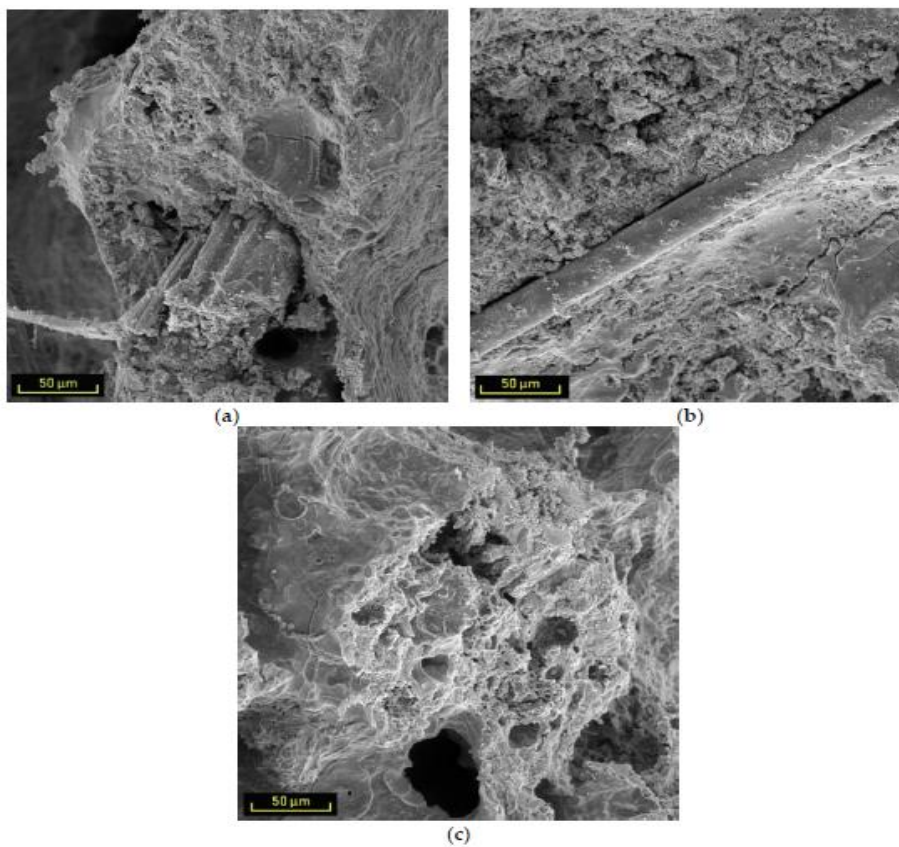
Figure 136. Impact of the addition of fibers on the nature of the joint failure (SEM images): (a) flax fiber-reinforced geopolymer, (b) basalt fiber-reinforced geopolymer, and (c) geopolymer without fibers.

Article D. Permeable water-resistant heat insulation panel based on recycled materials and its physical and mechanical properties

Stepan Hysek, Miroslav Frydrych, Miroslav Herclik, Ludmila Fridrichova, Petr Louda, Roman Knizek, Su Le Van and Hiep Le Chi. Molecules, 12, 2019.

This paper deals with the development and characteristics of the properties of a permeable water-resistant heat insulation panel based on recycled materials. The insulation panel consists of a thermal insulation core of recycled soft polyurethane foam and winter wheat husk, a layer of geopolymer that gives the entire sandwich composite strength (Figure 137) and fire-resistance, and a nanofibrous membrane that permits water vapor permeability, but not water in liquid form. The observed properties are the thermal conductivity coefficient, volumetric heat capacity, fire-resistance, resistance to long-term exposure of a water column, and the tensile strength perpendicular to the plane of the board. The results showed that while the addition of husk to the thermal insulation core does not significantly impair its thermal insulation properties (Figure 138), the tensile strength perpendicular to the plane of these boards was impaired by the addition of husk (Figure 139). The GF layer increased the fire-resistance of the panel for up to 13 min (Figure 140) and the implementation of the nanofibrous membrane resulted in a water flow of 154 cm^2 in the amount of 486 g of water per 24 h at a water column height of 0.8 m (Figure 141).

Figure 137. View of sandwich panel cut.
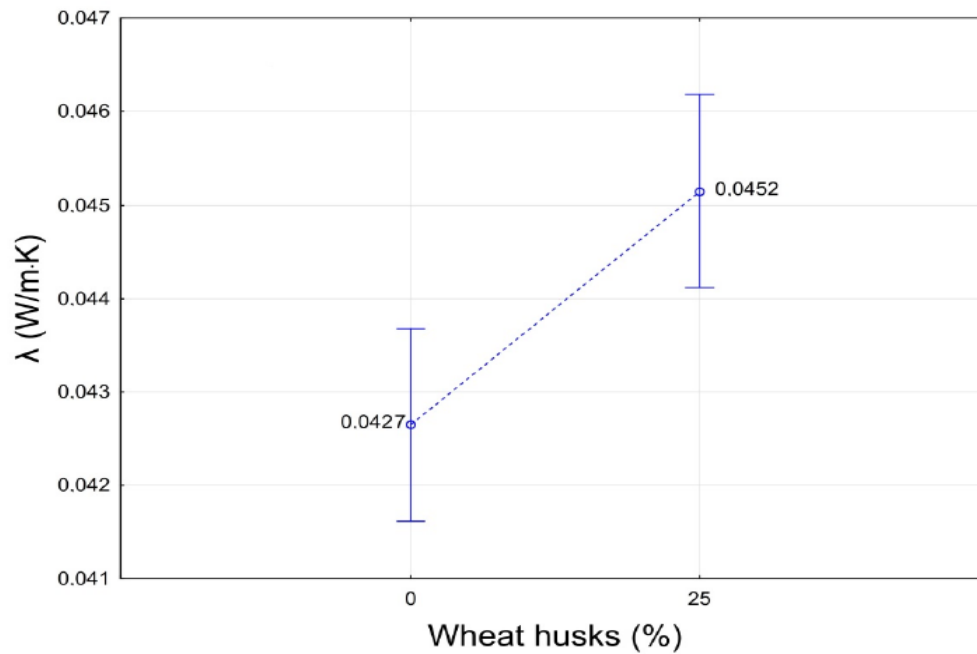
Figure 138. Influence of the proportion of the husk in the insulation board on the thermal conductivity coefficient.
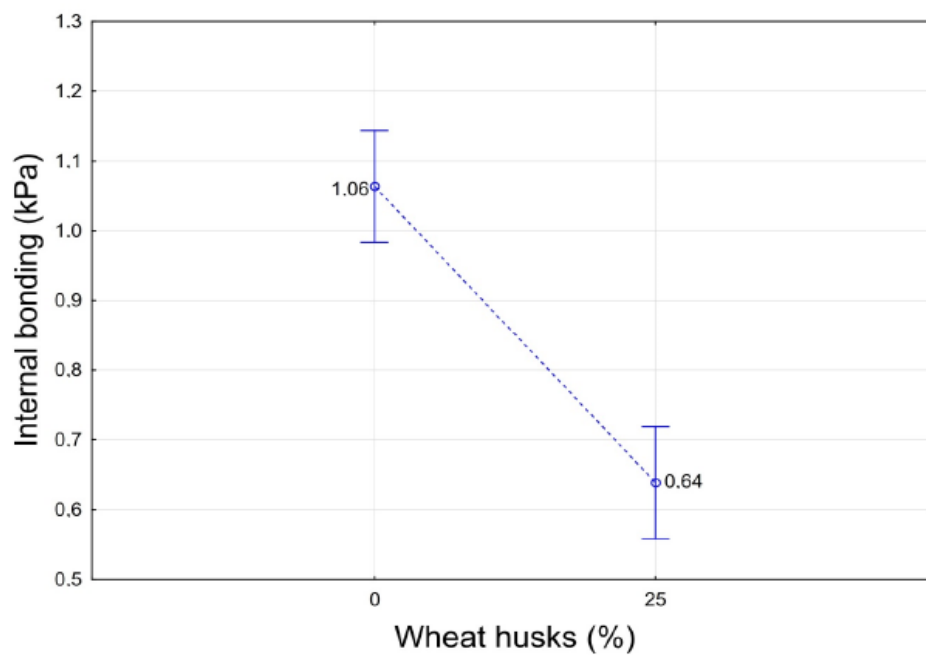
Figure 139. Influence of the proportion of the husk in the insulation board on the internal bonding of composite materials.
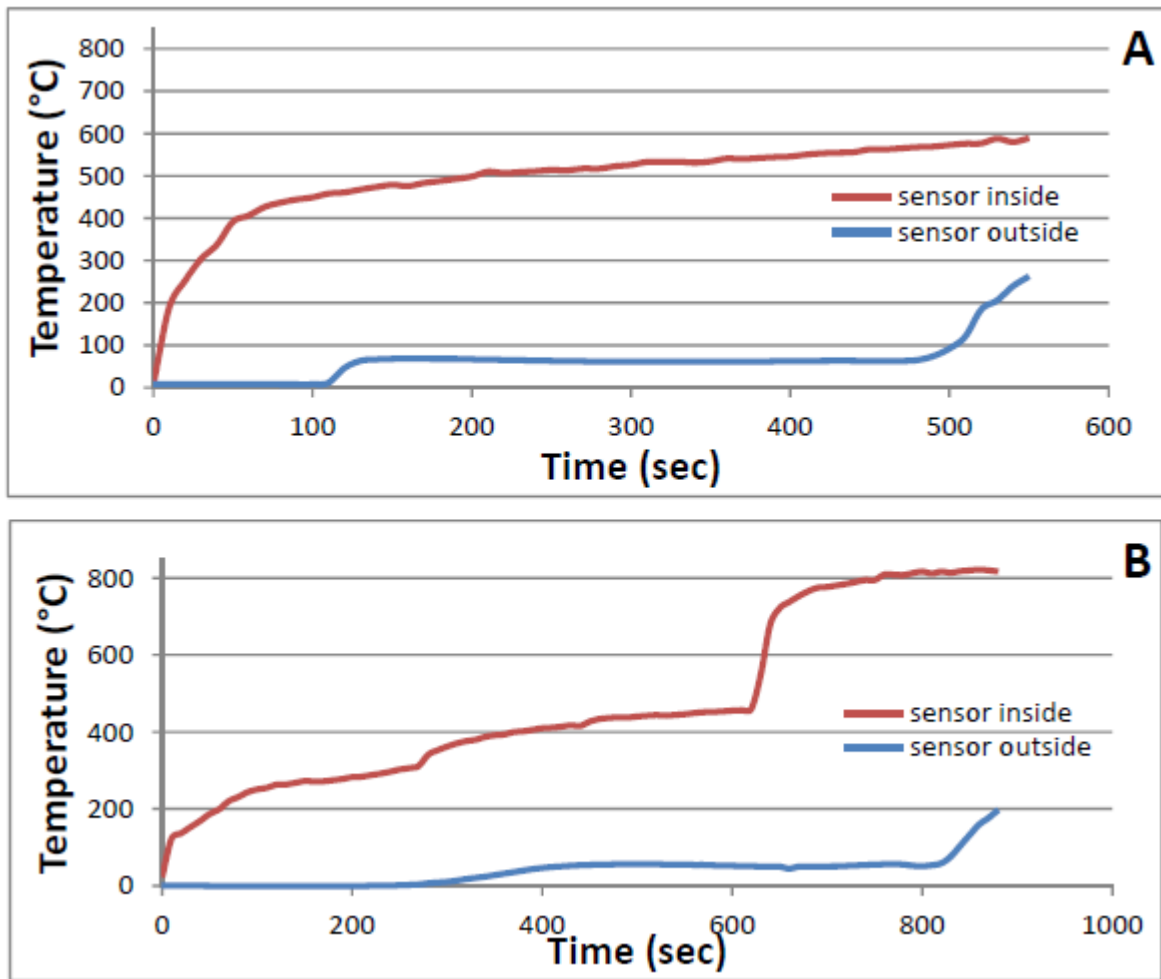
Figure 140. Burning characteristics of produced panels: (A) Rapid temperature increase; (B) gradual temperature increase.
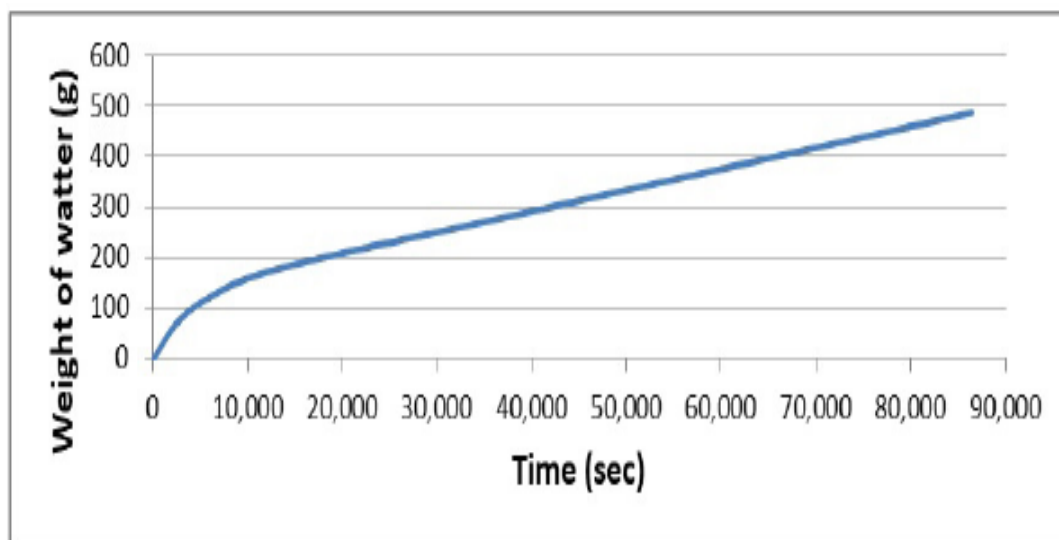
Figure 141. Effect of the nanofibrous membrane on the resistance of the sandwich panel against the long-term effects of the water column.

Article E. *Fire-resistant sandwich-structured composite material based on alternative materials and its physical and mechanical properties*

> Stepan Hysek, Miroslav Frydrych, Miroslav Herclik, Petr Louda, Ludmila Fridrichova, Su Le Van and Hiep Le Chi. Materials, 24(12), 2019.

The development of composite materials from alternative raw materials and the design of their properties for the intended purpose is an integral part of the rational management of raw materials and waste recycling. The submitted paper comprehensively assesses the physical and mechanical properties of composite sandwich material made from particles of winter rapeseed stalks, GF and reinforcing basalt lattices. The developed composite panel is designed for use as a filler in constructions (building or building joinery). The observed properties were: bending characteristics, internal bonding, thermal conductivity coefficient and combustion characteristics.

The results showed that the density of the particleboard has a significant effect on the resulting mechanical properties of the entire sandwich panel (Figure 142). On the contrary, the density of the second layer of the sandwich panel, geopolymer, did not have the same influence on its mechanical properties as the density of the particleboard (Figure 143). The basalt fiber reinforcement lattice positively affected the mechanical properties of sandwich composites only if it was sufficiently embedded in the structure of the particleboard. All of the manufactured sandwich composites resisted flame for more than 13 min, and the fire-resistance was positively affected by the density of the GF layer (Figure 144).
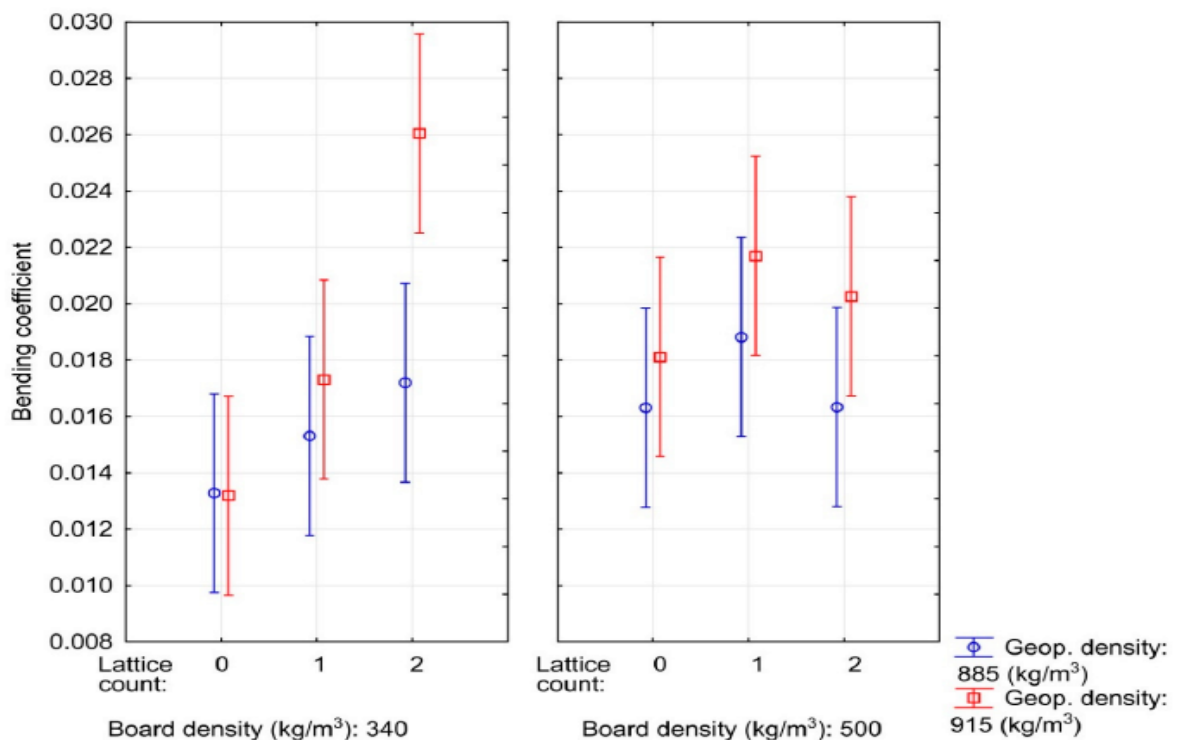
Figure 142. Influence of particleboard density, geopolymer composite density and the number of lattices on the bending coefficient of composite materials.
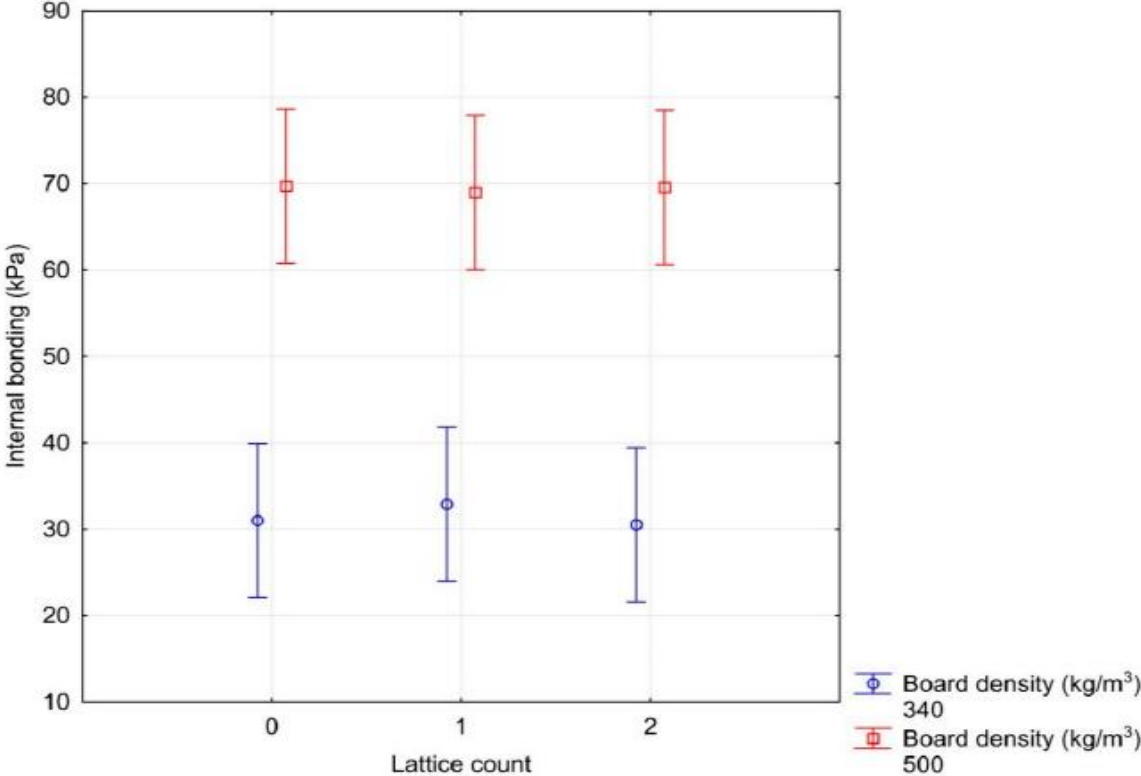
Figure 143. Influence of particleboard density and the number of lattices on the internal bonding of composite materials.
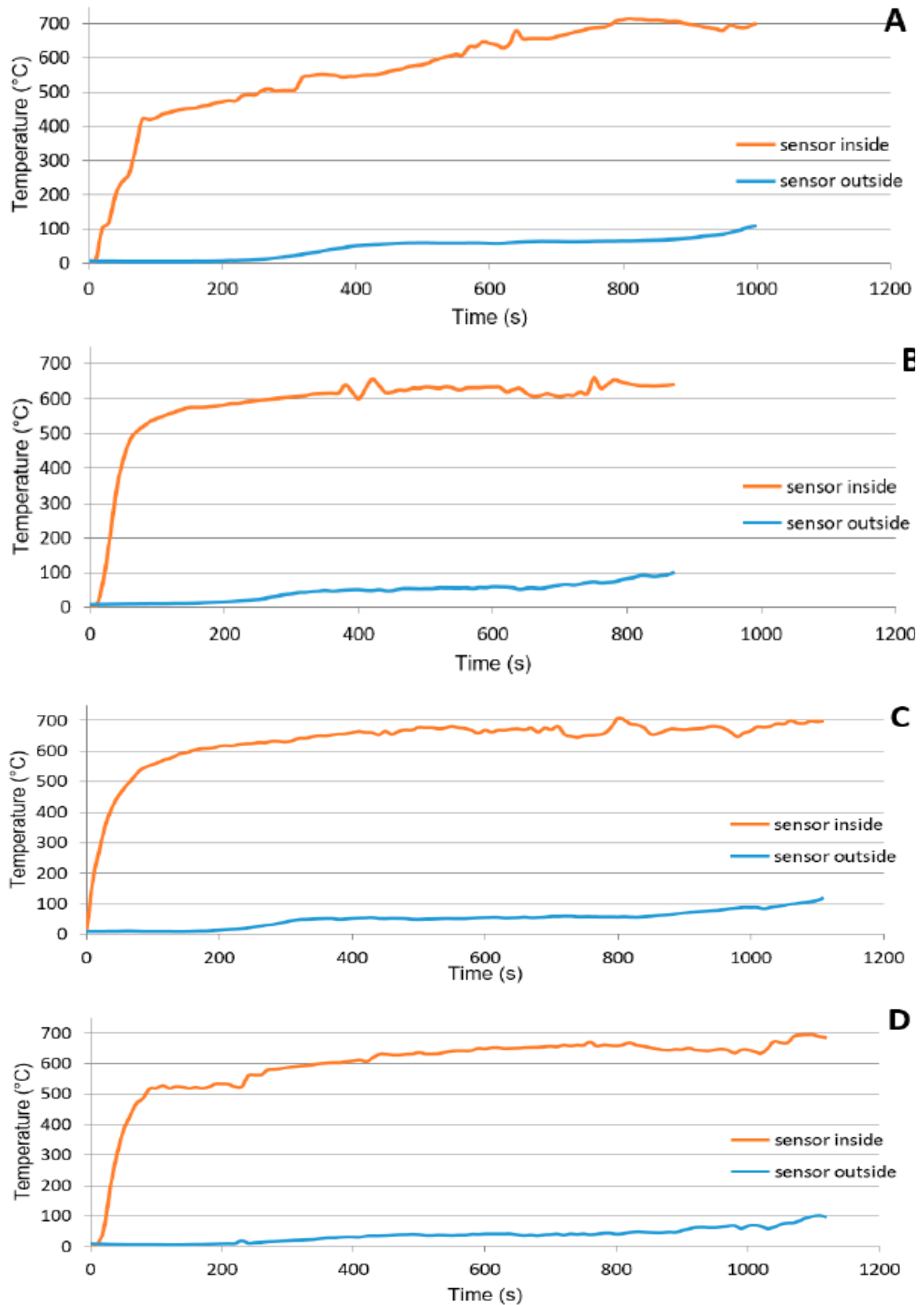
Figure 144. Influence of panel composition on burning characteristics, (**A**) board density 340 kg/m^3, geop. density 885 kg/m^3; (**B**) board density 500 kg/m^3, geop. density 885 kg/m^3; (**C**) board density 340 kg/m^3, geop. density 915 kg/m^3; (**D**) board density 500 kg/m^3, geop. density 915 kg/m^3.

Article F. *Water absorption properties of geopolymer foam after being impregnated with hydrophobic agents*

Hiep Le Chi, Pavlina Hajkova, Su Le Van, Petr Louda, Lukas Volesky. Materials, 24 (12), 2019.

GFs is classified as a lightweight material with high porous in its matrix which has an excellent offer for applications requiring fire-resistant, thermal, and acoustic properties. However, the high sensitivity to humid environments can be a major barrier to GFs that limits the variety of applications of this material. Based on this drawback, two types of the hydrophobic agent (Lukosil M130 and Lukofob ELX) were used as an impregnator to treat the surface of GFs samples. This paper presented the results of the water absorption properties of the untreated and treated GFs. The obtained properties were flexural strength, compressive strength, density, total water absorption, the rate of water absorption, and water absorption coefficient. The results showed that the samples after being impregnated with hydrophobic agents improved their waterproof property significantly, especially using Lukosil M130 (Figure 145). Moreover, the samples treated with Lukosil M130 had a positive impact on their mechanical strength (Figure 146).
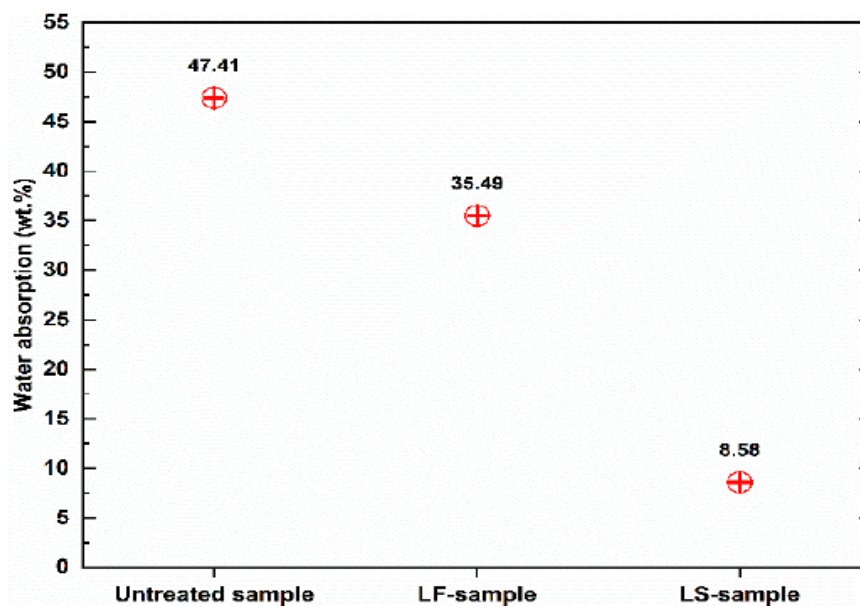
Figure 145. Total water absorption of the GFs.
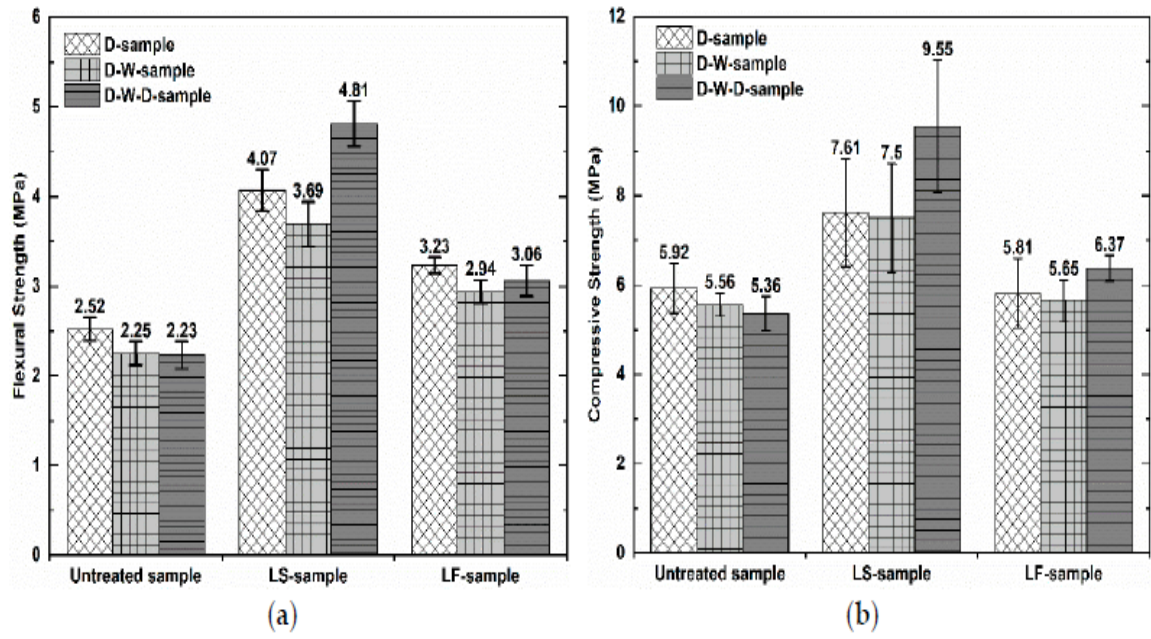
Figure 146. Mechanical properties of the GFs: (a) flexural strength; (b) compressive strength.

List publication of the author

- Louda Petr, Kovacic Vladimir, Hajkova Pavlina, Bakalova Totka, Volesky Lukas, Su Le Van, Hiep Le Chi. *Thermal insulation geopolymer composite*. Patent 33566 U1 20.12.2019. Available in PDF from https://isdv.upv.cz/doc/FullFiles/UtilityModels/FullDocuments/FDUM0033/uv033566.pdf

- Su Le Van, Hiep Le Chi, Petr Louda, Totka Bakalova, Marian Durak, Vladimir Kovacic, *Geopolymer foam for passive fire protection of the wooden structural panels,* SENM 2017 WORKSHOP, Lodz - Poland.

- Su Le Van, Iva Dufkova, Lukas Volesky, Vladimir Kovacic, Totka Bakalova, Hiep Le Chi, Petr Louda. *Geopolymer foams for passive fire protection of the steel structural and acoustic absorption*. GPCamp, 2019, Saint-Quentin, France. Available: https://www.geopolymer.org/conference/gpcamp/gpcamp-2019/

- Van Su Le, Michal M. Szczypinski, Pavlina Hajkova, Vladimir Kovacic, Totka Bakalova, LukasVolesky, Le Chi Hiep, and Petr Louda. *Mechanical properties of geopolymer foam at high-temperature.* Science and Engineering of Composite Materials. May 2020. 27(01):10. DOI: 10.1515/secm-2020-0013

- Le Van, Su., Hajkova, P., Kovacic, V., Bakalova, T., Volesky, L., Le Chi, H., Ceccon, S.K., Pereira, P.A., Louda, P. *Thermal conductivity of reinforced geopolymer foam.* Ceramics-Silikáty, Volume 63, 2019, Issue 4, p. 365-373. ISSN 0862-5468. Also available in PDF from: https://www.irsm.cas.cz/materialy/cs_content/2019_doi/Le_CS_2019_0032.pdf

- Szczypinski, M.M., Louda, P., Exnar, P., Chi, H.L., Kovacic, V., Van Su, L.V., Volesky, L., Bayhan, E., And Bakalova, T. *Evaluation of mechanical properties of composite geopolymer blocks reinforced with basalt fibers.* Manufacturing Technology. 2019, Vol. 18, no. 5, p. 861-865. ISSN 1213-2489. Also available in PDF from: https://arl.ujep.cz/arl-ep/cs/csg/?repo=ujeprepo&key=67492586428

- Chi, H.L., Louda, P., Van S.L., Volesky, L., Kovacic, V., And Bakalova, T. *Composite performance evaluation of basalt textile-reinforced geopolymer mortar.* Fibers, vol.7, 2019, no.7, art.no.63. ISSN 2079-6439. Also available in PDF from: https://www.mdpi.com/2079-6439/7/7/63/pdf

- Hysek, S., Frydrych, M., Herclik, M., Fridrichova, L., Louda, P., Knizek, R., Van, S.L., And Chi, H.L. *Permeable water-resistant heat insulation panel based on recycled materials and its physical and mechanical properties.* Molecules, 2019, vol.24, no.18, art. no. 3300. Also available in PDF from: https://www.mdpi.com/1420-3049/24/18/3300/pdf

- Hysek, S., Frydrych, M., Herclik, M., Louda, P., Fridrichova, L., Le Van, S., Le Chi, H. *Fire-resistant sandwich-structured composite material based on alternative materials and its physical and mechanical properties.* Materials, vol.12, (2019), no.9, art.no. 1432, ISSN 1996-1944.Also available in PDF from: https://www.mdpi.com/1996-1944/12/9/1432/pdf

- Frydrych, M., Hysek, S., Fridrichova, L., Le Van, S., Herclik, M., Pechociakova., Le Chi, H. Louda, P. *Impact of and basalt fire reinforcement on selected properties of geopolymer Composites.* Sustainability 2020, 12(1), 118; Also available in PDF from: https://doi.org/10.3390/su12010118

- Le Chi, H., Hajkova, P., Le Van, S., Kovacic, V., Louda, P., Volesky, L. *Water absorption properties of geopolymer foam after being impregnated with hydrophobic agents.* Materials 2019, 12(24), 4162; Also available in PDF from: https://doi.org/10.3390/ma12244162

Bibliography

[1]   J. Mehaffey, P. Cuerrier, and G. Carisse, "A model for predicting heat transfer through gypsum-board/wood-stud walls exposed to fire," *Fire and materials,* vol. 18, pp. 297-305, 1994.

[2]   N. Arjun. *Gypsum Products and Properties as a Building Material for Construction*. Available: https://theconstructor.org/building/gypsum-products-properties-building-construction/14949/#

[3]   B. Lomborg, *The skeptical environmentalist: measuring the real state of the world* vol. 1: Cambridge University Press Cambridge, 2003.

[4]   The Statistics Portal. (2018). *Global Cement Production From 1990 to 2030*. Available: https://www.statista.com/statistics/373845/global-cement-production-forecast/

[5]   Y. Chan, G. Peng, and M. Anson, "Residual strength and pore structure of high-strength concrete and normal strength concrete after exposure to high temperatures," *Cement and concrete composites,* vol. 21, pp. 23-27, 1999.

[6]   T. E. U. P. Regulation and 305/2011, "Eurocode 2: Design of concrete structures - Part 1-2: General rules - Structural fire design ", ed. European standard 2004.

[7]   V. S. Ramachandran, *Concrete admixtures handbook: properties, science and technology*: William Andrew, 1996.

[8]   L. T. Phan, T. P. McAllister, J. L. Gross, and M. J. Hurley, "Best practice guidelines for structural fire resistance design of concrete and steel buildings," *NIST technical note,* vol. 1681, p. 199, 2010.

[9]   R. Sarshar and G. Khoury, "Material and environmental factors influencing the compressive strength of unsealed cement paste and concrete at high temperatures," *Magazine of concrete research,* vol. 45, pp. 51-61, 1993.

[10]   N. Arjun. *Fire Resistance of Concrete Materials and Structures*. Available: https://theconstructor.org/concrete/fire-resistance-concrete-materials-structures/17540/

[11]   S. L. LeVan and J. E. Winandy, "Effects of fire retardant treatments on wood strength: a review," *Wood and fiber science,* vol. 22, pp. 113-131, 2007.

[12]   F. E. R. Du and D. L. Campbell, "Method for fireproofing wood and the treated wood," ed: Google Patents, 1967.

[13]   Wikipedia. (2019, 15/04). *Notre-Dame de Paris fire* Available: https://en.wikipedia.org/wiki/Notre-Dame_de_Paris_fire

[14]   W.-F. Chen and E. M. Lui, *Principles of structural design*: CRC Press, 2005.

[15]   M. Netopilová, *Materiály: Stavební materiály*: Sdružení požárního a bezpečnostního inženýrství, 2004.

[16]   B. C. David Doran, "construction materials reference book," in *construction materials* second edition ed London and new york: Routledge Taylor and Francis group.

[17]   W. Von Bonin and U. V. Gizycki, "Fire retardant elements," ed: Google Patents, 1991.

[18]   E. p. t. irreplaceable. *Intumescent coating for steel and aluminum protection*. Available: https://envirograf.com/product/intumescent-coating-for-steel-and-aluminum-protection/

[19]   cladspraysolution, "intumescent coatings," 2020.

[20]   U. S. D. o. Labor. Chemical Sampling Information (Fibrous Glass) [Online].

[21]   PNG. (2020). *Glass fiber Glass wool Building insulation materials, woolen glass, glass, company png*. Available: https://www.pngegg.com/en/png-eymhy

[22]   S.-H. Lin, C.-L. Pan, and W.-T. Hsu, "Monotonic and cyclic loading tests for cold-formed steel wall frames sheathed with calcium silicate board," *Thin-Walled Structures,* vol. 74, pp. 49-58, 2014.

[23]   F. f. p. Europe. (7/06). *Chanel for electrical wiring*. Available: https://www.fp-e.eu/en/schedule-of-services/fire-protection-covering/

[24]   Filip   Habart.   (2012).   *Geopolymer*.   Available: http://www.matrix-2012.cz/index.php/sekce-a-odkazy/rzne/1149-geopolymery

[25]   Wikipedia.   (2020).   *Ziggurat   of   Ur*.   Available: https://en.wikipedia.org/wiki/Ziggurat_of_Ur

[26]   M. Slackman, (2008, 17/10). *In the shadow of a Long Past, Patiently the Future*. Available: https://www.nytimes.com/2008/11/17/world/middleeast/17cairo.html

[27]   N. B. Jørgensen. (2019, 7-10). *The Great Pyramid: New Theory on God Symbolism and the Hidden Chambers*. Available: https://www.ancient-origins.net/ancient-places-africa/great-pyramid-0012684

[28]   Wikipedia.   (2020).   *Sacsayhuamán*.   Available: https://en.wikipedia.org/ wiki/Sacsayhuam%C3%A1n

[29]   WIKIPEDIA.   (2020).   *Colosseum*.   Available: https://en.wikipedia. org/wiki/Colosseum

[30]   J. Davidovits, "Process for the fabrication of sintered panels and panels resulting from the application of this process," ed: Google Patents, 1976.

[31]   J. Davidovits, "Years of successes and failures in geopolymer applications.Market trends and potential breakthroughs. ," *Geopolymer 2002 Conference.,* vol. 28, 2002.

[32]   J. Davidovits and J. L. Sawyer, "Early high-strength mineral polymer," ed: Google Patents, 1985.

[33]   J. Davidovits, "Properties of geopolymer cements," in *First international conference on alkaline cements and concretes*, 1994, pp. 131-149.

[34]   J. Davidovits and J. Orlinski, *'99 Geopolymer International Conference Proceedings*: Geopolymer Institute, 1999.

[35]   Y. Huang and M. Han, "The influence of α-Al2O3 addition on microstructure, mechanical and formaldehyde adsorption properties of fly ash-based geopolymer products," *Journal of hazardous materials,* vol. 193, pp. 90-94, 2011.

[36]   K. Pimraksa, P. Chindaprasirt, A. Rungchet, K. Sagoe-Crentsil, and T. Sato, "Lightweight geopolymer made of highly porous siliceous materials with various Na2O/Al2O3 and SiO2/Al2O3 ratios," *Materials Science and Engineering: A,* vol. 528, pp. 6616-6623, 2011.

[37]   J. Davidovits, "First international conference on alkaline cements and concretes," 1994.

[38]   H. Rahier, B. Van Mele, M. Biesemans, J. Wastiels, and X. Wu, "Low-temperature synthesized aluminosilicate glasses," *Journal of Materials Science,* vol. 31, pp. 71-79, 1996.

[39]   M. Sofi, J. Van Deventer, P. Mendis, and G. Lukey, "Bond performance of reinforcing bars in inorganic polymer concrete (IPC)," *Journal of Materials Science,* vol. 42, pp. 3107-3116, 2007.

[40]   I. García-Lodeiro, A. Fernández-Jiménez, A. Palomo, and D. E. Macphee, "Effect of calcium additions on N–A–S–H cementitious gels," *Journal of the American Ceramic Society,* vol. 93, pp. 1934-1940, 2010.

[41]   Y. Bao, M. W. Grutzeck, and C. M. Jantzen, "Preparation and properties of hydroceramic waste forms made with simulated hanford low-activity waste," *Journal of the American Ceramic Society,* vol. 88, pp. 3287-3302, 2005.

[42]   S. Mallicoat, P. Sarin, and W. Kriven, "Novel, alkali-bonded, ceramic filtration membranes," in *Developments in Advanced Ceramics and Composites: A Collection of Papers Presented at the 29th International Conference on Advanced Ceramics and Composites, January 23-28, 2005, Cocoa Beach, Florida, Ceramic Engineering and Science Proceedings*, 2009, p. 37.

[43]   A. Palomo, M. Grutzeck, and M. Blanco, "Alkali-activated fly ashes: a cement for the future," *Cement and concrete research,* vol. 29, pp. 1323-1329, 1999.

[44]   A. Fernández-Jiménez, A. Palomo, and M. Criado, "Microstructure development of alkali-activated fly ash cement: a descriptive model," *Cement and concrete research,* vol. 35, pp. 1204-1209, 2005.

[45]   J. Davidovits, *Geopolymer chemistry and application* Saint-Quentin: Institut geopolymere, 2015.

[46]   P. Duxson, A. Fernández-Jiménez, J. L. Provis, G. C. Lukey, A. Palomo, and J. S. van Deventer, "Geopolymer technology: the current state of the art," *Journal of materials science,* vol. 42, pp. 2917-2933, 2007.

[47]   M. Abdullah, K. Hussin, M. Bnhussain, K. Ismail, and W. Ibrahim, "Mechanism and chemical reaction of fly ash geopolymer cement-a review," *Int. J. Pure Appl. Sci. Technol,* vol. 6, pp. 35-44, 2011.

[48]   C. Panagiotopoulou, E. Kontori, T. Perraki, and G. Kakali, "Dissolution of aluminosilicate minerals and by-products in alkaline media," *Journal of Materials Science,* vol. 42, pp. 2967-2973, 2007.

[49]   D. Dimas, I. Giannopoulou, and D. Panias, "Polymerization in sodium silicate solutions: a fundamental process in geopolymerization technology," *Journal of materials science,* vol. 44, pp. 3719-3730, 2009.

[50]   D. Khale and R. Chaudhary, "Mechanism of geopolymerization and factors influencing its development: a review," *Journal of materials science,* vol. 42, pp. 729-746, 2007.

[51]   E. Hermann, C. Kunze, R. Gatzweiler, G. Kiebig, and J. Davidovits, "Solidification of various radioactive residues by geopolymere with special emphasis on long term stability," in *Proceedings of the Geopolymers Conference, Saint-Quentin, France*, 1999.

[52]   H. Xu and J. Van Deventer, "The geopolymerisation of alumino-silicate minerals," *International journal of mineral processing,* vol. 59, pp. 247-266, 2000.

[53]   H. Xu and J. S. Van Deventer, "Effect of source materials on geopolymerization," *Industrial & engineering chemistry research,* vol. 42, pp. 1698-1706, 2003.

[54]   V. F. Barbosa and K. J. MacKenzie, "Thermal behavior of inorganic geopolymers and composites derived from sodium polysialate," *Materials research bulletin,* vol. 38, pp. 319-331, 2003.

[55]   P. Rovnaník, "Effect of curing temperature on the development of hard structure of metakaolin-based geopolymer," *Construction and building materials,* vol. 24, pp. 1176-1183, 2010.

[56]   A. Palomo and F. Glasser, "Chemically-bonded cementitious materials based on metakaolin," *British ceramic. Transactions and journal,* vol. 91, pp. 107-112, 1992.

[57]   M. S. Cilla, P. Colombo, and M. R. Morelli, "Geopolymer foams by gelcasting," *Ceramics International,* vol. 40, pp. 5723-5730, 2014.

[58]   G. Görhan and G. Kürklü, "The influence of the NaOH solution on the properties of the fly ash-based geopolymer mortar cured at different temperatures," *Composites part b: engineering,* vol. 58, pp. 371-377, 2014.

[59]   P. Keawpapasson, C. Tippayasam, S. Ruangjan, P. Thavorniti, T. Panyathanmaporn, A. Fontaine*, et al.*, "Metakaolin-Based Porous Geopolymer with Aluminium Powder," *Key Engineering Materials,* vol. 608, pp. 132-138, 2014.

[60]   F. J. López, S. Sugita, M. Tagaya, and T. Kobayashi, "Metakaolin-based geopolymers for targeted adsorbents to heavy metal ion separation," *Journal of Materials Science and Chemical Engineering,* vol. 2, p. 16, 2014.

[61]   B.-h. Mo, H. Zhu, X.-m. Cui, Y. He, and S.-y. Gong, "Effect of curing temperature on geopolymerization of metakaolin-based geopolymers," *Applied clay science,* vol. 99, pp. 144-148, 2014.

[62]   H. S. Shiu, K. L. Lin, S. J. Chao, C. L. Hwang, and T. W. Cheng, "Effects of foam agent on characteristics of thin-film transistor liquid crystal display waste glass-metakaolin-based cellular geopolymer," *Environmental Progress & Sustainable Energy,* vol. 33, pp. 538-550, 2014.

[63]   M. A. Villaquirán-Caicedo, R. M. de Gutiérrez, S. Sulekar, C. Davis, and J. C. Nino, "Thermal properties of novel binary geopolymers based on metakaolin and alternative silica sources," *Applied Clay Science,* vol. 118, pp. 276-282, 2015.

[64]   G. F. Huseien, J. Mirza, M. Ismail, M. W. Hussin, M. Arrifin, and A. Hussein, "The effect of sodium hydroxide molarity and other parameters on water absorption of geopolymer mortars," *Indian Journal of Science and Technology,* vol. 9, pp. 1-7, 2016.

[65]   A. A. Aliabdo, A. E. M. A. Elmoaty, and H. A. Salem, "Effect of water addition, plasticizer and alkaline solution constitution on fly ash based geopolymer concrete performance," *Construction and Building Materials,* vol. 121, pp. 694-703, 2016.

[66]   T. Luukkonen, M. Sarkkinen, K. Kemppainen, J. Rämö, and U. Lassi, "Metakaolin geopolymer characterization and application for ammonium removal from model solutions and landfill leachate," *Applied Clay Science,* vol. 119, pp. 266-276, 2016.

[67]   N. U. Kockal, O. Beycan, and N. Gulmez, "Effect of binder type and content on physical and mechanical properties of geopolymers," *Sādhanā,* vol. 43, p. 49, 2018.

[68]   J. Swanepoel and C. Strydom, "Utilisation of fly ash in a geopolymeric material," *Applied Geochemistry,* vol. 17, pp. 1143-1148, 2002.

[69]   J. Van Jaarsveld, J. Van Deventer, and G. Lukey, "The characterisation of source materials in fly ash-based geopolymers," *Materials Letters,* vol. 57, pp. 1272-1280, 2003.

[70]   J. Davidovits, "Geopolymer chemistry and applications. 2008," *Saint Quentin: Geopolymer Institute,* 2008.

[71]   W. D. Rickard and A. Van Riessen, "Performance of solid and cellular structured fly ash geopolymers exposed to a simulated fire," *Cement and Concrete Composites,* vol. 48, pp. 75-82, 2014.

[72]   F. Skvara, R. Sulc, T. Zdenek, S. Petr, S. Vit, and Z. C. Zuzana, "Preparation and properties of fly ash-based geopolymer foams," *Ceramics-Silikaty,* vol. 58, pp. 188-197, 2014.

[73]   Z. Abdollahnejad, F. Pacheco-Torgal, T. Félix, W. Tahri, and J. B. Aguiar, "Mix design, properties and cost analysis of fly ash-based geopolymer foam," *Construction and Building Materials,* vol. 80, pp. 18-30, 2015.

[74]   A. Nazari and J. G. Sanjayan, "Hybrid effects of alumina and silica nanoparticles on water absorption of geopolymers: Application of Taguchi approach," *Measurement,* vol. 60, pp. 240-246, 2015.

[75]   R. M. Novais, L. Buruberri, G. Ascensão, M. Seabra, and J. Labrincha, "Porous biomass fly ash-based geopolymers with tailored thermal conductivity," *Journal of cleaner production,* vol. 119, pp. 99-107, 2016.

[76]   R. M. Novais, L. Buruberri, M. Seabra, and J. Labrincha, "Novel porous fly-ash containing geopolymer monoliths for lead adsorption from wastewaters," *Journal of hazardous materials,* vol. 318, pp. 631-640, 2016.

[77]   N. Toniolo and A. R. Boccaccini, "Fly ash-based geopolymers containing added silicate waste. A review," *Ceramics International,* vol. 43, pp. 14545-14551, 2017.

[78]   A. Hajimohammadi, T. Ngo, and A. Kashani, "Sustainable one-part geopolymer foams with glass fines versus sand as aggregates," *Construction and Building Materials,* vol. 171, pp. 223-231, 2018.

[79]   H. Xu and J. S. Van Deventer, "Ab initio calculations on the five-membered alumino-silicate framework rings model: implications for dissolution in alkaline solutions," *Computers & chemistry,* vol. 24, pp. 391-404, 2000.

[80]   V. Glukhovsky, "Slag-alkali concretes produced from fine-grained aggregate," *Kiev: Vishcha Shkolay,* 1981.

[81]   S. Kumar and R. Kumar, "Mechanical activation of fly ash: Effect on reaction, structure and properties of resulting geopolymer," *Ceramics International,* vol. 37, pp. 533-541, 2011.

[82]   B. Keertana, Sini Sara Mani, and M. Thenmozhi., "Utilization of ecosand and flyash in aerated concrete for a richest mix design.," *International Journal of Engineering Science and Technology,* vol. 3, 2011.

[83]   R. Arellano Aguilar, O. Burciaga Díaz, and J. I. Escalante García, "Lightweight concretes of activated metakaolin-fly ash binders, with blast furnace slag aggregates," *Construction and Building Materials,* vol. 24, pp. 1166-1175, 2010.

[84]   R. A. Aguilar, O. B. Díaz, and J. E. García, "Lightweight concretes of activated metakaolin-fly ash binders, with blast furnace slag aggregates," *Construction and building materials,* vol. 24, pp. 1166-1175, 2010.

[85]   A. Buchwald, H. Hilbig, and C. Kaps, "Alkali-activated metakaolin-slag blends—performance and structure independence of their composition," *Journal of materials science,* vol. 42, pp. 3024-3032, 2007.

[86]   J. Davidovits, "Mineral polymers and methods of making them," ed: Google Patents, 1982.

[87]   J. Davidovits, "Geopolymer chemistry and properties," in *Geopolymer*, 1988, pp. 25-48.

[88]   J. Davidovits, "Geopolymer chemistry and sustainable development. The poly (sialate) terminology: a very useful and simple model for the promotion and understanding of green-chemistry," in *Proceedings of the world congress Geopolymer*, 2005, pp. 9-15.

[89]   J. Davidovits, "years of successes and failures in geopolymer applications. Market trends and potential breakthroughs," in *Geopolymer 2002 Conference*, 2002, p. 29.

[90]   C. Bai, G. Franchin, H. Elsayed, A. Zaggia, L. Conte, H. Li*, et al.*, "High-porosity geopolymer foams with tailored porosity for thermal insulation and wastewater treatment," *Journal of Materials Research,* vol. 32, pp. 3251-3259, 2017.

[91]   Y. J. Zhang, L. C. Liu, Y. Xu, and Y. C. Wang, "A new alkali-activated steel slag-based cementitious material for photocatalytic degradation of organic pollutant from waste water," *Journal of hazardous materials,* vol. 209, pp. 146-150, 2012.

[92]   K. Sakkas, A. Sofianos, P. Nomikos, and D. Panias, "Behaviour of passive fire protection K-geopolymer under successive severe fire incidents," *Materials,* vol. 8, pp. 6096-6104, 2015.

[93]   Z. Zhang, J. L. Provis, A. Reid, and H. Wang, "Geopolymer foam concrete: An emerging material for sustainable construction," *Construction and Building Materials,* vol. 56, pp. 113-127, 2014.

[94]   K. Sakkas, D. Panias, P.P. Nomikos , and A.I. Sofianos, "Potassium based geopolymer for passive fire protection of concrete tunnels linings," *Tunnelling and Underground Space Technology,* vol. 43, pp. 148-156, 2014.

[95]   I. Lecomte, M. Liégeois, A. Rulmont, R. Cloots, and F. Maseri, "Synthesis and characterization of new inorganic polymeric composites based on kaolin or white clay and on ground-granulated blast furnace slag," *Journal of materials research,* vol. 18, pp. 2571-2579, 2003.

[96]   P. Palmero, A. Formia, P. Antonaci, S. Brini, and J.-M. Tulliani, "Geopolymer technology for application-oriented dense and lightened materials. Elaboration and characterization," *Ceramics International,* vol. 41, pp. 12967-12979, 2015.

[97]   P. Hlaváček, V. Šmilauer, F. Škvára, L. Kopecký, and R. Šulc, "Inorganic foams made from alkali-activated fly ash: Mechanical, chemical and physical properties," *Journal of the European Ceramic Society,* vol. 35, pp. 703-709, 2015.

[98]   E. Kamseu, B. Nait-Ali, M. Bignozzi, C. Leonelli, S. Rossignol, and D. S. Smith, "Bulk composition and microstructure dependence of effective thermal conductivity of porous inorganic polymer cements," *Journal of the European Ceramic Society,* vol. 32, pp. 1593-1603, 2012.

[99]   D. L. Kong and J. G. Sanjayan, "Damage behavior of geopolymer composites exposed to elevated temperatures," *Cement and Concrete Composites,* vol. 30, pp. 986-991, 2008.

[100] Y.-P. Chiu, Y.-M. Lu, and Y.-C. Shiau, "Applying inorganic geopolymers added with aluminium powder to fire-resistant fillers," *Materials Research Innovations,* vol. 19, pp. S5-642-S5-649, 2015.

[101] M. M. A. Abdullah, K. Hussin, M. Bnhussain, K. N. Ismail, Z. Yahya, and R. A. Razak, "Fly Ash-based Geopolymer Lightweight Concrete Using Foaming Agent," *International Journal of Molecular Sciences,* vol. 13, pp. 7186-7198, Jun 2012.

[102] C. Shi, "Composition of materials for use in cellular lightweight concrete and methods thereof," ed: Google Patents, 2002.

[103] Z. Zhang, J. L. Provis, A. Reid, and H. Wang, "Mechanical, thermal insulation, thermal resistance and acoustic absorption properties of geopolymer foam concrete," *Cement and Concrete Composites,* vol. 62, pp. 97-105, 2015.

[104] C. M. A. BUILDING, "Thermal insulation products for buildings. Factory-made mineral wool (MW) products. Specification," ed, 2015, p. 52.

[105] F. Asdrubali, F. D'Alessandro, and S. Schiavoni, "A review of unconventional sustainable building insulation materials," *Sustainable Materials and Technologies,* vol. 4, pp. 1-17, 2015.

[106] E. Kamseu, B. Ceron, H. Tobias, E. Leonelli, M. C. Bignozzi, A. Muscio, *et al.*, "Insulating behavior of metakaolin-based geopolymer materials assess with heat flux meter and laser flash techniques," *Journal of Thermal Analysis and Calorimetry,* vol. 108, pp. 1189-1199, 2011.

[107] X.-y. Zhou, F. Zheng, H.-g. Li, and C.-l. Lu, "An environment-friendly thermal insulation material from cotton stalk fibers," *Energy and Buildings,* vol. 42, pp. 1070-1074, 2010.

[108] L. Fridrichová, M. Frydrych, M. Herclík, R. Knížek, and K. Mayerová, "Nanofibrous membrane as a moisture barrier," in *AIP Conference Proceedings*, 2018, p. 030003.

[109] C. Bai and P. Colombo, "High-porosity geopolymer membrane supports by peroxide route with the addition of egg white as surfactant," *Ceramics International,* vol. 43, pp. 2267-2273, 2017.

[110] Y. Ge, Y. Yuan, K. Wang, Y. He, and X. Cui, "Preparation of geopolymer-based inorganic membrane for removing Ni2+ from wastewater," *Journal of hazardous materials,* vol. 299, pp. 711-718, 2015.

[111] M. Ahmaruzzaman, "Industrial wastes as low-cost potential adsorbents for the treatment of wastewater laden with heavy metals," *Advances in colloid and interface science,* vol. 166, pp. 36-59, 2011.

[112] M. Minelli, V. Medri, E. Papa, F. Miccio, E. Landi, and F. Doghieri, "Geopolymers as solid adsorbent for CO2 capture," *Chemical Engineering Science,* vol. 148, pp. 267-274, 2016.

[113] S. Sharma, D. Medpelli, S. Chen, and D.-K. Seo, "Calcium-modified hierarchically porous aluminosilicate geopolymer as a highly efficient regenerable catalyst for biodiesel production," *RSC Advances,* vol. 5, pp. 65454-65461, 2015.

[114] W. L. Weiliang Gong, Ian L. Pegg, "High-strength geopolymer composite cellular concrete," vol. US20140264140, ed: Google Patents, 2014.

[115] V. Vaou and D. Panias, "Thermal insulating foamy geopolymers from perlite," *Minerals Engineering,* vol. 23, pp. 1146-1151, 2010.

[116] J. Feng, R. Zhang, L. Gong, Y. Li, W. Cao, and X. Cheng, "Development of porous fly ash-based geopolymer with low thermal conductivity," *Materials & Design (1980-2015),* vol. 65, pp. 529-533, 2015.

[117] Y. P. Chiu, Y. M. Lu, and Y. C. Shiau, "Applying inorganic geopolymers added with aluminium powder to fire-resistant fillers," *Materials Research Innovations,* vol. 19, pp. S5-642-S5-649, 2015.

[118] J. G. Sanjayan, A. Nazari, L. Chen, and G. H. Nguyen, "Physical and mechanical properties of lightweight aerated geopolymer," *Construction and Building Materials,* vol. 79, pp. 236-244, 2015.

[119] A. Just and B. Middendorf, "Microstructure of high-strength foam concrete," *Materials Characterization,* vol. 60, pp. 741-748, 2009.

[120] A. Hajimohammadi, T. Ngo, P. Mendis, and J. Sanjayan, "Regulating the chemical foaming reaction to control the porosity of geopolymer foams," *Materials & Design,* vol. 120, pp. 255-265, 2017.

[121] B. Caijun Shi, "Composition of materials for use in cellular lightweight concrete and methods thereof," ed: advanced materials technologies, 2002.

[122] F. Han, G. Seiffert, Y. Zhao, and B. Gibbs, "Acoustic absorption behavior of an open-celled aluminum foam," *Journal of Physics D: Applied Physics,* vol. 36, p. 294, 2003.

[123] D. Tran, D. Kroisová, P. Louda, O. Bortnovsky, and P. Bezucha, "Effect of curing temperature on flexural properties of silica-based geopolymer-carbon reinforced composite," *Manufacturing Engineering,* vol. 37, pp. 492-497, 2009.

[124] T. D. Hung, P. Louda, D. Kroisová, O. Bortnovsky, and N. T. Xiem, "New generation of geopolymer composite for fire-resistance," in *Advances in Composite Materials-Analysis of Natural and Man-Made Materials*, ed: InTech, 2011.

[125] X. Thang, P. Louda, and D. Kroisova, "Thermophysical properties of woven fabrics reinforced geopolymer composites," *World Journal of Engineering,* vol. 10, pp. 139-144, 2013.

[126] G. Masi, W. D. A. Rickard, M. C. Bignozzi, and A. van Riessen, "The effect of organic and inorganic fibers on the mechanical and thermal properties of aluminate activated geopolymers," *Composites Part B: Engineering,* vol. 76, pp. 218-228, 2015.

[127] J. Henon, A. Alzina, J. Absi, D. S. Smith, and S. Rossignol, "Potassium geopolymer foams made with silica fume pore forming agent for thermal insulation," *Journal of Porous Materials,* vol. 20, pp. 37-46, 2012.

[128] František Škvára, Ros tislav Šulc, Zdeněk Tišler, Petr Skřičík, Vít Šmilauer, and Z. Z. Cílová, "Preparation and properties of fly ash-based geopolymer foams," vol. 58, pp. 188-197, 2014.

[129] E. P. Kearsley, & Wainwright, P. J, "The effect of porosity on the strength of foamed concrete," *Cement and concrete research,* vol. 23, pp. 233-239, 2002.

[130] J. Davidovits, "Geopolymers: man-made rock geosynthesis and the resulting development of very early high strength cement," *Journal of Materials Education,* vol. 16, pp. 91-91, 1994.

[131] J. Davidovits, "Geopolymer Chemistry and Applications. 2nd," *Institute Geopolymere, France,* 2008.

[132] J. Davidovits, "Geopolymers: inorganic polymeric new materials," *Journal of Thermal Analysis and calorimetry,* vol. 37, pp. 1633-1656, 1991.

[133] R. E. Lyon, P. Balaguru, A. Foden, U. Sorathia, J. Davidovits, and M. Davidovics, "Fire-resistant aluminosilicate composites," *Fire and materials,* vol. 21, pp. 67-73, 1997.

[134] C. Papakonstantinou, P. Balaguru, and R. Lyon, "Comparative study of high temperature composites," *Composites Part B: Engineering,* vol. 32, pp. 637-649, 2001.

[135] T. Alomayri, L. Vickers, F. U. A. Shaikh, and I.-M. Low, "Mechanical properties of cotton fabric reinforced geopolymer composites at 200–1000 °C," *Journal of Advanced Ceramics,* vol. 3, pp. 184-193, 2014.

[136] M. Chabannes, J.-C. Bénézet, L. Clerc, and E. Garcia-Diaz, "Use of raw rice husk as natural aggregate in a lightweight insulating concrete: An innovative application," *Construction and Building Materials,* vol. 70, pp. 428-438, 2014.

[137] G. Masi, W. D. Rickard, M. C. Bignozzi, and A. van Riessen, "The influence of short fibers and foaming agents on the physical and thermal behavior of geopolymer composites," *Advances in Science and Technology,* vol. 92, p. 56, 2014.

[138] J. H. S. Almeida, C. C. Angrizani, E. C. Botelho, and S. C. Amico, "Effect of fiber orientation on the shear behavior of glass fiber/epoxy composites," *Materials & Design (1980-2015),* vol. 65, pp. 789-795, 2015.

[139] H. Assaedi, T. Alomayri, F. U. A. Shaikh, and I.-M. Low, "Characterisation of mechanical and thermal properties in flax fabric reinforced geopolymer composites," *Journal of Advanced Ceramics,* vol. 4, pp. 272-281, 2015.

[140] V. Dhand, G. Mittal, K. Y. Rhee, S.-J. Park, and D. Hui, "A short review on basalt fiber reinforced polymer composites," *Composites Part B: Engineering,* vol. 73, pp. 166-180, 2015.

[141] P. S. Latha, M. V. Rao, V. V. K. Kumar, G. Raghavendra, S. Ojha, and R. Inala, "Evaluation of mechanical and tribological properties of bamboo–glass hybrid fiber reinforced polymer composite," *Journal of Industrial Textiles,* vol. 46, pp. 3-18, 2015.

[142] G. Wu, X. Wang, Z. Wu, Z. Dong, and G. Zhang, "Durability of basalt fibers and composites in corrosive environments," *Journal of Composite Materials,* vol. 49, pp. 873-887, 2015.

[143] S. Samal, B. Marvalová, I. Petríková, K. A. Vallons, S. V. Lomov, and H. Rahier, "Impact and post-impact behavior of fabric reinforced geopolymer composite," *Construction and Building Materials,* vol. 127, pp. 111-124, 2016.

[144] P. Timakul, W. Rattanaprasit, and P. Aungkavattana, "Improving compressive strength of fly ash-based geopolymer composites by basalt fibers addition," *Ceramics International,* vol. 42, pp. 6288-6295, 2016.

[145] Z. Lu, J. Xie, H. Zhang, and J. Li, "Long-term durability of basalt fiber-reinforced polymer (BFRP) sheets and the epoxy resin matrix under a wet-dry cyclic condition in a chloride-containing environment," *Polymers,* vol. 9, p. 652, 2017.

[146] H. Le Chi, P. Louda, A. P. Periyasamy, T. Bakalova, and V. Kovacic, "Flexural behavior of carbon textile-reinforced geopolymer composite thin plate," *Fibers,* vol. 6, p. 87, 2018.

[147] G. Taveri, E. Bernardo, and I. Dlouhy, "Mechanical performance of glass-based geopolymer matrix composites reinforced with cellulose fibers," *Materials,* vol. 11, p. 2395, 2018.

[148] S. Samal, "Effect of high temperature on the microstructural evolution of fiber reinforced geopolymer composite," *Heliyon,* vol. 5, p. e01779, 2019.

[149] B. a.s. (2019). *Processing of endless basalt fibers into technical products*. Available: http://www.basaltex.cz/cedic/cedic_charakteristika_cz.htm#08

[150] Z. Abdollahnejad, *Development of Foam One-Part Geopolymers*. Universidade do Minho Escola de Engenharia, 2016.

[151] J. Davidovits, "Global warming impact on the cement and aggregates industries," *World Resource Review,* vol. 6, pp. 263-278, 1994.

[152] D. Tran, P. Louda, O. Bortnovsky, and P. Bezucha, "Mechanical Properties of Silica-Based Geopolymer Composites Cured at Ambient Conditions in Accordance with Size-Independent Method," 2010.

[153] T. Hung, D. Pernica, D. Kroisová, O. Bortnovsky, P. Louda, and V. Rylichova, "Composites base on geopolymer matrices: Preliminary fabrication, mechanical properties and future applications," in *Advanced Materials Research*, 2008, pp. 477-480.

[154] P. Duxson, J. L. Provis, G. C. Lukey, and J. S. Van Deventer, "The role of inorganic polymer technology in the development of 'green concrete'," *cement and concrete research,* vol. 37, pp. 1590-1597, 2007.

[155] J. Davidovits, "Waste solidification and disposal method," ed: Google Patents, 1989.

[156] J. Van Jaarsveld, J. Van Deventer, and L. Lorenzen, "The potential use of geopolymeric materials to immobilise toxic metals: Part I. Theory and applications," *Minerals Engineering,* vol. 10, pp. 659-669, 1997.

[157] J. Van Jaarsveld, J. Van Deventer, and A. Schwartzman, "The potential use of geopolymeric materials to immobilise toxic metals: Part II. Material and leaching characteristics," *Minerals Engineering,* vol. 12, pp. 75-91, 1999.

[158] T. Hanzlíček, M. Steinerová, P. Straka, I. Perná, P. Siegl, and T. Švarcová, "Reinforcement of the terracotta sculpture by geopolymer composite," *Materials & Design,* vol. 30, pp. 3229-3234, 2009.

[159] G. INSTITUTE. (2006). *Chemical Structure and Applications*. Available: https://www.geopolymer.org/tag/ceramic/

[160] J. L. Provis, and Jan Stephanus Jakob Van Deventer, eds. Elsevier, *Geopolymers: structures, processing, properties and industrial applications*, 2009.

[161] E. Hartin, "Fire development and fire behavior indicators," ed, 2005.

[162] R. Bushnell, "Fire engineering for building structures and safety: 205 pp. ISBN 85825 492 1. Price: Australian $35· 00," ed: Elsevier, 1989.

[163] R. H. White, "Analytical methods for determining the fire resistance of timber members," in *SFPE handbook of fire protection engineering*, ed: Springer, 2016, pp. 1979-2011.

[164] D. Hardjito, S. E. Wallah, D. M. Sumajouw, and B. V. Rangan, "On the development of fly ash-based geopolymer concrete," *Materials Journal,* vol. 101, pp. 467-472, 2004.

[165]   J.-K. Kim, Y.-H. Moon and S.-H. Eo, "Compressive strength development of concrete with different curing time and temperature," *Cement and Concrete Research,* vol. 28, pp. 1761-1773, 1998.

[166]   V. Bhikshma, R. M. KOTI, and R. T. SRINIVAS, "An experimental investigation on properties of geopolymer concrete (no cement concrete)," 2012.

[167]   V. S. Le, P. Hájková, V. Kovačič, T. Bakalova, L. Voleský, C. H. Le*, et al.*, "thermal conductivity of reinforced geopolymer foams," *Ceramics-Silikaty,* 2019.

[168]   V. S. Le, M. M. Szczypinski, P. Hájková, V. Kovacic, T. Bakalova, L. Volesky*, et al.*, "Mechanical properties of geopolymer foam at high temperature," vol. 27, p. 129, 2020.

[169]   Š. Hýsek, M. Frydrych, M. Herclík, L. Fridrichová, P. Louda, R. Knížek*, et al.*, "Permeable Water-Resistant Heat Insulation Panel Based on Recycled Materials and Its Physical and Mechanical Properties," *Molecules,* vol. 24, p. 3300, 2019.

[170]   Š. Hýsek, M. Frydrych, M. Herclík, P. Louda, L. Fridrichová, S. Le Van*, et al.*, "Fire-Resistant Sandwich-Structured Composite Material Based on Alternative Materials and Its Physical and Mechanical Properties," *Materials,* vol. 12, p. 1432, 2019.

[171]   M. Frydrych, Š. Hýsek, L. Fridrichová, S. Le Van, M. Herclík, M. Pechočiaková*, et al.*, "Impact of Flax and Basalt Fibre Reinforcement on Selected Properties of Geopolymer Composites," *Sustainability,* vol. 12, p. 118, 2020.

[172]   H. L. Chi, P. Hájková, S. Le Van, P. Louda, and L. Voleský, "Water Absorption Properties of Geopolymer Foam after Being Impregnated with Hydrophobic Agents," *Materials,* vol. 12, p. 4162, 2019.

[173]   E. ČSN, "Natural stone test methods–Determination of real density and apparent density and of total and open porosity, 2000," 1936.

[174]   "ASTM C78/C78M - 10, Standard Test Method for Flexural Strength of Concrete (Using Simple Beam with Third-Point Loading)." in *ASTM C78/C78M - 10: Standard Test Method for Flexural Strength of Concrete (Using Simple Beam with Third-Point Loading).* ed, 2010, pp. 1-4.

[175]   "ASTM C348 - 08, Standard Test Method for Flexural Strength of Hydraulic-Cement Mortars.," in *ASTM C348 - 08: Standard Test Method for Flexural Strength of Hydraulic-Cement Mortars.*, ed, 2008, pp. 1-6.

[176]   a. s. České lupkové závody. (2019). *BAUCIS LK*. Available: http://www.cluz.cz/en/baucis-lk

[177]   p.-. kovyachemie.cz. (2018). *Aluminum powder*. Available: https://www.kovyachemie.cz/kontakty/

[178]   KEMA MORAVA - sanační centrum s.r.o. (2016). *Kema mikrosilika*. Available: http://www.kema-morava.cz/files/technicke_listy/CZ%20Kema%20 MIKROSILIKA.pdf

[179]   a. s. Sklopísek Střeleč. (2018). *Catalogue of Products*. Available: https://en.glassand.eu/getFile/case:show/id:432775??

[180]   Basalt.Today. (2018). *Chemical composition of basalt*. Available: https://basalt.today/2018/11/17329/

Part II. REPRINTS OF APPENDED ARTICLE

THERMAL CONDUCTIVITY OF REINFORCED GEOPOLYMER FOAMS

#VAN SU LE*, PAVLÍNA HÁJKOVÁ*, **, VLADIMIR KOVACIC*, TOTKA BAKALOVA*, VOLESKÝ LUKÁŠ*, CHI HIEP LE*, KEVIN CECCON SEIFERT*,***, AMANDA PEREIRA PERES*,***, PETR LOUDA*

*Faculty of Mechanical Engineering, Department of Material Science, Technical University of Liberec, Studentská 2, 461 17 Liberec, Czech Republic
**Unipetrol Centre for Research and Education, Revoluční 84, 400 01 Ústí nad Labem, Czech Republic
*** Department of Mechanical Engineering, Federal University of Rio Grande do Sul, Rua Sarmento Leite, no 425 – centro, Porto Alegre, RS, Cep 90050 – 170, Brazil

#E-mail: longsuvp90@gmail.com

Reinforced geopolymer foams were studied in this work as potential building materials. It has been widely assumed that for a given thermal conductivity λ [W·m⁻¹·K⁻¹], geopolymer foams can have a lighter density than other materials. The study sought to test this assumption by comparing the thermal conductivity between geopolymer foams. The thermal conductivity λ was measured using an ISOMET 2014 device. In all the experiments, the geopolymer foams were obtained by adding aluminium powder and several combinations: silica fume and fine sand reinforced by short basalt fibres. Curing was carried out at room temperature and then in a furnace at 70 °C. After the curing process, the properties of the samples were tested at 7 and 28 days. The results show that the thermal conductivity, porosity, compressive strength, flexural strength and density for all of the tests ranged in the following values: 0.13 - 0.359 W·m⁻¹·K⁻¹; 41.8 - 62.5 %; 1.94 - 9 MPa; 0.96 - 2.93 MPa; 546 - 1028 kg·m⁻³, respectively. It was proven that the filler in the geopolymer foams has a significant influence on the mechanical and physical properties of the tested samples.

INTRODUCTION

Geopolymer foams (GFs) have been widely investigated because of their unique properties, such as low thermal conductivity (TC), good mechanical properties, excellent high temperature stability [1], environmentally friendly, simple fabrication and lower sintering temperature [2-5]. Geopolymers were specified by Joseph Davidovits in the 1970s as a new class of 3-dimensional aluminosilicate materials. [6] Geopolymer materials have a number of advantages, such as excellent mechanical properties, good fire resistance and thermal stability, and they are resistant to acid attacks. A low density geopolymer can be considered as a potential material for applications in many fields. They have been used as thermal insulation, building materials [3, 7, 8], membranes and membrane supports [9, 10], adsorbents and fillers [11-14] or catalysts [15, 16]. Due to its low TC, geopolymers are designed for fire-resistance, which can be exposed to high temperature for an extended period of time [6, 17].

Nowadays, cement is very popular in the construction industry. The global cement production is expected to increase from 3.27 billion metric tonnes in 2010 to 4.83 billion metric tonnes in 2030 [18]. One of the weaknesses of cement is its low fire-resistance compared to some other materials, and it causes a global warming effect. The production of one tonne of cement generates one tonne of carbon-dioxide. That is a reason why a substitute for cement should be developed. Geopolymers are a good candidate for this, because they offer great properties, such as green materials, low cost and durability, low global warming potential (GWP), and excellent fire-resistance [20].

Concrete accounts for a large proportion of weight on a structure. The use of lower density GFs is beneficial in term of reduced structural load bearing with the further benefits of acoustic and thermal insulation [21-23]. However, the mechanical strength is strongly related to the density and low-density geopolymers can exhibit acceptably low strength. Sufficient mechanical strengths can be achieved with the controlled addition of foaming agents in order to achieve an optimum density and pore structure. Different foaming agents can be used to synthesise low-density geopolymers. Metallic aluminium powder is commonly used, which is very reactive in alkaline environments [22, 24, 25].

Fibre reinforcement has been used in various hardened binders to improve the mechanical properties [26-30]. Basalt fibres are inorganic and as such have

a much higher melting point (1450 °C) than organic fibres, making them a suitable candidate for high temperature resistant geopolymer composites [31-34]. Composite materials based on geopolymer matrices can be produced for various applications requiring good performances at elevated temperatures, but also for applications where thermal insulation at room temperature is necessary.

Foaming methods to reduce the density of the geopolymer have been investigated, as low density geopolymers are increasingly being reported in literature as effective in improving the insulating properties [35]. It was found that the addition of more metal powders to the foamed geopolymer resulted in a lower TC, which is caused by the higher porosity [36]. The macrospores are developed thanks to the release of gaseous hydrogen as a result of the aluminium reaction in the strong alkaline environment [24]. Meanwhile, two criteria were considered in selecting the mixtures for the TC testing:

- Mixtures with a compressive strength higher than 2 MPa;
- Mixtures with a bulk density lower than 1100 kg·m^{-3}.

The lowest TC performance (0.132 W·m^{-1}·K^{-1}) was recorded for the one-part geopolymer mortars and 1.2 % Al. Furthermore, a close value of the TC was measured for the same mixture with the 1.5 % aluminium powder [37]. The aluminium powder was used to create bubbles in the porous structure and provide information for the porous geopolymer production. It was introduced by adding the 0.05 - 1 % aluminium powder as a reactive material in the geopolymers to react with the water inside those materials and generate hydrogen gas inside the specimens [38, 39]. The TC diminished from 1.65 to 0.47 W·m^{-1}·K^{-1} for the density from 1800 to 600 kg·m^{-3} [40]. The addition of silica fume as a pore forming agent with an optimum at 5 - 10 wt. % [24] was used. The compressive strength of the geopolymer matrix without the basalt fibre added samples aged 28 days was 35 MPa which increased significantly by 37 percent when only the weight increase of 10 wt. % of basalt fibres were added [41]. As such, the thermal and fire resistance properties of the foamed geopolymers containing the fibre reinforcement were also investigated [33]. The TC measurements should be made at a certain moisture and humidity level for the same batch, as the moisture in the samples has a significant influence on the measurement [33].

This study has been undertaken to investigate the thermal, physical and mechanical properties of geopolymer foamed materials with and without fillers. Evaluating these properties is important for better manufacturing processes and adequate applications.

EXPERIMENTAL

Materials

The industrially supplied material BAUCIS LK (České Lupkové Závody, a.s, Czech Republic) was a two-component aluminosilicate binder based on metakaolin and activated by potassium alkaline [19]. An aluminium powder (pkchemie Inc., Czech Republic) was used to create pores inside the geopolymer. It had an aluminium content of 99 % and the average grain size was 65 µm [42]. The silica fume (produced by Kema Morava – sanační centrum a. s., Republic of Slovenia) contained 90 % SiO$_2$ and the average grain size was 1 mm [43]. A sand (produced by Sklopísek Střeleč a.s., type ST 03-08) was used with a grain size from 0.3 to 0.8 mm [44]. Two types of basalt fibre (Figure 1), a chopped basalt fibre and a waste ground basalt fibre from recycled mate-rial produced by Basaltex a.s. were used. The basalt fibre had a density of 2900 kg·m^{-3}, and thermal conductivity of 0.027 ÷ 0.033 W·m^{-1}·K^{-1} [45].

This work evaluates the impact of the component addition on the binder of the GFs, when one of them was changed and the other components remaining unchanged.

| a) air curing | b) raw brine immersion |
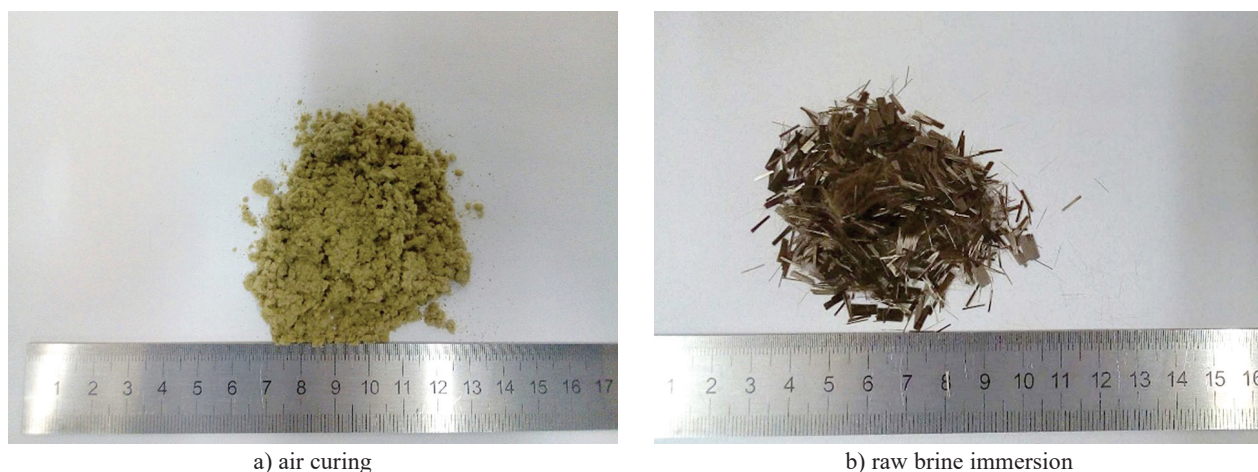
Figure 1. The waste ground basalt fibres (a), the chopped basalt fibre (b).

Table 1. The composition of the mixtures (all in the ratio of mass).

Mix.	A/B	SF\B	S/B	F1/B	F3/B	Note	Mix.	A/B	SF\B	S/B	F3/B	Note
S1	0.008						S5	0.008	0.026	0.066	0.018	
S2	0.008			0.053		I	S6	0.008	0.026	0.263	0.018	II
S3	0.008			0.158			S7	0.008	0.026	0.526	0.018	
S4	0.008			0.263			S8	0.008	0.026	1.05	0.018	
S9	0.00053	0.026	0.526		0,018		S14	0.008	0.026	0.526	0.0026	
S10	0.0026	0.026	0.526		0,018		S15	0.008	0.026	0.526	0.008	
S11	0.0053	0.026	0.526		0,018	III	S16	0.008	0.026	0.526	0.013	IV
S12	0.008	0.026	0.526		0,018		S17	0.008	0.026	0.526	0.018	
S13	0.016	0.026	0.526		0,018		S18	0.008	0.026	0.526	0.026	

*A – Aluminium Powder Agent, B – Activator LK/Baucis = 0.9 (ratio according to manufacturer), SF – Silica Fume, S – Sand, F1 – Waste Ground Basalt Fibres, F3 – Chopped Basalt Fibres.

The "Note" shown in Table 1:

I: A change in the content of the waste ground basalt fibres and chopped basalt fibres without changing the binder

II: The component of the GFs with a different concentration of the sand and constant other components (binder, silica fume, aluminium powder and chopper basalt fibres)

III: The component of the GFs with a different concentration of the aluminium powder and other constant components (binder, silica fume, sand and chopped basalt fibres)

IV: The component of the GFs with a different concentration of the chopped basalt fibres and other constant components (binder, silica fume, aluminium powder and sand)

Sample preparation

The preparation of the GF samples was made as follows: first, the geopolymer binder was prepared by mixing a potassium activator, which was recommended by the suppliers of the BAUCIS LK, and the mixture was stirred for 5 minutes at room temperature until the solution homogenised. Next, the geopolymer was mixed with different fibres, sand, silica fume content and the mixture were homogenised for a further 5 minutes. The aluminium powder was then added at the end of the mixture preparation for about one minute at high speed. Directly after mixing, the fresh GFs were cast into moulds. The geopolymer foam formation was allowed to stabilise after 2h to 4 h (depending on the composition). The samples were then covered by plastic sheets, cured at 70 °C for 24 h, aged for 27 days at room temperature, and then demoulded for testing and characterisation.

Characterisation of the test methods and the samples for measuring

The flexural strength was measured three times for each mixture, using prims with a size of $40 \times 40 \times 160$ mm^3 after 28 days at room temperature, and three cubes of 40 mm^3 were cut from the tested prims and used to test the compressive strength. The test was carried out on the Universal Testing Machine INSTRON Model 4202 (the maximum load of the sensor is 10 KN) at a loading speed of 1 mm·min^{-1}. The weight, height, width, and length of each sample was measured to calculate the volume density. For the strength and density measurements, the mean values of three samples for each mixture were used.

The TC λ was measured using an ISOMET 2014 device. The measurement was based on the analysis of the temperature response of the analysed material to the heat flow impulses. It was equipped with various planar or probes and a planar probe with a range of 0.015 to 6 W·m^{-1}·K^{-1}. The specimens were cast in moulds of $160 \times 160 \times 40$ mm^3. The samples were covered with a plastic film during setting in a furnace at 70 °C for 24 h. After de-moulding they were cured at room temperature for 6 days before the test.

The pore size distributions of two series of GFs were determined using an AutoPore IV 9510 mercury intrusion porosimeter, which operates at pressures from 0.01 to 414 MPa. All the samples of the tests were used on a $40 \times 40 \times 10$ mm^3 plate.

RESULTS AND DISCUSSION

Effect of the fillers and the basalt waste fibre reinforcement

The compressive strength of the GFs without the addition of the waste basalt fibre (sample S1) was 1.94 MPa which significantly increased by 36 %, 87.6 % and 97.4 % when 5, 15.6, 26.3 % of the waste basalt fibre was added, respectively, while on the other hand, the flexural strength of the GFs without the addition of the waste basalt fibre (sample S1), was 1.04 MPa which significantly increased by 32.7 %, 50.9 % when 15.6, 26.3 % of the waste basalt fibre was added, respectively (Figure 2.) Furthermore, group I has a lower volume density and thermal conductivity compared to the other group (Figure 3). However, their strength is the lowest.

Sample S4 is stronger than group I, while the same thermal conductivity can be found on samples S1 and S4. In group II, the results showed a significant increase in the compressive strength, and the same thing happened when comparing the GFs with the flexural strength. After the samples of the GFs were made with a sand aggregate as a filler, the result of sample S8 showed an increase in the compressive strength of 60 % compared to S5, and 300 % compared to S1 without the sand. Samples S6 and S7 had nearly the same strength value, but the volume density of S7 is larger than S6, while having a lower thermal conductivity. The typical compressive
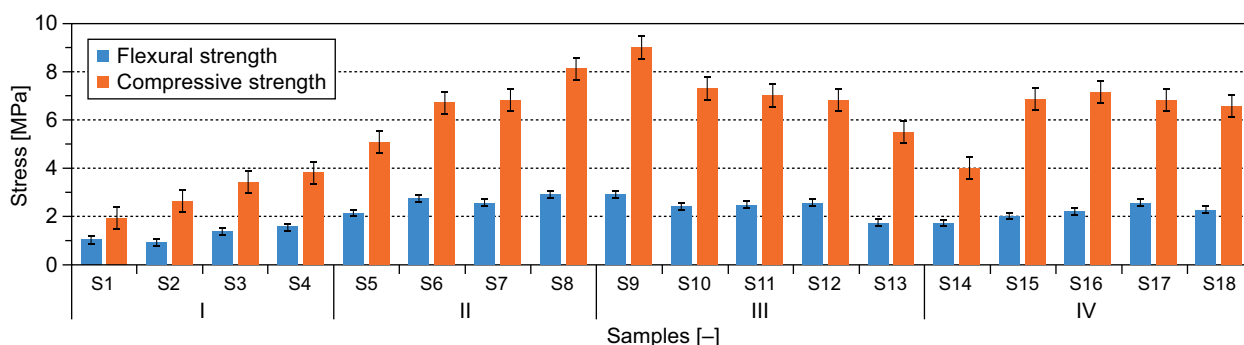
Figure 2. The compressive and flexural strength of the GFs with the reference samples.
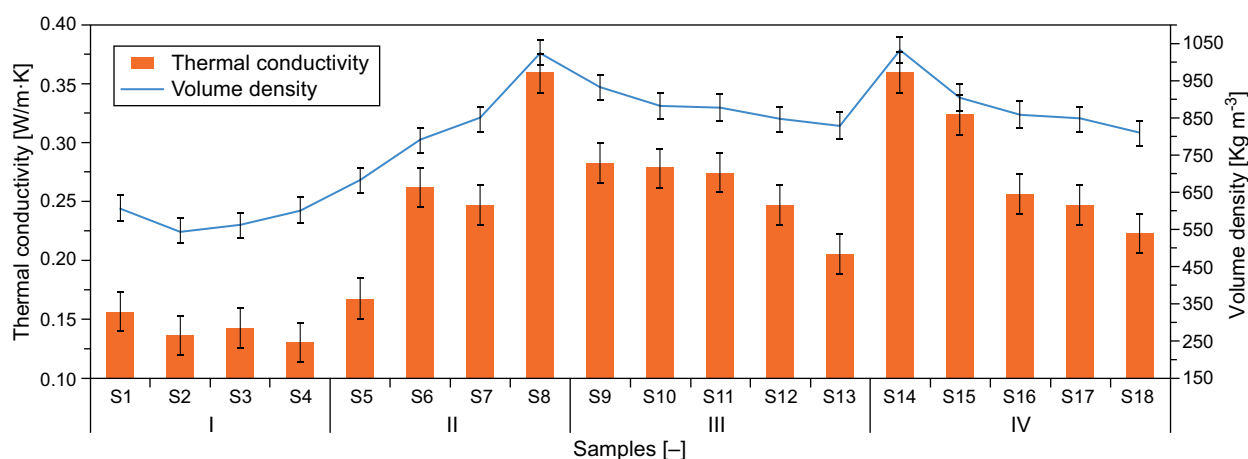
Figure 3. The thermal conductivity and volume density of the GFs with the reference samples.

Table 2. The values of the thermo-physical characteristics of the GFs from this work and literature.

RM	FAT	Density (g·cm^{-3})	Flexural Strength (MPa)	Compressive strength (MPa)	Thermal conductivity (W·m^{-1}·K^{-1})	Ref.
MK	AL	0.58 – 1.1	0.96 – 2.9	2 – 9	0.13 – 0.359	This work
MK	AL, Zn	0.7 – 1.2	–	1 – 7	0.17 – 0.55	[46]
MK	H$_2$O$_2$	0.37 – 0.74	–	0.3 – 11.6	0.11 – 0.17	[47]
MK	H$_2$O$_2$	0.3 – 0.58	–	0.3 – 4.4	0.09 – 0.16	[1]
MK	Al	0.36 – 0.59	–	–	0.12 – 0.17	[48]
MK	H$_2$O$_2$	0.3 – 0.6	–	1.8 – 5.2	0.15 – 0.17	[3]
MK	SI	0.3 – 1.1	–	–	0.08 – 0.12	[49]
MK	Al	0.8 – 1.1	–	4.4 – 9.5	0.3 – 0.65	[50]
Mk, FA	H$_2$O$_2$	0.44 – 0.84	–	0.3 – 6	0.08 – 0.17	[51]
MK, Glass	H$_2$O$_2$	0.5 – 1.45	–	3.1 – 24	0.42 – 0.75	[52]
MK, RHA, VA	Si	0.36 – 0.47	–	–	0.12 – 0.17	[8]
FA	AL	0.671	1	6	0.145	[5]
FA	Al	0.89 – 0.93	–	5.5 – 10.9	0.25 – 0.39	[53]
FA	H$_2$O$_2$	0.6 – 1.2	–	1.2 – 7	0.1 – 0.4	[4]
FA	Al	0.55 – 0.97	–	2 – 8	0.1 – 0.25	[24]
FA, Slag	SAC	0.6 – 1.2	–	2 – 30	0.1 – 0.5	[7]

RW – Raw Materials, FAT – Foam Agent Type, FA – Fly Ash, RHA – Rice Hush Ash, VA – Volcanic Ash, SAC – Surface-Active Concentrate, Ref. – Reference Literature

strength for the GFs with densities of 680 - 1028 kg·m⁻³ is 5 - 8 MPa. The presence of these minerals and aggregates may have provided a better strength. However, our results were high on the thermal conductivity of 0.16 - 0.36 W·m⁻¹·K⁻¹ in group III, when the different foaming aluminium powder agent amounts of 0.053, 0.26, 0.53, 0.8 and 1.6 % of mass were added to a binder geopolymer matrix. The compressive strength, volume density and thermal conductivity of the GFs decreased from 10 to 45 %. Sample S8 with a high compressive strength of 9 MPa was achieved within the samples containing 0.053 % aluminium powder. The use of the sand aggregate had a positive effect on the strength for the GFs. Samples S9 to S13 were added at a Baucis ratio: sand 1:1 due to these values, the volume density was around 850 - 950 kg·m⁻³. The average strength for samples S10, S11 and S12 was around 7 MPa. The addition of aluminium in the GFs had a bigger effect on the porosity, thermal conductivity and volume density. Because sample S13 has used a high amount of aluminium powder, an important decrease in the strength, due to the lack of time to create pores in the GFs, and faster hardening was observed. In group IV, the compressive strength was around 7 MPa except for sample S14, which was determined to be 4.04 MPa. The thermal conductivity and volume density were significantly reduced from 0.36 to 0.2 W·m⁻¹·K⁻¹ and from 1028 to 808 kg·m⁻³, respectively. The values of the thermal conductivity of samples S16 and S17 were the same at around 0.25 W·m⁻¹·K⁻¹. On the other hand, sample S17 had the highest flexural strength of all of the samples in group IV.

Analysis of the micro porosity using an Hg intrusion porosimeter

The pore size distribution in the range of 0.003 - - 300 µm, significantly influence the volume of porosity of the GFs when considering the reinforcing fibre, fillers, such as sand, the foaming agent. In Figure 4, it was shown that the volume of the porosity decreases when the basalt waste fibre percentage increases. When it was increased by up to 26.3 % via the weight of the binder (Table 1), it also increased. In Figure 5, it was clearly shown that when the amount of sand decreased, the volume of the porosity also decreased. In Figure 6, the percentage of the aluminium powder on the GFs increased, and, therefore, the volume of the porosity of the GFs also increased.

Analysis of the macro porosity by imaging

In Figure 7, the photographs of the porous samples S1-S4, S5-S8, S9-S13, and S14-S18 are shown. The pores seem irregular in the all of the samples. The reactivity of the foaming agent, the viscosity and homogeneity of the slurry influence the morphology of the pores (shape and diameter) and their distribution [48]. In Figure 7a, the degree of the pore generation and its size when the percentage of basalt waste fibre was increased can be visually observed. It appears that the size of the largest pores is one cm (Figure 7a). When the percentage of the fillers, such as the sand, increase in the GFs, the pore size is reduced, and the pores become more uniform in diameter (Figure 7b). An increase in the percentage of the aluminium powder or chopped basalt fibre significantly increases the size of the pores, as seen in
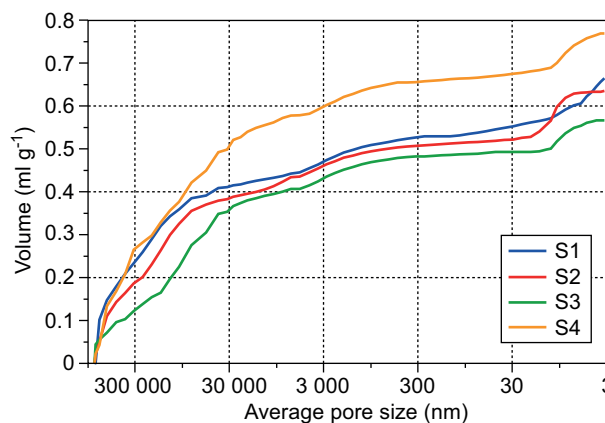
Figure 4. The average pore sizes of the different samples S1-S4.
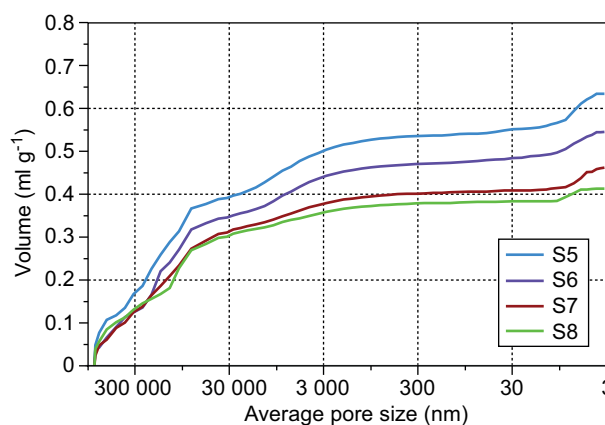
Figure 5. The average pore sizes of the different samples S5-S8.
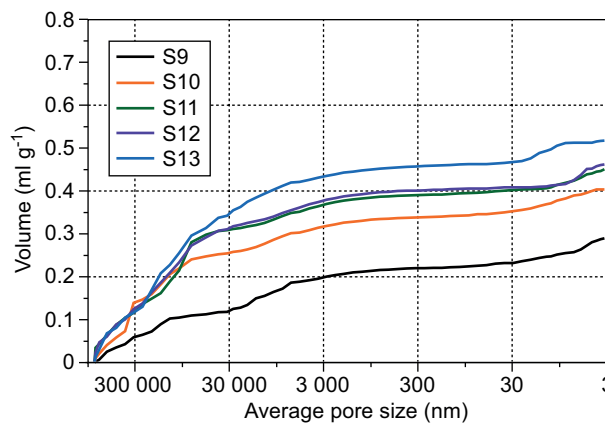
Figure 6. The average pore sizes of the different samples S9-S13.

a) S1 – S4

b) S5 – S8

c) S9 – S13

d) S14 – S18
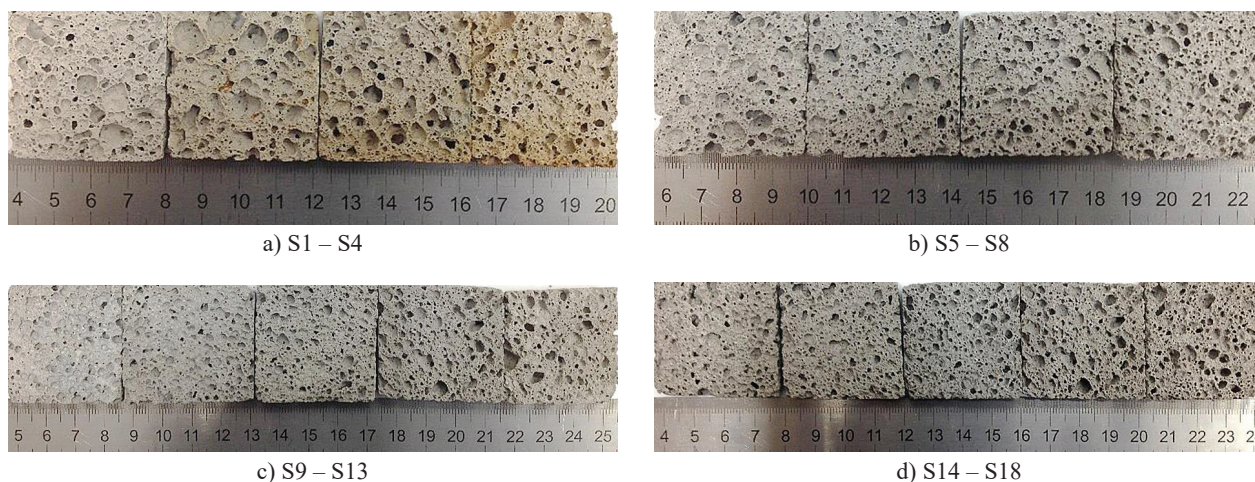
Figure 7. Photos of the different types of GFs with dimension 40×40 mm^2.

Figure 7c and Figure 7d, respectively. Several works can be mentioned to provide an explanation. Larger pores are created in the GFs based on a potassium activator [20]. The low viscosity and the high alkalinity of the slurry help in the creation and coalescence of the H$_2$ bubbles; however, this leads to the fast consolidation of the mixture, thereby, causing the wide statistical distribution of the pore size probability [51]. The circular shape and uniformity of the pore distribution improve the insulating properties of the foams [8, 54]. The broad and heterogeneous distribution of the pores are formed by the intricate network between the porous cavities, which in sum contain a large amount of air This leads to the significant dissipation of the sound waves within the porous matrix [8, 55]. The amount of irregularly formed therein increases the pores considerably. The smaller the formed air voids are, the more regular their shape and homogenous distribution increases the comparable thermal conductivity of the volume density.
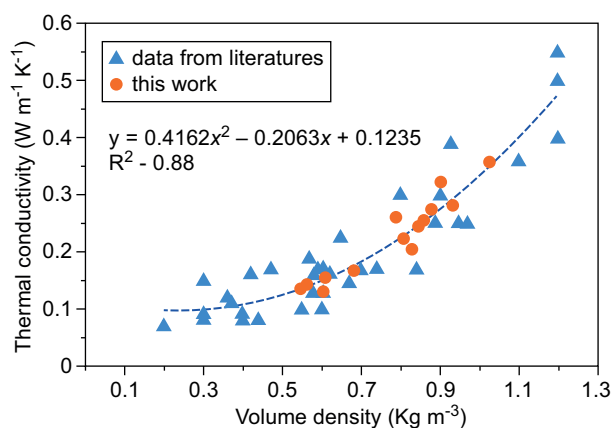
Figure 8. The relationship of the thermal conductivity with the volume density. Data from Ref. [1, 3-5, 7, 8, 33, 45-57] and this work.

Evaluate the relationship between the thermal conductivity and volume density

The exponential trend line with numeric values of $R^2 = 0.88$ shows that the congruent transformation is consistent with the individual measured values. In other words, the increase in the thermal conductivity depends on the volume density. The thermal conductivity also increases with the rising volume density. The values measured in this work are also in accordance with these rules. (Orange curve in Figure 8)

According to the description in Timakulov's work [41], the compressive strength of fly-ash geopolymer was reduced when a 15 - 30 wt. % basalt fibre addition was used. Nonetheless, the results of this work indicate the opposite trend. The concrete's density ranges from 2100 to 2415 kg·m^{-3} [28, 56], while the GFs have a volume density under 1200 kg·m^{-3} (see Table 2 and Figure 8). The thermal conductivity mostly depends on the composition, fillers and testing conditions [57, 58]. This reduction in the strength is due to the fact that the GF needs more aluminium powder in order to achieve large porosity, which decreases the volume density and thermal conductivity. GFs with a wide range of thermal conductivity were successfully synthesised by adding an aluminium powder. Compared to other works [46, 50], where a similar volume density and the same foaming method are shown, the strength and the thermal conductivity indexes do not achieve results as good as those in this work (Table 2). It is evident from the analysis of References 5 and 25 in Table 2 that the result is similar in this work; however, the description in Reference 35 is not in accordance with this work. Furthermore, many heavy metals are contained in the used fly-ash, and these may be hazardous substances that cause health risks [59]. This article shows the possibility to obtain a lower thermal conductivity or a low volume density from a potassium and Baucis (LK) alkaline environment and/or fumed silica and/or fillers

and/or reinforced fibre through the aluminium powder foaming method. The conclusion derived from this work and other literature summarises the dependence on the investigated parameters, such as fibres for reinforcement, fillers and a foaming agent.

The use of a fibre basalt waste as a by-product for reinforcing the GFs combined with the ambient temperature significantly improves the physical, thermal and mechanical properties of the GFs, enabling a reduction in the cost of the GFs and to create an environmentally friendly material. The lowest thermal conductivity of the GFs is 0.13 W·m^{-1}·K^{-1}.

Fillers such as sand, fibres and silica fume as an agent supporting the foaming properties, which improve the properties, were used in the GFs for the reinforcement. This is primarily manifested in the compressive and flexural strengths, whose measured values are around 5 - 9 MPa and 2 - 3 MPa, respectively. The use of silica fume as a waste by-product as an additional ingredient used to obtain the GFs is catalogued according to the risks to the health or the environment as a green material within the current description of the supplier and for concentrated product.

The results of this work allow for the design of the ratio of a proportional mixture (see Table 3).

With the growing demand for housing and of the

Table 3. The composition / information on the ingredients.

Ingredient name	% Wt.	Note
Baucis LK (clay)	41 – 49.6	
Potassium alkaline	37.3 – 44.7	Without fillers
Fibre waste basalt	13.5 – 20.7	
Aluminium	0.62 – 0.68	
Baucis LK (clay)	31.54 – 44.84	
Potassium alkaline	28.39 – 40.36	
Chopper fibres	0.42 – 5.6	With fillers
Sand	6.28 – 31.54	
Silica fume	1.58 – 2.24	
Aluminium powder	0.16 – 0.67	

construction industries in developed and developing countries, the demand for sustainable and friendly materials is increasing, as well as the growing popularity of geopolymers. These materials must be light and be able to withstand heat, have good sound absorption and be durable. Let us look at the common values in Table 2, where the values are shown as the results of this work. It is clear that they allow for the use of the investigated material as a thermal insulation and relative sound insulation.

CONCLUSIONS

The GF characterisation shows that a basalt waste fibre has a significant effect on the mechanical properties of the GFs and the necessary fillers' content.

It has been shown that a higher addition of basalt waste fibres reduces the thermal conductivity of the GFs due to small, homogenised and regular pore distribution.

The results also show that the thermal conductivity is increased after adding fillers with a larger proportion of chopped basalt fibres.

Acknowledgements

REFERENCE

1. C. Bai, G. Franchin, H. Elsayed, A. Zaggia, L. Conte, H. Li, et al., "High-porosity geopolymer foams with tailored porosity for thermal insulation and wastewater treatment," Journal of Materials Research, vol. 32, pp. 3251-3259, 2017. doi: 10.1557/jmr.2017.127

2. I. Lecomte, M. Liégeois, A. Rulmont, R. Cloots, and F. Maseri, "Synthesis and characterization of new inorganic polymeric composites based on kaolin or white clay and on ground-granulated blast furnace slag," Journal of materials research, vol. 18, pp. 2571-2579, 2003. doi: 10.1557/JMR.2003.0360

3. P. Palmero, A. Formia, P. Antonaci, S. Brini, and J.-M. Tulliani, "Geopolymer technology for application-oriented dense and lightened materials. Elaboration and characterization," Ceramics International, vol. 41, pp. 12967-12979, 2015. doi: 10.1016/j.ceramint.2015.06.140

4. R. M. Novais, L. Buruberri, G. Ascensão, M. Seabra, and J. Labrincha, "Porous biomass fly ash-based geopolymers with tailored thermal conductivity," Journal of cleaner production, vol. 119, pp. 99-107, 2016. doi: 10.1016/j.jclepro.2016.01.083

5. P. Hlaváček, V. Šmilauer, F. Škvára, L. Kopecký, and R. Šulc, "Inorganic foams made from alkali-activated fly ash: Mechanical, chemical and physical properties," Journal of the European Ceramic Society, vol. 35, pp. 703-709, 2015. doi: 10.1016/j.jeurceramsoc.2014.08.024

6. J. Davidovits, "years of successes and failures in geopolymer applications. Market trends and potential breakthroughs," in Geopolymer 2002 Conference, 2002, p. 29.

7. Z. Zhang, J. L. Provis, A. Reid, and H. Wang, "Mechanical, thermal insulation, thermal resistance and acoustic absorption properties of geopolymer foam concrete," Cement and Concrete Composites, vol. 62, pp. 97-105, 2015. doi: 10.1016/j.cemconcomp.2015.03.013

8. E. Papa, V. Medri, D. Kpogbemabou, V. Morinière, J. Laumonier, A. Vaccari, et al., "Porosity and insulating properties of silica-fume based foams," Energy and Buildings, vol. 131, pp. 223-232, 2016. doi: 10.1016/j.enbuild.2016.09.031

9. Y. Ge, Y. Yuan, K. Wang, Y. He, and X. Cui, "Preparation of geopolymer-based inorganic membrane for removing Ni^{2+} from wastewater," Journal of hazardous materials, vol. 299, pp. 711-718, 2015. doi: 10.1016/j.jhazmat.2015.08.006

10. C. Bai and P. Colombo, "High-porosity geopolymer membrane supports by peroxide route with the addition of egg white as surfactant," Ceramics International, vol. 43, pp. 2267-2273, 2017. doi: 10.1016/j.ceramint.2016.10.205

11. M. Minelli, V. Medri, E. Papa, F. Miccio, E. Landi, and F. Doghieri, "Geopolymers as solid adsorbent for CO_2 capture," Chemical Engineering Science, vol. 148, pp. 267-274, 2016. doi: 10.1016/j.ces.2016.04.013

12. R. M. Novais, L. Buruberri, M. Seabra, and J. Labrincha, "Novel porous fly-ash containing geopolymer monoliths for lead adsorption from wastewaters," Journal of hazardous materials, vol. 318, pp. 631-640, 2016. doi: 10.1016/j.jhazmat.2016.07.059

13. T. Luukkonen, M. Sarkkinen, K. Kemppainen, J. Rämö, and U. Lassi, "Metakaolin geopolymer characterization and application for ammonium removal from model solutions and landfill leachate," Applied Clay Science, vol. 119, pp. 266-276, 2016. doi: 10.1016/j.clay.2015.10.027

14. F. J. López, S. Sugita, M. Tagaya, and T. Kobayashi, "Metakaolin-based geopolymers for targeted adsorbents to heavy metal ion separation," Journal of Materials Science and Chemical Engineering, vol. 2, p. 16, 2014. doi: 10.4236/msce.2014.27002

15. S. Sharma, D. Medpelli, S. Chen, and D.-K. Seo, "Calcium-modified hierarchically porous aluminosilicate geopolymer as a highly efficient regenerable catalyst for biodiesel production," RSC Advances, vol. 5, pp. 65454-65461, 2015. doi: 10.1039/C5RA01823D

16. Y. J. Zhang, L. C. Liu, Y. Xu, and Y. C. Wang, "A new alkali-activated steel slag-based cementitious material for photocatalytic degradation of organic pollutant from waste water," Journal of hazardous materials, vol. 209, pp. 146-150, 2012. doi: 10.1016/j.jhazmat.2012.01.001

17. M. S. Cilla, P. Colombo, and M. R. Morelli, "Geopolymer foams by gelcasting," Ceramics International, vol. 40, pp. 5723-5730, 2014.

18. The Statistics Portal. (2018). Global Cement Production From 1990 to 2030. Available: https://www.statista.com/statistics/373845/global-cement-production-forecast/

19. a. s. České lupkové závody. (2019). BAUCIS LK. Available: http://www.cluz.cz/en/baucis-lk

20. Z. Abdollahnejad, F. Pacheco-Torgal, T. Félix, W. Tahri, and J. B. Aguiar, "Mix design, properties and cost analysis of fly ash-based geopolymer foam," Construction and Building Materials, vol. 80, pp. 18-30, 2015. doi: 10.1016/j.conbuildmat.2015.01.063

21. Y.-P. Chiu, Y.-M. Lu, and Y.-C. Shiau, "Applying inorganic geopolymers added with aluminium powder to fire-resistant fillers," Materials Research Innovations, vol. 19, pp. S5-642-S5-649, 2015. doi: 10.1179/1432891714Z.0000000001168

22. M. M. A. Abdullah, K. Hussin, M. Bnhussain, K. N. Ismail, Z. Yahya, and R. A. Razak, "Fly Ash-based Geopolymer Lightweight Concrete Using Foaming Agent," International Journal of Molecular Sciences, vol. 13, pp. 7186-7198, Jun 2012. doi: 10.3390/ijms13067186

23. C. Shi, "Composition of materials for use in cellular lightweight concrete and methods thereof," ed: Google Patents, 2002.

24. F. Skvara, R. Sulc, T. Zdenek, S. Petr, S. Vit, and Z. Cílová, "Preparation and properties of fly ash-based geo-polymer foams," Ceramics-Silikaty, vol. 58, pp. 188-197, 2014.

25. A. Hajimohammadi, T. Ngo, P. Mendis, and J. Sanjayan, "Regulating the chemical foaming reaction to control the porosity of geopolymer foams," Materials & Design, vol. 120, pp. 255-265, 2017. doi: 10.1016/j.matdes.2017.02.026

26. T. Alomayri and I. M. Low, "Synthesis and characterization of mechanical properties in cotton fiber-reinforced geopolymer composites," Journal of Asian Ceramic Societies, vol. 1, pp. 30-34, 2013.

27. T. Alomayri, L. Vickers, F. U. Shaikh, and I.-M. Low, "Mechanical properties of cotton fabric reinforced geopolymer composites at 200–1000 C," Journal of Advanced Ceramics, vol. 3, pp. 184-193, 2014. doi: 10.1007/s40145-014-0109-x

28. K. Vijai, R. Kumutha, and B. Vishnuram, "Properties of glass fibre reinforced geopolymer concrete composites," 2012.

29. Š. Hýsek, R. Wimmer, and M. Böhm, "Optimal processing of flax and hemp fibre nonwovens," BioResources, vol. 11, pp. 8522-8534, 2016.

30. Š. Hýsek, M. Podlena, H. Bartsch, C. Wenderdel, and M. Böhm, "Effect of wheat husk surface pre-treatment on the properties of husk-based composite materials," Industrial Crops and Products, vol. 125, pp. 105-113, 2018. doi: 10.1016/j.indcrop.2018.08.035

31. P. Amuthakkannan, V. Manikandan, J. W. Jappes, and M. Uthayakumar, "Effect of fibre length and fibre content on mechanical properties of short basalt fibre reinforced polymer matrix composites," Materials Physics and Mechanics, vol. 16, pp. 107-117, 2013.

32. T. D. Hung, P. Louda, D. Kroisová, O. Bortnovsky, and N. T. Xiem, "New generation of geopolymer composite for fire-resistance," in Advances in Composite Materials-Analysis of Natural and Man-Made Materials, ed: InTech, 2011.

33. G. Masi, W. D. Rickard, M. C. Bignozzi, and A. Van Riessen, "The effect of organic and inorganic fibres on the mechanical and thermal properties of aluminate activated geopolymers," Composites Part B: Engineering, vol. 76, pp. 218-228, 2015. doi: 10.1016/j.compositesb.2015.02.023

34. K. Sakkas, D. Panias, P. Nomikos, and A. Sofianos, "Potassium based geopolymer for passive fire protection of concrete tunnels linings," Tunnelling and underground space technology, vol. 43, pp. 148-156, 2014. doi: 10.1016/j.tust.2014.05.003

35. G. Masi, W. D. Rickard, M. C. Bignozzi, and A. van Riessen, "The influence of short fibres and foaming agents on the physical and thermal behaviour of geopolymer composites," Advances in Science and Technology, vol. 92, p. 56, 2014. doi: 10.4028/www.scientific.net/AST.92.56

36. T.-Y. Yang, C.-C. Chou, and C.-C. Chien, "The effects of foaming agents and modifiers on a foamed-geopolymer," in The 2012 World Congress on Advances in Civil, Environmental, and Materials Research (ACEM'12) Seoul, Korea, 2012.

37. Z. Abodollahnejad, Development Of Foam One-Part Geopolymer. Universidade do Minho Escola de Engenharia, 2016.

38. P. Keawpapasson, C. Tippayasam, S. Ruangjan, P. Thavorniti, T. Panyathanmaporn, A. Fontaine, et al., "Metakaolin-Based Porous Geopolymer with Aluminium Powder," Key Engineering Materials, vol. 608, pp. 132-138, 2014. doi: 10.4028/www.scientific.net/KEM.608.132

39. Z. Q. Guo, X. Li, X. G. Yuan, and H. J. Huang, "Effects of

extrusion methods and powder carriers on powder forming and precursor foaming behavior in the preparation process of aluminum foam," in Advanced Materials Research, 2013, pp. 1734-1739.

40. R. A. Aguilar, O. B. Díaz, and J. E. García, "Lightweight concretes of activated metakaolin-fly ash binders, with blast furnace slag aggregates," Construction and building materials, vol. 24, pp. 1166-1175, 2010. doi: 10.1016/j.conbuildmat.2009.12.024

41. P. Timakul, W. Rattanaprasit, and P. Aungkavattana, "Improving compressive strength of fly ash-based geopolymer composites by basalt fibers addition," Ceramics International, vol. 42, pp. 6288-6295, 2016. doi: 10.1016/j.ceramint.2016.01.014

42. p.-. kovyachemie.cz. (2018). Aluminum powder. Available: https://www.kovyachemie.cz/kontakty/

43. KEMA MORAVA – sanační centrum s.r.o. (2016). KEMA MIKROSILIKA. Available: http://www.kema-morava.cz/files/technicke_listy/CZ%20Kema%20MIKROSILIKA.pdf

44. a. s. Sklopísek Střeleč. (2018). CATALOGUE OF PRODUCTS. Available: https://en.glassand.eu/getFile/case:show/id:432775??

45. B. a.s. (2019). Processing of endless basalt fibers into technical products. Available: http://www.basaltex.cz/cedic/cedic_charakteristika_cz.htm#08

46. Tsung-Yin Yang, Chia-Ching Chou, and a. C.-C. Chien, "the effects of foaming agents and modifiers on a foamed-geopolymer," Advances in Civil, Environmental, and Materials Research (ACEM' 12), 2012.

47. C. Bai, T. Ni, Q. Wang, H. Li, and P. Colombo, "Porosity, mechanical and insulating properties of geopolymer foams using vegetable oil as the stabilizing agent," Journal of the European Ceramic Society, vol. 38, pp. 799-805, 2018. doi: 10.1016/j.jeurceramsoc.2017.09.021

48. E. Kamseu, Z. N. Ngouloure, B. N. Ali, S. Zekeng, U. Melo, S. Rossignol, et al., "Cumulative pore volume, pore size distribution and phases percolation in porous inorganic polymer composites: Relation microstructure and effective thermal conductivity," Energy and buildings, vol. 88, pp. 45-56, 2015. doi: 10.1016/j.enbuild.2014.11.066

49. E. Prud'homme, E. Joussein, and S. Rossignol, "Use of silicon carbide sludge to form porous alkali-activated materials for insulating application," The European Physical Journal Special Topics, vol. 224, pp. 1725-1735, 2015. doi: 10.1140/epjst/e2015-02494-7

50. W. D. Rickard, L. Vickers, and A. Van Riessen, "Performance of fibre reinforced, low density metakaolin geopolymers under simulated fire conditions," Applied Clay Science, vol. 73, pp. 71-77, 2013. doi: 10.1016/j.clay.2012.10.006

51. R. M. Novais, G. Ascensão, L. Buruberri, L. Senff, and J. Labrincha, "Influence of blowing agent on the fresh-and hardened-state properties of lightweight geopolymers," Materials & Design, vol. 108, pp. 551-559, 2016. doi: 10.1016/j.matdes.2016.07.039

52. H. S. Shiu, K. L. Lin, S. J. Chao, C. L. Hwang, and T. W. Cheng, "Effects of foam agent on characteristics of thin-film transistor liquid crystal display waste glass-metakaolin-based cellular geopolymer," Environmental Progress & Sustainable Energy, vol. 33, pp. 538-550, 2014. doi: 10.1002/ep.11798

53. W. D. Rickard and A. Van Riessen, "Performance of solid and cellular structured fly ash geopolymers exposed to a simulated fire," Cement and Concrete Composites, vol. 48, pp. 75-82, 2014. doi: 10.1016/j.cemconcomp.2013.09.002

54. J. Feng, R. Zhang, L. Gong, Y. Li, W. Cao, and X. Cheng, "Development of porous fly ash-based geopolymer with low thermal conductivity," Materials & Design (1980-2015), vol. 65, pp. 529-533, 2015. doi: 10.1016/j.matdes.2014.09.024

55. F. Han, G. Seiffert, Y. Zhao, and B. Gibbs, "Acoustic absorption behaviour of an open-celled aluminium foam," Journal of Physics D: Applied Physics, vol. 36, p. 294, 2003.

56. R. S. Ravindrarajah and W. Jones, "Properties of adjusted density high-performance concrete," Futures in Mechanics of Structures and Materials, p. 351, 2008.

57. Z. Zhang, J. L. Provis, A. Reid, and H. Wang, "Geopolymer foam concrete: An emerging material for sustainable construction," Construction and Building Materials, vol. 56, pp. 113-127, 2014.

58. N. Narayanan and K. Ramamurthy, "Structure and properties of aerated concrete: a review," Cement and Concrete composites, vol. 22, pp. 321-329, 2000. doi: 10.1016/S0958-9465(00)00016-0

59. M. Ahmaruzzaman, "Industrial wastes as low-cost potential adsorbents for the treatment of wastewater laden with heavy metals," Advances in colloid and interface science, vol. 166, pp. 36-59, 2011. doi: 10.1016/j.cis.2011.04.005

Research Article

Van Su Le*, Michal M. Szczypinski, Pavlína Hájková, Vladimir Kovacic, Totka Bakalova, Lukas Volesky, Le Chi Hiep, and Petr Louda

Mechanical properties of geopolymer foam at high temperature

Abstract: In this work, geopolymer foam composites containing waste basalt fibre (10, 30, and 50%wt) were exposed to elevated temperatures of 200, 400, 600, 800 and 1000°C. With an increase in high temperature, the geopolymer foams material exhibits a decrease in compressive strength and bending strength. When heated above 600°C, geopolymer foams materials exhibit a significant reduction in mechanical properties. It shows clearly with the naked eye that surface cracks in case of samples containing 10% of basalt filler. However, when increasing fillers with basalt fibres up to 30% and 50%, the cracking of the sample surface is no longer visible to the naked eye. Especially when the temperature increases, the mechanical properties also increase without decreasing in the sample of 50% by weighing to the binder. The results show that reinforcing the geopolymer foams with basalt ground fibre improves the mechanical properties at high temperatures.

Keywords: aluminium, compressive strength, flexural strength, agent powder, basalt fibre

1 Introduction

Cement and their variants are widely used in the construction industry. By 2030, about 4.83 billion tons of cement will be produced globally [1]. Cement is the primary aggre-gate to produce concrete. One of the weaknesses of concrete is its low fire-resistance compared to some other construction materials, and it causes global warming to affect the production of one tonne of cement generates one tonne of carbon dioxide [2].

Geopolymer is a break-through material. The production of one tonne of kaolinite-based geopolymeric cement generates only 0.18 tons of CO_2, compared with 1 tonne of CO_2 for Portland cement (six times less) [3]. Fly ash-based geopolymeric cement has attracted intensive research word-wide because it emits even less CO_2, up to nine times less than Portland cement.
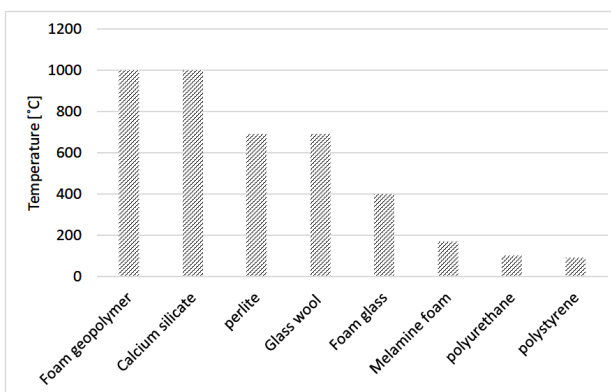
Figure 1: Maximum application temperature of some insulation materials [4].

Geopolymer materials have several advantages such as high durability, suitable fire-resistant and thermal stability, excellent mechanical properties, and resistance to acid attacks. Low-density geopolymers could be considered as potential materials for applications in many fields such as thermal insulation, fire resistance and other high-temperature applications (Figure 1). Due to its low thermal conductivity, geopolymer designed for fire resistance applications could be exposed to high temperature for an extended period.

The construction made of concrete usually has a large net mass [5]. The use of geopolymers of lower density is beneficial in term of reduced structural load-bearing with

*Corresponding Author: Van Su Le: Faculty of Mechanical Engineering, Department of Material Science, Technical University of Liberec, Studentská 2, 461 17 Liberec, Czech Republic; Email: longsuvp90@gmail.com
Michal M. Szczypinski, Vladimir Kovacic, Totka Bakalova, Lukas Volesky, Le Chi Hiep, Petr Louda: Faculty of Mechanical Engineering, Department of Material Science, Technical University of Liberec, Studentská 2, 461 17 Liberec, Czech Republic
Pavlína Hájková: Faculty of Mechanical Engineering, Department of Material Science, Technical University of Liberec, Studentská 2, 461 17 Liberec, Czech Republic; Unipetrol Centre for Research and Education, Revoluční 84, 400 01 Ústí nad Labem, Czech Republic

further benefits of acoustic and thermal insulation [6, 7]. Different foaming agents can be used to synthesise low-density geopolymers. Metallic aluminium powder is commonly used and is very reactive in alkaline environments and react at room temperatures [7–9].

Fibre reinforcement has been used in various hardened binders to improve mechanical properties [10–15]. Reinforced geopolymer adds either steel fibres, glass fibres or carbon fibres or basalt fibres to carry mechanical properties and for high temperature resistant geopolymer composites [16–19].

This study was conducted to study the physical and mechanical properties of geopolymers with enhanced fillers. Evaluating these properties is essential for better material use purposes.

2 Materials and Methods

2.1 Used materials

During the experiments, the following raw materials were used: binder, grounded basalt fibre and foaming agent. The used binder material was *Baucis Lk*, supplied by *České Lupkové Závody* (Czech Republic). This is an inorganic two-component aluminosilicate material based on metakaolin and potassium alkaline silicate solution [20]. Grounded basalt fibre was used in the experimental work as reinforcement material. To obtain grounded fibres, the stone wool *Isover N* (manufactured by *Saint-Gobain Construction Product CZ a.s.*) was milled (see Figure 2).

The preparation of geopolymer coatings was carried out using aluminium powder (foaming agent). This powder produces bubbles in the material volume, which increases porosity and reduces the weight of the geopolymer coating. The chemical composition and particle size of the aluminium powder are shown in Table 1.

Table 1: The chemical composition and size of the aluminium powder.

Name	Diameter	Al	FeO	SiO	Cu
D50	65μm	98%	0.35%	0.4%	0.02%

Figure 2: Photograph of basalt fibre grounded using the mill.

2.2 Geopolymer synthesis

Geopolymers were synthesized using cement and the activator. The materials were homogenized with a stirrer for 5 minutes. After homogenization, the filler (basalt fibre) and aggregate (fine sand) were added to the mixture, and they were stirred for a further 5 minutes to full homogenization. Aluminium powder was added to the geopolymer slurry after 10 minutes of mixing period, and they were mixed for a further 30 s at high RPM. Immediately after mixing, samples were poured into test moulds. The synthesis of geopolymers was carried out according to Figure 3.

Afterwards, the polymer paste was poured into moulds of dimensions 40×40×160 mm (see Figure 4). In 2 to 8 minutes, geopolymer began to expand (pores formation) and finished after 20 to 30 minutes. Samples were cured at room temperature for 1 to 2 hours, and then the test specimens cut by hand-saw.

In this work, three samples of geopolymer foams with different weight percentages of basalt waste fibre (Table 2) were prepared and tested. All samples were made modules on 40×40×160 mm. They were cured after 28 days at room temperature. They were heated in a furnace at various temperatures of 200, 400, 600, 800 and 1000°C. The
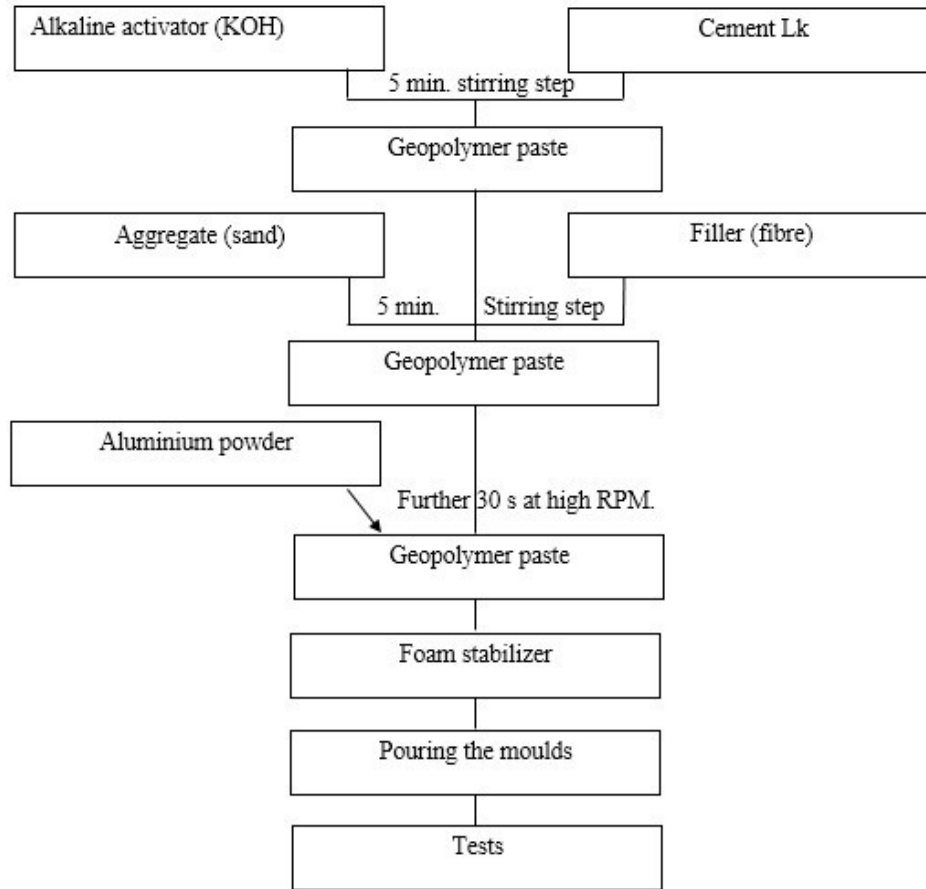
Figure 3: Schematic flowchart of geopolymer foams processing.

Table 2: Composition of geopolymer foams.

Binder	Activator	Grounded basalt fibre	Aluminium powder
1	0.9	0.1	0.015
1	0.9	0.3	0.015
1	0.9	0.5	0.015

(column headers under "Mix ratio by weight")

heating rate of the furnace was set to 5°C per minute until it reached the desired temperature, and the final temperature was kept for two hours. After they were holding them in the furnace until they lowered room temperature and then take to test.

2.3 Test procedures

The evaluation of the samples was carried out using mechanical tests, and subsequently, the structure of the tested samples was analysed. Drying of samples was done in a designated room at room temperature or an elevated temperature until the test requirements were met. The final result value was determined as the average of three measurements.

2.3.1 Apparent density

Apparent density was calculated with the following equation:

$$Apparent\ density = \frac{Mass}{Volume} \tag{1}$$

Where:
Apparent density (Kg/m^3);
Mass is the mass of the specimen (Kg);
Volume is the volume of the specimen (m^3);

(a)

(b)

(c)

Figure 4: Prepared samples: a) in moulds of size 40×40×160 mm, b) after cut by hand-saw c) samples removed from moulds.

2.3.2 Flexural strength and compressive strength

The strength was evaluated by a hydraulic press, universal Testing Mechanical INSTRON Model 4202 (Figure 5). Flexural strength was calculated from a three-point bending test on the samples of size 40×40×160 mm [21, 22]. Three cubes of 40 mm were cut from the test bar, and they were used for compressive strength testing. Continuously tested three samples were performed after 28 days.

The compressive strength of geopolymer foams (f_{cm}) was calculated by the equation:

$$f_{cm} = \frac{F_{max}}{A_c} \qquad (2)$$

Where:

f_{cm} is compressive strength (MPa);

F_{max} is the maximum applied load indicated by the testing machine (N);

A_c is the original cross-sectional area of a specimen in a compression test (mm^2);

The flexural strength (R_{mo}) was calculated by the equation:

$$R_{mo} = \frac{3F_{max}L}{2bh^2} \qquad (3)$$

Where:

R_{mo} is the flexural strength (MPa);

F_{max} is the maximum applied load indicated by the machine (N);

b is the average width of the specimen (mm);

h is the average depth of the specimen (mm);

L is span length (mm);

2.3.3 Weight loss

Weight loss was calculated using the equation:

$$W_L = \frac{W_0 - W}{W_0} \star 100 \qquad (4)$$

Where:

W_L is the weight loss (%);

W_0 is the initial mass (g);

W is the remaining mass at any given time(g);

2.3.4 Dry shrinkage

Dry shrinkage was calculated using the following equation:

$$S_L = \frac{L_0 - L}{L_0} \times 100 \qquad (5)$$
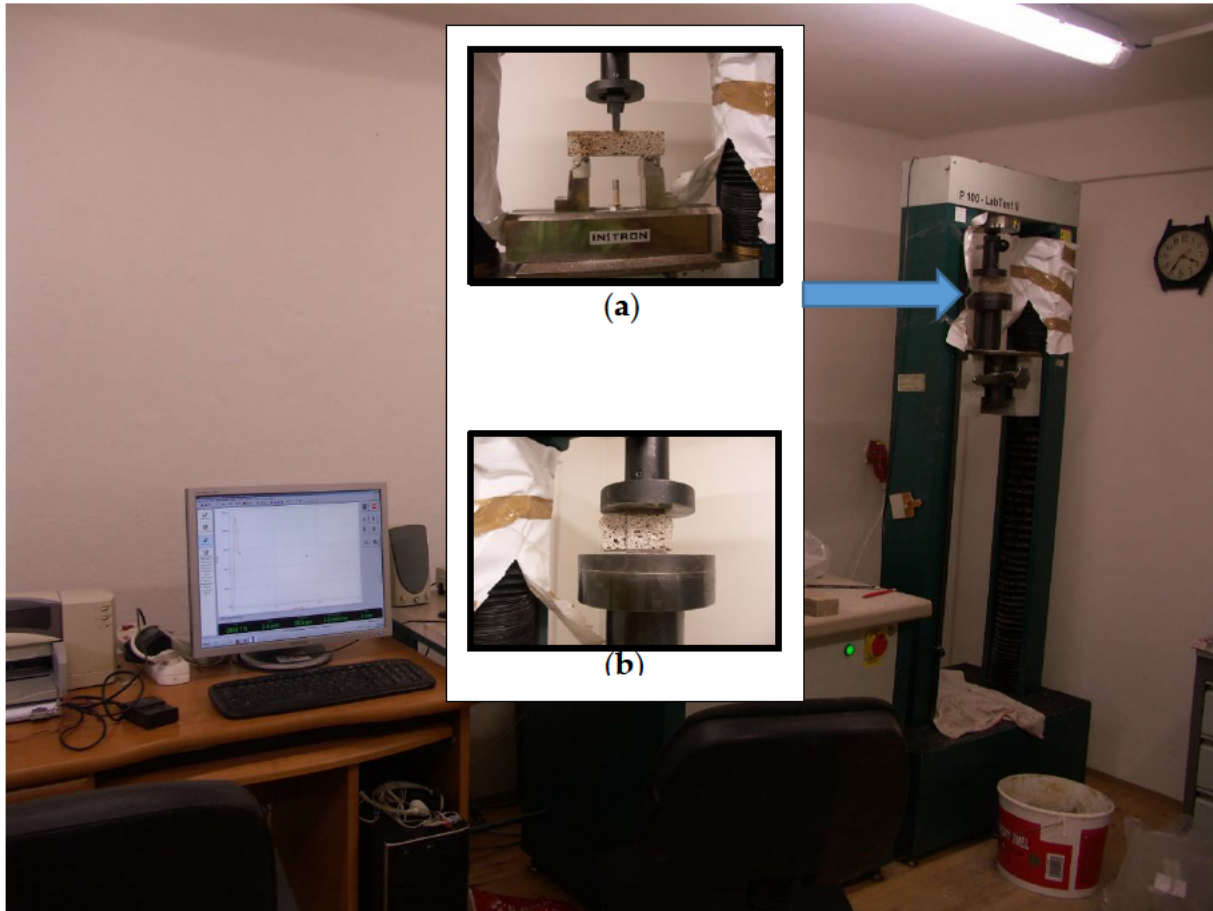
Figure 5: Universal testing machine INSTRON (Model 4202): a) test set-up for flexural strength b) test set-up for compressive strength.

Where:

S_L is the dry shrinkage (%);

L_0 is the length of the specimen (mm);

L is the remaining length of the specimen at any given time (mm);

2.3.5 Water Absorption

Water absorption is used to measure the permeability of geopolymer foams. The test made on the specimen (40×40×80) mm. All the samples were kept in room temperature for 28 days before they were tested. Each result was calculated from the average of three samples. According to ASTM C642 06 regulation, the samples were cured in an oven at a temperature of 100 to 110°C for not less than 24 h and determine the mass A. The samples were soaked in water for interval 24h. Surface-dry the sample by removing surface moisture with a towel, and determine the mass B.

Water absorption was calculated using the following equation:

$$\% = \left[\frac{B - A}{A}\right] \times 100 \qquad (6)$$

Where:

A is the mass of the dry sample (g);

B is the mass of the wet sample (g);

3 Results and discussion

As part of this work, research was carried out that is relevant to building materials and those that have fireproofing properties. The physical characteristics of the material at room temperature and subjected to elevated temperatures were characterized. The density, water absorption, pore size, compressive and flexural strength were tested, and the weight loss and shrinkage of the materials after heating were examined. The building material that is to constitute a fire barrier must be characterized by the smallest
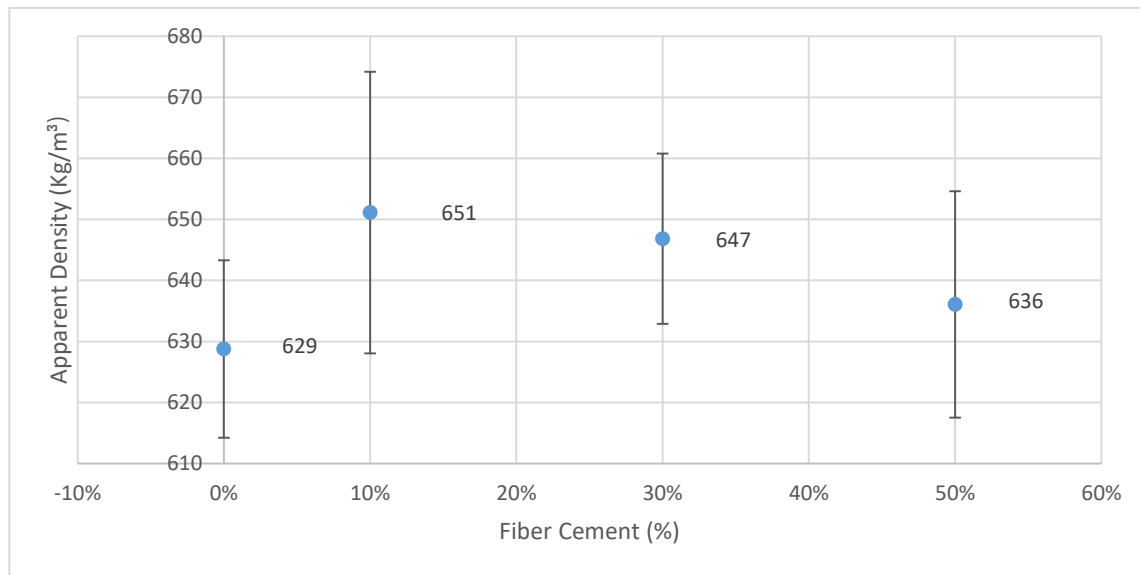
Figure 6: The density of geopolymer foams with increasing basalt waste fibre concentration at room temperature.
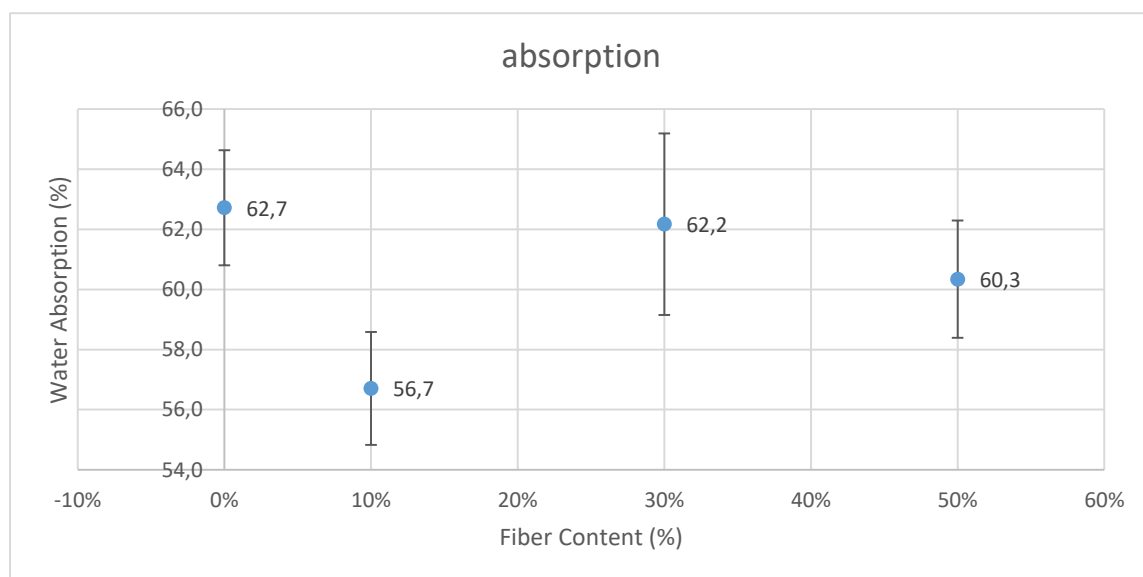
Figure 7: The absorption coefficient of geopolymer foams with increasing basalt waste fibre concentration.

possible change in physical parameters - otherwise a building disaster may occur during a fire. Compressive and flexural stregth testing will give an answer as to whether the material will continue to withstand when exposed to high temperatures.

3.1 Characterization of materials in room temperature

The addition of fibres contributes to the increase in the geopolymer foam density. However, it is not a significant increase (Figure 6). Furthermore, the addition of the fibre leads to reduced water absorption (Figure 7).

The fibre content also affects the pore size (Figure 8). The smallest pores occur in samples with a 50% fibre content (Figure 8c), the largest in samples with a content of 10% (Figure 8a).
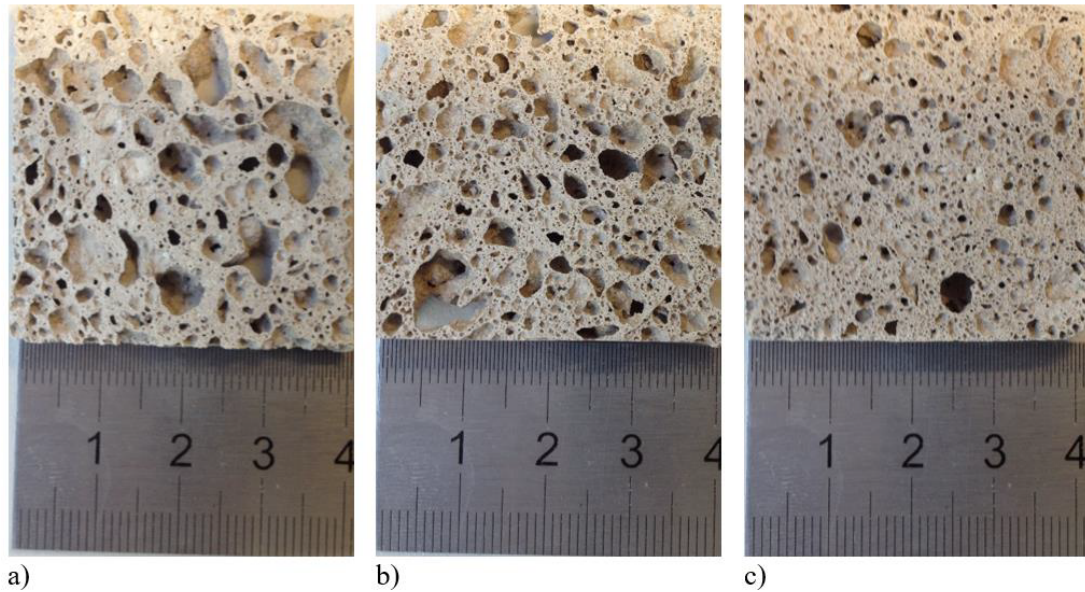
Figure 8: Pores size of geopolymer foams with various content of reinforcing fibre a) 10%, b) 30%, c) 50 % (total image width: 40 mm).

3.2 Characterization of material subjected to elevated temperature

All samples exhibit a colour change after heating from 200°C to 1000°C as follow: grey at 200°C, blackish-grey from 400°C to 800°C, yellowish-grey at 1000°C (Figure 9). There are visible cracks on samples containing 10% which were heated up to 600, 800 and 1000°C (Figure 9a). Samples reinforced with a larger amount of basalt fibre tend to crack less (Figure 9b and 9c). It is clearly seen that the fibers contribute to a change in the transfer of stress associated with sintering the material and thus inhibit the propagation of cracks from the places where these stresses arise.

The temperature of the material has a significant influence on the absorption coefficient. It decreases rapidly at 200°C, 400°C, and 600°C. However, at 600°C, 800°C, 1000°C, it doesn't decrease, and it's stable (Figure 10). This is particularly evident in the case of a sample with 50% fibre content, where coefficient doesn't decrease at range from 400°C to 1000°C. A similar situation occurs in the case of weight loss of tested samples at different temperatures (Figure 11). Weight loss increases in range from 200°C to 600°C. A further increase in temperature does not result in weight loss. The weight loss of unreinforced and the low fiber content samples is associated with the evaporation of water and gases in the pores, which are much larger than those of samples reinforced with more fibers. For the same reason, there is a significant change in the water absorption of samples with low (or no) fiber content.

Temperature also has a significant impact on the density (Figure 13) and shrinkage (Figure 12) of geopolymer composites – both increase with the temperature. The fastest growth is visible at high temperatures, above 400°C. In the case of density changes, a slight decrease was observed in all samples at a temperature of 400°C. The highest density changes at increasing temperature were observed in samples with less (10% and 30%) fibre content. Shrinkage is associated with the chemical nature of the material from which geopolymers are made. At high temperature there is a transformation from an amorphous to a crystalline phase. This happens following the crystallization of amorphous sodium aluminosilicates into nephelin.

Figures 14 and 15 show changes in strength (compression and flexural, respectively) depending on the temperature. The increasing dependence of strength on the temperature in the range from 400°C to 1000°C was observed. However, samples with a temperature of 200°C than 400°C were characterized by much higher strength. This is particularly evident in the case of samples with a lower fibre content (10% and 30%). Samples with 50% fibre content are characterized by the highest strength at temperatures above 400°C. At 1000°C, a sudden increase in strength in the sample with a 50% fibre content was observed (at 1000°C the compressive strength is 83.61% higher than compressive strength at 200°C). Samples reinforced with a higher fiber content are characterized by higher bending strength due to the smaller number of pores, which dramatically affect the strength of the material, increasing its fragility. In addition, the crystallization of aluminosilicate mentioned above occurs at a high temperature, which further promotes mechanical strength.
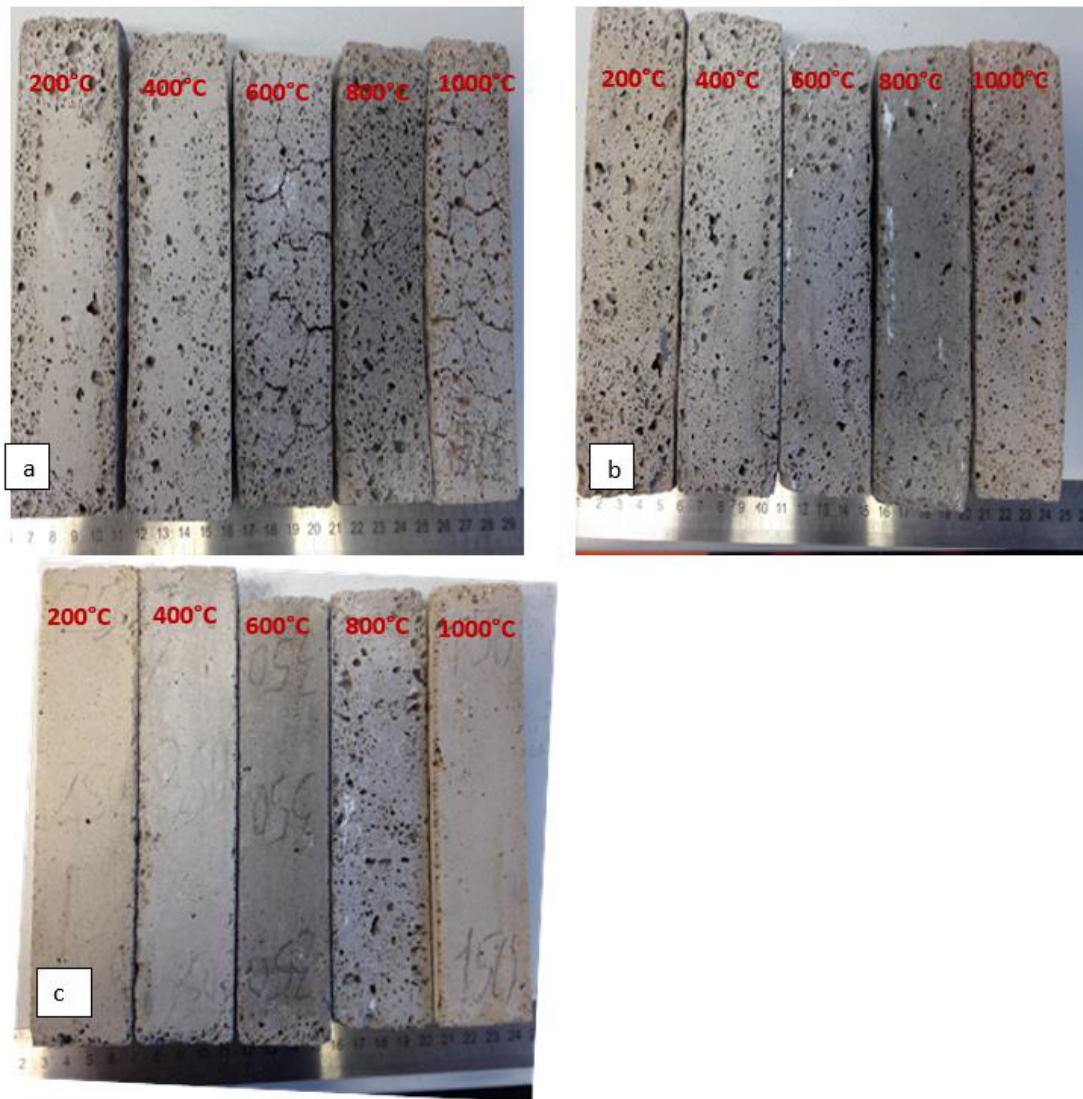
Figure 9: Colour change and cracks occurrence of geopolymer foams with different content of basalt waste fibre a) 10%, b) 30% and c) 50% after heating at various temperatures.
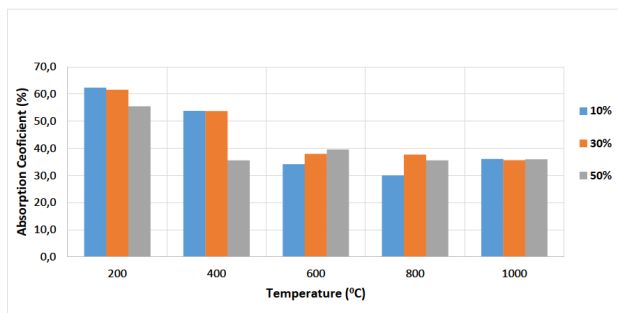
Figure 10: The absorption coefficient of geopolymer foams with different content of basalt waste fibre at high temperature.
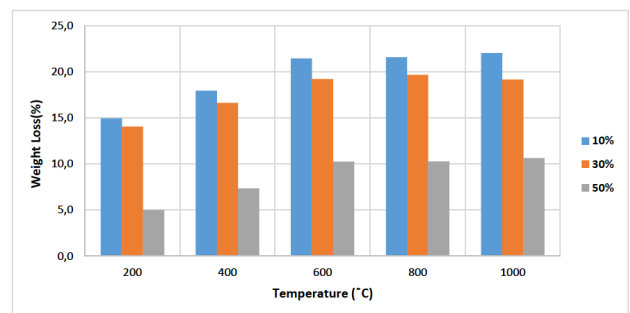
Figure 11: Weight loss of geopolymer foams with different content of basalt waste fibre at high temperature.

4 Conclusions

The results showed that the reinforcement of geopolymers with different content of basalt fibres influences the me-
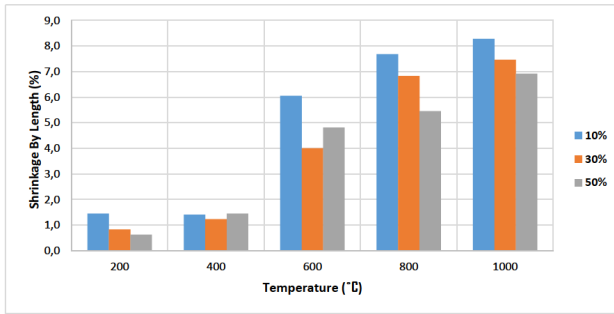
Figure 12: Shrinkage by the length of geopolymer foams with different content of basalt waste fibre at high temperature.
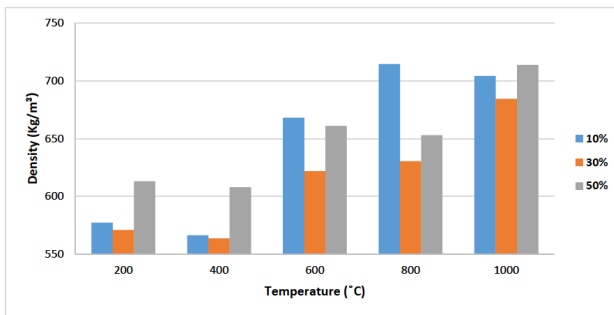
Figure 13: The density of geopolymer foams with different content of basalt waste fibre at high temperature.
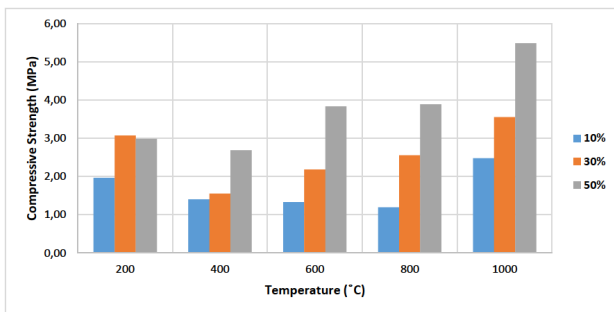
Figure 14: Change of compressive strength of geopolymer foams vs. heating temperatures.
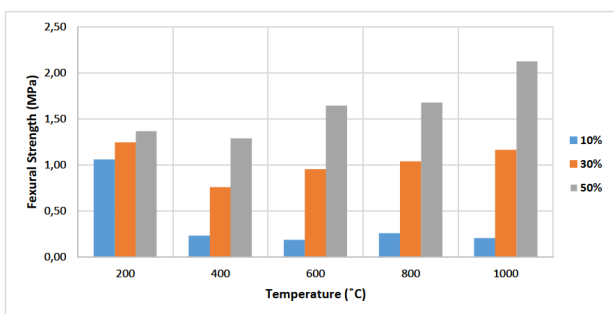
Figure 15: Evolution of Flexural strength of geopolymer foams vs. heating temperatures.

chanical properties of the obtained composites. The high fibre content improves practically all of the tested parameters, making the material also stable at very high temperatures. Through the reinforcement of the geopolymer composite with the right amount of basalt fibres, it's possible to obtain heat-resistant material. The research showed the influence of the content of introduced fibres in the formation of pores, crack propagation and in the formation of structural changes of the material, which ultimately result in its mechanical properties.

The obtained results are promising and lead us to further research towards the development of fireproof composite materials based on geopolymers.

References

[1] (2018). *Cement: global production 1990-2030*. Available: https://www.statista.com/statistics/373845/global-cement-production-forecast/

[2] Davidovits J. Global warming impact on the cement and aggregates industries. World Resour Rev. 1994;6:263–78.

[3] Davidovits J. "Geopolymer chemistry and applications," in *Geopolymer Chemistry & Applications*, ed: Geopolymer Institute, 2008.

[4] Liefke E. Industrial applications of foamed inorganic polymers. Geopolymere. 1999;99:189–200.

[5] Just A, Middendorf B. Microstructure of high-strength foam concrete. Mater Charact. 2009;60(7):741–8.

[6] Feng J, Zhang R, Gong L, Li Y, Cao W, Cheng X. "Development of porous fly ash-based geopolymer with low thermal conductivity," *Materials & Design (1980-2015),* vol. 65, pp. 529-533, 2015.

[7] Chiu YP, Lu YM, Shiau YC. "Applying inorganic geopolymers added with aluminium powder to fire-resistant fillers," *Materials Research Innovations,* vol. 19, pp. S5-642-S5-649, 2015.

[8] Caijun Shi B. "Composition of materials for use in cellular lightweight concrete and methods thereof," ed: advanced materials technologies, 2002.

[9] Škvára F. Ros tislav Šulc, Zdeněk Tišler, Petr Skřičík, Vít Šmilauer, and Z. Z. Cílová, "Preparation and properties of fly ash-based geopolymer foams," vol. 58, pp. 188-197, 2014.

[10] Almeida JH, Angrizani CC, Botelho EC, Amico SC. "Effect of fiber orientation on the shear behavior of glass fiber/epoxy composites," *Materials & Design (1980-2015),* vol. 65, pp. 789-795, 2015.

[11] Alomayri T, Low IM. Synthesis and characterization of mechanical properties in cotton fiber-reinforced geopolymer composites. Journal of Asian Ceramic Societies. 2013;1(1):30–4.

[12] Alomayri T, Shaikh FU, Low IM. Mechanical and thermal properties of ambient cured cotton fabric-reinforced fly ash-based geopolymer composites. Ceram Int. 2014;40(9):14019–28.

[13] Alomayri T, Vickers L, Shaikh FU, Low IM. Mechanical properties of cotton fabric reinforced geopolymer composites at 200–1000°C. Journal of Advanced Ceramics. 2014;3(3):184–93.

[14] V. Sathish Kumar, Blessen Skariah Thomas, and Alex Christopher., "An Experimental Study on the Properties of Glass Fibre Reinforced Geopolymer Concrete," 2012.

[15] Hung TD, Louda P, Kroisová D, Bortnovsky O, Xiem NT. "New generation of geopolymer composite for fire-resistance," in *Advances in Composite Materials-Analysis of Natural and Man-Made Materials*, ed: InTech, 2011.

[16] Hung TD, et al. New generation of geopolymer composite for fire-resistance. Advances in Composite Materials-Analysis of Natural and Man-Made Materials. InTech; 2011.

[17] Masi G, Rickard WD, Bignozzi MC, van Riessen A. The effect of organic and inorganic fibres on the mechanical and thermal properties of aluminate activated geopolymers. Compos, Part B Eng. 2015;76:218–28.

[18] Timakul P, Rattanaprasit W, Aungkavattana P. Improving compressive strength of fly ash-based geopolymer composites by basalt fibers addition. Ceram Int. 2016;42(5):6288–95.

[19] D. Tran, P. Louda, O. Bortnovsky, and P. Bezucha, "Mechanical Properties of Silica-Based Geopolymer Composites Cured at Ambient Conditions in Accordance with Size-Independent Method," 2010.

[20] AS. České lupkové závody. (2019). *BAUCIS LK*. Available: http://www.cluz.cz/en/baucis-lk

[21] "ASTM C348 - 08, Standard Test Method for Flexural Strength of Hydraulic-Cement Mortars.," in *ASTM C348 - 08: Standard Test Method for Flexural Strength of Hydraulic-Cement Mortars.*, ed, 2008, pp. 1-6.

[22] "ASTM C78/C78M - 10, Standard Test Method for Flexural Strength of Concrete (Using Simple Beam with Third-Point Loading)." in *ASTM C78/C78M - 10: Standard Test Method for Flexural Strength of Concrete (Using Simple Beam with Third-Point Loading)*. ed, 2010, pp. 1-4.

Impact of Flax and Basalt Fibre Reinforcement on Selected Properties of Geopolymer Composites

Miroslav Frydrych [1], Štěpán Hýsek [2,3,*], Ludmila Fridrichová [1], Su Le Van [2], Miroslav Herclík [1], Miroslava Pechočiaková [4], Hiep Le Chi [2] and Petr Louda [2]

[1] Department of Textile Evaluation, Faculty of Textile Engineering, Technical University of Liberec, Studentska 2, 461 17 Liberec, Czech Republic; miroslav.frydrych@tul.cz (M.F.); ludmila.fridrichova@tul.cz (L.F.); miroslav.herclik@tul.cz (M.H.)

[2] Department of Material Science, Faculty of Mechanical Engineering, Technical University of Liberec, Studentska 2, 461 17 Liberec, Czech Republic; longsuvp90@gmail.com (S.L.V.); lechihieptul09@gmail.com (H.L.C.); petr.louda@tul.cz (P.L.)

[3] Department of Wood Processing and Biomaterials, Faculty of Forestry and Wood Sciences, Czech University of Life Sciences in Prague, 16521 Praha, Czech Republic

[4] Department of Material Engineering, Faculty of Textile Engineering, Technical University of Liberec, Studentska 2, 461 17 Liberec, Czech Republic; miroslava.pechociakova@tul.cz

* Correspondence: hysekstepan@seznam.cz; Tel.: +420-607-501-858

Abstract: The submitted paper deals with the physical and mechanical properties of geopolymer composite materials reinforced with natural fibres. For this study, we aimed to develop a geopolymer composite reinforced with long flax fibres, which were implemented in the geopolymer in the form of a nonwoven fabric that reinforced the structure of the geopolymer over the entire thickness of the board. In order to compare the properties of the developed composite with natural fibres, a geopolymer without fibres and a geopolymer reinforced with basalt fibres were also produced. The monitored mechanical properties were impact bending, bending strength and compressive strength. Differential scanning calorimetry (DSC), thermogravimetric analysis (TGA), Fourier transform infrared spectroscopy (FTIR) and microscopic analysis were also carried out. The results clearly showed the positive effect of the addition of natural fibres on impact bending and bending strength. However, the addition of natural fibres in the form of a nonwoven fabric significantly increased the variability of the properties of the developed composites. In addition, a different pattern of joint failure was noted between geopolymer reinforced with flax fibres and geopolymer reinforced with basalt fibres.

Keywords: geopolymer; natural fibre; flax; basalt; reinforcement

1. Introduction

Reinforcing polymers with fibres can create high-performance materials. The specific mechanical properties of the materials that use high-quality natural fibres achieved better values than composites reinforced by man-made fibres that had already been developed [1]. Flax is a very strong natural fibre with a tensile strength of 1.5 GPa and a specific tensile strength of GPa·m^3·kg^{-1}. Thanks to these properties and their renewability, flax fibres are considered an environmentally friendly alternative to glass fibres for use in composites. These fibres have a number of other advantages compared to glass, basalt or carbon fibres: they do not cause skin irritation, their edges blunt less, they do a very good job of absorbing energy, vibration and UV radiation, they do not create static charge, they are resistant to insects and bacteria, they are harmless to health, they are biodegradable and they do not release VOCs.

Combined with low density and high strength, they are designed for material use in composites [2,3]. On the other hand, their disadvantages are degradation at lower temperatures, higher variability of mechanical properties, lower maximum tensile strength, lower relative elongation and low resistance to natural impacts. The free and bound water content also poses problems in the manufacture of composites made from natural fibres [2,4,5].

The higher absorption capacity of natural fibre composites makes them an intuitive choice for use in automobiles, where they are able to absorb a significant amount of impact energy. In addition, composites with these fibres are not fragmented [4,6]. Adversely, the high variability of their properties makes it more difficult to use them in the automotive industry, and it is therefore necessary to seek out other applications. One solution may be to use natural fibres in building composites. In recent years, geopolymer composites have appeared as a progressive material [7,8].

A geopolymer is formed by the alkaline activation of aluminosilicates and consists of a repeating unit of sialate monomer (–Si–O–Al–O–). This material is considered a third-generation cement and has many interesting properties [9]. Geopolymers are environmentally friendly building materials that have excellent fire, strength, thermal insulation and acoustic properties. Another of their advantages is the possibility of foaming, which makes it possible to regulate and optimise their properties [10–12]. Geopolymers can be well reinforced, for example, with basalt fibres. This combination is suitable for high-temperature applications [13].

If a geopolymer mixture is produced by mixing, it is not possible, for technological reasons, to use reinforcing fibres that are longer than 32 mm. Longer fibres tend to wind around the mixing propeller and it is not possible to distribute them by blending throughout the whole mixture. If we want to use natural fibres made from flax, which can be longer than 10 cm [14], it is necessary to choose an appropriate application method. The submitted research describes a method of reinforcing geopolymer with long flax fibres in the form of nonwoven fabric. We assume that the implementation of fibres into the geopolymer in the form of nonwoven fabric will have a synergistic effect, and the resulting composite will achieve high strength characteristics due to the oriented fibre structure. In order to compare the properties of the developed reinforced flax fibre composite, a geopolymer reinforced with basalt fibres and a geopolymer without reinforcement were produced.

2. Materials and Methods

2.1. Materials

The flax fibres were supplied by Holstein Flachs GmbH (Alte Ziegelei, Germany) and consisted of purified flax fibres. The average fibre length was 5.9 mm and the softness was 67 dtex. Before fibre processing, the fibres were not dried, however they were air conditioned at 20 °C and 65% relative humidity for four weeks and they reached an equilibrium moisture content of 10%. The flax fibres were implemented in the composites in the form of fibre mat. The flax fibre clusters were fed into a carding machine (Figure 1) equipped with a set of rollers with wire working coatings. The fibre web emerging from the carding machine was laminated to form a non-reinforced fibre mat with a base weight of 225 g/m^2.

Basalt chopped fibres supplied by Orlimex CZ (Czech Republic, Usti nad Orlici) with a length of 6 mm were used. The fibre diameter was 18 μm. The suitability of basalt fibres for use with concrete is declared by the producer. The basalt fibres were implemented into the geopolymer by mixing, as opposed to flax fibres, which were implemented into the geopolymer in the form of a fibre mat.

Figure 1. Production of a flax fibre mat.

The following manufacturing process was used to produce geopolymer composites. Alkaline Activator Baucis Lk (ČESKÉ LUPKOVÉ ZÁVODY, as, Nové Strašecí Czech Republic) was poured into a Heidolph RZR 2020 rack mixer (Heidolph Instruments GmbH & CO. KG, Schwabach, Germany) and a weighed amount of Baucis Lk metakaolin cement inorganic two-component aluminosilicate binder (ČESKÉ LUPKOVÉ ZÁVODY, as, Nové Strašecí, Czech Republic) was added. The two components were mixed vigorously for 5 min. The mixture was then mixed for 5 min with added fibres (basalt variant only). In the last step, aluminium powder with a purity of at least 99% and an average particle size of 52 μm (PK CHEMIE, Czech Republic) was added, followed by mixing for 30 s. The prepared mixture was poured into moulds with dimensions of 300 × 300 mm. According to the variants, the height of the samples was in the range of 17–20 mm, depending on the interaction of the individual components. The percentage of the individual components used in the production of geopolymers is shown in Table 1. Basalt fibres (6 mm long) were mixed into the geopolymer, and a fibre mat made from flax fibres with a length of 5.9 cm was placed in the prepared mould and the geopolymer mixture was subsequently cast.

Table 1. Materials used to produce geopolymers by weight.

Component	Percentage of Individual Components
Cement Baucis Lk	50.45%
Activator Baucis Lk	44.90%
Fibres (flax or basalt)	2.16%
Aluminium powder	2.49%

2.2. Methods

2.2.1. Mechanical Properties

All of the mechanical properties tests were performed after air conditioning the samples at 20 °C and a relative humidity (RH) of 65% for one month. The bending strength test was carried out on the basis of standard ČSN EN 789 [15], where three-point bending was tested and the distance of the supports was 240 mm. The universal testing machine P 100—LabTest II from LaborTech (Opava, Czech Republic) was used, and the test duration was between 45 and 90 s. For this test, specimens with dimensions of 300 × 50 mm and a height of 20 mm were cut from the produced boards. A total of 20 specimens were used. The compressive strength test was carried out on the basis of standard ČSN ISO 1920-10 [16], the universal testing machine P 100—LabTest II from LaborTech was used and the

test duration was between 45 and 90 s. For this test, specimens with dimensions of 50 × 50 mm and a height of 20 mm were cut, and 20 pieces were used in total. The impact strength test was carried out on the basis of standard ČSN EN 10045 [17] and the pendulum impact testing machine from Wance was used. For that test, specimens with dimensions of 20 × 20 × 150 mm were cut, and 20 pieces were used in total.

2.2.2. Thermogravimetric Analysis (TGA), Differential Scanning Calorimetry (DSC) and Fourier Transform Infrared Spectroscopy (FTIR) Analysis

Samples for TGA, DSC and FTIR analyses were milled and homogenised using a laboratory ball mill and the obtained powder was analysed. A TGA analysis was carried out using the device TGA/SDTA 851 (Mettler Toledo, Greifensee, Switzerland). A temperature program from 25 to 1000 °C was chosen with steps of 10 K/min in the presence of a nitrogen atmosphere with a nitrogen flow rate of 50 mL/min. The DSC analysis was performed using a DSC 3+ device (Mettler Toledo, Greifensee, Switzerland). A temperature program from −50 to 700 °C was chosen with steps of 10 K/min in the presence of a nitrogen atmosphere with a nitrogen flow rate of 50 mL/min. The measuring commenced by conditioning the samples at −50 °C for 10 min. Infrared spectroscopy was performed using a Spectrum One spectrometer (PerkinElmer, Waltham, MA, USA). Obtained powder from composites was placed directly on the attenuated total reflection crystal and pressed with reproducible pressure. The spectral range was recorded from 4000 to 400 cm^{-1} with a count of 10 scans each.

2.2.3. Scanning Electron Microscopy

The shape characteristics of the used fibres and the evaluation of composite joint failure were performed using scanning electron microscopy (Tescan Orsay Holding, a.s., Brno, Czech Republic). Ruptured samples from the bending strength tests were used in order to assess the joint failure. The samples of both fibres and composites taken were gold coated using a laboratory coater, and a microscopic analysis was performed using scanning electron microscope MIRA 3 (Tescan Orsay Holding, a.s., Brno, Czech Republic). The following conditions were used: secondary electron detector, acceleration voltage 10 kV, working distance 7 mm.

2.2.4. Statistical Data Processing

Descriptive statistics (arithmetic mean, standard deviation) and analysis of variance were used to characterise the obtained data. Tukey's post-hoc test was used to determine if any of the differences between the pairwise means were statistically significant. A significance level of $\alpha = 0.05$ was selected for all of the analyses. The fibre type acts as a factor in the analysis of variance. The impacts of the fibre type on the physical and mechanical properties were shown graphically, and the vertical columns represent 95% confidence intervals.

3. Results and Discussion

3.1. Characteristics of the Used Fibres

Figure 2a,b shows the surface morphology of the used flax fibres. The figure shows the rough and rugged surface of fibres, but also variability in surface structure. In terms of replacing glass fibres (with a smooth surface and circular cross-section) as reinforcement in the geopolymer with these rough surface fibres, an increase in adhesion between the geopolymer and the reinforcing fibres can be expected, which should lead to higher strength of the resulting composite. This hypothesis will be verified by comparing the geopolymer with flax fibres and with basalt fibres, as shown in Figure 2c.
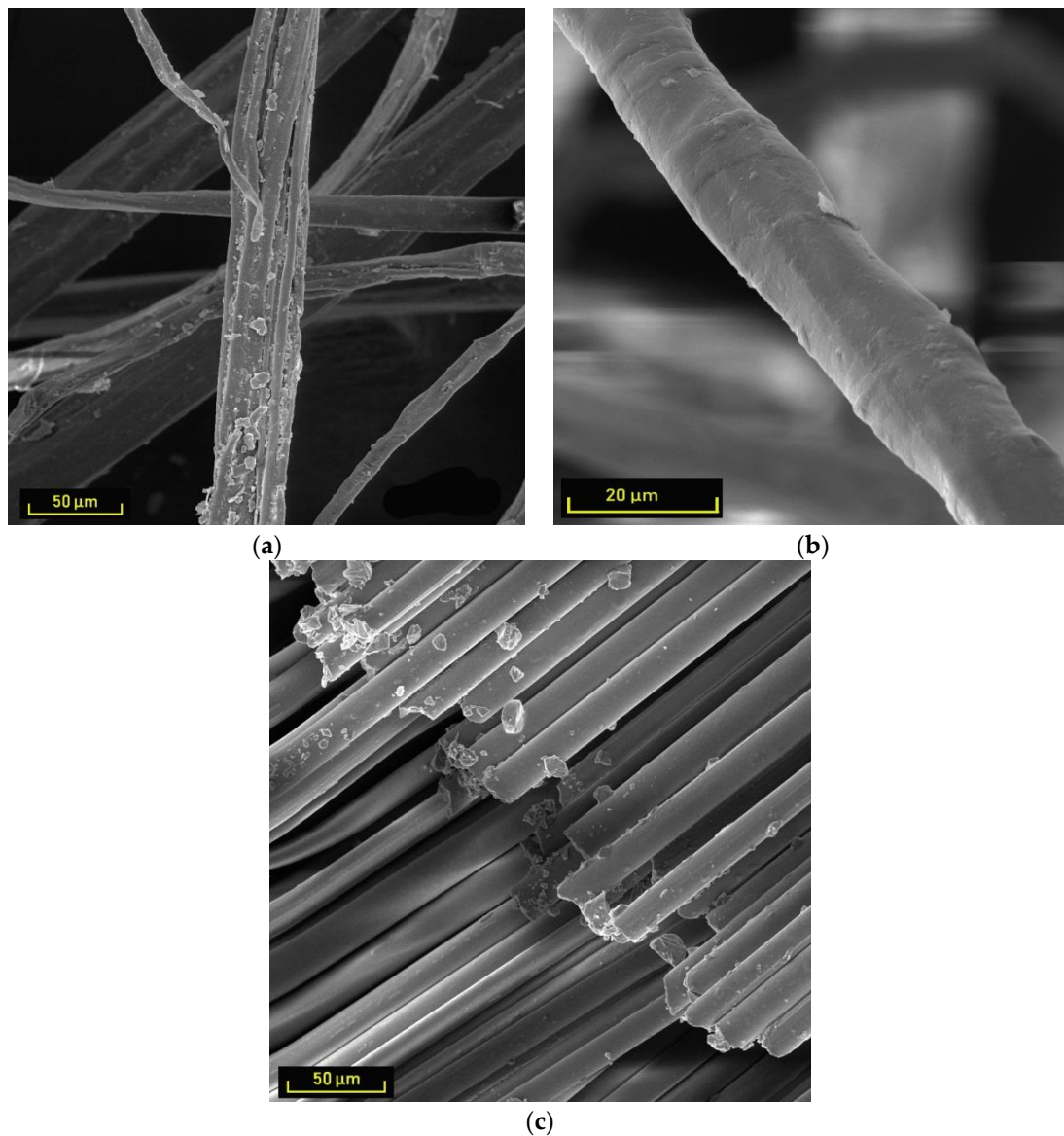
Figure 2. SEM figures of used fibres: (**a**) flax fibres, magnification 1000×, (**b**) flax fibre, magnification 4000×, and (**c**) basalt fibres.

3.2. Impact of the Addition of Fibres on the Mechanical Properties of the Composite

Table 2 shows the average densities of the produced composites. Due to manual production, there was a higher density variability in samples due to variability in the basis weight of the composites. Flax-reinforced geopolymer composites showed the highest variability due to the higher variability of natural fibres [4] and variability in the basis weight of flax nonwoven fabric [3]. Flax-reinforced geopolymer composites also showed the lowest density due to the highest foaming of geopolymer composites, and therefore the occurrence of larger pores.

Table 2. Average densities of composites at 20 °C and relative humidity (RH) 65%.

No.	Type of Fibres	Density (kg/m^3)
1	Flax	448 (51)
2	Basalt	456 (22)
3	Without reinforcement	556 (35)

Values in parentheses are the standard deviations.

Figure 3 shows the effect of added fibres in the geopolymer on impact bending. Samples of the geopolymer reinforced with flax fibre were tested, as well as samples reinforced with basalt fibre, and samples without the addition of fibres were used as a reference set. The graph in the figure shows that the highest impact bending value of 0.62 J/cm^2 was achieved by the material reinforced by flax fibres. This difference is statistically significant, at a significance level of 0.05. At the same time however, there was also a high variability of the measured values for this material. This high variability originates both in the high variability of natural fibre properties [4], in the variability of nonwoven fabric properties (caused mainly by the variability of the basis weight) [3], and also in the variability of the basis weight of the resulting composite, caused by worse spillage of geopolymer in the nonwoven textile form. Basalt fibre reinforcement also increased impact bending compared to the reference set, and for samples with added basalt fibres, impact bending was measured at an average of 0.32 J/cm^2, and 0.21 J/cm^2 for samples without fibres. However, this difference is not statistically significant at a significance level of 0.05. In addition to adding fibres, the impact bending of fibre-reinforced geopolymers can be further increased by increasing the proportion of cement in the geopolymer [18] or by adding a small amount of carbon nanomaterials such as carbon nanotubes or nanofibers [19].
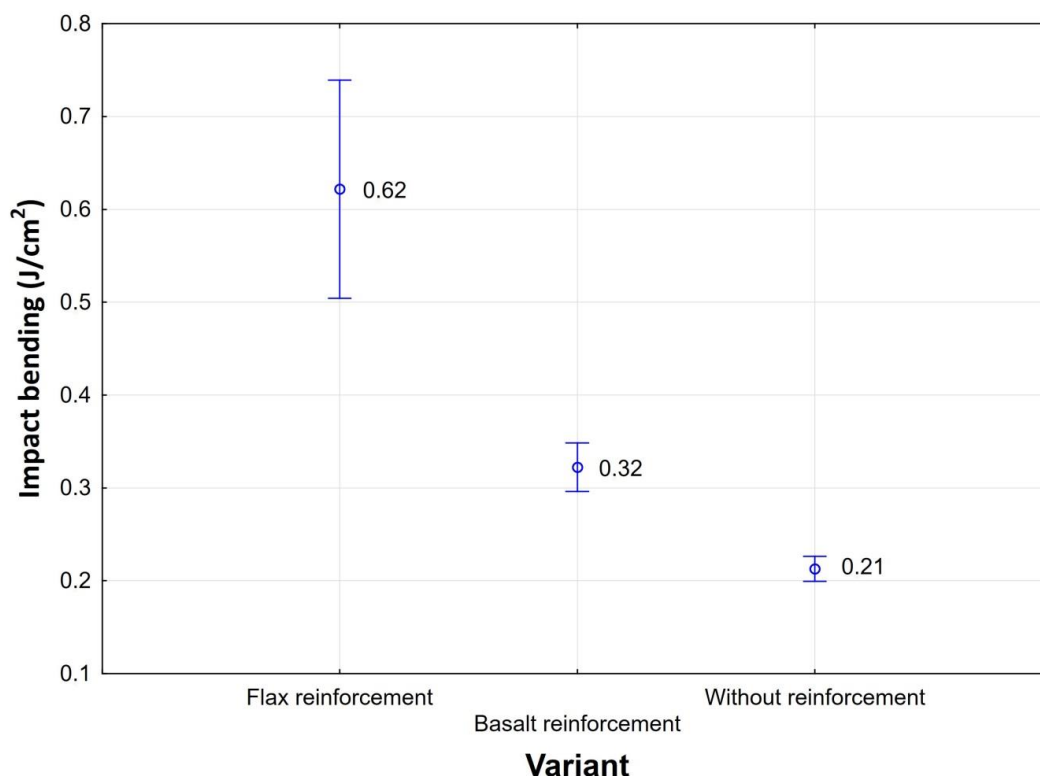
Figure 3. Impact of the addition of fibres on impact bending.

Figure 4 shows the effect of fibre reinforcement on flexural strength. It was found that in both cases the flexural strength of geopolymers with added fibres was statistically significantly increased, that is, from 0.59 MPa for samples without added fibres, to 0.91 MPa for samples with basalt fibres, and

to 0.95 MPa for samples with flax fibres. Unlike the dynamic test, this static test did not demonstrate the effect of the fibre type on flexural strength. This finding corresponds to the literature [2,5] where natural fibres are reported to have a higher absorption capacity than artificial fibres. Overall, the bending strength values are set lower than in similar research on geopolymers reinforced with flax fibres [18], but in this research, the developed composites have a density several times higher. The resultant properties of impact bending and bending strength could be significantly improved by using a coupling agent or functionalising the fibre surfaces [20], however, the goal of this study was not to maximise the properties of composites.
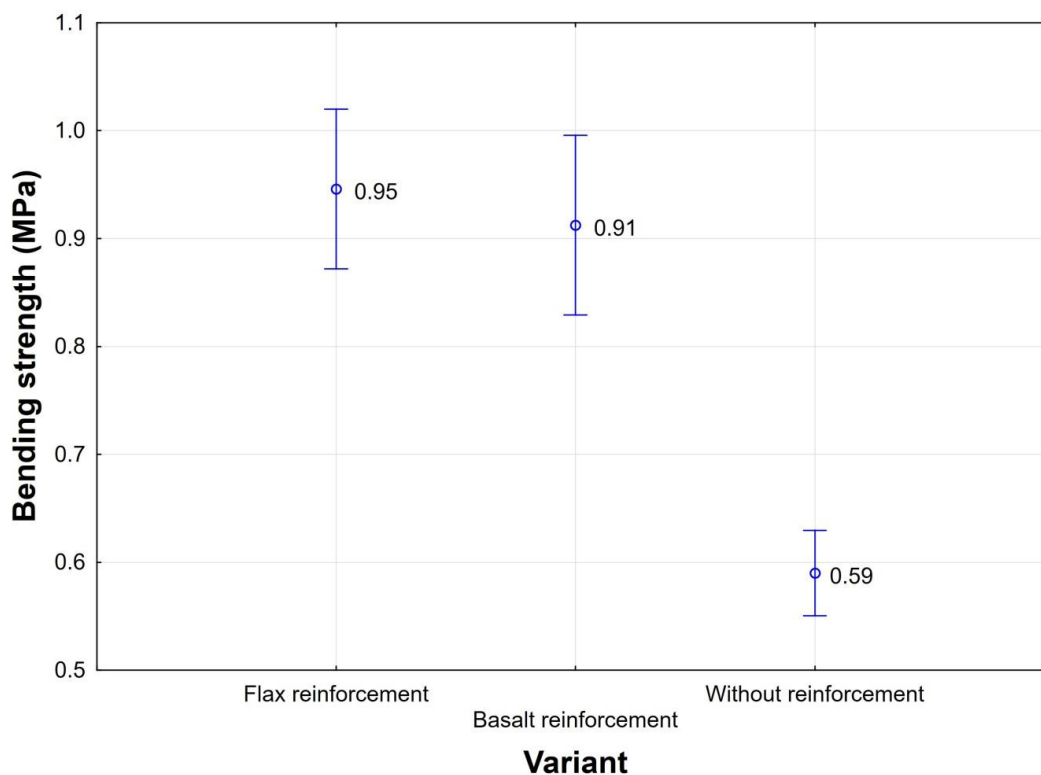
Figure 4. Impact of the addition of fibres on bending strength.

The durability of natural fibres as reinforcements in geopolymer composites is affected by the alkalinity of the activators of geopolymer matrices. The alkaline environment is the main reason for natural fibre degradation in cementitious matrices [21]. The results of the tests showed that the mechanical properties (either static or dynamic) of the geopolymer were significantly improved by the addition of flax fibres. Thus, the activator used in the form of an aluminium powder caused sufficiently rapid curing of the geopolymer, and the flax fibres were not decomposed by the alkaline mixture. Further reduction of the curing time of the geopolymer can be achieved, for example, by using nanoclay [22] or nanosilica [23].

The results of the compressive strength test are shown in Figure 5. The graph shows that by adding fibres to the geopolymer, the composite properties are not improved in terms of compressive strength. The highest compressive strength of 0.62 MPa was measured for samples without added fibres. The lowest compressive strength value of 0.33 MPa was measured in samples reinforced with flax fibres. The difference between the compressive strength in samples without fibres and samples with basalt fibres is not statistically significant; the decrease of compressive strength in the samples with flax fibres is statistically significant, at a significance level of 0.05. The low compressive strength of samples with flax fibres is given by the low density of these samples (Table 2), or by the higher number of pores in the geopolymer. The bending strength and the impact bending of the flax fibre

composite was improved, however, the compressive strength decreased significantly. Based on these results, it could be pointed out that the fibres exert a toughening effect on the material, acting as an impact modifier.
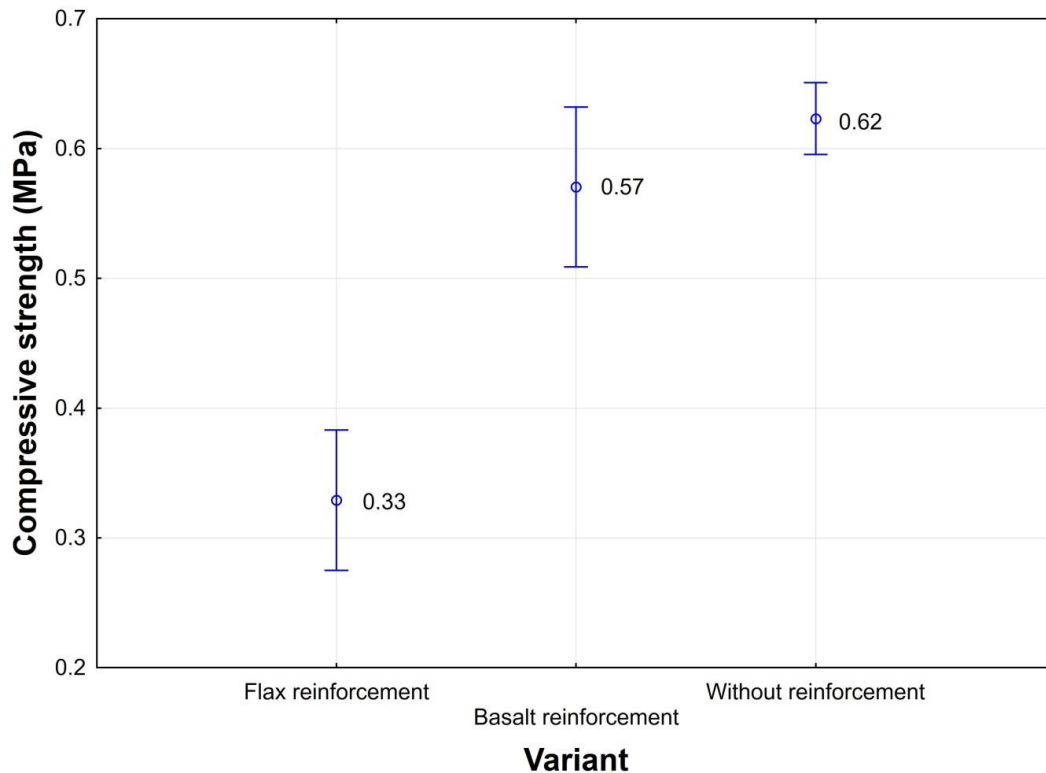
Figure 5. Impact of the addition of fibres on compressive strength.

3.3. Characteristics of Joint Failure

Electron microscopy showed a different pattern of joint failure for composites with flax and basalt and without fibres. Both flax and basalt fibres exhibited reinforcing properties in the geopolymer, and during bending they were able to transfer the tensile load. Because of the rough surface, flax fibres were better anchored in the geopolymer matrix than basalt fibres, which have a smooth surface. Basalt fibres have higher tensile strength, but due to their smooth surface, they are not able to transfer the maximum possible tensile stress. The mechanisms of failure for flax and basalt fibre composites are therefore different. Figure 6a shows the failure of the geopolymer with flax fibre—breakage of the flax fibre that is fully anchored in the geopolymer matrix. This failure mode in these types of composite materials corresponds to the literature [24]. In terms of basalt fibres (Figure 6b), the fibres do not break, but rather peel off from the geopolymer. This is due not only to the high tensile strength of basalt fibres [25,26], but also to their smooth surface. In Figure 6c, only geopolymer breakage is visible; the fibres were not present in the reference set.

(a)

(b)

(c)
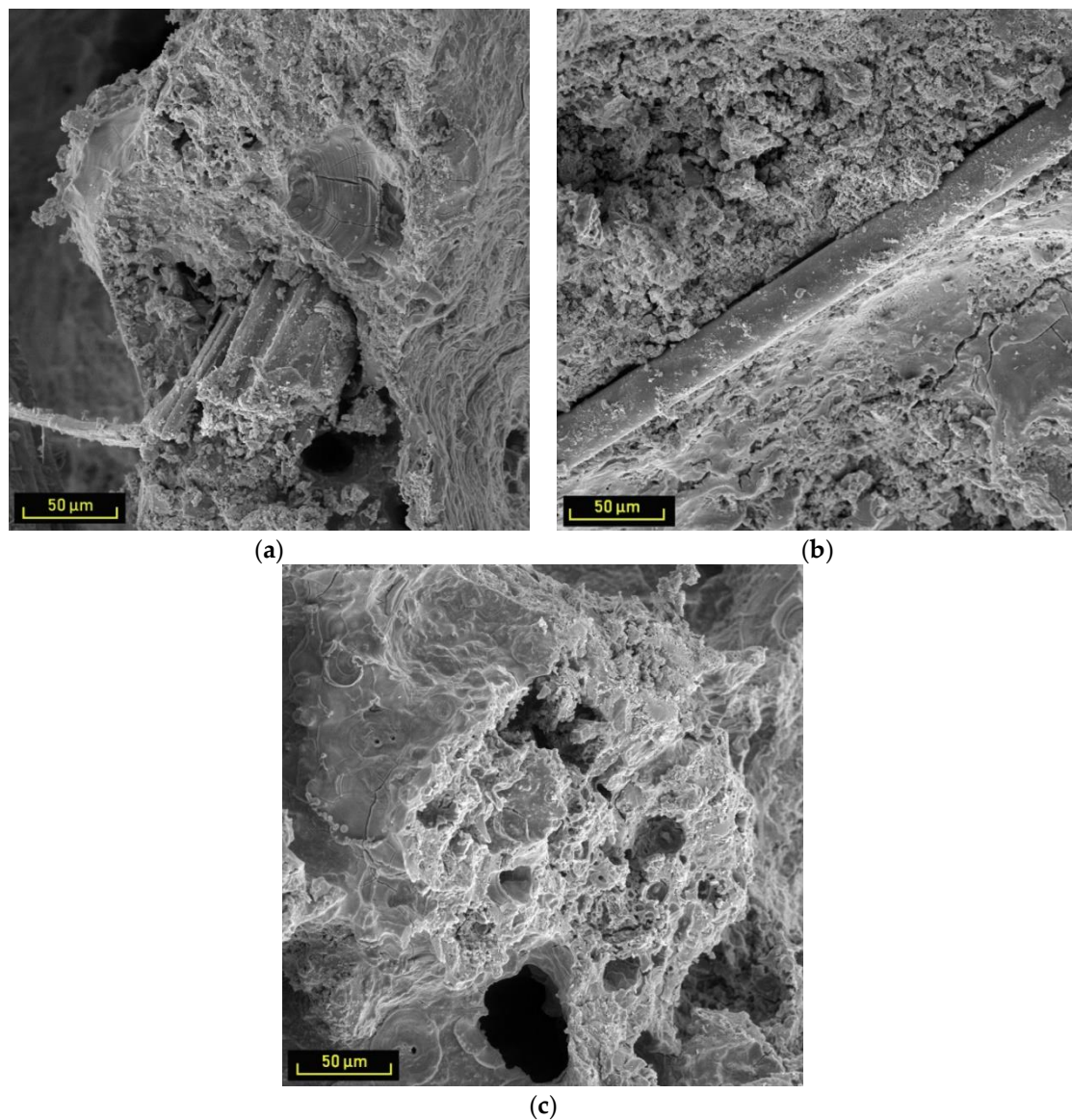
Figure 6. Impact of the addition of fibres on the nature of the joint failure (SEM figures): (**a**) flax fibre-reinforced geopolymer, (**b**) basalt fibre-reinforced geopolymer, and (**c**) geopolymer without fibres.

3.4. TGA, DSC and FTIR Analysis

Figure 7 captures the measured curves from the TGA analysis. Cellulose degradation is apparent at a temperature of 260.74 °C in the geopolymer filled with flax. This does not occur in the case of the two remaining composites. For all three types of geopolymers, over a temperature range of about 690 to about 700 °C, there is evident melting of the aluminium that was added to the geopolymers in order to activate the foaming reaction. The analysis shows that all three types of composite materials are thermally stable and the captured curves contain no significant jumps. The highest weight loss of the sample is manifested in the temperature range from 25 to 200 °C, which is caused by a loss of moisture (both loose and bound) due to heating. The individual relative decreases are 4.3% for geopolymer without fibres, 4% for geopolymer with flax fibres and 5.7% for geopolymer with basalt fibres. Most of the water in the geopolymers evaporates to 100 °C, whereas the remaining hydrated water leaves at the interval from 100 to 200 °C. Further weight loss is above 600 °C, probably due to sialate bonds and the release of hydroxyl ions [27].
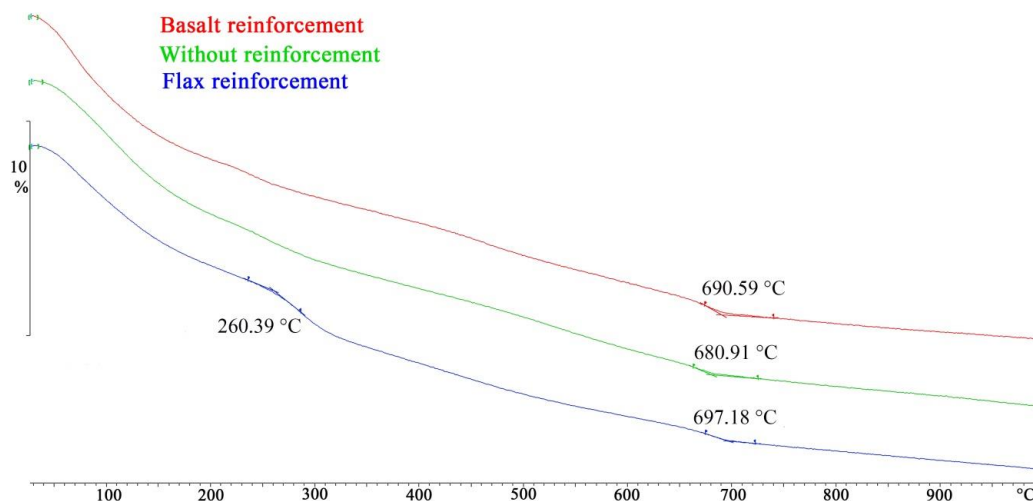
Figure 7. Thermogravimetric analysis (TGA) of geopolymer samples.

Figure 8 captures measured curves from the DSC analysis, and these results correspond to the performed TGA analysis. All three types of composite materials show a significant decrease in water content at temperatures ranging from 60 to approximately 90 °C. Endothermic peaks in the range of 250 to 290 °C can be caused by the melting of geopolymer components or by the breakdown of their bonds. IR spectroscopy could be used for their precise specification. In the case of fibre-reinforced composites (flax and basalt), a slight endothermic reaction is evident at 374 °C for geopolymer with flax and at 376 °C for geopolymer with basalt. This reaction can be attributed to degradation of the bonds between the fibres and the geopolymer. At the end of the observed temperature range, the melting range of aluminium is again apparent for all three types of geopolymers.
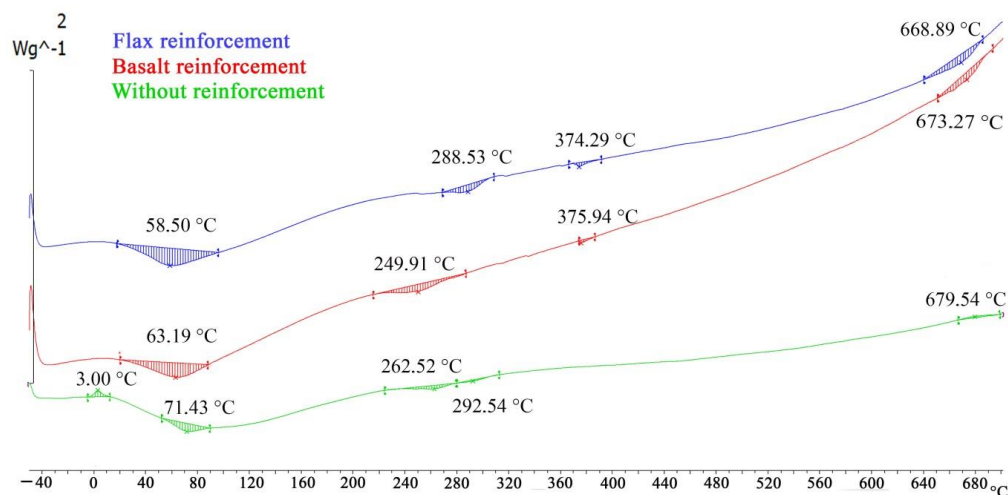
Figure 8. Differential scanning calorimetry (DSC) of geopolymer samples.

Figure 9 captures measured spectra from the FTIR analysis. From the figure can be seen that the obtained signals exhibited only slight differences between the variants. Very few differences are due to the absolutely prevailing inorganic matrix. The weight ratio of the fibres used was only 2.16%. The differences caused by the types of reinforcing fibres used can be seen at the wavelengths of 1430–1460 cm^{-1}, which correspond to C–H deformation (asymmetric) and aromatic skeletal vibration [28]. The high peak around 1000 cm^{-1} represents vibration Si–O from silicate, and vibration C–O from cellulose and skeletal vibration. From the performed chemical analyses, it can be concluded that the reinforced inorganic matrix is stable and is not negatively affected by the reinforcing fibres.
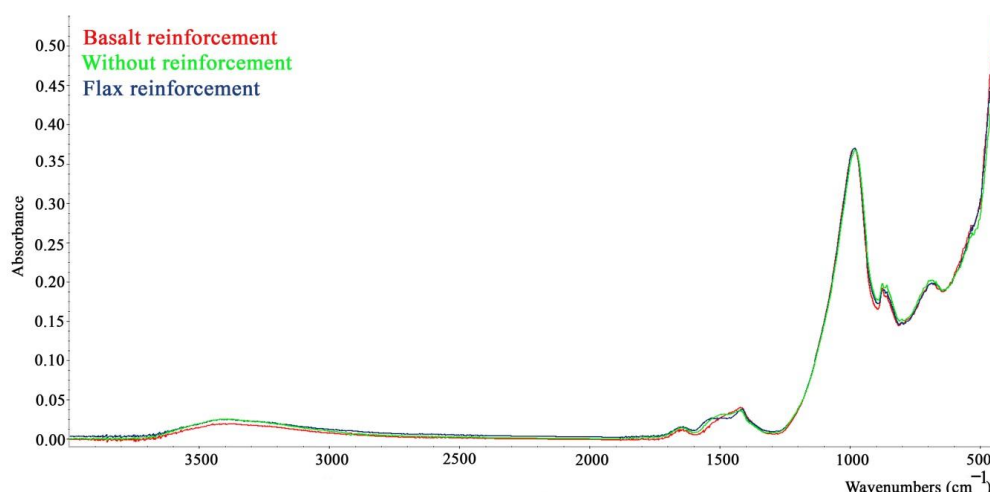
Figure 9. Fourier transform infrared spectroscopy (FTIR) of geopolymer samples.

4. Conclusions

In the present research, the geopolymer was reinforced with flax fibres, with the flax fibres being implemented in the geopolymer as a nonwoven fabric and the fibres spread over the entire board thickness. The following conclusions can be drawn from the results. Flax reinforcement of geopolymer composites with a density of 448 kg/m^3 increased the impact bending of composites up to 0.62 J/cm^2; however, the variability also increased. While impact bending of flax-reinforced geopolymers was statistically significantly higher than basalt-reinforced geopolymers, the bending strength of both composites reinforced with fibres was comparable. Geopolymers reinforced with basalt exhibited a different pattern of joint failure than geopolymers reinforced with flax. While basalt fibres peeled off when the composite was breached, flax fibres remained anchored in the geopolymer and ruptured.

References

1. Defoirdt, N.; Biswas, S.; De Vriese, L.; Van Acker, J.; Ahsan, Q.; Gorbatikh, L.; Van Vuure, A.V.; Verpoest, I. Assessment of the tensile properties of coir, bamboo and jute fibre. *Compos. Part A Appl. Sci. Manuf.* **2010**, *41*, 588–595. [CrossRef]

2. Maity, S.; Gon, D.; Paul, P. A Review of Flax Nonwovens: Manufacturing, Properties, and Applications. *J. Nat. Fibers* **2014**, *11*, 365–390. [CrossRef]

3. Hýsek, Š.; Wimmer, R.; Böhm, M. Optimal processing of flax and hemp fibre nonwovens. *BioResources* **2016**, *11*, 8522–8534. [CrossRef]

4. Anajiwala, R.D.; Blouw, S. Composites from bast fibres—Prospects and potential in the changing market environment. *J. Nat. Fibers* **2007**, *4*, 91–109. [CrossRef]

5. Sgriccia, N.; Hawley, M.C.; Misra, M. Characterization of natural fiber surfaces and natural fiber composites. *Compos. Part A Appl. Sci. Manuf.* **2008**, *39*, 1632–1637. [CrossRef]

6.　Das, D.; Pradhan, A.K.; Chattopadhyay, R.; Singh, S.N. Composite Nonwovens. *Text. Prog.* **2012**, *44*, 1–84. [CrossRef]

7.　Pernica, D.; Reis, P.N.B.; Ferreira, J.A.M.; Louda, P. Effect of test conditions on the bending strength of a geopolymer-reinforced composite. *J. Mater. Sci.* **2010**, *45*, 744–749. [CrossRef]

8.　Hýsek, Š.; Frydrych, M.; Herclík, M.; Louda, P.; Fridrichová, L.; Le Van, S.; Le Chi, H. Fire-resistant sandwich-structured composite material based on alternative materials and its physical and mechanical properties. *Materials* **2019**, *12*, 1432. [CrossRef]

9.　Singh, B.; Ishwarya, G.; Gupta, M.; Bhattacharyya, S.K. Geopolymer concrete: A review of some recent developments. *Constr. Build. Mater.* **2015**, *85*, 78–90. [CrossRef]

10.　Nguyen, T.X.; Louda, P.; Kroisova, D.; Kovacic, V.; Chi, H.L.; Vu, N.L. Effects of Commercial Fibers Reinforced on the Mechanical Properties of Geopolymer Mortar. *Chem. Listy* **2012**, *106*, 560–563.

11.　Zheng, Y.Z.; Wang, W.W.; Brigham, J.C. Flexural behaviour of reinforced concrete beams strengthened with a composite reinforcement layer: BFRP grid and ECC. *Constr. Build. Mater.* **2016**, *115*, 424–437. [CrossRef]

12.　Le Chi, H.; Louda, P. Experimental Investigation of Four-Point Flexural Behavior of Textile Reinforcement in Geopolymer Mortar. *Int. J. Eng. Technol.* **2019**, *11*, 10–15. [CrossRef]

13.　Behera, P.; Baheti, V.; Militky, J.; Louda, P. Elevated temperature properties of basalt microfibril filled geopolymer composites. *Constr. Build. Mater.* **2018**, *163*, 850–860. [CrossRef]

14.　Cook, J.G. *Handbook of Textile Fibres*, 5th ed.; Woodhead Pub: Cambridge, UK, 2003.

15.　*Timber Structures—Test Methods—Determination of Mechanical Properties of Wood Based Panels*; EN 798:2004; Eur. Comm. for Stand: Brussels, Belgium, 2004.

16.　*Testing of Concrete—Determination of Static Modulus of Elasticity in Compression*; ISO 1920-10; Eur. Comm. for Stand: Brussels, Belgium, 2016.

17.　*Test Method—Metallic Materials—Charpy Impact Test*; EN 10045; Eur. Comm. for Stand: Brussels, Belgium, 1990.

18.　Yan, L.; Kasal, B.; Huang, L. A review of recent research on the use of cellulosic fibres, their fibre fabric reinforced cementitious, geo-polymer and polymer composites in civil engineering. *Compos. Part B Eng.* **2016**, *92*, 94–132. [CrossRef]

19.　Meng, W.; Khayat, K.H. Mechanical properties of ultra-high-performance concrete enhanced with graphite nanoplatelets and carbon nanofibers. *Compos. Part B Eng.* **2016**, *107*, 113–122. [CrossRef]

20.　Xu, M.; Bao, Y.; Wu, K.; Shi, H.; Guo, X.; Li, V.C. Multiscale investigation of tensile properties of a TiO_2-doped Engineered Cementitious Composite. *Constr. Build. Mater.* **2019**, *209*, 485–491. [CrossRef]

21.　Assaedi, H.; Alomayri, T.; Shaikh, F.; Low, I.M. Influence of Nano Silica Particles on Durability of Flax Fabric Reinforced Geopolymer Composites. *Materials* **2019**, *12*, 1459. [CrossRef]

22.　Assaedi, H.; Shaikh, F.U.A.; Low, I.M. Effect of nanoclay on durability and mechanical properties of flax fabric reinforced geopolymer composites. *J. Asian Ceram. Soc.* **2017**, *5*, 62–70. [CrossRef]

23.　Assaedi, H.; Shaikh, F.U.A.; Low, I.M. Influence of mixing methods of nano silica on the microstructural and mechanical properties of flax fabric reinforced geopolymer composites. *Constr. Build. Mater.* **2016**, *123*, 541–552. [CrossRef]

24.　Yan, L.; Chouw, N.; Jayaraman, K. Flax fibre and its composites—A review. *Compos. Part B Eng.* **2013**, *56*, 296–317. [CrossRef]

25.　Raj, S.; Kumar, V.R.; Kumar, B.H.B.; Lyer, N.R. Basalt: Structural insight as a construction material. *Sādhanā* **2017**, *42*, 75–84. [CrossRef]

26.　Sim, J.; Park, C.; Moon, D.J. Characteristics of basalt fiber as a strengthening material for concrete structures. *Compos. Part B Eng.* **2005**, *36*, 504–512. [CrossRef]

27.　Davidovits, J. *Geopolymer Chemistry and Applications*, 2nd ed.; Institut Geopolymere: Saint-Quentin, France, 2008.

28.　Tran, T.P.T.; Bénézet, J.-C.; Bergeret, A. Rice and Einkorn wheat husks reinforced poly (lactic acid) (PLA) biocomposites: Effects of alkaline and silane surface treatments of husks. *Ind. Crop. Prod.* **2014**, *58*, 111–124. [CrossRef]

Permeable Water-Resistant Heat Insulation Panel Based on Recycled Materials and Its Physical and Mechanical Properties

Štěpán Hýsek [1,*], **Miroslav Frydrych [2]**, **Miroslav Herclík [2]**, **Ludmila Fridrichová [2]**,
Petr Louda [1], **Roman Knížek [2]**, **Su Le Van [1] and Hiep Le Chi [1]**

[1]   Department of Material Science, Faculty of Mechanical Engineering, Technical University of Liberec, Studentska 2, 461 17 Liberec, Czech Republic
[2]   Department of Textile Evaluation, Faculty of Textile Engineering, Technical University of Liberec, Studentska 2, 461 17 Liberec, Czech Republic
*   Correspondence: hysekstepan@seznam.cz; Tel.: +420-607-501-858

check for updates

Abstract: This paper deals with the development and characteristics of the properties of a permeable water-resistant heat insulation panel based on recycled materials. The insulation panel consists of a thermal insulation core of recycled soft polyurethane foam and winter wheat husk, a layer of geopolymer that gives the entire sandwich composite strength and fire resistance, and a nanofibrous membrane that permits water vapor permeability, but not water in liquid form. The observed properties are the thermal conductivity coefficient, volumetric heat capacity, fire resistance, resistance to long-term exposure of a water column, and the tensile strength perpendicular to the plane of the board. The results showed that while the addition of husk to the thermal insulation core does not significantly impair its thermal insulation properties, the tensile strength perpendicular to the plane of these boards was impaired by the addition of husk. The geopolymer layer increased the fire resistance of the panel for up to 13 min, and the implementation of the nanofibrous membrane resulted in a water flow of 154 cm^2 in the amount of 486 g of water per 24 h at a water column height of 0.8 m.

Keywords: heat insulation; sandwich panel; polyurethane foam; geopolymer; nanofiber membrane

1. Introduction

One of the most important challenges for the construction industry is to reduce the energy demands of buildings throughout their entire life cycle. During the use of a building, its thermal demands are undoubtedly influenced by its insulation. Commonly used thermal insulation materials for building insulation are produced from petrochemical products or from natural sources, but their production is highly energy intensive (glass, rock, wool) [1]. From this perspective, the use of recycled and plant materials is very promising for the production of thermal insulation. In the case of plant materials, rice husks [2], sunflower stalks [3], wheat straw [4], wheat husks [5] flax fibers [6], hemp fibers [7], larch bark [8], and many others can be considered for thermal insulation production. Recycling synthetic materials or using agricultural or industrial residues can be an effective way to reduce virgin materials consumption [9]. Products from recycled plastics such as polyethylene terephthalate [10] and recycled textile fibers [11] provide very good thermal insulation properties.

However, a significant disadvantage of plant materials consisting mainly of cellulose, hemicelluloses, lignin, and pectins is their flammability [12]. In terms of building materials, their resistance to burning by geopolymer applications [13,14] can be improved significantly. Geopolymers are materials usually synthesized using an aluminosilicate raw material and an activating solution

mainly composed of alkalis of sodium or potassium and water glass [15,16]. Due to the properties of geopolymers in the form of high strength, resistance to chemicals and, in particular, thermal stability and fire resistance, applications of these geopolymers in the form of protective coatings or coatings on structures [17–21] have been studied in recent years. In the past, the fire resistance of particleboards based on winter rapeseed stalks [13] has been successfully increased by the geopolymer layer. Even better geopolymer properties can be achieved, for example, via the implementation of carbon fibers, which result in better mechanical properties of the entire composite [22].

An important property of cellulose-based plant fibers is hygroscopicity. This property may be an advantage in some applications and a disadvantage in other applications. However, in terms of thermal insulation of structures, high humidity in the insulation is undesirable, as water reduces the thermal insulation properties of the material [23]. On the other hand, we require, from natural fiber, thermal insulation interior vapor permeability through the building envelope to the exterior [24,25]. Preventing the permeability of liquid water from the exterior into the building envelope and, at the same time ensuring the transport of water vapor from the interior through the building envelope to the exterior, is ensured by a suitably-selected wall structure [26]. One of the elements that can be used in the wall structure for this purpose can be a nanofibrous membrane, which provides water vapor permeability, but prevents the permeability of water in the liquid state [27]. In addition, a suitably-designed nanofibrous membrane can withstand a very high water column, which can affect the building, for example during floods [27].

This paper deals with the use of post-harvest residues of winter wheat and recycled polyurethane foam in combination with geopolymer foam and a nanofibrous membrane for the production of composite materials with properties for the given purpose of use. The aim of this work is to determine the influence of winter wheat husk and the implementation of a nanofibrous membrane and a geopolymer layer into the sandwich panel structure on its mechanical and physical properties. This paper contributes to finding material utilization of wheat husks, which provides storage of CO_2 in comparison with energetic utilization of this raw material. Moreover, addition of husks into the heat insulation panel may bring additional benefits during manufacturing of these panels. Since wheat husks contain 12.7% moisture [5], no steam injection would be necessary for hardening of polyurethane adhesive.

2. Materials and Methods

2.1. Heat Insulation Board Manufacturing

The insulation boards were made of crushed flexible polyurethane (PUR) foam, winter wheat husk, and PU4349/3 one component moisture curing binder (Leeson Polyurethanes Ltd., Warwick, UK). The crushed flexible PUR foam was supplied by the Molitan company (Molitan a. s., Breclav, Czech republic) as recyclate from manufacturing rests. The apparent density of the used PUR foam was 24 kg/m^3 and the bulk density was 11.3 kg/m^3. The PUR particle fraction analysis is shown in the results. Winter wheat husks were mixed into the boards at 0% and 25% to the weight of the PUR recycled material. The analysis of the husk fraction is presented in the results. The adhesive was applied to the particles by spraying in a laboratory adhesive applicator, and the proportion of adhesive on the dry matter was 15%. The carpet was manually layered and compressed between the steel screens, and curing was carried out in a heat chamber at an air temperature of 120 °C for 15 min. The boards were then air conditioned at 20 °C and 65% relative humidity (RH) for 3 days. Figure 1 shows the surface view of the thermal insulation boards.

Figure 1. Surface view of the thermal insulation layer, board without husks on the **left**, board with addition of husks on the **right**.

2.2. Geopolymer and Nanofiber Membrane Application

A geopolymer layer of 1 cm thickness and a density of 880 kg/m^3 was applied to one side of the insulation board to increase its fire resistance. The composition of the geopolymer is shown in Table 1. A more detailed identification of its composition is given in previously published research [13]. A nanofibrous membrane was manually deposited on the surface of the freshly-applied and uncured geopolymer. The nanofibrous membrane was implemented into the composite due to the above-described reason in order to prevent the permeability of water molecules in a liquid state, but allowing for the permeability of water vapor. In order to protect the nanofiber membrane from damage, it was laminated between two non-woven fabrics made from polyester with a basic weight of 55.6 g/m^2. The nanofiber membrane was made of polyurethane via electrospinning using Nanospider technology (Elmarco s.r.o., Liberec, Czech Republic). The solution was spun in an electric field with a voltage of 80.7 kV, the distance of the condenser was 190 mm, the velocity of the supporting base fabric was 0.1 m/min, the relative humidity in the spinning chamber was 21%, and the surface weight of the produced nanofibrous layer was 6 g/m^2.

Table 1. Geopolymer composition.

Component	Percentage of Individual Components
Cement Baucis Lk	43.2%
Activator Baucis Lk	38.9%
KEMA MIKROSILIKA	4.3%
Mineral wool ISOVER	13.0%
Aluminum powder	0.6%

Table 2 shows the variants of the sandwich composites being developed. Two variants of the percentage husk representation were chosen and composites with and without a membrane were made. The geopolymer layer was always constant. Figure 2 shows a cut of the sandwich panel.

Table 2. Variants of the manufactured sandwich-structured panel.

	Permeable Water-Resistant Heat Insulation Panel			
Recycled PUR:wheat husk ratio	1:0		3:1	
Nanofiber membrane	0	1	0	1

Note: polyurethane (PUR).

Figure 2. View of sandwich panel cut.

2.3. Physical and Mechanical Properties Estimation

All of the tests were carried out after air conditioning of the material under conditions of 20 °C and 65% relative humidity. The distribution of husks and crushed PUR foam fraction was determined via a screen analysis and the results were then graphically expressed. The density of the material was determined according to standard EN 323 [28] and internal bonding (tensile strength perpendicular to the plane of the board) according to EN 319 [29]. The methodology of these experiments is described in more detail in [13]. The thermal insulation properties of boards were measured using the Isomet 2104 device (Applied Precision, Ltd., Bratislava, Slovakia) according to the method described previously in [30], using a probe with a measuring range of 0.015 to 2 W/(m·K). The thermal conductivity coefficient of the entire sandwich panel was determined by a calculation, because the thermal insulation properties of the sandwich materials cannot be measured by the used method. The calculation was carried out according to the thermal resistances of the individual layers (Equation (1)) and; therefore, the total thermal conductivity coefficient of the developed sandwich panels is a theoretical value that is based on the thermal resistance values of the individual layers and does not include thermal resistance during heat transfer.

$$\lambda_{tot} = \frac{d_{tot}}{\sum R_i} = \frac{d_{tot}}{\sum \frac{d_i}{\lambda_i}}, \tag{1}$$

where λ_{tot}. is the total thermal conductivity coefficient of the sandwich panel, d_{tot} is the total thickness of the sandwich panel, d_i. is the thickness of one layer in the sandwich panel, λ_i is the thermal conductivity coefficient of one layer in the sandwich panel, and R_i is the thermal resistance of one layer in the sandwich panel.

The fire resistance of the panels was performed via a thermal loading test. This test was performed according to the methodology previously published in [13], and comes from slightly modified standard EN 1363-2 [31]. A custom-designed furnace that allows for testing samples with dimensions of 300 mm × 300 mm was employed in order to characterize the behavior of the developed panels in different types of fire. Chosen external fire curves are presented in the results. Two temperature sensors were used, the first located in the burner chamber and the second on the outside of the flame.

The course of temperatures was monitored over time. The flame intensity was controlled by the flow of gas and the flame was directed parallel to the plane of the tested sample.

The water permeability of sandwich composites was measured on our developed prototype. Unlike similar devices used to measure, for example, water column resistance, the used prototype measures the actual amount of liquid that the test sample releases over time at a defined hydrostatic pressure [27]. Samples with a circular cross section with a diameter of 17 cm were mounted in a test capsule using a seal and, subsequently, the surface of the sample of 154 cm^2 was exposed to a water column 80 cm in height, corresponding to a pressure of 7.8 kPa. The water that passed through the composite was measured for 24 h. Throughout the experiment, the constant height of the water column to which the composite was exposed was maintained.

2.4. Statistical Analysis

Data was statistically processed using Statistica12 software (Tulsa, OK, USA). Descriptive statistics and graphical representations were used to describe the data. The influence of the observed factors on the variables was shown graphically: Thermal conductivity coefficient, thermal capacity, tensile strength perpendicular to the level of the board. The vertical columns correspond to 95% confidence intervals. Subsequently, a Tukey posthoc test was performed to determine if any of the differences between sample means were statistically significant. A significance level of $\alpha = 0.05$ was used for all analyses. The temperature course during the thermal loading test was depicted using point chart as a function of time.

3. Results and Discussion

Figures 3 and 4 show the distribution of the PUR foam crushed fraction and the winter wheat husk. While the predominant part of the crushed PUR foam particles is in the range of 5 to 15 mm, the predominant part of the husk can be characterized by dimensions of 1.5 to 3 mm. The particle size has a major influence on the mechanical properties of the boards [32]; however, in the case of the sandwich panels, where one layer is significantly stronger than the other, the geopolymer layer takes over all the flexural strength [33]. In this research, the particle size affected tensile strength perpendicular to the level of the board.
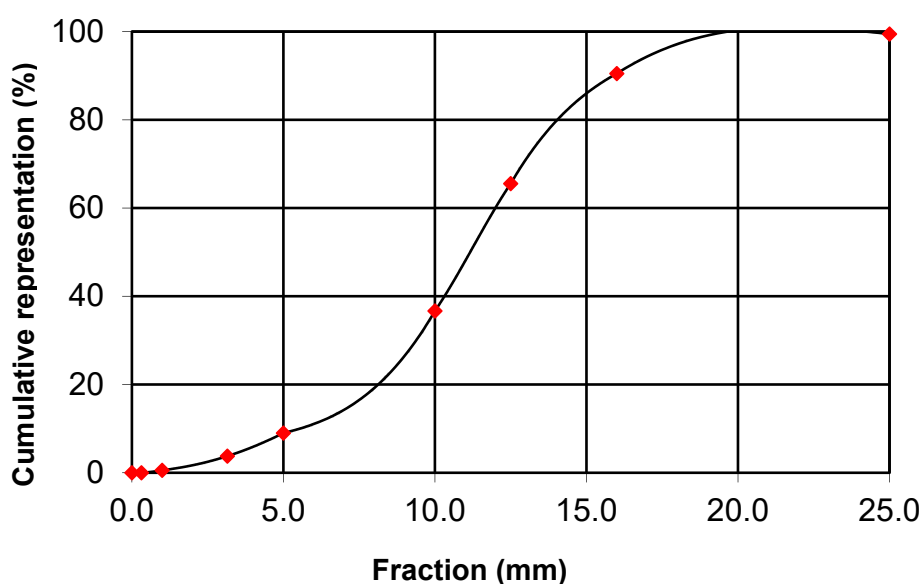
Figure 3. Fraction of crushed PUR foam.
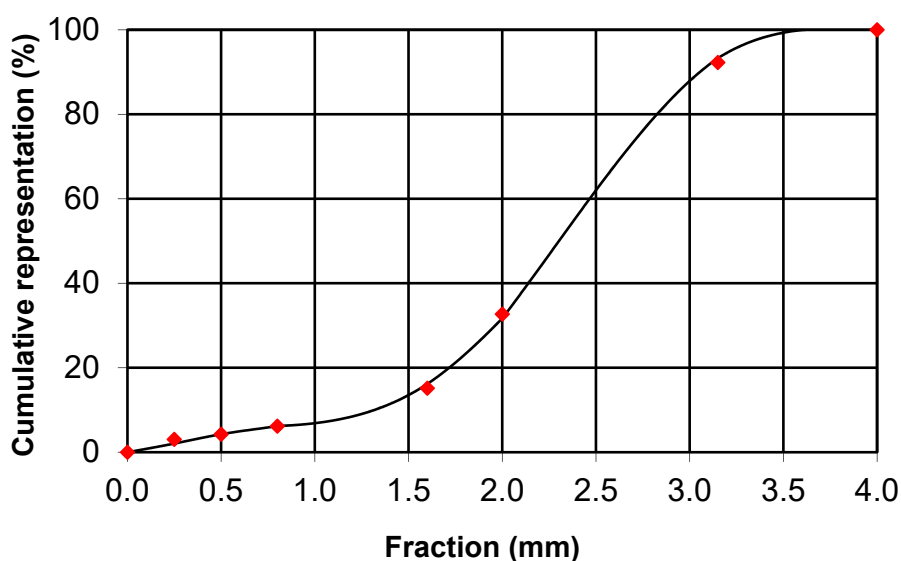
Figure 4. Fraction of winter wheat husk.

Figure 5 shows the effect of the weight ratio of husk in the insulation board on the thermal conductivity coefficient. The picture shows that in both cases the measured thermal insulation cores achieved very good thermal conductivity values in the range from 0.0427 to 0.0452 W/(m·K). The addition of the husk to the crushed PUR foam resulted in a slight deterioration of 0.0025 W/(m·K) (a statistically significant difference); nevertheless, these are still very good values compared to other alternative raw materials. The achieved thermal conductivity values are slightly lower than in the case of thermal insulation boards made from reeds [1], bagasse [34], or cotton stalks [35]. However, it should be noted that, in the above competing products, the manufactured boards had a higher density. For example, 30 kg/m^3 recycled polyethylene terephthalate boards achieved a thermal conductivity coefficient of 0.0355 W/(m·K) [10].
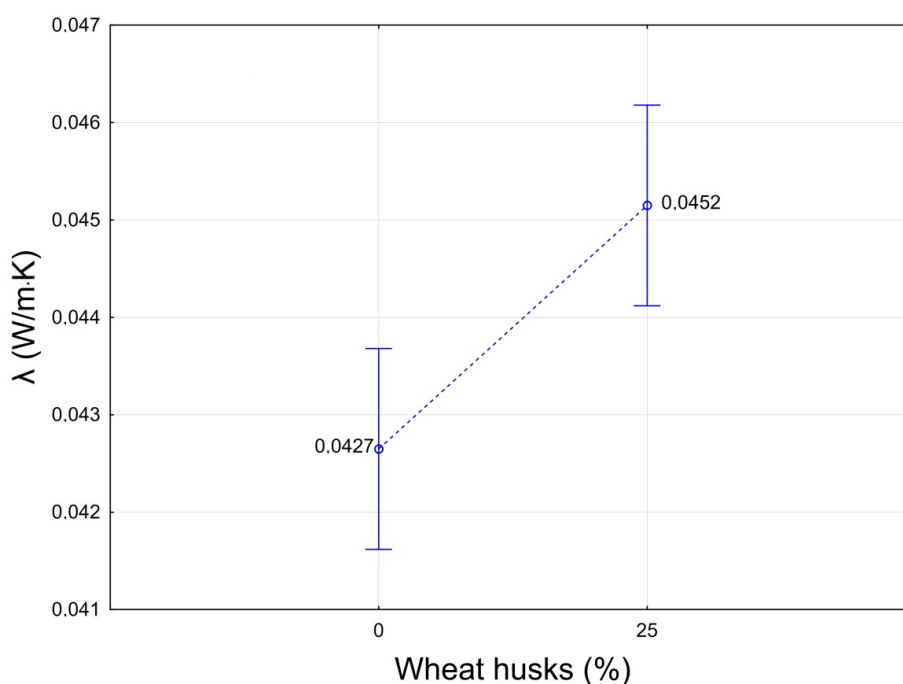
Figure 5. Influence of the proportion of the husk in the insulation board on the thermal conductivity coefficient.

Figure 6 shows the effect of the weight proportion of husk in the insulation board on the volumetric heat capacity. The difference between the individual variants is statistically significant at a level of 0.05. As with the thermal conductivity coefficient, the addition of husk increased this characteristic. However, in this case, this is an improvement in the characteristic that can compensate for the increase in the thermal conductivity coefficient, in the form of a higher accumulation capability of the material and the retention of heat in the walls at a slight decrease in exterior temperature [36]. However, panel cores containing husks achieved, still, a much lower volumetric heat capacity than another agriculture by-product—corn husks [37].
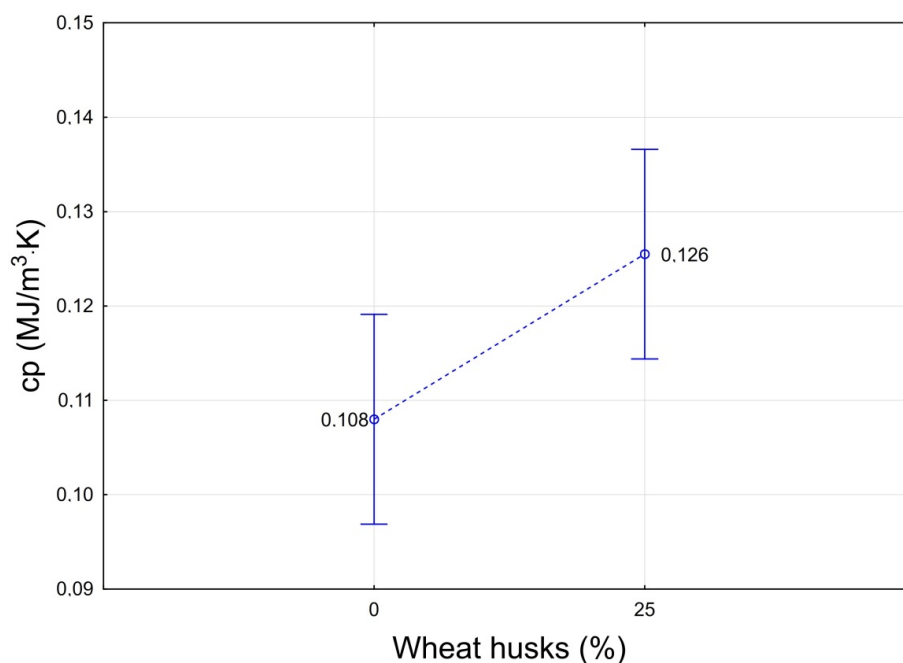
Figure 6. Influence of the proportion of the husk in the insulation board on volumetric heat capacity (cp).

Table 3 shows the calculated thermal conductivity coefficient values of the entire sandwich composite panels and the measured density values of the individual materials. There were slight deviations in the actual thermal insulation board densities from their nominal values. The influence of nanofiber membranes on thermal insulation properties or fire resistance was not evaluated. The geopolymer layer only slightly worsened the thermal insulation properties of the sandwich composite. The total thermal conductivity coefficient is around 0.05 W/(m·K), which is a fully adequate value for thermal insulation materials [9], and produced panels are comparable to other commonly used materials [38]. The reached thermal conductivity coefficients are higher than the thermal conductivity coefficients of commercially-produced heat insulation panels from PUR or PIR (polyisocyanurate) panels; however, the developed panels are from recycled materials and from recycled PUR that was initially not produced for thermal insulation.

Table 3. Average densities of materials and thermal conductivity of sandwich panels.

Recycled PUR:Wheat Husk Ratio	Heat Insulation Board Density (kg/m^3)	Geopolymer Density (kg/m^3)	λ20/65 (W/(m·K))
1:0	49.4 (1.7)	885 (32)	0.049 (0.006)
3:1	51.6 (4.2)	885 (32)	0.051 (0.006)

Note: Values in parentheses are the standard deviations. Polyurethane (PUR).

There was a statistically significant effect of the proportion of husk in the thermal insulation core on its internal bonding (Figure 7). With an increase in the proportion of husk in the material, internal bonding was reduced to 0.64 kPa, which is already insufficient for thermal insulation materials according to standard EN 13162+A1 [39]. For the production of industrially-useable thermal insulation panels with winter wheat husk admixtures, it would then be necessary either to select a higher proportion of adhesive [40] or to include pre-treatment of wheat husks in the production process, in order increase their surface energy and thus reach higher bonding [5].
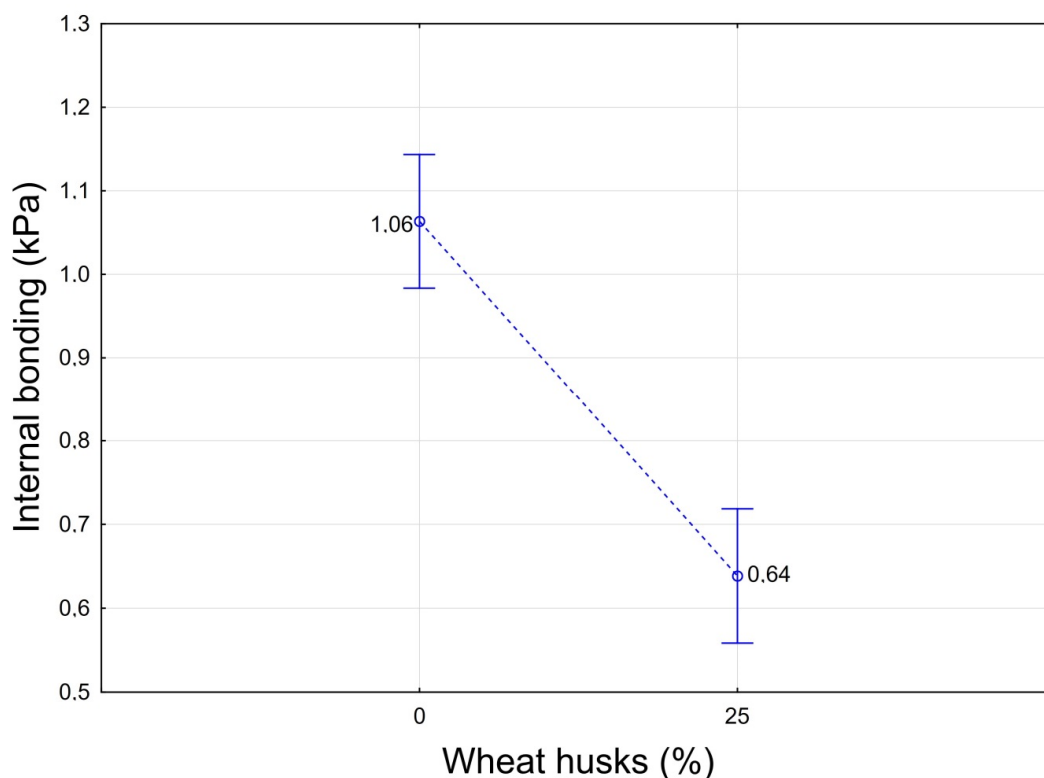
Figure 7. Influence of the proportion of the husk in the insulation board on internal bonding of composite materials.

The graphs in Figure 8 show the behavior of the entire panel under fire load. The samples were exposed to a flame with rapid (Figure 8a) and gradual (Figure 8b) temperature increases. No effect of the wheat husk additive on fire resistance was observed. However, the fire resistance of the boards was affected by the rate of temperature increase. In the case of a fast onset, the boards withstood the effect of flame for approximately 500 s, and more than 800 s in the case of gradual onset. Regardless of the steepness of the onset temperature curve, it was observed that when the temperature inside the furnace rises to around 400 °C, the temperature on the outer surface of thermal insulation boards increases to around 60 °C, which is then held constant until the material burns. These results correspond with results for sandwich-structured composites made from rapeseed stalks [13], and, because of the flammable insulation core, the panel withstood lower temperatures than in [16], where geopolymer composites were filled only by basalt microfibrils.
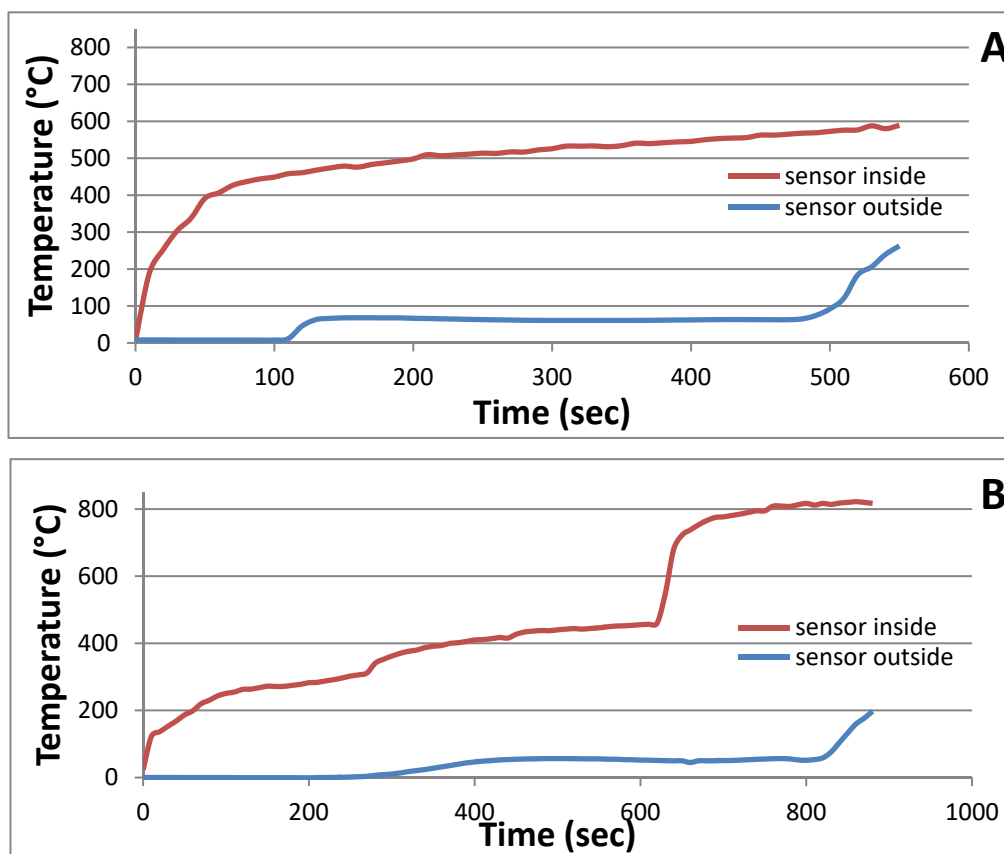
Figure 8. Burning characteristics of produced panels: (**A**) Rapid temperature increase; (**B**) gradual temperature increase.

The developed sandwich panels were able to withstand fairly long-term exposure to a water column with a height of 80 cm. In 24 h, only 486 g of water flowed through the 154 cm^2 area (Figure 9). There was no difference found between the sandwich panel with the addition of husk and no husk. All of the resistance of the sandwich composite to the long-term effect of the water column is due to the used nanofibrous membrane and the interface between the nanofibrous membrane and the geopolymer. With regard to the thermal insulation sandwich panel without a nanofibrous membrane, this sandwich is virtually unable to prevent water flow. When the sandwich without a nanofibrous membrane was encumbered with a water column with a height of 80 cm, 3700 g of water flowed through the 154 cm^2 area over 4 min.
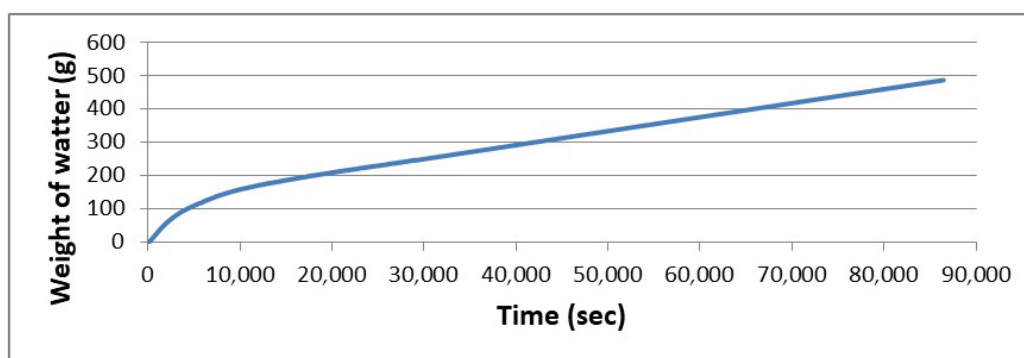
Figure 9. Effect of the nanofibrous membrane on the resistance of the sandwich panel against the long-term effects of the water column.

The results show that the geopolymer layer in the entire sandwich panel suitably complements the thermal insulation core. The geopolymer layer provided the material with fire resistance, and it can be assumed that it would increase flexural strength [41], while only slightly worsening the overall thermal conductivity coefficient. The geopolymer layer was thoroughly bonded to the thermal insulation core, and in the tensile strength test perpendicular to the plane of the board, there was no breach between these layers, but in the insulation core. The nanofibrous membrane also contributed to improving the properties of the entire sandwich composite. It gave the material resistance to long-term exposure to the water column, while not negatively affecting any other material properties.

4. Conclusions

The paper presented properties of a sandwich panel from recycled materials enhanced by a geopolymer layer and a nanofibrous membrane. It was shown that the addition of husk to the thermal insulation core increased the thermal conductivity coefficient up to the value of 0.0452 W/(m·K), but this negative increase can be compensated by the increase in specific heat capacity of the insulation core with husks up to the value of 0.126 MJ/(m^3·K). The theoretical value of the thermal conductivity coefficient of the developed panels achieves excellent values on the level of 0.05 W/(m·K). The geopolymer layer and nanofibrous membrane provided the sandwich panel with the necessary properties for use as thermal insulation in exposed building walls, and fire resistance and water resistance increased nominally. The panel resisted fire with a gradual temperature increase for more than 13 min, and incorporation of a nanofibrous membrane provided enhanced resistance to a water column with a height of 0.8 m.

References

1. Asdrubali, F.; D'Alessandro, F.; Schiavoni, S.; Mencarelli, N. Sound absorption properties of reed. In Proceedings of the 22nd International Congress on Sound and Vibration, Florence, Italy, 12–16 July 2015.
2. Yarbrough, D.W.; Wikes, K.E.; Olivier, P.A.; Graves, R.S.; Vohra, A. Apparent thermal conductivity data and related information for rice hulls and crushed pecan shells. *Therm. Cond.* **2005**, *27*, 222–230.
3. Binici, H.; Eken, M.; Dolaz, M.; Aksogan, O.; Kara, M. An environmentally friendly thermal insulation material from sunflower stalk, textile waste and stubble fibres. *Constr. Build. Mater.* **2014**, *51*, 24–33. [CrossRef]
4. Goodhew, S.; Griffiths, R. Sustainable earth walls to meet the building regulations. *Energy Build* **2005**, *37*, 451–459. [CrossRef]
5. Hýsek, Š.; Podlena, M.; Bartsch, H.; Wenderdel, C.; Böhm, M. Effect of wheat husk surface pre-treatment on the properties of husk-based composite materials. *Ind. Crops Prod.* **2018**, *125*, 105–113. [CrossRef]
6. Kozłowski, R.; Mieleniak, B.; Muzyczek, M.; Mankowski, J. Development of insulation composite based on FR bast fibers and wool. In *International Conference on Flax and Other Bast Plants*; Saskatchewan Flax Development Commission: Saskatoon, SK, Canada, 2008; ID number: 68; pp. 353–363.
7. Battegazzore, D.; Alongi, J.; Duraccio, D.; Frache, A. Reuse and valorisation of hemp fibres and rice husk particles for fire resistant fibreboards and particleboards. *J. Polymers Env.* **2018**, *26*, 3731–3744. [CrossRef]

8.　Kain, G.; Lienbacher, B.; Barbu, M.C.; Senck, S.; Petutschnigg, A. Water vapour diffusion resistance of larch (Larix decidua) bark insulation panels and application considerations based on numeric modeling. *Constr. Build. Mater.* **2018**, *164*, 308–316. [CrossRef]

9.　Asdrubali, F.; D'Alessandro, F.; Schiavoni, S. A review of unconventional sustainable building insulation materials. *Sustain. Mater. Technol.* **2015**, *4*, 1–17. [CrossRef]

10.　Intini, F.; Kühtz, S. Recycling in buildings: an LCA case study of a thermal insulation panel made of polyester fiber, recycled from post-consumer PET bottles. *Int. J. Life Cycle Assess.* **2011**, *16*, 306–315. [CrossRef]

11.　Briga-Sá, A.; Nascimento, D.; Teixeira, N.; Pinto, J.; Caldeira, F.; Varum, H.; Paiva, A. Textile waste as an alternative thermal insulation building material solution. *Constr. Build. Mater.* **2013**, *38*, 155–160. [CrossRef]

12.　Das, D.; Pradhan, A.K.; Chattopadhyay, R.; Singh, S.N. Composite nonwovens. *Text. Prog.* **2012**, *44*, 1–84. [CrossRef]

13.　Hýsek, Š.; Frydrych, M.; Herclík, M.; Louda, P.; Fridrichová, L.; Le Van, S.; Le Chi, H. Fire-resistant sandwich-structured composite material based on alternative materials and its physical and mechanical properties. *Materials* **2019**, *12*, 1432. [CrossRef] [PubMed]

14.　Dufkova, I.; Kovacic, V.; Louda, P. The effect of adding micro and inorganic nanoparticles on properties of geosilicate cured at temperature. In Proceedings of the 9th International Conference on Nanomaterials-Research and Application (Nanocon), Brno, Czech, 18–20 October 2017.

15.　Toniolo, N.; Boccaccini, A.R. Fly ash-based geopolymers containing added silicate waste. A review. *Ceramics Int.* **2017**, *43*, 14545–14551. [CrossRef]

16.　Behera, P.; Baheti, V.; Militky, J.; Louda, P. Elevated temperature properties of basalt microfibril filled geopolymer composites. *Constr. Build. Mater.* **2018**, *163*, 850–860. [CrossRef]

17.　Rovnaník, P.; Al, S.O. Effect of curing temperature on the development of hard structure of metakaolin-based geopolymer. *Constr. Build. Mater.* **2010**, *24*, 1176–1183. [CrossRef]

18.　Degirmenci, F.N. Freeze-thaw and fire resistance of geopolymer mortar based on natural and waste pozzolans. *Ceram. Silik.* **2017**, *62*, 1–9. [CrossRef]

19.　Bakharev, T. Resistance of geopolymer materials to acid attack. *Cem. Concr. Res.* **2005**, *35*, 658–670. [CrossRef]

20.　Villaquirán-Caicedo, M.A.; de Gutiérrez, R.M.; Sulekar, S.; Davis, C.; Nino, J.C. Thermal properties of novel binary geopolymers based on metakaolin and alternative silica sources. *Appl. Clay Sci.* **2015**, *118*, 276–282. [CrossRef]

21.　Hung, T.D.; Pernica, D.; Kroisova, D.; Bortnovsky, O.; Louda, P.; Rylichova, V. Composites Base on Geopolymer Matrices: Preliminary Fabrication, Mechanical Properties and Future Applications. *Adv. Mater. Res.* **2018**, *55–57*, 477–480. [CrossRef]

22.　Le Chi, H.; Louda, P.; Periyasamy, A.P.; Bakalova, T.; Kovacic, V. Flexural behavior of carbon textile-reinforced geopolymer composite thin plate. *Fibers* **2018**, *6*, 87. [CrossRef]

23.　Bastien, D.; Winther-Gaasvig, M. Influence of driving rain and vapour diffusion on the hygrothermal performance of a hygroscopic and permeable building envelope. *Energy* **2018**, *164*, 288–297. [CrossRef]

24.　Arundel, A.V.; Sterling, E.M.; Biggin, J.H.; Sterling, T.D. Indirect health effects of relative humidity in indol environments. *Environ. Health Perspect.* **1986**, *65*, 351–361 101289/ehp8665351.

25.　Simonson, C.J.; Salaonvaara, M.; Ojanen, T. Heat and mass transfer between indoor air and a permeable and hygroscopic building envelope: Part I – field measurements. *J. Build. Phys.* **2004**, *28*, 63–101 101177/1097196304044395. [CrossRef]

26.　Simonson, C.J.; Salaonvaara, M.; Ojanen, T. Heat and mass transfer between indoor air and a permeable and hygroscopic building envelope: Part II – verification and numerical studies. *J. Build. Phys.* **2004**, *28*, 161–185. [CrossRef]

27.　Fridrichová, L.; Frydrych, M.; Herclík, M.; Knížek, R.; Mayerová, K. Nanofibrous membrane as a moisture barrier. In Proceedings of the AIP Conference, Milano, Italy, 3–7 August 2018.

28.　*EN 323:1993—Wood-Based Panels. Determination of Density*; Eur. Comm. for Stand.: Brussels, Belgium, 1993.

29.　*EN 319:1993—Particleboards and Fibreboards. Determination of Tensile Strength Perpendicular to the Plane of the Board*; Eur. Comm. for Stand.: Brussels, Belgium, 1993.

30.　Neuberger, P.; Kic, P. The use of unsteady method for determination of thermal conductivity of porous construction materials in real conditions. *Agronomy Res.* **2017**, *15*, 1119–1126.

31.　*EN 1363-2:1999—Fire Resistance Tests. Alternative and Additional Procedures*; Eur. Comm. for Stand.: Brussels, Belgium, 1999.

32. Ferrández-García, C.-E.; Ferrández-García, A.; Ferrández-Villena, M.; Hidalgo-Cordero, J.F.; García-Ortuño, T.; Ferrández-García, M.-T. Physical and mechanical properties of particleboard made from palm tree prunings. *Forests* **2018**, *9*, 755. [CrossRef]

33. Yuan, L.; Batra, R.C. Optimum first failure load design of one/two-core sandwich plates under blast loads, and their ultimate loads. *Compos. Struct.* **2019**, *224*. [CrossRef]

34. Panyakaew, S.; Fotios, S. New thermal insulation boards made from coconut husk and bagasse. *Energy Build.* **2011**, *43*, 1732–1739. [CrossRef]

35. Zhou, X.; Zheng, F.; Li, H.; Lu, C. An environment-friendly thermal insulation material from cotton stalk fibers. *Energy Build.* **2010**, *42*, 1070–1074. [CrossRef]

36. Pavelek, M.; Prajer, M.; Trgala, K. Static and dynamic thermal characterization of timber frame/wheat (*Triticum Aestivum*) chaff thermal insulation panel for sustainable building construction. *Sustainability* **2018**, *10*, 2363. [CrossRef]

37. Czajkowski, L.; Wojcieszak, D.; Olek, W.; Prybyl, J. Thermal properties of fractions of corn stover. *Construct. Building Mater.* **2019**, *210*, 709–712. [CrossRef]

38. Asdrubali, F.; Pisello, A.L.; DˇAlessandro, F.; Bianchi, F.; Fabiani, C.; Cornicchia, M.; Rotili, A. Experimental and numerical characterization of innovative cardboard-based panels: Thermal and acoustic performance analysis and life cycle assessment. *Building Env.* **2016**, *95*, 145–159. [CrossRef]

39. *EN 13162:2012+A1:2015—Thermal Insulation Products for Buildings. Factory Made Mineral Wool (MW) Products. Specification*; Eur. Comm. for Stand.: Brussels, Belgium, 2015.

40. Tayeb, A.H.; Amini, E.; Ghasemi, S.; Tajvidi, M. Cellulose nanomaterials-binding properties and applications: A review. *Molecules* **2018**, *23*, 2684. [CrossRef] [PubMed]

41. Taveri, G.; Bernardo, E.; Dlouhy, I. Mechanical performance of glass-based geopolymer matrix composites reinforced with cellulose fibers. *Materials* **2018**, *11*, 2395. [CrossRef] [PubMed]

Sample Availability: All samples are available from the authors.

Fire-Resistant Sandwich-Structured Composite Material Based on Alternative Materials and Its Physical and Mechanical Properties

Štěpán Hýsek [1],* , **Miroslav Frydrych [1]**, **Miroslav Herclík [1]**, **Petr Louda [1]** ,
Ludmila Fridrichová [2], **Su Le Van [1] and Hiep Le Chi [1]**

[1] Department of Material Science, Faculty of Mechanical Engineering, Technical University of Liberec, Studentska 2, 461 17 Liberec, Czech Republic; miroslav.frydrych@tul.cz (M.F.); miroslav.herclik@tul.cz (M.H.); petr.louda@tul.cz (P.L.); longsuvp90@gmail.com (S.L.V.); lechihieptul09@gmail.com (H.L.C.)

[2] Department of Textile Evaluation, Faculty of Textile Engineering, Technical University of Liberec, Studentska 2, 461 17 Liberec, Czech Republic; ludmila.fridrichova@tul.cz

* Correspondence: hysekstepan@seznam.cz; Tel.: +420-607-501-858

Abstract: The development of composite materials from alternative raw materials, and the design of their properties for the intended purpose is an integral part of the rational management of raw materials and waste recycling. The submitted paper comprehensively assesses the physical and mechanical properties of sandwich composite material made from particles of winter rapeseed stalks, geopolymer and reinforcing basalt lattices. The developed composite panel is designed for use as a filler in constructions (building or building joinery). The observed properties were: bending characteristics, internal bonding, thermal conductivity coefficient and combustion characteristics. The results showed that the density of the particleboard has a significant effect on the resulting mechanical properties of the entire sandwich panel. On the contrary, the density of the second layer of the sandwich panel, geopolymer, did not have the same influence on its mechanical properties as the density of the particleboard. The basalt fibre reinforcement lattice positively affected the mechanical properties of sandwich composites only if it was sufficiently embedded in the structure of the particle board. All of the manufactured sandwich composites resisted flame for more than 13 min and the fire resistance was positively affected by the density of the geopolymer layer.

Keywords: composite material; sandwich panel; rapeseed; geopolymer; reinforcing lattice

1. Introduction

Through their properties, basalt fibres are intended for use as a reinforcement in composite materials. These fibres have a higher tensile strength than E-glass fibres, larger strain to failure than carbon fibres and good resistance to alkaline exposure; they are also non-flammable, chemically stable, non-toxic and, overall, can be used in conditions from −200 °C to 600 °C [1–3]. Basalt fibres may be used separately as microfibers, successfully fulfilling the function of a reinforcing agent in composite materials based on inorganic matrices [4–7], or as a reinforcement element in the form of a surface fabric, the use of which appears to be very effective [1,8]. In addition, basalt fibres arranged in the form of a surface fabric have been successfully used in the past, for example in reinforcing concrete beams [9], historical pillars [10] or surface panels [1,11,12]. In all of the mentioned cases, basalt fibres, whether as single fibres, fibre bundles or fibre lattices, function as a reinforcement element in a matrix made of concrete, mortar or other material. In the presented research, the basalt fibre surface fabric was used to reinforce the particleboard from winter rapeseed stalks.

Winter rapeseed stalks are an abundant raw material in the European Union, with about 45 million tonnes produced annually [13], which would approximately two times suffice for the annual consumption of wood for the production of particleboard in the EU [14]. In addition to the production of bioethanol [15], it can be successfully used in the production of particleboard [16].

In terms of carbon dioxide binding, their use for further production of material is far more meaningful than their use for energy purposes. Boards made from these stems can also have very good properties [17]. However, the combination of these post-harvest residues with cheap urea-formaldehyde adhesive is very attractive, which offers a very cost-effective composite material with acceptable properties [18]. Geopolymer was used in order to improve the mechanical properties and fire resistance of this cheap composite reinforced with basalt surface fabric.

Geopolymers are amorphous three-dimensional alkali-activated aluminosilicates [19] and are considered an environmentally friendly building material [20]. These are materials that have great potential in various applications due to their specific properties (thermal insulation, fire resistance, strength, acoustics). Due to the possible foaming of the geopolymer, a lightweight material is produced while maintaining the fire and strength characteristics. Examples include a geopolymer-based composite and basalt fibre, which is suitable for high-temperature applications [4] or geopolymer foam concrete (GFC) panel with excellent sound absorption [21].

The sustainable development of production, processing and consumption cannot be achieved without the responsible waste management [22] and efficient use of materials [23,24]. This paper responds to the latest research trends and deals with the development of a new lightweight composite material from alternative raw materials for the production of highly functional composite materials with properties for the intended use. The aim of the work is to determine the influence of density of individual layers of sandwich composite material and reinforcing lattices on its mechanical and physical properties.

2. Materials and Methods

Particles from winter rape stalks were used to produce particleboards. The producer of particles from winter rape stalks was Mikó Stroh (Borota, Hungary). The dimensional characteristics of the used particles are given in Table 1. The dimensional characteristics of particles were determined using screen analysis (Imal, Modena, Italy).

Table 1. Dimensional characteristics of particles.

Dimension (mm)	0–0.25	0.25–0.5	0.5–0.8	0.8–1.6	1.6–2	2–3.15	3.15–8
Percentage (%)	1.2	2.8	4.8	39.4	20.1	23.1	8.6

2.1. Lattice

Lattices made from basalt fibre with loop dimensions of 25 mm were supplied by Alligard (Libavské Údolí, Czech Republic). According to the producer's declaration from the technical data sheet, each bundle of fibres contained 6500 microfibers with a diameter of 11–18 μm. The linear mass density of the bundle was 2400 tex and the density of microfibers was 2700 kg/m^3. The tensile strength of the individual bundles was 600 MPa. According to the variants, two, one or no lattices were pressed into the particleboard. In the composite material with the two-lattice variant, the lattices were placed in the surface layer, and in the variant with one lattice it was pressed in the middle of the board. The lattices were inserted into the particles during the layering of the particle carpet, according to the variant in the middle of the carpet, or on its surface from both sides (Figure 1).

Figure 1. Lattice placed in the surface of the board. From the left: layered carpet in the form for pre-pressing, carpet after cold pre-pressing, pressed board.

2.2. Adhesive Mixture Application

A urea-formaldehyde adhesive (UF) was used to manufacture particleboards, which was applied to particles using a laboratory adhesive applicator. The used hardener was $(NH_4)(NO_3)$, and the ratio between the solids hardener and dry adhesive was 10%. The hydrophobizing agent used was paraffin emulsion. The solid content of whole adhesive mixture was 50%. A resin dosage of 10% solids on particle dry mass was used. The detailed composition of the adhesive is given in [25].

2.3. Pre-Pressing and Hot-Pressing

Particleboards were pressed from particles dried to 8% moisture content. The first step was cold pre-pressing with conditions: pressure 4 bars, time 1 min. The pre-pressed board was pressed using a heated HLP350 hydraulic press (Höfer Presstechnik GmbH, Taiskirchen, Austria) at 165 °C. Pressing was carried out according to the press cycle (Table 2). The nominal board thickness was 12 mm. Plates were pressed in two variants according to density and in three variants according to the number of grids. An illustration of the various composite variants is given in Table 3. After pressing, the boards were conditioned at 20 °C and at a relative humidity (RH) of 65% until moisture stabilization.

Table 2. Pressing Cycle.

Phase No.	Thickness at the End (mm)	Moving Time (s)	Remaining Time (s)
1	40	0.1	0
2	18	3	0
3	11.8	8	12
4	12	5	10
5	12.3	3	0
6	12	3	141
7	12.5	25	0
8	500	0.1	0

2.4. Geopolymer Application

In order to increase the fire resistance of the manufactured materials, geopolymer was applied to the manufactured board from one side with a nominal height of the layer of 1 cm and a nominal density of 885 and 915 kg/m^3. The variants of the manufactured sandwich-structured panel are listed in Table 3. In order to compare the developed material with commercially-sold products, a commercially-sold oriented strand board (OSB) (class 3, density 620 kg/m^3) was selected. This board was used for reference

samples instead of particleboard from rapeseed stalks and reinforced lattices. Both geopolymer variants were also applied to the OSB.

The mixture for the geopolymer production consists of the following five components.

(1)   inorganic, two-component, aluminosilicate binder based on metakaolin Cement Baucis Lk (České Lupkové Závody, a.s., Nové Strašecí, Czech Republic),

(2)   alkaline activator in liquid form Activator Baucis Lk (České Lupkové Závody, a.s., Nové Strašecí, Czech Republic),

(3)   anticorrosive powder additive for concrete and malt based on amorphous SiO_2 Kema Mikrosilika (Kema Mikrosilika-sanační centrum s.r.o., Sviadnov Czech Republic),

(4)   basalt fibres Mineral wool Isover Uni—basalt fibres (Saint-Gobain Construction Product CZ a.s., Praha, Czech Republic),

(5)   aluminium powder with a purity of at least 99% and an average particle size of 65 μm Aluminium powder-Alpra—very fine, (PK Chemie, Třebíč Czech Republic). The geopolymer was manufactured according the methodology previously published in [8]. Two manufactured geopolymer density variants were selected; the percentage of all components in each variant is shown in Table 4.

Table 3. Variants of manufactured sandwich-structured panel.

Layer Specification	Fire-Resistant Sandwich-Structured Panel											
Board density (kg/m^3)	340						500					
Geopolymer density (kg/m^3)	885			915			885			915		
Lattice count	0	1	2	0	1	2	0	1	2	0	1	2

Table 4. Geopolymer composition.

Component	Percentage Share of Individual Components	
	Geopolymer Density 885 kg/m^3	Geopolymer Density 915 kg/m^3
Cement Baucis Lk	43.2%	43.4%
Activator Baucis Lk	38.9%	39.1%
Kema Mikrosilika	4.3%	4.3%
Mineral wool Isover	13.0%	13.0%
Aluminium powder	0.6%	0.2%

2.5. Composite Material Properties Estimation

Before all of the tests, the panels we air-conditioned at 20 °C and a relative humidity (RH) of 65% for three weeks. After this period, the equilibrium moisture was achieved. The density, the tensile strength of the composite material perpendicular to the board's plane and the three-point bending characteristics were measured according international standards. The density of boards was measured according to EN 323 [26], the internal bonding was measured according to EN 319 [27] and the measurements of three-point bending characteristics were carried out according to EN 798 [28]. The bending test bodies were placed on the universal testing machine so that the geopolymer layer was directed upward in order to be subjected to compressive stress during bending, and the layer with reinforcing lattice to tensile stress. The measurement accuracy of the universal tensile machine was 0.25% of reading. For a more thorough characterization of the bending properties of sandwich composites, the bending coefficient was calculated according to the following Formula [29]:

$$K_{bendC} = \frac{h}{R_{minC}} = \frac{h}{\frac{l_0^2}{12 \cdot y_{max}}} \tag{1}$$

where:

R_{minC}—The minimum curve radius based on the basic bending equations.
K_{bendC}—The coefficient of bendability based on the basic bending equations.
y_{max}—The maximum deflection.
l_0—The distance between supports.
h—The thickness of the sample.

The tensile and bending tests were performed using universal testing machine TIRA test 2850. The thermal conductivity of boards was estimated using Isomet 2104 (Applied Precision, Ltd., Bratislava, Slovakia) according the method described previously in [30], the thermal conductivity was measured using a probe with a range of 0.015–2 W/(m·K). According to the technical data specification of the probe, the measurement accuracy is 5% of reading +0.001 W/(m·K). The thermal conductivity coefficient of the entire sandwich panel was subsequently calculated. The recalculation was performed according to the thermal resistances of the individual layers according to Formula (2). The total coefficient of thermal conductivity of the developed sandwich panels is therefore the theoretical value based on the values of the thermal resistances of the individual layers and does not include thermal resistance during heat transfer.

$$\lambda_{tot} = \frac{d_{tot}}{\sum R_i} = \frac{d_{tot}}{\sum \frac{d_i}{\lambda_i}} \tag{2}$$

where:

λ_{tot}—The total thermal conductivity of the sandwich panel.
d_{tot}—The total thickness of the sandwich panel.
d_i—The thickness of one layer in the sandwich panel.
λ_i—The thermal conductivity of one layer in the sandwich panel.
R_i—The thermal resistance of one layer in the sandwich panel.

The thermal loading test was carried out for the purpose of characterizing the fire resistance of the panels. Slight deviations from the standard EN 1363-2 [31] were used. Alternative external fire curves were chosen for the behavioural characteristics of the developed material in different types of fire. These curves are shown in the results. A custom designed furnace was used for the fire testing. Samples with dimensions of 300 mm × 300 mm were placed in a vertical position and were exposed to flames in a direction parallel to the plane of the board. The flame intensity was managed by controlling the flow of gas and was increased over time. Two sensors for temperature monitoring were used to characterize the behaviour of the material in this test. The first was placed in a chamber with a burner and the second on the outside of the flame. The temperature measurement accuracy was 0.1 °C. The temperature was monitored over time.

The number of measured samples for each variant was 30 for density, internal bonding and bending tests. The thermal conductivity was measured on 10 samples for each variant and one sample from each variant was used for the thermal loading test.

2.6. Statistical Analysis

The data was characterized using descriptive statistics (sample mean and sample standard deviation) and a multi-factor analysis of variance. The sample standard deviation was calculated according to Formula (3). For the analysis of variance, the following factors were used: lattice count, board density and geopolymer density. Graphically were depicted the influences of the factors on the following variables: bending strength, modulus of elasticity, bending coefficient and internal bonding. Vertical columns in the graphical representation of the analysis of variance represent 95 percent confidence intervals. Limits of the confidence intervals were calculated according to

Formula (4). The graphics are listed for illustration of the descriptive statistics. The Tukey HSD test was used to determine if any of the differences between the sample means were statistically significant. A significance level of $\alpha = 0.05$ was selected. The temperature course during the thermal loading test was depicted using point chart as a function of time.

$$s = \sqrt{\frac{\sum_{i=1}^{N}(x_i - \bar{x})^2}{n-1}} \tag{3}$$

where:

s—The sample standard deviation.
x—The observed value.
n—The number of observations.

$$L_{1,2} = \bar{x} \pm \frac{s}{\sqrt{n}} \times t_{n-1}(\alpha) \tag{4}$$

where:

$L_{1,2}$—The upper and lower limits of the confidence interval.
s—The sample standard deviation.
$\bar{x}$—The sample mean.
n—The number of observations.
$t_{n-1}(\alpha)$—The percentile of the t distribution.

3. Results and Discussion

Figure 2 shows the effect of the density of the particleboard, the number of lattices and the density of the geopolymer on the bending strength of the sandwich boards. It was found that particleboard density has the greatest impact on bending strength, whereas geopolymer density did not have a statistically significant effect on composite panel properties. In addition, the influence of the inserted lattices was observed where, in the case of the use of one lattice, the bending strength of the test material increased compared to the variants without lattices. With the increasing number of reinforcement elements in the composite, its bending strength generally increases [12]. However, when two reinforcing lattices were used, the bending strength dropped, surprisingly. This seemingly paradoxical phenomenon can be explained by the anchor of the lattices in the composite. Whereas in the case of one-lattice variants, the lattice is firmly anchored in the middle of the particleboard material, for two-lattice variants these lattices are on the surface and are not fully anchored in the composite material. In the variant with two lattices, the lattice is on the borderline of the particleboard and the geopolymer in the neutral zone during bending, and it therefore does not impact the strength of the material [29]. It can be assumed that this lattice located in the neutral zone would affect the impact strength, i.e., a property that is also important in security doors. While the lattice at the bottom edge of the sandwich composite is exactly in the tensile zone during bending and the used lattice has a tensile strength of 600 MPa, due to insufficient anchoring in the particleboard, it did not have a positive effect on the resulting bending strength of the tested material. The geopolymer reference samples with an OSB showed a bending strength of 0.66 MPa for a lower density geopolymer and 0.65 MPa for a higher density geopolymer. The differences between these averages are within statistical error. The reference samples from commercially sold OSB thus achieved a significantly higher bending strength, but this high strength was caused by the significantly higher density of the OSB (620 kg/m^3) compared to particleboards from rapeseed stalks (340 and 500 kg/m^3) and a smaller dimension of glued particles [32–34].
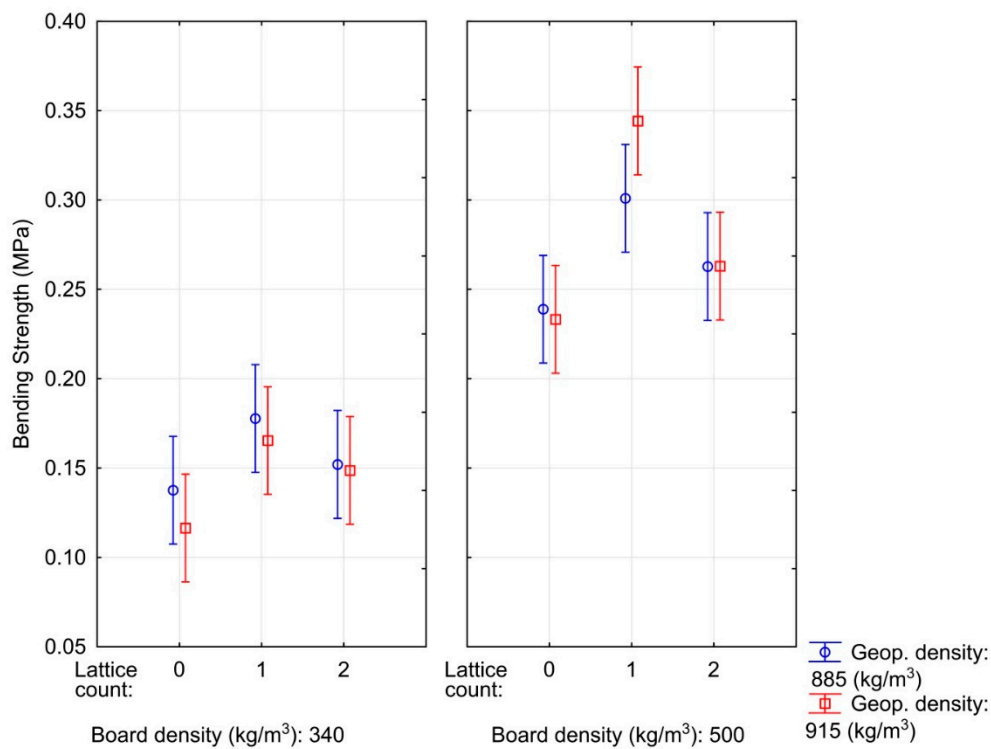
Figure 2. Influence of particleboard density, geopolymer density and the number of lattices on the bending strength of composite materials.

The developed material exhibited high elasticity, the average modulus of elasticity (MOE) values reached 0.14–0.28 MPa (Figure 3). These are considerably lower MOE values compared to the material on the same rapeseed base [16]; however, in the previous research, another adhesive and another press cycle were used, which implied a different vertical density profile of particleboard. Reference samples with an OSB reached a modulus of elasticity of 0.37 MPa for a lower density geopolymer and 0.29 MPa for a higher density geopolymer. A decrease in MOE was observed along with the decreasing particleboard density used in the sandwich panel, which is consistent with theoretical assumptions [35]. Adversely, the influence of geopolymer density was not observed. When using higher rapeseed particleboard densities, it is apparent (however, not statistically significant) that MOE increases with the number of lattices, but it does not increase at a lower particleboard density. This phenomenon may be due to the anchoring of reinforcing lattices in the board, where these lattices are better embedded in a higher density board and are able to transfer a certain load.

A bending coefficient KbendC (Figure 4) was determined for another characteristic of the bending properties of the developed material. The proportion of material thickness to its minimum bending radius was highest for the sandwich panel with a particleboard density of 340 kg/m^3 in combination with two lattices and a layer of geopolymer with a density of 300 kg/m^3. Other differences are not statistically significant at a significance level of 0.05. Compared to wood-based sandwich materials [29,36], the developed material exhibited a lower bending coefficient. However, wood or sandwich material based on lamellae is characterized by high elasticity and a high bending coefficient. The bending coefficient (KbendC) of beechwood is about 0.033 [29]. However, a higher bending coefficient was achieved than in a commercially available wood particleboard (0.01), and values comparable to those of composite material of higher density were obtained, and only from rapeseed particles bonded with epoxy-polyester adhesive [37]. The developed sandwich material thus makes it possible to use boards from rapeseed particles of lower density and bonded with a cheaper, less flexible UF adhesive while maintaining good bending characteristics.
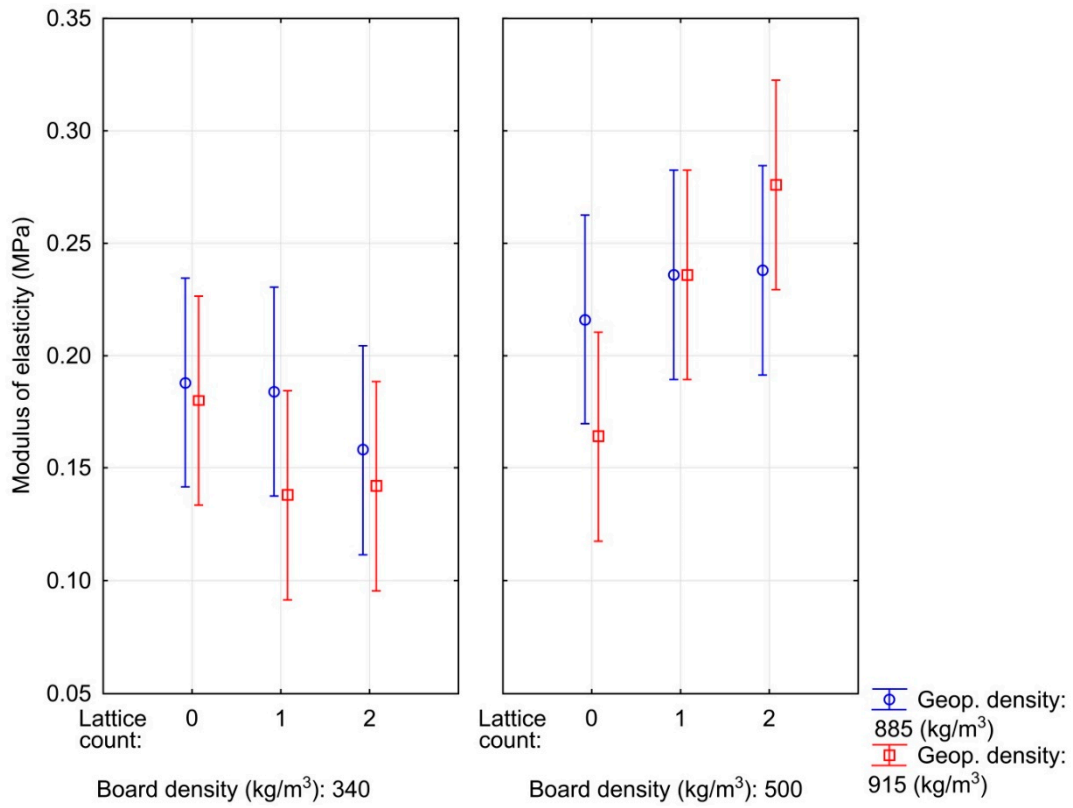
Figure 3. Influence of particleboard density, geopolymer density and the number of lattices on the modulus of elasticity of composite materials.
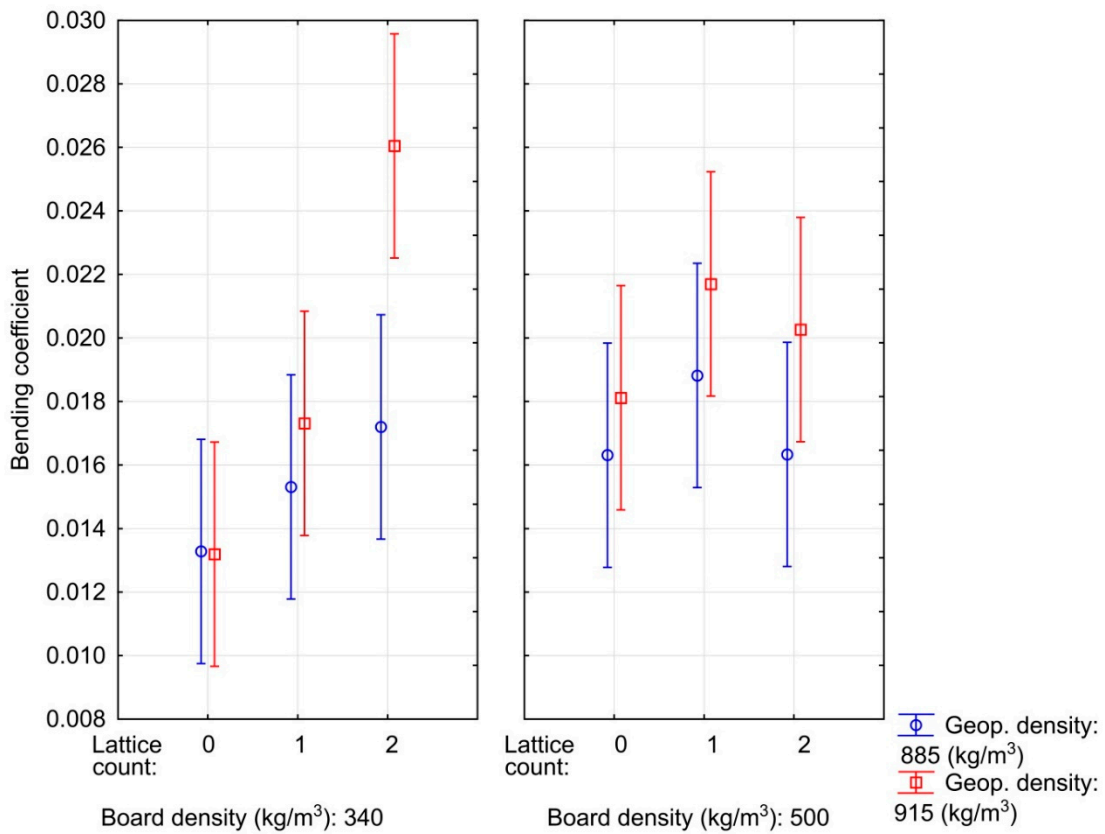
Figure 4. Influence of particleboard density, geopolymer density and the number of lattices on the bending coefficient of composite materials.

Figure 5 captures the effect of the observed factors on the tensile strength perpendicular to the plane of the boards of the developed sandwich panels. There was a clear influence of particleboard density on the internal bonding of the sandwich composite. With an increasing density of particleboard, the internal bonding of composite panel increases according to theoretical assumptions [32]. On the other hand, the effect of using reinforcing lattices and density of geopolymer on internal bonding was not observed. We can positively assess the fact that there was no breach in the joint between the particleboard and the geopolymer. (As there is no breach of the test specimens in the geopolymer material, this factor is not stated in the chart). The material was breached in the middle of the particleboard at the lowest density point. The lowest particleboard density was attained at its centre thanks to the chosen high-speed closing of the press [38].
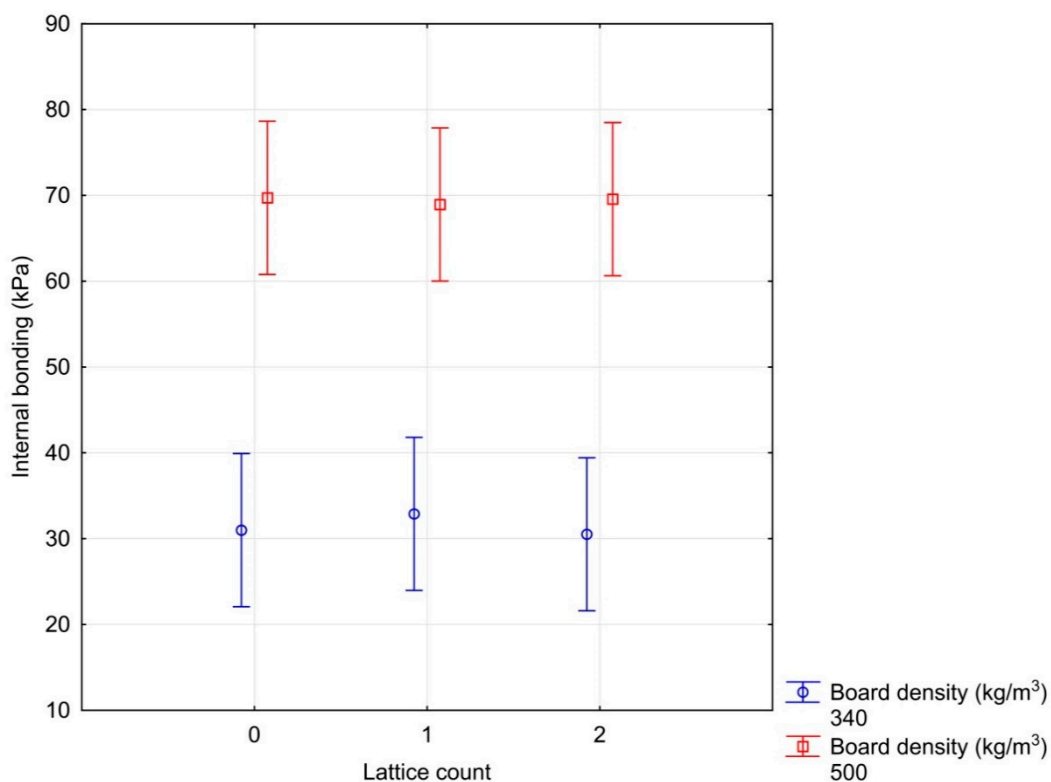
Figure 5. Influence of particleboard density and the number of lattices on the internal bonding of composite materials.

The ascertained values of the thermal conductivity coefficient of manufactured panels and the actual measured values of the density of the individual materials are specified in Table 5. Mild variations in the actual density of the particleboard and the geopolymer from their nominal values were found. The effect of reinforcing lattices on thermal insulation properties and on combustion resistance was not assessed. The thermal conductivity coefficient of the sandwich composite with the lowest density value was 0.111 W/(m·K) and just exceeded the value of 0.1 W/(m·K), which is considered a threshold value for thermal insulating materials. According to theoretical assumptions, the highest values of the thermal conductivity coefficient were obtained [39] for the highest density sandwich composite; nevertheless, the value of 0.214 W/(m·K) can be considered an acceptable thermal conductivity value compared to other load-bearing building materials, such as a wall made from wet pine wood [40]. The good thermal insulation properties of geopolymer foam concretes due to air-cavity content were described earlier, the thermal conductivity coefficient ranged from 0.15–0.48 W/(m·K), which is a better thermal insulation compared to the foamed Portland cement concrete of the same density [21]. Low thermal conductivity (0.15–0.4 W/(m·K)) is also described by [41], who prepared geopolymer foams with Al powder as a foaming agent.
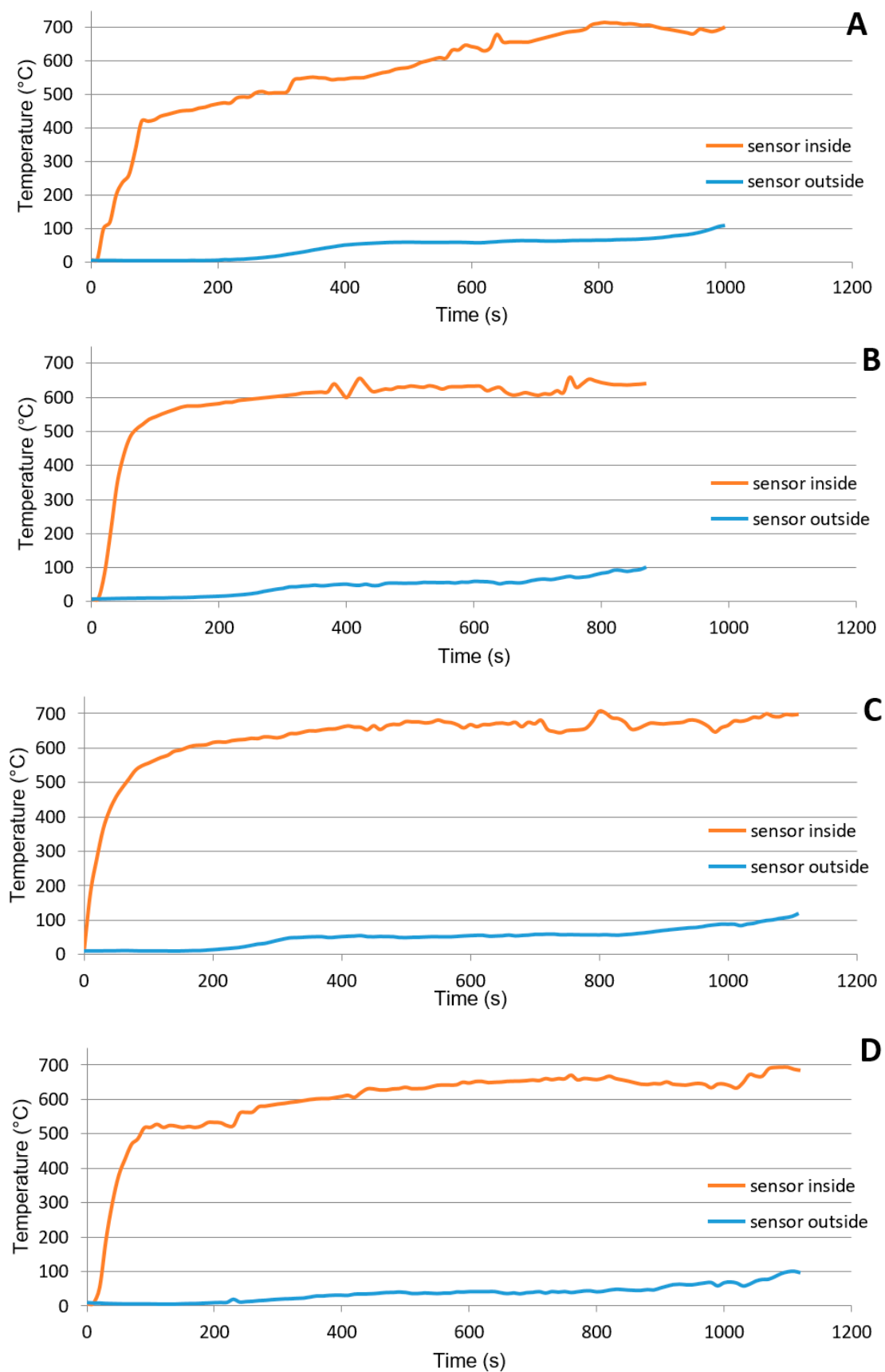
Figure 6. Influence of panel composition on burning characteristics, (**A**) board density 340 kg/m^3, geop. density 885 kg/m^3; (**B**) board density 500 kg/m^3, geop. density 885 kg/m^3; (**C**) board density 340 kg/m^3, geop. density 915 kg/m^3; (**D**) board density 500 kg/m^3, geop. density 915 kg/m^3.

Table 5. Average densities of materials and thermal conductivity of boards.

Sandwich Panel Combination	Board Density (kg/m^3)	Geopolymer Density (kg/m^3)	λ20/65 (W/(m·K))
1	340 (18)	885 (32)	0.111 (0.009)
2	340 (18)	916 (28)	0.113 (0.014)
3	498 (17)	885 (32)	0.134 (0.008)
4	498 (17)	916 (28)	0.214 (0.013)

Values in parentheses are the standard deviations.

Geopolymers can be successfully used to increase the fire resistance of materials [42,43]. Figure 6 captures the burning characteristics of developed panels. The effect of the particleboard and geopolymer density on the fire resistance of the panels was observed. Despite slight variations in temperature rise in the furnace, there was a clear influence of geopolymer density on the resistance time of the panel (the time of reaching the temperature of 100 °C on the outside of the panel). On the contrary, the density of the particleboard layer did not affect its fire resistance as the density of the geopolymer layer. This is the opposite effect of the individual layers, rather than the influence of the individual layers on the mechanical properties where the density of the particleboard is the most important parameter.

4. Conclusions

The submitted paper evaluates the physical and mechanical properties of the developed sandwich composite material based on particles of winter rapeseed stalks, geopolymer and reinforcing lattices. The fundamental influence of particleboard density on the resulting mechanical properties of the entire sandwich panel was demonstrated. The density of the second layer of the sandwich panel and the geopolymer did not have the same impact on its mechanical properties as the particleboard density. The reinforcing lattice made of basalt fibre positively influenced the mechanical properties of sandwich composites only if it was sufficiently anchored in the particleboard structure. The developed materials reached a higher bending strength than 0.3 MPa in only two cases, and the tensile strength perpendicular to the board plane was also low. However, these low values are due to the low density of the material and the low adhesive content. On the contrary, good thermal and fire protection properties were achieved, namely the thermal conductivity coefficient of the sandwich composite with the lowest density value was 0.111 W/(m·K) and all developed sandwich composites resisted flame for more than 13 min.

Author Contributions: Š.H. conceived, designed the experiments, analyzed the data and wrote the paper; M.F. performed the experiments and graphics; M.H. performed the experiments and graphics; P.L. consulted and co-wrote the paper; L.F. consulted and co-wrote the paper; S.L.V. prepared the samples and performed the experiments; H.L.C. prepared the samples and performed the experiments.

Conflicts of Interest: The authors declare no conflict of interest.

References

1. Marcari, G.; Basili, M.; Vestroni, F. Experimental investigation of tuff masonry panels reinforced with surface bonded basalt textile-reinforced mortar. *Compos. Part B* **2017**, *108*, 131–142. [CrossRef]
2. Raj, S.; Kumar, V.R.; Kumar, B.H.B.; Lyer, N.R. Basalt: Structural insight as a construction material. *Sādhanā* **2017**, *42*, 75–84.
3. Sim, J.; Park, C.; Moon, D.J. Characteristics of basalt fiber as a strengthening material for concrete structures. *Compos. Part B Eng.* **2005**, *36*, 504–512. [CrossRef]

4. Behera, P.; Baheti, V.; Militky, J.; Louda, P. Elevated temperature properties of basalt microfibril filled geopolymer composites. *Constr. Build. Mater.* **2018**, *163*, 850–860. [CrossRef]

5. Di Ludovico, M.; Prota, A.; Manfredi, G. Structural upgrade using basalt fibers for concrete confinement. *J. Compos. Constr.* **2010**, *14*, 541–552. [CrossRef]

6. Pernica, D.; Reis, P.N.B.; Ferreira, J.A.M.; Louda, P. Effect of test conditions on the bending strength of a geopolymer-reinforced composite. *J. Mater. Sci.* **2010**, *45*, 744–749. [CrossRef]

7. Nguyen, T.X.; Louda, P.; Kroisova, D.; Kovacic, V.; Chi, H.L.; Vu, N.L. Effects of Commercial Fibers Reinforced on the Mechanical Properties of Geopolymer Mortar. *Chemické Listy* **2012**, *106*, 560–563.

8. Le Chi, H.; Louda, P. Experimental Investigation of Four-Point Flexural Behavior of Textile Reinforcement in Geopolymer Mortar. *Int. J. Eng. Technol.* **2019**, *11*, 10–15. [CrossRef]

9. Zheng, Y.Z.; Wang, W.W.; Brigham, J.C. Flexural behaviour of reinforced concrete beams strengthened with a composite reinforcement layer: BFRP grid and ECC. *Constr. Build. Mater.* **2016**, *115*, 424–437. [CrossRef]

10. Mezrea, P.E.; Yilmaz, I.A.; Ispir, M.; Binbir, E. External Jacketing of Unreinforced Historical Masonry Piers with Open-Grid Basalt-Reinforced Mortar. *J. Compos. Constr.* **2017**, *21*, 4016110. [CrossRef]

11. Ismail, N.; El-Maaddawy, T.; Khattak, N.; Najmal, A. In-Plane Shear Strength Improvement of Hollow Concrete Masonry Panels using a Fabric-Reinforced Cementitious Matrix. *J. Compos. Constr.* **2018**, *22*, 4018004. [CrossRef]

12. Szczypinski, M.M.; Louda, P.; Exnar, P.; Le Chi, H.; Kovačič, V.; Van Su, L.; Voleský, L.; Bayhan, E.; Bakalova, T. Evaluation of mechanical properties of composite geopolymer blocks reinforced with basalt fibres. *Manuf. Technol.* **2018**, *18*, 861–865. [CrossRef]

13. Eurostat. *Agriculture, Forestry and Fishery Statistics*; Publications Office of the European Union: Luxembourg, 2015.

14. Klímek, P.; Wimmer, R. Alternative Raw Materials for Bio-Based Composites. In Proceedings of the International Conference Wood Science and Engineering in the Third Millennium, Brasov, Rumania, 2–4 November 2017.

15. Haq, F.; Ali, H.; Shuaib, M.; Badshah, M.; Hassan, S.W.; Munis, M.F.H.; Chaudhary, H.J. Recent progress in bioethanol production from lignocellulosic materials: A review. *Int. J. Green Energy* **2016**, *13*, 1413–1441. [CrossRef]

16. Hýsek, Š.; Gaff, M.; Sikora, A.; Babiak, M. New composite material based on winter rapeseed and his elasticity properties as a function of selected factors. *Compos. Part B Eng.* **2018**, *153*, 108–116. [CrossRef]

17. Dukarska, D.; Czarnecki, R.; Dziurka, D.; Mirski, R. Construction particleboards made from rapeseed straw glued with hybrid pMDI/PF resin. *Eur. J. Wood Wood Prod.* **2017**, *75*, 175–184. [CrossRef]

18. Gajdačová, P.; Hýsek, Š.; Jarský, V. Utilisation of winter rapeseed in wood based materials as a solution of wood shortage and forest protection. *Bioresources* **2018**, *13*, 2546–2561. [CrossRef]

19. Timakul, P.; Rattanaprasit, W.; Aungkavattana, P. Improving compressive strength of fly ash-based geopolymer composites by basalt fibers addition. *Ceram. Int.* **2016**, *42*, 6288–6295. [CrossRef]

20. Zhang, L.; Zhang, F.; Liu, M.; Hu, X. Novel sustainable geopolymer based syntactic foams: An eco-friendly alternative to polymer based syntactic foams. *Chem. Eng. J.* **2017**, *313*, 74–82. [CrossRef]

21. Zhang, Z.; Provis, J.L.; Reid, A.; Wang, H. Mechanical, thermal insulation, thermal resistance and acoustic absorption properties of geopolymer foam concrete. *Cem. Concr. Compos.* **2015**, *62*, 97–105. [CrossRef]

22. Toniolo, N.; Boccaccini, A.R. Fly ash-based geopolymers containing added silicate waste. A review. *Ceram. Int.* **2017**, *43*, 14545–14551. [CrossRef]

23. Velenturf, A.P.M.; Purnell, P.; Tregent, M.; Ferguson, J.; Holmes, A. Co-Producing a Vision and Approach for the Transition towards a Circular Economy: Perspectives from Government Partners. *Sustainability* **2018**, *10*, 1401. [CrossRef]

24. Kidalova, L.; Stevulova, N.; Terpakova, E.; Sicakova, A. Utilization of alternative materials in lightweight composites. *J. Clean. Prod.* **2012**, *34*, 116–119. [CrossRef]

25. Hýsek, Š.; Podlena, M.; Bartsch, H.; Wenderdel, C.; Böhm, M. Effect of wheat husk surface pre-treatment on the properties of husk-based composite materials. *Ind. Crops Prod.* **2018**, *125*, 105–113. [CrossRef]

26. *EN 323:1993—Wood-Based Panels. Determination of Density*; Eur. Comm. for Stand.: Brussels, Belgium, 1993.

27. *EN 319:1993—Particleboards and Fibreboards. Determination of Tensile Strength Perpendicular to the Plane of the Board*; Eur. Comm. for Stand.: Brussels, Belgium, 1993.

28. *EN 798:2004—Timber Structures—Test Methods—Determination of Mechanical Properties of Wood Based Panels*; Eur. Comm. for Stand.: Brussels, Belgium, 2004.

29. Gaff, M.; Vokatý, V.; Babiak, M.; Bal, B. Coefficient of wood bendability as a function of selected factors. *Constr. Build. Mater.* **2016**, *126*, 632–640. [CrossRef]

30. Neuberger, P.; Kic, P. The use of unsteady method for determination of thermal conductivity of porous construction materials in real conditions. *Agron. Res.* **2017**, *15*, 1119–1126.

31. *EN 1363-2:1999—Fire Resistance Tests. Alternative and Additional Procedures*; Eur. Comm. for Stand.: Brussels, Belgium, 1999.

32. Wong, E.D.; Zhang, M.; Wang, Q.; Kawai, S. Formation of the density profile and its effects on the properties of particleboard. *Wood Sci. Technol.* **1999**, *33*, 327–340. [CrossRef]

33. Hegazy, S.; Ahmed, K. Effect of Date Palm Cultivar, Particle Size, Panel Density and Hot Water Extraction on Particleboards Manufactured from Date Palm Fronds. *Agricult* **2015**, *5*, 267–285. [CrossRef]

34. Nguyen, D.M.; Grillet, A.C.; Diep, T.M.H.; Thuc, C.N.H.; Woloszyn, M. Hygrothermal properties of bio-insulation building materials based on bamboo fibers and bio-glues. *Constr. Build. Mater.* **2017**, *155*, 852–866. [CrossRef]

35. Wong, E.D.; Yang, P.; Zhang, M.; Wang, Q.; Nakao, T.; Li, K.F.; Kawai, S. Analysis of the effects of density profile on the bending properties of particleboard using finite element method (FEM). *Holz als Roh- und Werkstoff* **2003**, *61*, 66–72. [CrossRef]

36. Gaff, M.; Gašparík, M.; Borůvka, V.; Haviarová, E. Stress simulation in layered wood-based materials under mechanical loading. *Mater. Des.* **2015**, *87*, 1065–1071. [CrossRef]

37. Gaff, M.; Hýsek, Š.; Sikora, A.; Babiak, M. Newly developed boards made from crushed rapeseed stalk and their bendability properties. *BioResources* **2018**, *13*, 4776–4794.

38. Wong, E.D.; Zhang, M.; Wang, Q.; Kawai, S. Effects of mat moisture content and press closing speed on the formation of density profile and properties of particleboard. *J. Wood Sci.* **1998**, *44*, 287–295. [CrossRef]

39. Asdrubali, F.; D'Alessandro, F.; Schiavoni, S. A review of unconventional sustainable building insulation materials. *Sustain. Mater. Technol.* **2015**, *4*, 1–17. [CrossRef]

40. Raji, S.; Jannot, Y.; Lagière, P.; Puiggali, J.R. Thermophysical characterization of a 377 laminated solid-wood pine wall. *Constr. Build. Mater.* **2009**, *23*, 3189–3195. [CrossRef]

41. Kamseu, E.; Nait-Ali, B.; Bignozzi, M.C.; Leonelli, C.; Rossignol, S.; Smith, D.S. Bulk composition and microstructure dependence of effective thermal conductivity of porous inorganic polymer cements. *J. Eur. Ceram. Soc.* **2012**, *32*, 1593–1603. [CrossRef]

42. Vickers, L.; Pan, Z.; Tao, Z.; van Riessen, A. In Situ Elevated Temperature Testing of Fly Ash Based Geopolymer Composites. *Materials* **2016**, *9*, 445. [CrossRef] [PubMed]

43. Sakkas, K.; Sofianos, A.; Nomikos, P.; Panias, D. Behaviour of Passive Fire Protection K-Geopolymer under Successive Severe Fire Incidents. *Materials* **2015**, *8*, 6096–6104. [CrossRef]

Water Absorption Properties of Geopolymer Foam after Being Impregnated with Hydrophobic Agents

Hiep Le Chi [1,*] , **Pavlína Hájková** [1,2] , **Su Le Van** [1] , **Petr Louda** [1] and **Lukáš Voleský** [1]

1   Department of Material Science, Faculty of Mechanical Engineering, Technical University of Liberec, Studenstká 2, 461 17 Liberec, Czech Republic; pavlina.hajkova@unicre.cz (P.H.); longsuvp90@gmail.com (S.L.V.); petr.louda@tul.cz (P.L.); lukas.volesky@tul.cz (L.V.)
2   Unipetrol Centre for Research and Education, Revoluční 84, 400 01 Ústí nad Labem, Czech Republic
*   Correspondence: lechihieptul09@gmail.com

Abstract: Geopolymer foam is classified as a lightweight material with high porous in its matrix which has great offer for applications requiring fire-resistant, thermal, and acoustic properties. However, the high sensitivity to humid environments can be a major barrier of geopolymer foam that limits the variety of applications of this material. Based on this drawback, two types of hydrophobic agent (Lukosil M130 and Lukofob ELX) were used as an impregnator to treat the surface of geopolymer foam samples. This paper presented the results of water absorption properties of the untreated and treated geopolymer foam composites. The obtained properties were flexural strength, compressive strength, density, total water absorption, the rate of water absorption, and water absorption coefficient. The results showed that the samples after being impregnated with hydrophobic agents improved significantly their waterproof property especially using Lukosil M130. Moreover, the samples treated with Lukosil M130 had positive impact on their mechanical strength.

Keywords: geopolymer foam; Lukosil M130; Lukofob ELX; water absorption; water uptake; water absorption coefficient; flexural strength; compressive strength

1. Introduction

The term "geopolymer" introduced by Davidovits in the 1970s [1] is the inorganic aluminosilicate polymers which is produced by a combination of rich source materials in silica and alumina such as metakaolin, fly-ash, blast furnace slag, etc., with strongly alkali activators [2–6]. When considering a proper mixing ratio of raw materials, type and concentration of alkaline activator geopolymers can exhibit a wide variety of desired properties and characteristic such as high compressive strength, low shrinkage, high temperature resistance, acid resistance, and fire resistance up to 1200 °C, etc., [7–13]. In recent years, this type of material has become an attractive topic in research for the reason that geopolymer concrete offers great potential for alternative to Portland cement-based concrete because of the issue of CO_2 emission in production of the Portland cement causing the environment pollution [14,15].

Among many products that are established on geopolymer binders, geopolymer foam belongs to the class of lightweight materials with high porous in its structure which has great use in some areas of the construction requiring fire-resistant, thermal, and acoustic insulation properties [16–23]. It is well-known that geopolymer foam is formed from solid geopolymers with addition of foam agents such as metals (silica, alumina, zinc powders), H_2O_2, etc., thus pure geopolymer foam is very sensitive to brittle fracture because of the large number of void spaces in structure. The addition of various types of the fillers including particles and fibers will help to improve significantly the mechanical properties of geopolymer foams [19]. However, the existence of fillers especially fiber reinforcements in matrix

has a strong influence on the long-term durability of the composite when considering the weathering aspect. The structural performance of geopolymer foam makes it very sensitive to humidity because of easy water ingress through the highly porous structure. The water carrying aggressive agents in the environment, such as H_2O, O_2, CO_2, Cl^-, SO_4, cause reinforcement corrosion leading to the deterioration of the structures, such that its service-life is reduced.

Microstructure of geopolymers defines the possibility for water ingress in the material, and therefore microstructure is a key criterion in geopolymer long-term durability. The high sensitivity to humid environments can be considered as a major barrier of geopolymer foams that limits the variety of applications of this material. Therefore, the surface treatment of these composites should be adapted to increase their service life. There are three basic approaches used in applying surface protection to concrete [24]: (i) Hydrophobic impregnation is to produce a water-repellent surface, and the pores and capillaries are internally coated, but they are not filled; (ii) impregnation is to reduce the surface porosity by filling partially or totally the concrete pores; (iii) coating is to produce a continuous protective layer on the concrete surface. Some hydrophobic agents can ingress deep into the inner structure and fill a large number of matrix pores resulting in reduction of surface porosity and improvement of mechanical strength of the treated concrete. The others produce a pore lining effect or form a protective layer at the concrete surface, which acts as a barrier to prevent and/or delay the water penetration.

In the previously reported findings, many researches have been performed on the techniques, various raw materials, foam agents, etc., to achieve improved physical-mechanical properties of geopolymer foam such as fire resistant, thermal, and acoustic properties. In this work, the surface impregnation treatment will be carried out in order to evaluate the water absorption properties of the geopolymer composites. Two types of hydrophobic agents based on siloxane was used, and geopolymer foam is a composite material which was produced by a combination of geopolymer paste and the fillers such as quartz sand, silica fume, chopped basalt fiber, and foam agent.

2. Materials and Methods

2.1. Raw Materials

Geopolymer Baucis L_k, supplied by Ceske Lupkove Zavody, a.s Czech Republic, was used as the aluminosilicate source for producing geopolymer paste (in weight percent: SiO_2—47.4; Al_2O_3—29.7; CaO—14.5; MgO—2.6; TiO_2—1.8; Fe_2O_3—0.5; K_2O—0.3; Na_2O—1) along with potassium silicate activator of modul 1.71 (in weight percent: SiO_2—19.56; K_2O—17.87; H_2O—62.57). In order to prepare geopolymer paste, the mixing ratio of two components (solid, liquid) was taken out according to the requirement of the manufacturer.

Quartz sand with brand name ST 03/08, supplied by Sklopisek Strelec a. s. Czech, was used as the fine aggregates for the geopolymer mortar matrix (grain size: 0.315–0.80 mm). Powder additive (microsilica) based on amorphous SiO_2 for concrete and mortar was purchased from Kema Mikrosilika–Sanační centrum s.r.o., Sviadnov Czech Republic. The chemical composition of microsilica as follows (wt. %): SiO_2—90, CaO—0.8, MgO—max. 1.5, Al_2O_3—max. 1, Na_2O—0.5. This additive was added into geopolymer mortar to enhance both the workability of the fresh mortar and mechanical strength of the hardened mortar. The chopped basalt fiber (BF) was provided by Kamenny Vek, and the tows were about 6.4 mm long with the individual fiber diameters of 13 μm, the density of 2.67 g/cm^3, tensile strength in the range of 2700–3200 MPa, and tensile modulus of 85–95 GPa. An aluminum powder, supplied by Pkchemie Inc., Czech Republic, was used to make geopolymer foam.

Two different types of the hydrophobic agents with the commercial names Lukosil M130 and Lukofob ELX, provided by Lucebni zavody Kolin a.s., Czech Republic, were used as impregnator for the geopolymer foam samples. Lukosil M130 product is a transparent solution of methyl-silicon resin in xylene, in which the presence of methyl group in the polysiloxane chain makes it hydrophobic with density of 1000–1020 kg/m^3, viscosity of 30–40 mPa.s/20 °C, heat resistance of max. 230 °C. Its thermal

curing enhances hardness and marked improvement in mechanically and mainly chemically resistant film. After drying, it forms a thin, non-stick, heat and weather-resistant film. Lukofob ELX product is a milk-white aqueous emulsion of methyl-silicone resin designed for the final surface waterproof impregnation of porous or less porous silicate materials, which has density of 1000–1010 kg/m^3, viscosity of 60–80 mPa.s/20 °C [25,26].

2.2. Preparation of Geopolymer Foam Composite

The raw materials and mixing ratio for producing geopolymer foam composite are shown in Table 1. Geopolymer mortar was prepared as the following steps. First, geopolymer cement and activator with a given ratio were mechanically stirred for about 3 min to gain homogenous geopolymer paste. Second, silica fume was added to the slurry and mixture was stirred for about 2 min more. Next, rough quartz sand along with chopped basalt fiber was added to prepared mixture followed by mixing for a few minutes until ensuring a homogenous mortar. Finally, Al powder was added into prepared mixture and stirred for about 1 min to create pores inside the geopolymer composite. It should be said that the mixing ratio used in Table 1 was optimized in our lab. The freshly prepared mortar was poured immediately into the molds with a dimension of $40 \times 40 \times 160$ mm^3. After casting, all the specimens were wrapped using a polypropylene film, and cured at room temperature, ~22 °C, with 45% relative humidity for 24 h. Afterward, the specimens were demolded, and wrapped again using a polypropylene film, and kept at room temperature until 7 days. Finally, the specimens were unwrapped and put into the drying oven at the temperature of 70 °C until an unchanged weight is reached so that they can be used to impregnate with silicone solutions.

Table 1. Mixture of geopolymer foam composite.

By wt.% of Geopolymer Cement			By Weight Ratio (-)		
BF content	Silica fume	Al powder	Geopolymer cement	Activator	Silica sand
15	5	1.5	1	0.9	1

2.3. Impregnation Process of the Samples with Silicone Solutions

Before performing this step, all the specimens were carefully weighed. Because of the large porous size of the geopolymer foam, the impregnation approach (wet out) was selected to easily apply the silicone solutions to all surfaces of the geopolymer foam specimens. The specimens prepared in the previous step were placed in a clean bath followed by pouring the silicone solution into the bath until the specimens are immersed in solution to a depth of 20 mm. It should be noted that during immersion the bottom surface of the samples was changed to ensure that the solution is uniformly absorbed into the matrix at all surfaces. They were left for about 30 min to ensure the visible pores in matrix are completely drenched with the solution. The specimens are then removed and drained for about two hours before being placed in the drying oven at the temperature of 70 °C for 48 h. All specimens are removed out of the oven after 48 h and weighed again. The final sample of the impregnation process can be clearly seen in Figure 1. It was found that it consumed about 45.92 g of Lukosil M130 to impregnate each specimen, whereas for Lukofob ELX is about 22.38 g, and this consumed value is calculated only after the impregnated specimens were dried in the oven.
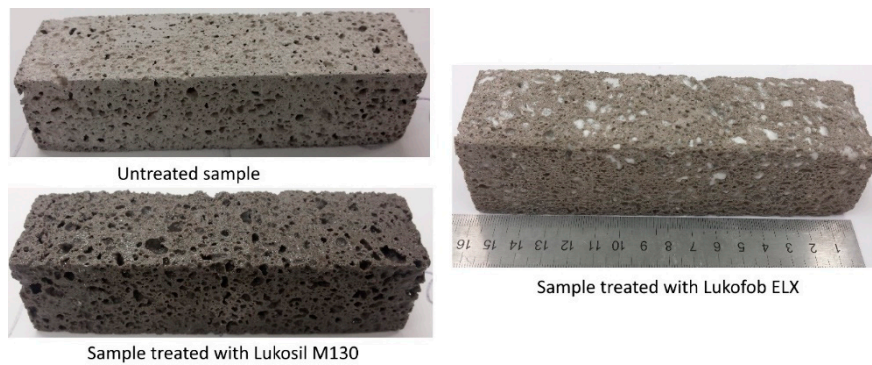
Figure 1. Photographs of the samples without and with impregnation of the silicone solutions.

2.4. Geopolymer Foam Composite Estimation

The water absorption test of the specimens was performed to know the total water absorption capacity of untreated and treated geopolymer foam. It was determined in accordance with ČSN EN 13755 standard. The samples after being dried to constant mass in the early step were placed in a container of boiled water (to remove dissolve gases) at a room temperature of ~22 °C with a level reaching half the height. Water is gradually added after 1 h to $\frac{3}{4}$ of the height, after 2 h to complete immersion to a depth of 25 ± 5 mm. The samples are removed from the water after 48 h, wiped with a damp cloth, and weigh quickly. The test was measured for five samples and an average value of measurements was taken. The total water absorption is calculated as per the Equation (1):

$$A = \frac{m_w - m_d}{m_d} \times 100 \ (\%) \tag{1}$$

where A is total water absorption (%), m_d is mass of oven-dried sample in air in gram, m_w is mass of the sample saturated with water in gram.

The determination of the water absorption coefficient by capillary action is performed according to ČSN EN 1925. The samples with a dimension of $40 \times 40 \times 40 \ mm^3$ that were cut from $40 \times 40 \times 160 \ mm^3$ samples were weighed and the area of the submerged base is calculated and expressed in square meters. The sample is placed on thin pads in a closed container so that only a part of the base rests on them. The base was immersed in water to a depth of 3 mm and the water level during test was kept constant. The amount of absorbed water is found out through the weight of the sample in a period of time throughout the contact with water. The mass of water soaked in grams divided by the area of the immersed base of the sample in square meters as a function of the square root of time expressed in seconds is expressed by the graph. The water absorption coefficient was defined as equivalent to the slope of the linear regression line of the first part of the graph.

The flexural strength and compressive strength tests were applied to evaluate the mechanical properties of the geopolymer foam specimens, in which the test method is conducted according to EN 196-1 [27]. The testing machine with load cell capacity of 100 kN (FP Lab Test II, from LABORTECH s.r.o. Opava, Czech Republic), located at the Technical University of Liberec Laboratory, with the applied load under displacement control at a loading rate of 4 mm/min, was used. The mechanical strength of the specimens was tested as the following procedure: (i) The samples with label D-sample mean that they were dried at 70 °C in oven to constant mass in order to perform water absorption tests, as mentioned early; (ii) the samples with label D-W-sample mean that the number of the samples were selected in step 1 and then soaked in water for 48 h; (iii) the samples with label D-W-D-sample mean that the number of the samples were selected in step 2, then they were again dried in oven at 70 °C to constant mass. In other words, the samples that were impregnated by Lukosil M130 are named the LS-sample while those were impregnated by Lukofob ELX are named the LF-sample. Five samples for each recipe was tested and an average value of measurements was taken.

3. Results and Discussion

Figure 2 shows the influence of the impregnators on bulk density of the geopolymer foam composite samples. The bulk density value of the reference sample was 758.2 kg/m^3 which increased by 23.66% and 14.99% when the specimens were impregnated by Lukosil M130 and Lukofob ELX solutions, respectively. The higher value of bulk density in LS-sample can be explained by the fact that Lukosil M130 has significantly lower viscosity compared to Lukofob ELX, which can be attributed to better penetration into geopolymer matrix leading to greater bulk density. Moreover, Lukosil M130 uses xylene liquid as a solvent, which attributed to the superior dissolving of methyl-silicone component in solution resulting in better ingress into the matrix pores. On the other way Lukofob ELX uses water as a solvent which results in largecluster size of methyl-silicone resin because of its insolubility in water leading to poor ingress into the matrix pores.
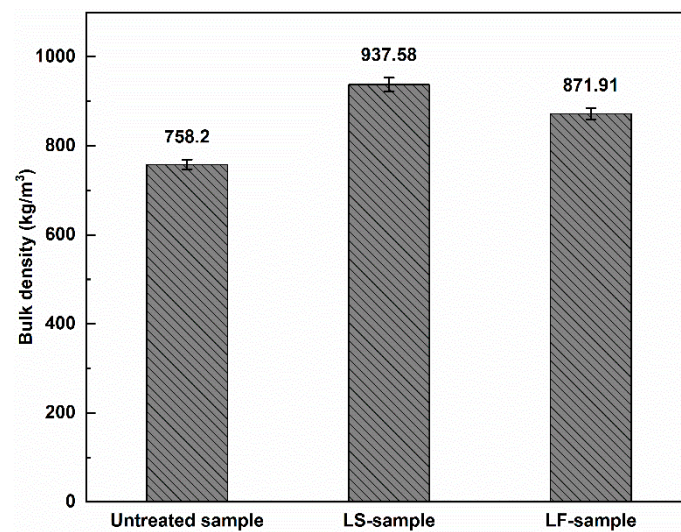
Figure 2. Bulk density value of the geopolymer foam composites.

Figure 3 shows the flexural strength and compressive strength of the geopolymer foam composite samples. It can be observed that when all samples were saturated in water after 48 h of immersion, they did not show a significant reduction in mechanical strength compared to dry samples. The average mechanical strength of the untreated samples is 2.52 MPa in flexural and 5.92 MPa in compressive strength. The average mechanical strength of the LS-samples and LF-samples increases by 61.51% (4.07 MPa), 28.55% (3.23 MPa) in flexural and 28.17% (7.61 MPa), −1.85% (5.81 MPa) in compressive strength, respectively, compared to untreated samples. It showed that the LS-samples show a marked improvement in their mechanical strength, while the LF-samples have the enhanced flexural strength value, compared to the untreated those. The improved mechanical strength of the LS-samples can be explained by the fact that the greater precipitation of the methyl silicone components in the matrix acts as a reinforcing agent, contributing to enhanced mechanical strength. Moreover, the LS-samples showed an increase in mechanical strength again when they were oven-re-dried after immersion in water. This finding can be said that it seems that the initial oven-dry mode at 70 °C for 48 h of the LS-samples after impregnation is not effective enough for Lukosil M130 to fully utilize its effects, as a result of the maximum unsatisfactory mechanical strength of those samples. The effect of Lukosil M130 on the marked improvement in mechanical properties of the substrates is clearly mentioned by the manufacturer if they are reasonably cured at high temperatures [24].

Figure 4 shows the total water absorption capacity of the geopolymer foam composite samples after 48 h of immersion in water. It is notable that the water-resistant performance of treated geopolymer foam was improved significantly, especially those treated with Lukosil M130. The total water absorption

of untreated samples is 47.41%, which significantly decreased by 25.14% and 81.90% when the samples were treated with Lukofob ELX and Lukosil M130, respectively.
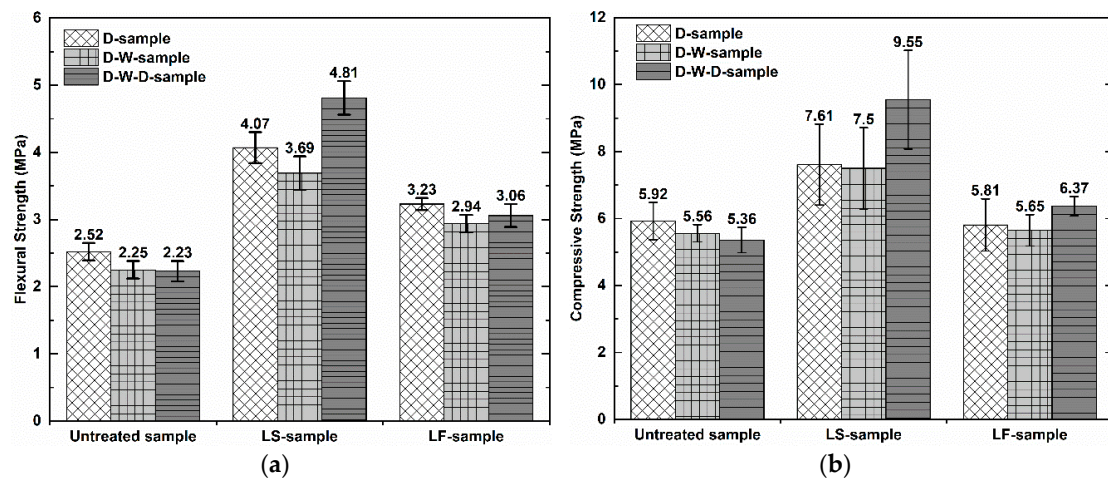
Figure 3. Mechanical properties of the geopolymer foam composites: (**a**) flexural strength; (**b**) compressive strength.

The loss rate of absorbed water of the samples under oven-drying is shown in Figure 5. It is found that the amount of absorbed water is released from the samples very quickly during the first 2 h of the oven-drying process, and the geopolymer foam samples almost achieve constant weight after 5 h of oven-dried, except for the LF-samples. The residual percentage of water after this duration was 1.2%, 2.2%, and 13.04%, respectively for the untreated samples, LS-samples, and LF-samples. This is attributed to the penetration of hydrophobic agent of Lukofob ELX caused by its material characteristics. Lukofob ELX is an aqueous emulsion with high viscosity, which limits good penetration into pore spaces and deep transportation into matrix. Moreover, the pores at the surface layer of the samples are sealed partially (see in Figure 1). Thus, a barrier in the surface layer is formed which hinders the water penetration and migration. As a result, it takes longer time for water to escape from the material. In the contrast, because of the complete dissolving of methyl silicone in xylene solvent, the hydrophobic agent of Lukosil M130 is transported deeper into the matrix and fills in a greater number of matrix pores as well, as a result of better elimination of water absorption capacity. This result is consistent with the results of the bulk density and mechanical strength performance of the LS-samples and LF-samples.
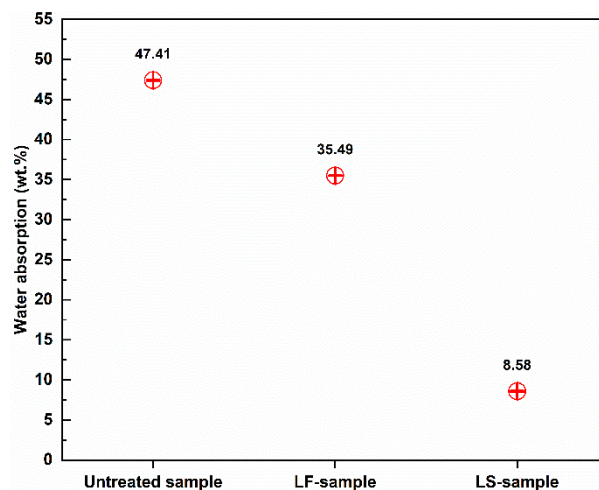
Figure 4. Total water absorption of the geopolymer foam composites.
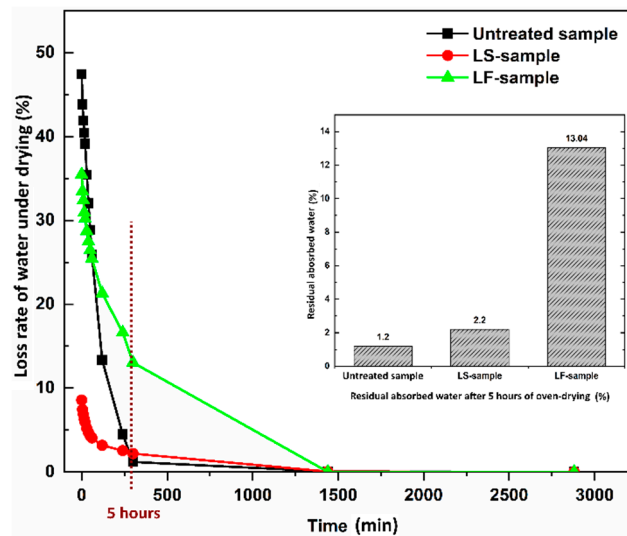
Figure 5. The rate of water loss during the oven-dried process of the geopolymer foam composite.

Figure 6 shows the results of capillary water uptake curves with different service duration, whereas the water uptake rate at the initial period is indicated in Figure 7, and the results of the water uptake coefficient of geopolymer foam composite are listed in Table 2. It can be observed that there is a large reduction in capillary water uptake of samples treated with two types of hydrophobic agents, despite high open porosity in geopolymer foam. The untreated samples quickly absorbed a large amount of water during test, and the high rate of capillary water uptake happened in the initial period and this degree was gradually decreased over time. For the LF-samples the low rate of capillary water uptake occurred in the initial period but then increased in the intermediate period and finally a reduction of the water uptake rate exhibited for further periods. This phenomenon is consistent with the above explanation regarding the slow loss rate of water under oven-dried process. The initial capillary uptake is controlled by the surface layer of the sample which acts as a barrier that hinders water penetration. However, once the water gets over this obstacle, an observed rapid increase of capillary suction because of water requirement of the inner pores can be seen in the intermediate period of 30 min to 2 h. Eventually a subsequent decrease of the capillary suction indicated for the longer periods because of higher water content in the interior of the sample and the slow progressive participation of the less accessible pores [28]. The rate of capillary water uptake of the LS-samples is lower in the initial period compared to the LF-samples and tends to reach saturation after 6 days of test. The water absorption coefficient is defined as equivalent to the slope of linear regression line of the initial period of the graph which is selected from 0.5 min to 10 min (Figure 7). However, because of the higher capillary suction in the intermediate period, the authors think that the water absorption coefficient of the LF-sample should be mentioned over the period of time that ranges from 30 min to 2 h (Figure 8). The water absorption coefficient of the untreated samples is 90.39, which decreased significantly by 97.49% when the samples are treated by Lukosil M130 (Table 2). On the other hand, it decreased marked by 95.31% and 92.84% when the LF-sample considered in the initial and intermediate period, respectively (Table 2). It is observed that capillary water uptake test revealed better waterproofing ability of the LF-samples compared to test method of total water absorption, in which the samples were immersed in water up to full saturation.
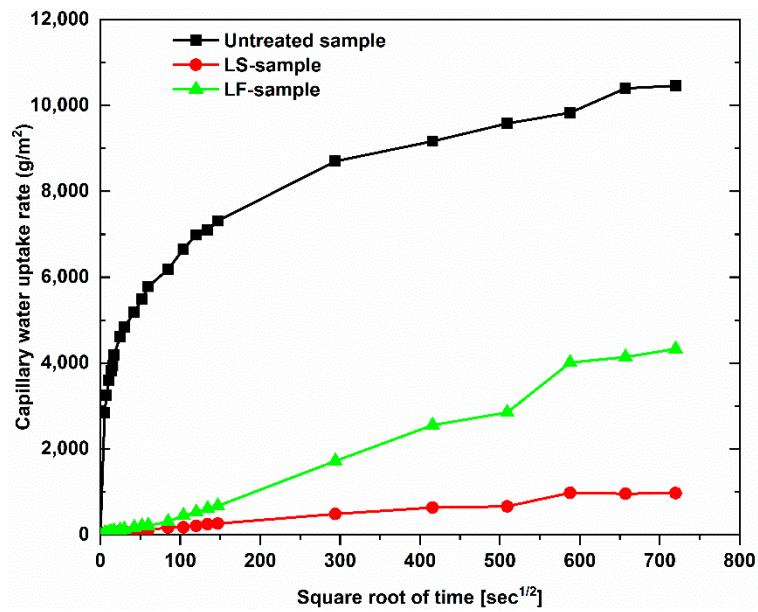
Figure 6. Capillary water uptake for geopolymer foam composite with different service duration.

(**a**)　　　　　　　　　　　　　　　　　　　　(**b**)
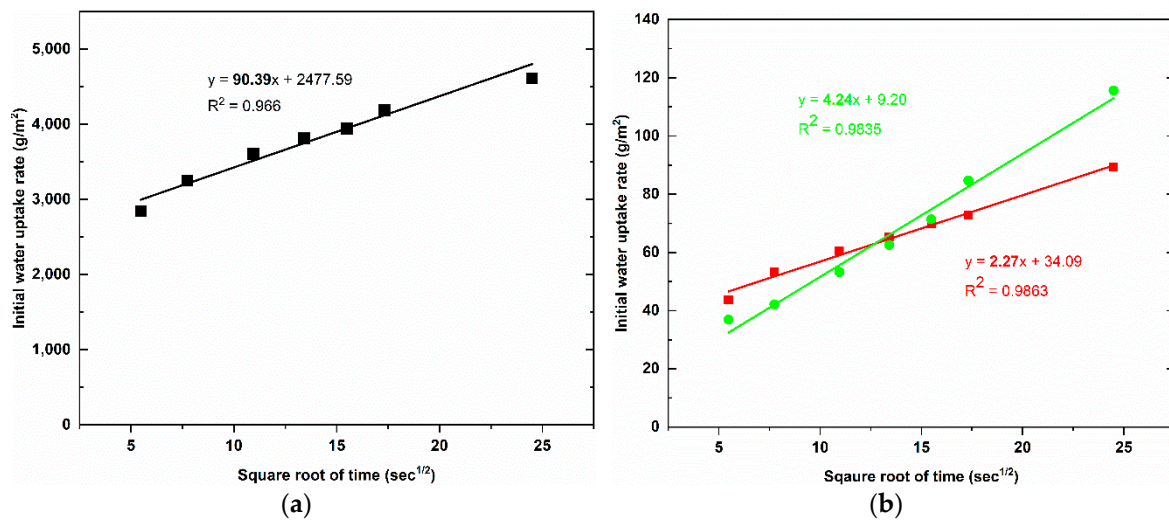
Figure 7. Water uptake rate of the geopolymer foam samples at the first period of 0.5 min to 10 min: (**a**) the untreated samples; (**b**) the LS-sample (red line) and the LF-sample (green line).

Table 2. Water absorption coefficient of geopolymer foam composites.

No. Sample	Water Absorption Coefficient ($g/m^2/s^{0.5}$)	Correlation Coefficient (R^2)
Untreated sample	90.39	0.97
LF-sample	(Initial) 4.24	0.98
	(Intermediate) 6.47	0.99
LS-sample	2.27	0.99
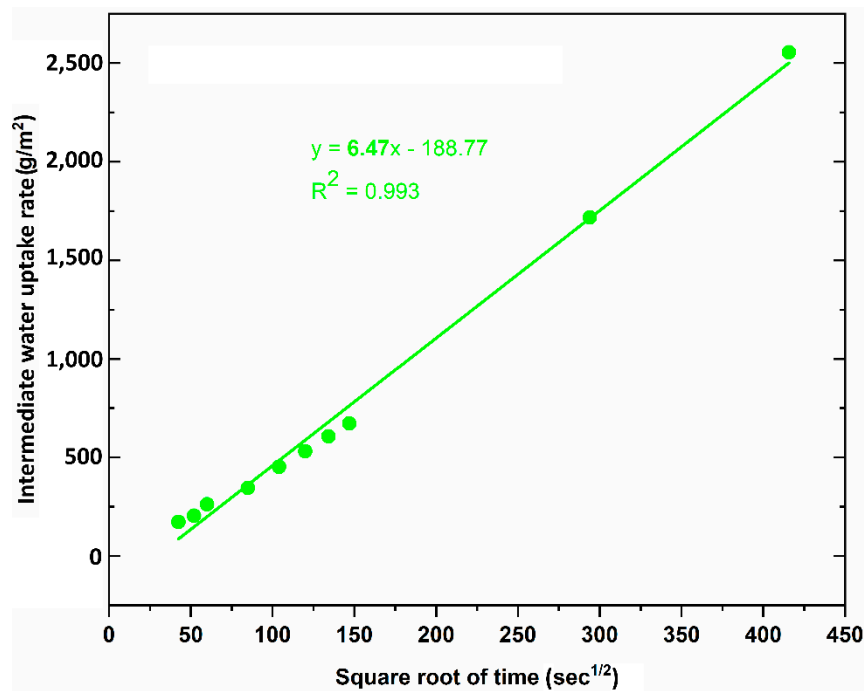
Figure 8. Water uptake rate at the intermediate period of 30 min to 2 h of the LF-sample.

4. Conclusions

In the present research, the geopolymer foams were treated with two types of hydrophobic agent at the age of 7 days after casting and their physical-mechanical properties such as flexural strength, compressive strength, bulk density, water absorption capacity, and water absorption coefficient were analyzed. Based on the experimental results achieved, the following conclusions are outlined: The higher bulk density of the LS-sample revealed that the hydrophobic agent of Lukosil M130 filled in the greater number of pores in the matrix leading to better physical-mechanical properties of the geopolymer foam composite compared to that of Lukofob ELX. Moreover, using Lukosil M130 for impregnating samples also helps significantly in the improvement of mechanical strength of geopolymer foams if they are reasonably cured at high temperatures.

The LF-samples indicate that their total water absorption capacity is much higher than that of LS-sample. The LS-samples with water absorption capacity of 8.58% decreased significantly by 81.90%, while the LF-samples with this value of 35.49% decreased by 25.14%, compared to untreated samples with value of 47.41%. However, under capillary water uptake test, the water absorption coefficient of the LF-samples was quite good compared to that of the LS-samples. The untreated sample obtained water absorption coefficient with 90.39 while this value was 6.47 and 2.27 for LF-sample, LS sample, respectively.

Lukosil M130 has proved that it is an excellent hydrophobic agent for geopolymer foam as it is applied by the impregnation method. The authors recommend that further work is required to find out the optimal oven-dried regime (temperature and time) of the LS-sample which influences significantly on their mechanical strength. Moreover, the preliminary results obtained in this work were tested at the early-age impregnated samples. Therefore, the long-term performance of waterproof property of geopolymer foam treated with Lukosil M130 and Lukofob ELX should be considered. On the other hand, Lukofob ELX is considered as a hydrophobic agent with high environmental friendliness.

Author Contributions: H.L.C. designed the experiments, analyzed the data, and wrote the paper; P.H. conceived, designed the experiments, consulted, and co-wrote the paper; S.L.V. prepared and performed the experiments; L.V. designed the experiments; P.L. supervision.

References

1. Davidovits, J. Geopolymers: Ceramic-like inorganic polymers. *J. Ceram. Sci. Technol.* **2017**, *8*, 335–350.
2. Da Silva Rocha, T.; Dias, D.P.; França, F.C.C.; de Salles Guerra, R.R.; de Oliveira, L.R.D.C. Metakaolin-based geopolymer mortars with different alkaline activators. *Constr. Build. Mater.* **2018**, *178*, 453–461. [CrossRef]
3. Hemalatha, T.; Mapa, M.; George, N.; Sasmal, S. Physico-chemical and mechanical characterization of high volume fly ash incorporated and engineered cement system towards developing greener cement. *J. Clean. Prod.* **2016**, *125*, 268–281. [CrossRef]
4. Yu, X.; Chen, L.; Komarneni, S.; Hui, C. Fly ash-based geopolymer: Clean production, properties and applications. *J. Clean. Prod.* **2016**, *125*, 253–267.
5. Barbosa, V.F.F.; MacKenzie, K.J.D.; Thaumaturgo, C. Synthesis and characterisation of materials based on inorganic polymers of alumina and silica: Sodium polysialate polymers. *Int. J. Inorg. Mater.* **2000**, *2*, 309–317. [CrossRef]
6. Duxson, P.; Provis, J.L.; Lukey, G.C.; Mallicoat, S.W.; Kriven, W.M.; van Deventer, J.S.J. Understanding the relationship between geopolymer composition, microstructure and mechanical properties. *Colloids Surf. A Physicochem. Eng. Asp.* **2005**, *269*, 47–58. [CrossRef]
7. Duan, P.; Yan, C.; Zhou, W. Compressive strength and microstructure of fly ash based geopolymer blended with silica fume under thermal cycle. *Cem. Concr. Compos.* **2017**, *78*, 108–119. [CrossRef]
8. Allahverdi, A.L.I. Sulfuric Acid Attack on Hardened Paste of Geopolymer Cements Part 2. Corrosion Mechanism At Mild and Relatively Low Concentrations. *Ceram. Silik.* **2005**, *4*, 3–6.
9. Allahverdi, A.; Škvára, F. Sulfuric acid attack on hardened paste of geopolymer cements Part 2. Corrosion mechanism at mild and relatively low concentrations. *Ceram. Silik.* **2006**, *50*, 1–4.
10. Ramujee, K.; Potharaju, M. Abrasion Resistance of Geopolymer Composites. *Procedia Mater. Sci.* **2014**, *6*, 1961–1966. [CrossRef]
11. Degirmenci, F.N. Freeze-Thaw and Fire Resistance of Geopolymer Mortar Based on Natural and Waste Pozzolans. *Ceram. Silik.* **2017**, *62*, 1–9. [CrossRef]
12. Kong, D.L.Y.; Sanjayan, J.G. Effect of elevated temperatures on geopolymer paste, mortar and concrete. *Cem. Concr. Res.* **2010**, *40*, 334–339. [CrossRef]
13. Chindaprasirt, P.; Rattanasak, U. Fire-resistant geopolymer bricks synthesized from high-calcium fly ash with outdoor heat exposure. *Clean Technol. Environ. Policy* **2018**, *20*, 1097–1103. [CrossRef]
14. Meyer, C. The greening of the concrete industry. *Cem. Concr. Compos.* **2009**, *31*, 601–605. [CrossRef]
15. Verian, K.P.; Behnood, A. Effects of deicers on the performance of concrete pavements containing air-cooled blast furnace slag and supplementary cementitious materials. *Cem. Concr. Compos.* **2018**, *90*, 27–41. [CrossRef]
16. Rickard, W.D.A.; van Riessen, A. Cement & Concrete Composites Performance of solid and cellular structured fly ash geopolymers exposed to a simulated fire. *Cem. Concr. Compos.* **2014**, *48*, 75–82.
17. Zhang, Z.; Provis, J.L.; Reid, A.; Wang, H. Cement & Concrete Composites Mechanical, thermal insulation, thermal resistance and acoustic absorption properties of geopolymer foam concrete. *Cem. Concr. Compos.* **2015**, *62*, 97–105.
18. Hýsek, Š.; Frydrych, M.; Herclík, M.; Louda, P.; Fridrichová, L.; Le Van, S.; Le Chi, H. Fire-resistant sandwich-structured composite material based on alternative materials and its physical and mechanical properties. *Materials* **2019**, *12*, 1432. [CrossRef]

19. Van, S.; Hájková, P.; Kovacic, V.; Bakalova, T.; Lukáš, V.; Le, C.H.; Seifer, K.C.; Peres, A.P.; Louda, P. Thermal Conductivity of Reinforced. *Ceram. Silik.* **2019**, *63*, 365–373.

20. Soltan, H.; Abdel-gawwad, H.A.; García, S.R.V.; Israde-alcántara, I. Fabrication and characterization of thermally-insulating coconut ash-based geopolymer foam. *Waste Manag.* **2018**, *80*, 235–240.

21. Leiva, C.; Arenas, C. A porous geopolymer based on aluminum-waste with acoustic properties. *Waste Manag.* **2019**, *95*, 504–512. [CrossRef] [PubMed]

22. Duan, P.; Song, L.; Yan, C.; Ren, D.; Li, Z. Novel thermal insulating and lightweight composites from metakaolin geopolymer and polystyrene particles. *Ceram. Int.* **2017**, *43*, 5115–5120. [CrossRef]

23. Yong, M.; Liu, J.; Alengaram, U.J.; Jumaat, M.Z.; Mo, K.H. Evaluation of thermal conductivity, mechanical and transport properties of lightweight aggregate foamed geopolymer concrete. *Energy Build.* **2014**, *72*, 238–245.

24. En, B. Products and systems for the protection and repair of concrete structures. In *Definitions, Requirements, Quality Control and Evaluation of Conformity—Part 2: Surface Protection Systems for Concrete*; International standard EN 1504-2:2004; British Standard: London, UK, 2004; Volume 3.

25. a. s. Lučební závody. Lukosil M130. Available online: https://www.lucebni.cz/cs/lukosil/85-silikonovy-lak-lukosil-m-130.html. (accessed on 15 November 2019).

26. a. s. Lučební závody. Lukofob ELX. Available online: https://www.lucebni.cz/cs/lukofob/70-hydrofobizacni-pripravek-lukofob-elx.html. (accessed on 15 November 2019).

27. En, B.S. *Methods of Testing Cement—Part 1: Determination of Strength*; European Committee for Standardization: Brussels, Belgium, 2005; Volume 169, p. 36.

28. Bogas, J.A.; Glo, M.; Real, S. Capillary absorption of structural lightweight aggregate concrete. *Mater. Struct.* **2015**, *48*, 2869–2883. [CrossRef]